The control of centrosome duplication after genotoxic stress

Burcu İnanç

Centre for Chromosome Biology,

School of Natural Sciences,

National University of Ireland Galway.

A thesis submitted to the National University of Ireland Galway for the degree of Doctor of Philosophy

September 2011

Supervisor: Prof. Ciaran Morrison

Table of Contents

List of Figures

List of Tables

Abbreviations

γ-TuRC	γ-tubulin ring complex
APC/C	anaphase-promoting complex/cyclosome
APS	ammonium persulphate
ATM	ataxia telangiectasia, mutated
ATP	adenosine-5'-triphosphate
ATR	ATM-Rad3 related
ALV	avian leukosis virus
BER	base excision repair
BRCA1	breast cancer associated gene1
BRCA2	breast cancer associated gene 2
BLAST	basic local alignment search tool
bp	base pair(s)
BrdU	5-bromo-2`-deoxyuridine
BSA	bovine serum albumin
cDNA	complementary DNA
Cdk	cyclin-dependent kinase
CAK	cyclin-dependent kinase-activating kinases
CENP-F	centromere protein F
Chk(1/2)	checkpoint kinase (1/2)
CHO	chinese hamster ovary cells
CIN	chromosome instability
CKI	cyclin-dependent kinase-inhibitors
CLAP	chymostatin, leupeptin, antipain, pepstatin A
CMAC	CellTracker™ Blue 7-amino-4-chloromethylcoumarin
C-Nap1	centrosomal NEK2-associated protein 1
C-terminus	carboxy terminus
DABCO	1,4-diazabicyclo[2.2.2]octane
DAPI	4',6-diamidino-2-phenylindole
DDR	DNA damage response
DEPC	diethylpyrocarbonate
DMSO	dimethylsulfoxide
dsDNA	double-stranded DNA
ssDNA	single-stranded DNA
DNA-PK	DNA-dependent protein kinase
dNTP	deoxyribonucleotide-5'-triphosphate
DSB	double-strand break
EB1	microtubule end-binding protein 1
ECL	enhanced chemiluminesence
EDTA	ethylenediaminetetraacetic acid
EGTA	ethylene glycol tetraacetic acid
ES	mouse embryonic stem cells
FACS	fluorescence-activated cell sorting
FBS	fetal bovine serum
FITC	fluorescein isothiocyanate
FRAP	fluorescence recovery after photobleaching
g	gravity
GADD45a	growth arrest and DNA damage inducible 45a
GFP	green fluorescent protein
GTP	guanosine triphosphate
HR	homologous recombination
HU	hydroxyurea
IF	immunofluorescence microscopy
IR	ionizing radiation
kb	kilobase pair(s)

kDa	kilodaltons
Kiz	kizuna
LB	luria-Bertani medium
M	mitosis
MAD	mitotic arrest deficient
MEFs	microtubule
MCC	mitotic checkpoint complex
MTOC	microtubule organizing centre
NEK2	NIMA (never in mitosis gene a)-related kinase 2
NER	nucleotide excision repair
NHEJ	non-homologous end joining
NIN	ninein
ns	non-significant
NPM/B23	nucleophosmin
N-terminus	amino terminus
OD	optical density
PBS	phosphate buffered saline
PCM	pericentriolar material
PCM1	pericentriolar material 1
PEG	polyethylene glycol
PH3	phosphorylated histone H3
PCR	polymerase chain reaction
Pen/Strept	penicillin/streptomycin
PIKK	phosphoinositide 3-kinase related protein kinas
Plk	polo-like kinase
PMSF	phenylmethylsulfonyl fluoride
PP1	protein phosphatase 1
PP2A	protein phosphatase 2A
Rb	retinoblastoma protein
RISC	RNA-induced silencing complex
RNA	ribonucleic acid
RNAi	RNA interference
RNase	ribonuclease
RPA	replication protein A
RT-PCR	reverse-transcriptase PCR
SAC	spindle assembly checkpoint
SAP	shrimp alkaline phosphatese
SCC1	sister chromatid cohesion 1
SDS	sodium dodecyl sulphate
SMC	structural maintenance of chromosomes protein
SDS-PAGE	SDS polyacrylamide gel electrophoresis
SEM	standard error of the mean
Ser/Thr	serine/threonine
shRNA	short hairpin-like RNA
siRNA	small interfering RNA
SPB	spindle pole body
ssDNA	single stranded DNA
TAE	tris acetate EDTA
TEMED	N,N,N',N'-tetramethylethylenediamine
TG	tris-glycine
TEM	transmission electron microscopy
Tris	tris(hydroxymethyl)aminomethane
TRIzol	total RNA isolation reagent
UV	ultraviolet
XLF	XRCC4-like factor
WT	Wild-type
Xpa	Xeroderma pigmentosum, complementation group A

Acknowledgements

First and foremost, I would like to thank my supervisor Prof. Ciaran Morrison for giving me the opportunity to come to Ireland and carry out my PhD work in his group. I am deeply grateful for his constant support, guidance, encouragement and helpful discussions while working on my project and writing my thesis.

I would also like to thank Dr. Helen Dodson for her help in so many ways during my PhD, especially for her supervision, never-ending scientific advice and her assistance with corrections during my write up phase.

I would like to thank all members of the Chromosome Biology Laboratory for providing a great atmosphere to work in and always being ready to help: A big thanks to Anna for all the scientific help, for always being truly supportive and wishing me the best. Thanks to Tiago for the valuable scientific help and discussion. Thanks to Loretta for helping with corrections in my thesis and for fun chats in the lab. Many thanks to Maciek, Pauline, Sinead, David and Yifan for helping me and making my time in the lab enjoyable by sharing lunches and tea breaks. Many thanks to all my colleagues from the Genome Stability Cluster for all their help. It has been nice working with all of you!

Many thanks to all my friends in Galway, in particular Chiara, Emilie, Simona, Sylvie and my housemate Danielle, thank you for supporting me and making my staying here more joyful and less lonely.

I also would like to thank my family ‘my parents, my brother, my sister in law and my lovely cat Karamel’ and my friends for always being there for me and for their continual support and encouragement throughout my whole life and especially during my PhD. Canım Anneciğim ve Babacığım hayatım boyunca bana her zaman inandığınız ve yanımda olduğunuz için ve en önemlisi doktoram sürecinde iyi günümde de kötü günümde de beni hep anlayışla karşılayıp pozitif enerjiniz ve sevginizle beni hiç yalnız bırakmadığınız ve desteklediğiniz için sizlere çok ama çok teşekkür ederim.

Burcu

‘to all my beloved ones’

Abstract

The centrosome is the major microtubule organising center in animal cells. Following DNA damage, centrosome amplification can occur, which in turn can result in the formation of multipolar mitotic cells, and cell death. DNA damage-induced centrosome amplification requires G2-to-M checkpoint function. In the first part of this thesis, we tested if IR-induced centrosome amplification is allowed through a diffusible stimulatory signal or by the loss of a duplication-inhibiting signal, using cell fusion assays. Cell fusion experiments revealed that only the irradiated centrosome can reduplicate following IR treatment. These findings support a model in which centrosome amplification results from a centrosome-limited license to duplicate in G2 in response to DNA damage. In addition, we observed a notable increase in centriole disengagement following DNA damage, suggesting a link between IR-induced centriole disengagement and centrosome amplification. Moreover, pharmacological inhibition of Plk1 resulted in a decrease of centrosome amplification in irradiated cells, suggesting that Plk1 might be a licensing factor in IR-induced centrosome amplification.

Cep135 is a core centrosome protein that is important for the assembly and the maintenance of functional centrosomes in several organisms. In the second part of this study, we attempted to elucidate the role of chicken Cep135 in centrosome duplication and structure in chicken DT40 cells, using gene targeting. We found that *Cep135*$^{-/-}$ cells were viable and showed no obvious phenotypic differences in terms of cell cycle progression, mitosis and microtubule nucleation compared to wild-type DT40 cells. In addition, we showed that the loss of Cep135 does not cause any change in the overall centrosome composition, configuration and centrosome duplication, indicating that Cep135 is not an essential structural or functional component of centrioles in DT40 cells. Interestingly, ultrastructural analysis of Cep135-deficient centrosomes revealed an unusual electron-dense structure within the barrel of the centrioles. Furthermore, *Cep135*$^{-/-}$ cells displayed high levels of HU-induced centrosome amplification in comparison to wild-type DT40 cells, indicating that Cep135 deficiency causes DT40 cells to become more permissive to multiple rounds of centriole duplication. Together, the results presented in this thesis provide new insights into how cells control centrosome duplication after genotoxic stress.

Chapter 1
Introduction

1.1 Cell cycle

The cell cycle is an ordered series of events that leads to cell division and the production of two daughter cells each containing chromosomes identical to those of the parental cell. Regulation of the cell cycle is critical since loss of its control may lead to the generation of non-viable or transformed daughter cells and cancer. The cell cycle consists of four stages: G1, S, G2, and M (Figure 1.1). In the synthesis (S) phase, replication of parental DNA occurs and chromosomes are equally distributed to each daughter cell during mitosis (M). S phase is preceded by a gap called G1 during which the cell prepares for DNA synthesis and chromosome replication and this is followed by a gap called G2 during which the cell readies itself for mitosis. The two gap phases are the periods of times that allow the cell to monitor the external environment for growth factors or cell density and the internal environment for DNA damage or abnormal cellular structure. Under certain conditions such as the absence of growth stimuli or after terminal differentiation, cells can exit the cell cycle during early G1 phase and enter a quiescent phase called G0. All together, G1, S and G2 are called interphase (reviewed by Morgan, 2007).

In a typical mammalian cell, the interphase is about 24 hours, whereas passage through mitosis takes about 1 hour. The M phase is divided into 5 stages: prophase, pro-/metaphase, anaphase, telophase and cytokinesis. In prophase the chromatin becomes highly condensed and the nuclear envelope breaks down. In metaphase, sister chromatids align at the metaphase plate of the bipolar spindle. In anaphase, each chromatid starts to move to opposite sides of the spindle. During telophase the nuclear envelope is reformed and chromosomes start to decondense. Finally, during cytokinesis the mother cell divides into two daughter cells each containing the same genetic information (reviewed by Hunt & Kirschner, 1993).

The progression of cells through the cell cycle is regulated by cyclin proteins and cyclin dependent kinases (Cdks) (Figure 1.1). Since cyclins lack enzyme activity their action is mediated by binding to Cdks to form cyclin/Cdk complexes. The activity

of Cdks depends on association with their respective cyclins, in a cell cycle specific manner (Morgan, 1997), to positive phosphorylation by cyclin-dependent kinase (Cdk)-activating kinases (CAKs). The inactivation of Cdks requires the removal of inhibitory phosphates by cyclin-dependent kinase-inhibitors (CKIs), as well as the ubiquitin-dependent degradation of cyclins (Glotzer et al., 1991; Desai et al., 1995; Zachariae et al., 1998; Obaya and Sedivy, 2002; Lukas et al., 2004).

In mammalian cells, only four Cdks (Cdk1, Cdk2, Cdk4, Cdk6) are directly involved in cell cycle regulation. Cdk1 binds to cyclin B and forms the M-phase promoting factor, which is the key kinase for mitosis (Takizawa and Morgan, 2000). Cdk2/cyclin E are the main regulators of the G1/S transition. Cdk2 binds also to cyclin A at the beginning of S-phase and promotes DNA replication and centrosome duplication. Cdk4 and Cdk6 bind to cyclin D and regulate the G0/G1 transition as well as G1-progression (Lucibello et al., 1993; Sherr et al., 1994). There are other Cdks that are involved indirectly in cell cycle progression, such as Cdk7 and Cdk8 and Cdk9 (Fisher and Morgan, 1994; Pinhero et al., 2004).

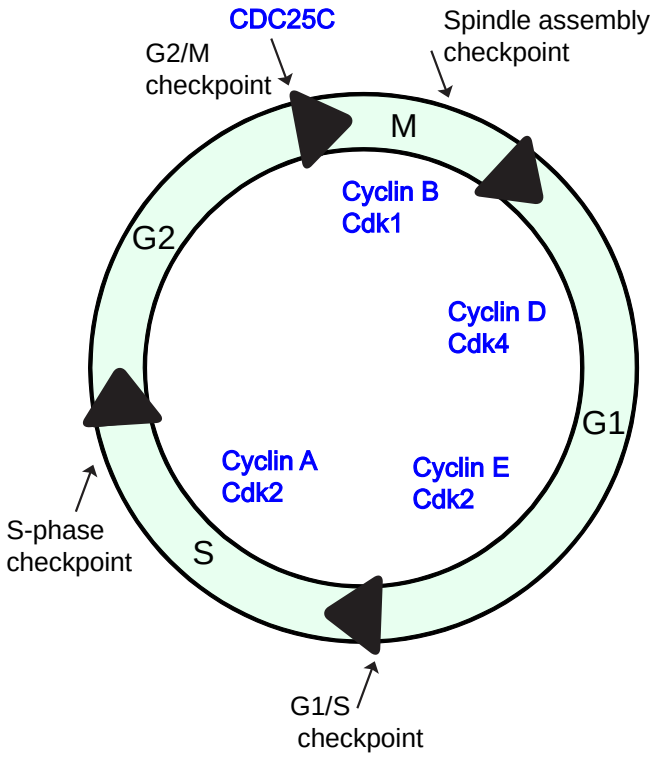

Figure 1.1 The cell cycle.
Schematic representation of the cell cycle progression and the various phases (G1, S, G2 and M) of the cell cycle. Activation of specific CDK/cyclin complexes drives progression through the cell cycle.

1.1.1 The G1/S transition

During early G1 and in quiescent cells the activity of Cdk/cyclin complexes is down-regulated. Once retinoblastoma protein (Rb) binds to the transcription factors of E2F family, this interaction blocks transcription of G1/S and S-phase specific cyclins. In the presence of growth factors, signal transduction via the ERK pathway leads to activation of critical transcription factors, such as AP-1, that stimulate synthesis of cyclin D. Cyclin D in the cytoplasm interacts with Cdk4 and Cdk6 and then these complexes move into the nucleus (Brown et al., 1998; Albanese et al., 1999). Phosphorylation of Rb by cyclin D/Cdk complexes causes Rb to move away from E2F, allowing it to activate the transcription of many genes including cyclin E and c-Myc (Nevins et al., 1997; Brehm et al., 1999; Harbour and Dean, 2000; Kaye, 2002). Cyclin E associates with Cdk2 to form the cyclin E/Cdk2 complex that has two main functions. Firstly, it further phosphorylates Rb protein allowing G1 progression. Secondly, it contributes to the onset of DNA synthesis. As cells progress towards S phase, cyclin A is expressed and Cdk2 is released to associate with cyclin A. Cyclin A/Cdk2 phosphorylates Cdc6 (the essential regulator of DNA replication) and DNA replication is initiated. Cyclin A/Cdk2 activity remains high from S phase until the G2/M transition (Pines and Hunter, 1991; reviewed by Hochegger et al., 2008).

1.1.2 The G2/M transition

Until the completion of DNA replication, cyclin B/Cdk1 accumulates in the cytoplasm and at the centrosomes (Jackman et al., 2003). During this period, cyclin B/Cdk1 is kept inactive by Wee1 kinase. Once DNA replication is completed, cyclin B/Cdk1 is activated by Cdc25 phosphatases action on theronine 14 and tyrosine 15 and the transition into mitotic prophase starts. Active cyclin B/Cdk1 also phosphorylates Cdc25B and Cdc25C phosphatases and thereby creates a positive feedback loop leading to increased Cdc25B and Cdc25C activity, while inhibiting Wee1 (Xiong and Ferrell, 2003; reviewed by Boutros et al., 2007). Other mitotic kinases such as Plk1 and Aurora-A also contribute to the activation of Cdk1 (Toyoshima-Morimoto et al., 2001; Hirota et al., 2003). Onset of mitosis requires the translocation of active cyclin B/Cdk1 from the cytoplasm to the nucleus, where it phosphorylates nuclear lamin, induces the breakdown of the nuclear envelope, and catalyses chromosome condensation. Cdk1 activity is also required for the formation of the mitotic spindle that aligns condensed chromosomes at the metaphase plate. Once all the chromosomes are attached to the spindle, cyclin B is

rapidly degraded by the activity of the anaphase promoting complex/cyclosome (APC/C), which is an E3 ubiquitin ligase. APC/C is also involved in cohesin cleavage through separase activity. Following cohesin cleavage, chromatid separation occurs and cells progress from metaphase into anaphase (reviewed by Hochegger et al., 2008).

1.2 The Centrosome

The centrosome was first discovered in the early 1900s by Theodor Boveri (Boveri, 1901). It was described as a small focus of dense material within a cell that anchored the end of thin cytoplasmic spindle fibres. It is now known that this electron-dense structure is the centrosome, which is the major microtubule organising centre (MTOC) in animal cells. In proliferating cells, the centrosome is required for the nucleation of microtubules (MTs), whereas in differentiated or quiescent cells the core centrosomal components, the centrioles, form basal bodies that are needed for cilium formation. The centrosomes have functions in many cellular activities including cell division, cell cycle progression, cell motility, polarity, maintenance of cell shape, transport of vesicles, and targeting of numerous signalling molecules (reviewed by Doxsey, 2001; Schatten, 2008; Azimzadeh and Bornens, 2007). In recent years, the centrosome has gained increased scientific attention, as various functions that are important for the survival and reproduction of the cells have been attributed to it.

Although centrosomes are evolutionarily conserved, they were lost from many eukaryotic phyla over the course of evolution. For example, higher plants lack centrioles yet still organise a bipolar mitotic spindle via a centrosome-independent pathway. Fungi and yeast have developed a structure that is known as the spindle pole body. Similar to the animal centrosome, it plays a role at the spindle poles during cell division (reviewed by Marshall, 2009). Even though centrosomes are not essential for spindle assembly and organisation, recent discoveries have revealed that centrosomes and in particular centrioles have a vital function in the production of flagella and cilia (reviewed by Luders and Stearns, 2007).

1.2.1 Centrosome structure

The centrosome is a non-membranous cell organelle of approximately 1 μm^3 in size and usually found in close proximity to the nucleus and the Golgi apparatus. (reviewed by Doxsey, 2001; Bettencourt-Dias and Glover, 2007). The centrosome is composed of a pair of centrioles which are characterised by their orthogonal orientation (Figure 1.2). Centrosomes consist of a large number of centrosome proteins including γ-tubulin and the γ-tubulin ring complex (γ-TURC) and are surrounded by the pericentriolar material (PCM). The PCM is an electron-dense matrix that contains proteins which mostly harbour protein-interaction motifs such as coiled-coil domains and functions as the primary site of microtubule nucleation (Bettencourt-Dias and Glover, 2007; Andersen et al., 2003). Centrioles are cylindrical structures formed by nine microtubule triplets organised in a radially symmetric manner around a cartwheel structure (Figure 1.2). The cartwheel is located at the proximal procentriole lumen and is required for the establishment of the ninefold symmetry of the centriole (reviewed by Azimzadeh and Marshall, 2010). In human cells, centrioles are approximately 200 nm in diameter and 400 nm in length (reviewed by Doxsey, 2001; Bettencourt-Dias and Glover, 2007). Each centriole is formed from arrays of nine microtubule triplets, which are referred to as the A-, B- and C-tubules. The A-tubule connects the triplets to the cartwheel and is the only complete microtubule that extends across the proximal to distal end of a fully grown centriole. The C-tubule is shorter than the A- and B- tubules and does not stretch to the distal end of the tube. The distal end of the centriole consists of a transition zone where microtubule triplets are reduced to doublets (reviewed by Azimzadeh and Marshall, 2010). In this region an array of fine fibres links the alternate microtubule doublets to each another. These fibres are enriched in Centrin, a ubiquitous calcium-binding centrosome component (reviewed by Salisbury, 2007).

The two centrioles within each centrosome are referred to as the mother (older) and daughter (younger) centrioles. The mother centriole can be recognised by two sets of specialised appendages at its distal end: the distal and sub-distal appendages. The distal appendages act as basal bodies and are required for ciliogenesis, whereas subdistal appendages are required for microtubule anchoring (reviewed by Azimzadeh and Marshall, 2010; Azimzadeh and Bornens, 2007). Several proteins have been characterised as components of those appendages such as ε-tubulin, Cep164, Cep170, ninein, and the ODF-2 splice variant hCenexin1 (Mogensen et al., 2000; Chang et al.,

2003; Guarguaglini et al., 2005; Ishikawa et al., 2005; Graser et al., 2007; Soung et al., 2009).

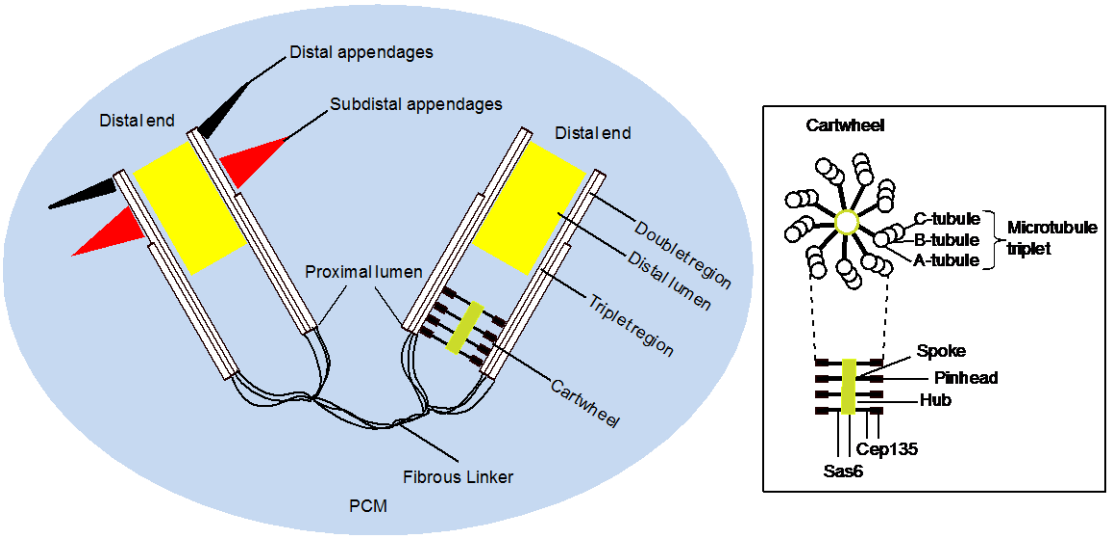

Figure 1.2 Centrosome structure.
Schematic view of the G2 phase centrosome structure. The centrosome is composed of a pair of centrioles, linked at their proximal ends by a proteinaceous fibrous linker and surrounded by pericentriolar material (PCM). Centrioles are composed of nine triplets of microtubules. The mature `mother` centriole carries two types of appendage, distal and subdistal, which the `daughter` procentriole lacks. The procentriole has an internal cartwheel structure in its proximal end. The mother centriole does not have a cartwheel structure. The cartwheel structure establishes the ninefold symmetry of the centriole and consists of a central hub and nine radial spokes, which are terminated by pinhead structures. The nine triplets of microtubules are connected to the cartwheel through the A-tubule on the pinhead structure. The B- and C- tubules follow the A-tubule in the microtubule triplets. Assembly of the cartwheel depends on Sas-6 on the hub and inner spokes and Cep135 on the spokes or/and pinheads (Adapted from Azimzadeh and Marshall, 2010 and Hatch and Stearns, 2010).

1.3 Centrosome Functions

1.3.1 Microtubule nucleation

Microtubules are hollow filaments made up by polymerisation of α- and β-tubulin heterodimers. Microtubules possess minus and plus ends and assemble in such a way that the β-tubulin subunit is exposed at the plus end and the α-tubulin subunit is exposed at the minus end. The GTP-binding capacity of the tubulin heterodimer controls the dynamic instability of microtubules, which can switch rapidly between growing and shrinking phases. If bound to GTP, the dimers of α- and β-tubulin assemble into microtubules and microtubule growth occurs, whereas if GTP molecules are hydrolyzed, microtubules depolymerize (reviewed by Etienne-Manneville, 2010; Kline-Smith and Walczak, 2004). When cells are treated with microtubule-depolymerizing drugs which are then washed out, microtubules mainly grow out of the

centrosomes. The two main drugs that are used to study microtubules in cells are taxol and nocodazole. Taxol prevents microtubule depolymerisation by stabilization of microtubules (Amos and Lowe, 1999; Nogales et al., 1995). Nocodazole is a derivative of benzimidazole and it promotes microtubule polymer disassembly. Therefore, it is possible to study different aspects of microtubule behaviour using different concentrations of these drugs in cells (Jordan et al., 1993; Vasquez et al., 1997).

The main microtubule nucleation site in most cells is the centrosome. Interphase centrosomes organise microtubule arrays to regulate intracellular trafficking, cell mobility, adhesion and contribute to the cytoskeleton, giving a cell its shape and polarity (reviewed by Luders and Stearns, 2007). Similar to other microtubules, the centriolar microtubules are polar polymers. The unstable minus end forms the proximal end of centrioles whereas the more dynamic plus end forms the distal end of the centrioles and extends away from the centrosome. To achieve this organisation, centriole MTs are stabilised by post-translational modifications such as polyglutamylation and acetylation (reviewed by Doxsey, 2001; Bornens, 2002).

Organisation of microtubule arrays depends on the ability of centrosomes to nucleate, anchor and release microtubules. The PCM is a key component of the centrosome which serves as a site of microtubule anchorage and nucleation during interphase and mitosis (reviewed by Bettencourt-Dias and Glover, 2007). Nucleation of centrosomal microtubules requires a third type of tubulin, γ-tubulin. Together with at least 6 additional proteins including GCP-WD/NEDD1, Cep192/hSPD2, pericentrin, Cep215/Cdk5Rap2, γ-tubulin forms a circular structure in the pericentriolar matrix, called the γ-tubulin ring complex (γ-TuRC) (Wiese and Zheng, 2006; Luders and Stearns, 2007). Centrosomal microtubules are nucleated by γ-TuRCs. The γ-TuRC caps the minus ends of the microtubules, thereby stabilising them and preventing their depolymerization (Luders and Stearns, 2007). Microtubule anchoring occurs on subdistal appendages in addition to PCM. Anchoring of MTs requires molecules including ninein, Centriolin, dynactin and the p150-glued subunit of the dynactin complex in association with EB1 (Askham et al., 2002; Dammermann and Merdes, 2002). Ninein, which is a component of the subdistal appendages of the mother centriole, is connected to the centriole through its C-terminus and also interacts with γ-TuRC through its N-terminus. Although the mechanism of microtubule anchoring is not

yet known, the capacity of γ-TuRCs to anchor the microtubules at centrosomes is disrupted in the absence of ninein (Mogensen et al., 2000; Ou et al., 2002).

The release of microtubules from the centrosome to the cytoplasm requires MT-severing proteins, such as katanin, which has an important role in remodelling MTs in the interphase-mitosis transition (reviewed by Bettencourt-Dias and Glover, 2007). During the G2/M transition, when the cell is preparing to assemble the mitotic spindle, microtubule nucleating activity increases. This process is called centrosome maturation and is promoted by both Polo-like kinases and Aurora-A, which recruit additional pericentriolar material (PCM) to the centrosomes (reviewed by Blagden and Glover, 2003). Inhibition of MT nucleation is mediated by the action of several phosphatases like PP1, PP2A and by the BRCA1-mediated ubiquitylation of γ-tubulin (Cazales et al., 2007; Sankaran et al., 2007; Tournebize et al., 1997).

1.3.2 Mitotic spindle organisation and cytokinesis

During mitosis in animal somatic cells, centrosomes organise a microtubule network into the bipolar mitotic spindle, which is necessary for the equal segregation of chromosomes. However, plants as well as the female germline of many organisms in the animal kingdom, lack centrosomes, but can still organise a normal mitotic spindle and undergo cell division (reviewed by Luders and Stearns, 2007). Unexpectedly, laser ablation or micro-needle removal of centrosomes in mammalian cells still allows the formation of a functional bipolar spindle (Hinchcliffe et al., 2001). Despite the fact that centrosomes are not essential for bipolar spindle assembly, they still play a key role in mitosis, ensuring the correct positioning of the spindle and establishing the site of cell cleavage furrow during cytokinesis. In cells lacking centrosomes, spindles are mispositioned and cleavage furrow placement becomes irregular and disorganised due to movement of the spindle apparatus. This usually results in cells that are unequally cleaved (Hinchcliffe et al., 2001; Khodjakov et al., 2002). In addition, many centrosomal proteins such as CP110, CEP55 and Centriolin have been reported to localise to the midbody and to be involved in cytokinesis and cleavage furrow formation (reviewed by Debec et al., 2010).

1.3.3 Ciliogenesis

In contrast to the mitotic functions of centrosomes, ciliogenesis is a complex and highly coordinated process that strictly requires centrioles. Cilia or flagella are evolutionarily conserved organelles that are required for cell motility and movement of substances around the cell (reviewed by Pedersen and Rosenbaum, 2008). The centrosome translocates from the periphery of the nucleus to the cell membrane to form the basal body for the generation of cilia and flagella. The mature basal body, which is anchored to the plasma membrane, functions as a template for the growth of the axoneme (a membrane-bound microtubule based structure) that extends out from the cell membrane to the extracellular environment (reviewed by Bettencourt-Dias and Glover, 2007). In vertebrate cells, only the mature mother centriole can grow a primary cilium. Deletion of ODF2, an appendage protein, in mouse results in centrioles that cannot form cilia, indicating that the appendages of the mother centriole are important for cilia formation (Ishikawa et al., 2005). Flagella or cilia can be motile or static, such as the primary cilium. Motile flagella or cilia have a 9+2 arrangement of microtubules in the axoneme in which nine doublets of microtubules are organised around a central pair, whereas the primary cilia have a nine-fold arrangement of microtubules, with no central pair (reviewed by Nigg and Raff, 2009). The functions of flagella or the primary cilium are diverse and indispensable for several cellular and developmental processes. These include the motile cilia in the sperm and fallopian tubes and the primary cilia which are present on sensory organelles, photoreceptors, fibroblasts, neurons, trachea and bronchial tubes (Satir and Christensen, 2008).

1.4 The centrosome cycle

In contrast to the *de novo* centrosome duplication pathway, which occurs in some specialized cell types and under unusual conditions, the canonical centrosome duplication pathway requires pre-existing centrioles (Tsou and Stearns, 2006a). Centrosome duplication is tightly coordinated with the cell cycle and occurs only once per cell cycle. The centrosome duplication cycle can be divided into four main steps. 1) centriole disengagement, 2) centrosome duplication, 3) centrosome maturation and 4) centrosome separation (Figure 1.3), (reviewed by Tsou and Stearns, 2006a; Nigg, 2007). Duplication of the centrosome starts at the G1/S transition and finishes in G2 phase. In G1 phase, cells contain only one centrosome which is composed of two centrioles attached loosely by cohesion fibres. During the G1/S transition, one new

procentriole starts growing at the proximal end of each centriole. The procentriole continues to elongate until late G2 phase and becomes mature by recruiting extra proteins to the PCM. At the G2/M transition, mature centrosomes separate and form the poles of the bipolar spindle in mitosis. During S phase, G2 phase and early mitosis, the old and the new centrioles are tightly associated and have an orthogonal orientation. The tight link between the two centrioles is lost in co-ordination with chromatid segregation at the metaphase to anaphase transition, in a process referred to as `disengagement`. This centriole disengagement process licences the two centrioles for a new round of duplication (reviewed by Tsou and Stearns, 2006a; Nigg, 2007).

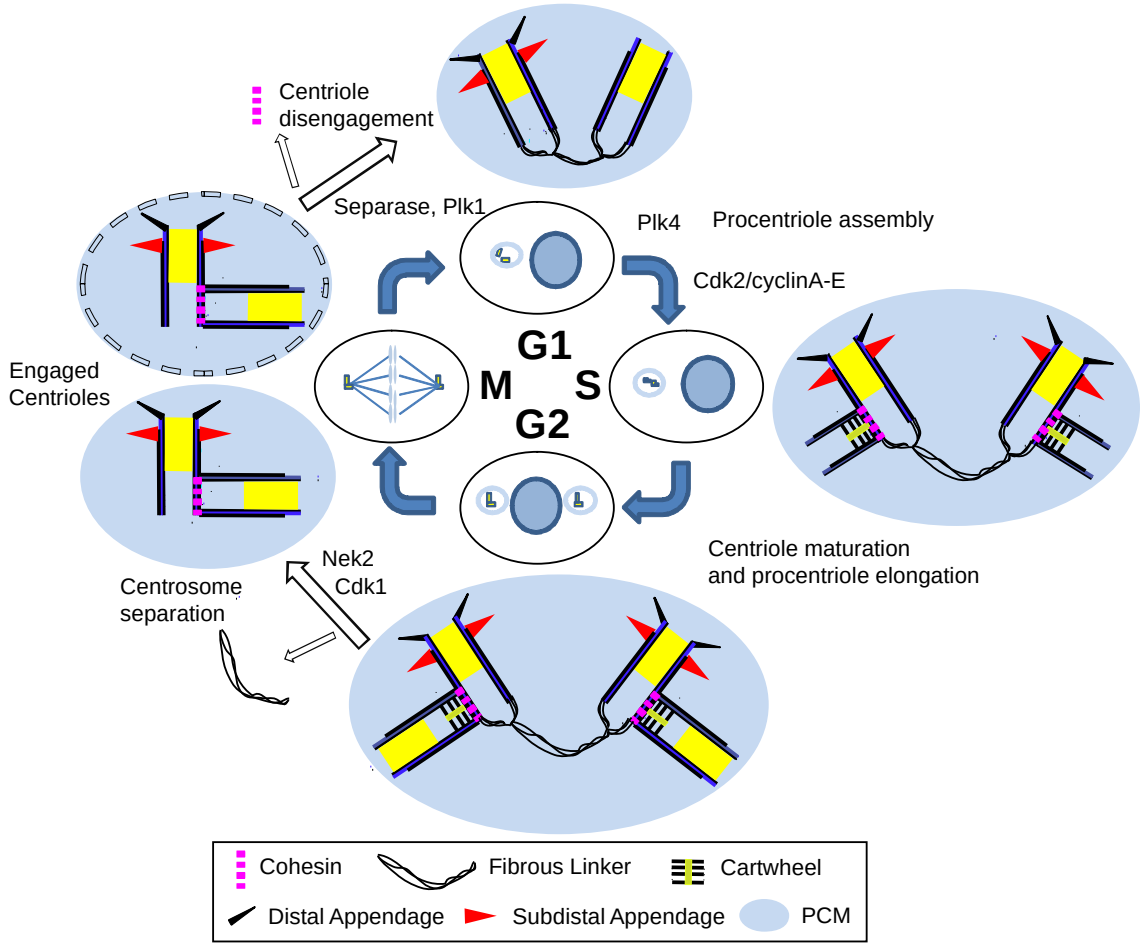

Figure 1.3 The centrosome cycle. Schematic representation of the cell cycle and the five major events of the centrosome cycle: centriole disengagement, procentriole assembly and elongation, centriole maturation and centrosome separation. Mature centrioles are depicted with distal and subdistal appendages, procentrioles are depicted with a cartwheel structure. Important regulators of the centrosome cycle are indicated (See text for details), (Adapted from Hatch and Stearns, 2010).

1.4.1 Centriole disengagement

Centrosomes duplicate only once in S phase. In untransformed cell lines, when progression through the cell cycle is blocked, centrosomes do not reduplicate, indicating

the presence of a mechanism that limits centrosome duplication to once per cell cycle (Nigg, 2007). Evidence for cell cycle control of centrosome duplication came from cell fusion studies (Wong and Stearns, 2003). These fusion experiments demonstrated that, although unduplicated G1 centrosomes were able to duplicate in S or G2 phase cytoplasm, recently duplicated G2 centrosomes were not able to reduplicate even in the presence of permissive S phase cytoplasm, suggestive of a centrosome-intrinsic block to centrosome reduplication in G2 phase (Wong and Stearns, 2003). Using *Xenopus* egg extracts and purified human centrosomes, Wong and Stearns showed that engaged S phase centrioles became disengaged after being added to the mitotic extract, indicating that the engagement of centrioles provides an intrinsic block to further duplication and the disengagement event in mitosis licenses the two centrioles for a new round of duplication (Tsou and Stearns, 2006b; reviewed by Nigg, 2006a). These elegant experiments provided a "block-and-license" model for centriole duplication (Tsou and Stearns, 2006b; reviewed by Nigg, 2007). According to this model, the presence of a daughter centriole on the wall of mother centriole blocks the formation of new daughter centrioles even though cytoplasmic conditions are permissive for duplication. Laser ablation experiments on S-phase arrested HeLa cells provided direct support for this model. Removal of daughter centrioles by laser micro-irradiation allows mother centrioles to initiate centriole duplication, clearly showing that the capacity of a mother centriole to duplicate depends on its engagement or disengagement status (Loncarek and Khodjakov, 2009).

Recent studies have indicated that Separase and Polo-like kinase 1 (Plk1) are the major regulators of centriole disengagement (Figure 1.3), (Tsou and Stearns, 2006b; Tsou et al., 2009). Separase is a protease that becomes active at anaphase onset and is responsible for triggering the cleavage of sister-chromatid cohesion. Separase activity is regulated via its inhibition by Securin and Cyclin B1, which are both targeted for degradation by the anaphase promoting complex/cyclosome (APC/C) (Zou et al., 1999; Holland and Taylor, 2006; Gorr et al., 2005). Treatment of purified human centrosomes in *Xenopus* egg extracts with nondegradable Securin or Cyclin B1 provided evidence for the requirement of Separase activity for centriole disengagement (Tsou and Stearns, 2006b). Later studies have demonstrated that Plk1, a centrosomally-localised kinase, is a parallel activator of centriole disengagement (Tsou et al., 2009). Tsou and colleagues have shown that homozygous inactivation of ESPL1 (Separase) in human tissue culture

cells resulted in strong inhibition of centriole disengagement in the short term and that these cells were able to progress into G1 phase with engaged centrioles. However, long-term observations revealed that these centrioles disengaged later in the cell cycle, indicating the activity of another licensing pathway. Treatment of cells with the Plk1 inhibitor BI2536 resulted in inhibition of centriole disengagement before the onset of anaphase. These findings suggest the involvement of Plk1 as an additional disengagement factor prior to Securin destruction and Separase activation. Moreover, combined inhibition of Separase and Plk1 activity led to complete abrogation of centriole disengagement and centriole duplication in the following S phase (Tsou et al., 2009). Taken together, these results indicate that both Plk1 and Separase play crucial roles in the mitotic dissolution of centriole engagement, thereby licensing centriole duplication.

Recent studies have started to investigate the centriolar substrates of Separase and Plk1. It has been proposed that the members of the cohesin ring complex, in addition to their role in the regulation of sister chromatid separation during mitosis, associate with the centrosome and act as centriole engagement factors (Wang et al., 2008; Tsou et al., 2009; Schockel et al., 2011; Gimenez-Abian et al., 2010). Sister chromatids are held together by the cohesin ring complex, which consists of structural maintenance of chromosomes protein 1 (SMC1), SMC3, sister chromatid cohesion protein 1 (SCC1) and SCC3 (Gruber et al., 2003; Haering et al., 2008). The cohesin complex resides along the chromosome arms and at centromeres and is removed by two different pathways during mitosis (Waizenegger et al., 2000). Removal of cohesin from chromosome arms occurs in prophase and involves phosphorylation of SCC3 by Plk1. However, the centromeric cohesin complex, which also involves phosphatase 2A (PP2A) and Shugoshin1 (Sgo1), is protected from this pathway and removed only at the metaphase to anaphase transition when SCC1 is cleaved by Separase (Kitajima et al., 2006).

Nakamura and co-workers have shown that SCC1 is found at the centrosomes and is cleaved by Separase, in a manner similar to chromosomal SCC1 (Nakamura et al., 2009). Another study also showed that SCC1 localises at the centrosome and is required for centrosome integrity (Gimenez-Abian et al., 2010). Furthermore, Wang and colleagues have suggested that sSgo1, a smaller splice variant of Sgo1, is another

centriole engagement factor, which localizes to centrosomes in interphase and to spindle poles in mitosis (Wang et al., 2008). They have proposed that the function of sSgo1 as a protector of centriole cohesion is regulated by Plk1. A very recent study on centriole cohesin as a centriole engagement factor has provided more details on this enigmatic process (Schockel et al., 2011). It has been shown that while ectopic activation of Separase or depletion of Sgo1 results in both premature sister chromatid separation and centriole disengagement, expression of non-cleavable SCC1 or inhibition of the prophase pathway (by Plk1 inhibition and the depletion of cohesin-associated factor Wap1) suppresses these events. Moreover, it has been found that artificial endoproteolysis of SCC1 or SMC3 triggers centriole disengagement. Taken together, these findings suggest that, in a similar way to sister chromatids, the cohesin complex may work as a glue to hold the paired centrioles together in an engaged state, before their disengagement by Separase and Plk1 in late mitosis (Schockel et al., 2011).

1.4.2 Cell-cycle regulators of centriole duplication

Centrosome duplication is tightly linked to DNA duplication and occurs in S phase (Figure 1.3). Similar to DNA replication, the rise of Cyclin dependent kinase 2 (Cdk2) activity coincides with procentriole formation in early S phase. It has been proposed that cyclinE/Cdk2 and/or cyclinA/Cdk2 activation are the key elements that link centrosome duplication and DNA replication (Matsumoto et al., 1999; Meraldi et al., 1999; Hinchcliffe et al., 1999; Hinchcliffe et al., 2001; Matsumoto and Maller, 2004). However, *Cdk2* null mice cells are able to duplicate their centrioles without any defects, suggesting that Cdk1 activity might compensate for Cdk2 function (Berthet and Kaldis, 2007; Ortega et al., 2003). Moreover, chicken DT40 cells that lack Cdk2 require Cdk1 to duplicate their centrosomes, suggesting the redundancy of the two kinases in this pathway (Hochegger et al., 2007).

Three substrates of Cdk2 have been implicated in centrosome duplication: nucleophosmin (NPM/B23) (Okuda et al., 2000), CP110 (Chen et al., 2002) and Mps1 (Kasbek et al., 2007). Nucleophosmin is only found in G1 centrosomes and its phosphorylation by Cdk2/cyclin E results in nucleophosmin removal from the centrosome and initiation of procentriole formation. In addition, inhibition of nucleophosmin phosphorylation blocks centriole duplication (Okuda et al., 2000; Tokuyama et al., 2001). Mps1 is an essential protein kinase for the spindle assembly

checkpoint (Stucke et al., 2002). Although Mps1 has been shown to be necessary for duplication of the spindle pole body in yeast, its exact contribution to centriole duplication in higher eukaryotes has not been fully defined. One group has indicated that the involvement of Mps1 is not required for centriole duplication in human cells (Stucke et al., 2002), whereas other groups have suggested that the accumulation of Mps1 is necessary for centriole duplication (Fisk and Winey, 2001; Fisk et al., 2003; Kasbek et al., 2007). CP110 is another centrosomal protein, which is phosphorylated by Cdks. CP110 protein levels increase at the G1/S transition and remain high until the end of mitosis. It has been shown that CP110 physically interacts with centrin and calmodulin *in vivo* and upon its depletion, cells display defects in cytokinesis and binucleation after mitosis (Tsang et al., 2006). Moreover, siRNA-mediated depletion of CP110 inhibites centriole reduplication in HU (hydroxyurea) arrested U2OS cells (Chen et al., 2002; Kleylein-Sohn et al., 2007).

1.4.3 Centriole Biogenesis

Centriole assembly is an evolutionarily highly conserved pathway between all organisms including protists, invertebrates and vertebrates (Figure 1.4), (Carvalho-Santos et al., 2010). Polo-like kinase 4 (Plk4), the master regulator of centriole assembly in human cells, is a functionally conserved protein and its functional homologues have been identified as SAK in *Drosophila melanogaster* and as ZYG-1 in *C. elegans*. Overexpression of Plk4 induces supernumerary centriole formation and its depletion inhibits centriole duplication, indicating that the cellular activity of Plk4 needs to be tightly regulated to control centriole copy number (Habedanck et al., 2005; Duensing et al., 2007; Kleylein-Sohn et al., 2007). Although the mechanism of ZYG-1/SAK/Plk4 activation is not known, it starts accumulating at the parental centrioles before the initiation of centriole assembly and continues to accumulate at the centrioles during S, G2 and mitosis (Bettencourt-Dias et al., 2005; Kleylein-Sohn et al., 2007).

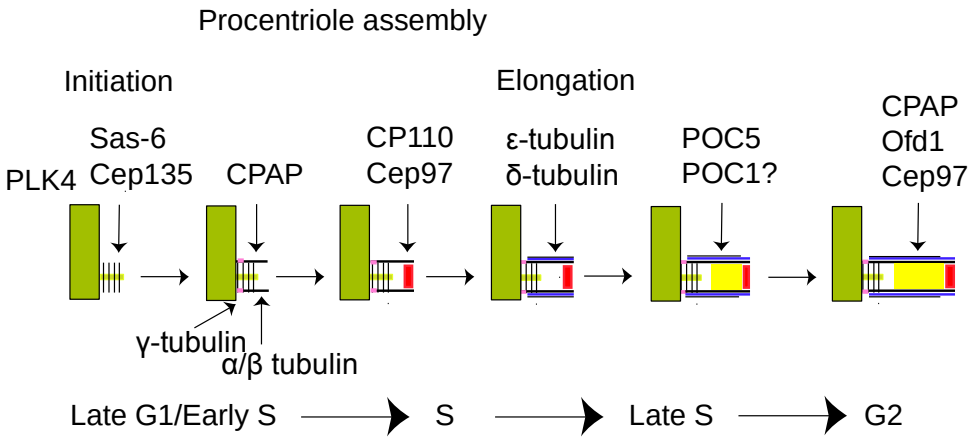

Figure 1.4 Model for centriole assembly in human cells.
Procentriole assembly starts during late G1 or early S phase with the assembly of the cartwheel structure that contains Sas-6 and Cep135. Important regulators (Plk4) and structural components of centriole assembly (Cep135, Sas-6, CPAP, CP110, γ/α/β/ε/δ-tubulins, Cep97, POC1, POC5, and Ofd1) are depicted in the image (See text for details), (Adapted from Azimzadeh and Marshall, 2010).

In human cells, the initiation of procentriole assembly, which occurs during late G1 or early S phase, requires many proteins together with Plk4: Sas-6 (Leidel et al., 2005), Cep135 (Hiraki et al., 2007; Mottier-Pavie and Megraw, 2009), Sas-4 (CPAP/CENPJ) (Leidel and Gonczy, 2003; Dammermann et al., 2008), γ/α/β-tubulin (Kleylein-Sohn et al., 2007), Cep97 (Spektor et al., 2007) and CP110 (Chen et al., 2002). An siRNA screen in U2OS cells revealed that Sas-6, Cep135 and CP110 are essential for centriole biogenesis in human cells (Kleylein-Sohn et al., 2007). Procentriole assembly begins with the formation of a cartwheel located at the proximal end of centrioles. In *C. elegans*, ZYG-1 controls the recruitment of Sas-6 to the centriole (Kitagawa et al., 2009). It has been proposed that Sas-6 and Cep135 establish the nine-fold symmetry of the cartwheel by localising at the central hub and at the pin heads of the cartwheel, respectively (reviewed by Azimzadeh and Marshall, 2010). The *Chlamydomonas reinhardtii* homologue of *Sas-6* is *Bld12* and mutations in this gene lead to the formation of a cartwheel without the central hub and structurally defective basal bodies (Nakazawa et al., 2007). Moreover, depletion of DmSas-6 in primary spermatocytes of *Drosophila* results in the formation of centrioles which are shorter in diameter than controls, with missing microtubule blades (Rodrigues-Martins et al., 2007). Sas-6 protein levels increase at the end of G1 phase and decline in mitosis. In keeping with this observation, it has been shown Sas-6 no longer remains associated with mother and daughter centrioles. Recent evidence has indicated that Sas-6 is targeted for 26S proteasome-mediated degradation through APC^{Cdh1} activity at the end of mitosis (Strnad et al., 2007). Therefore, Sas-6 levels and the activity of APC^{Cdh1} need

to be tightly regulated through the cell cycle in order to ensure the initiation of procentriole assembly in late G1 phase (reviewed by Strnad and Gonczy, 2008; Azimzadeh and Marshall, 2010).

It has been shown that the expression of a C-terminal mutant form of Bld10 (Cep135 orthologue) in *Chlamydomonas* cells results in the formation of shortened cartwheel spokes and centrioles with 8-fold symmetry (Hiraki et al., 2007; Jerka-Dziadosz et al., 2010). Similarly, RNAi-mediated depletion of *Bld10* in *Paramecium* gives rise to the formation of centrioles that lack cartwheel spokes but retain the central hub (Jerka-Dziadosz et al., 2010). Also, ultrastructural studies in flies have revealed that sperm centrioles in *Bld10* mutant male flies are shorter than those seen in wild-type flies and the central pair of microtubules is missing in sperm flagella, resulting in sterility (Blachon et al., 2009). However, in contrast to observations in *Chlamydomonas*, depletion of Bld10 in *Paramecium* and mutation of *Bld10* in *Drosophila* did not indicate a role for Bld10 in determining the ninefold symmetry of the microtubule triplets (Jerka-Dziadosz et al., 2010). Immuno-electron microscopy studies in human and mouse cells have shown that Cep135 also localizes to the proximal lumen of the centrioles and to the surface of the parental centriolar cyclinder. Similar to *Chlamydomonas* Bld10, Cep135 has been found to be essential for centriole assembly in Chinese hamster ovary (CHO) and U2OS cells (Ohta et al., 2002; Kleylein-Sohn et al., 2007). In addition to its role in cartwheel formation, Cep135 has been implicated in the organisation and nucleation of microtubules (Ryu et al., 2000; Ohta et al., 2002; Uetake et al., 2004). When Cep135 is overexpressed or depleted via RNAi, microtubule organisation is altered both in interphase and mitotic CHO cells (Ohta et al., 2002). In addition, it has been proposed that Cep135 functions as a platform protein by holding C-NAP1 at the proximal ends of the centrioles (Kim et al., 2008).

In mammalian cells, following cartwheel formation, procentriole wall organisation is initiated by the assembly of nine microtubule triplets around a cartwheel in late G1 phase and early S phase. Microtubule triplet formation occurs sequentially. First, the A-microtubule, which is nucleated by γ-TuRC, attaches to the spokes of the cartwheel. Then, the B- and C-microtubules grow bidirectionally, by a γ-TuRC independent mechanism, around the wall of A- and B-microtubules, respectively (Figure 1.2) (Guichard et al., 2010). The microtubule triplets are stabilised by the recruitment of δ- and ε-tubulin and centriole elongation begins during S phase (Figure

1.4). Recruitment of microtubules to form the wall of the procentriole is triggered by the activity of CENPJ (CPAP)/Sas-4 (Kohlmaier et al., 2009; Schmidt et al., 2009; Tang et al., 2009). Immuno-electron microscopy studies have revealed that Sas-4 is concentrated at the centriole walls in *C. elegans* (Kirkham et al., 2003) and CPAP localises at the centriole lumen in human cells (Kleylein-Sohn et al., 2007). During procentriole formation, a cap structure forms at the distal end of the procentriole. This structure contains CP110 and Cep97 and protects the centrioles from extensive growth and depolymerisation (reviewed by Azimzadeh and Marshall, 2010). Recent studies have demonstrated that CPAP and CP110 determine the extent of centriole elongation by the addition of tubulin subunits to the growing centrioles, thereby controlling the length of centrioles (Kohlmaier et al., 2009; Schmidt et al., 2009; Tang et al., 2009). Several other centriolar proteins have been recently identified as regulators of centriole length. Procentriole elongation requires POC1 and POC5 during S phase (Keller et al., 2009; Azimzadeh et al., 2009). In addition, another centriolar protein called Ofd1 localises to the distal end of the procentrioles and parental centrioles, and plays a role in controlling the length of centrioles (Singla et al., 2010). Finally, procentriole formation continues by the addition of tubulin during G2 phase, and microtubules are stabilized by post-translational polyglutamylation (reviewed by Azimzadeh and Marshall, 2010).

1.4.4 Centrosome maturation and separation

Centrosome maturation begins in late G2 and is characterized by structural changes in centrioles such as an increase in centrosome size due to recruitment of several PCM proteins, in particular γ-TURC (Zheng et al., 1995; reviewed by Meraldi and Nigg, 2002; Lukasiewicz and Lingle, 2009). At the onset of mitosis, the centrosome becomes attached to the spindle pole and acquires additional microtubule nucleation sites. Centrosome maturation is regulated by Plk1 (Lane and Nigg, 1996), Nek2 (Prigent et al., 2005), protein phosphatase 1 (PP1) (Helps et al., 2000) and Aurora-A (reviewed by Meraldi and Nigg, 2002). Plk1 and Aurora-A, the key regulators of centrosome maturation, phosphorylate their substrates to allow the recruitment of PCM proteins to the centrosome (reviewed by Meraldi and Nigg, 2002; Lukasiewicz and Lingle, 2009). Recent studies have shown that Aurora-A also phosphorylates Plk1 at mitotic entry (Macurek et al., 2008). The centrosome maturation pathway involves many proteins such as centrosomin (Terada et al., 2003), Hef1 (Pugacheva and Golemis, 2005), TACC or TPX2 (De Luca et al., 2006), Bora (Hutterer et al., 2006), NDEL1 (Mori et al., 2007),

and LATS2 (Toji et al., 2004). Surprisingly, all of these proteins play a role either in the recruitment of Aurora-A to centrosomes or as downstream targets of Aurora-A (reviewed by Lukasiewicz and Lingle, 2009).

Centrosome maturation is followed by the separation of the duplicated centrosomes into two spindle poles (Figure 1.3). Centrosome separation starts with the disruption of cohesion between the proximal ends of the two parental centrioles by the activity of Nek2 kinase (reviewed by Meraldi and Nigg, 2002). Nek2 is a cell cycle-regulated centrosomal kinase and its overexpression is correlated with the formation of extra centrosomes (Hayward et al., 2004). Kinase activity of Nek2 increases towards the end of G2 phase since the activity of its negative regulator PP1 is inhibited by increased Cdk1 activity (Helps et al., 2000). The fibrous linker between the two centrioles contains C-NAP1 and Rootletin (Mayor et al., 2000; Bahe et al., 2005). Phosphorylation of C-NAP1 and Rootletin by Nek2 leads to displacement of these proteins from centrosomes and thereby disassembly of the fibrous linker (Fry et al., 1998; Bahe et al., 2005). β-catenin, an integral component of the Wnt signalling pathway which regulates cell proliferation and gene expression during development, is also a component of the fibrous centriole linker (Bahmanyar et al., 2008). β-catenin is associated with Rootletin in interphase. Phosphorylation of β-catenin is required for Nek2-induced centrosome separation. Although the exact mechanism underlying the requirement for β-catenin in Nek2-mediated centrosome separation is still not fully understood, these findings suggests that β-catenin is a negative regulator of centrosome cohesion (Bahmanyar et al., 2008).

Beyond its well-characterised roles in mitosis and microtubule organisation, the centrosome is also known to function in the cellular response to DNA damage. In the next section, first I will summarize the DNA damage responses and then discuss centrosome amplification in response to DNA damage and other factors.

1.5 DNA damage responses

DNA is the essential carrier of genetic information in all living cells. DNA is not a chemically stable molecule since the primary structure of DNA is constantly subjected to alterations by endogenous and exogenous sources of DNA damage. The endogenous sources include the products of cellular metabolism such as reactive oxygen species and replication errors, such as stalled and collapsed replication forks. The exogenous sources include threats from the external environment such as ionizing radiation (IR), ultraviolet light (UV) and genotoxic chemicals. Alterations in DNA structure can result in simple base changes or more complex changes including deletions, fusions, translocations, or aneuploidy (reviewed by Lieber, 2010; Sancar et al., 2004).

To protect genomic integrity, cells have evolved a surveillance mechanism, termed 'the DNA damage response'. The DNA damage response includes the recognition of DNA damage, DNA repair and the activation of signal transduction pathways that activate cell cycle checkpoints to arrest cell cycle progression or induce apoptosis (Zhou and Elledge, 2000; Halazonetis et al., 2008). All these processes are coordinated to achieve faithful maintenance, replication and segregation of the genetic material. Defects in any of these pathways may cause genomic instability, immunodeficiency, aging, neoplastic transformation and cell death. (reviewed by Lieber, 2010; Sancar et al., 2004).

1.5.1 The DNA damage checkpoint network

The DNA damage checkpoint is composed of proteins that function as sensors, transducers, mediators, and effectors (Figure 1.5). Following DNA damage, sensor proteins detect DNA lesions, and recruit and/or activate mediators and transducers. Transducer kinases transmit damage signal to downstream effectors, and mediators mediate the signal from the transducer kinases to the effectors, which then trigger specific cellular responses, such as cell cycle arrest, DNA repair or cell death. DNA damage sensor proteins are multiprotein complexes, such as the Mre11-Rad50-Nbs1 (MRN) complex which recruits ATM and the Rad17 and Rad9-Rad1-Hus1/9-1-1 complex which recruits ATR. ATM and ATR transduce the damage signal to checkpoint kinases, such as Chk1 and Chk2. Activation of ATM/ATR and ATM/ATR-mediated phosphorylation of sensor proteins result in recruitment of mediator proteins, such as 53BP1, BRCA1, MDC1, FANCD2, Claspin and H2AX. Activation of mediator

proteins further induces ATM and ATR-dependent activation of Chk1 and Chk2, respectively. Chk1 and Chk2 phosphorylate and promote the degradation of effector proteins such as Cdc25s (Cdc25A, B, and C), which in turn results in deactivation of cyclin-dependent kinases (Cdk1 and Cdk2). Another effector protein that is phosphorylated by Chk1/Chk2 and ATM/ATR is p53 (Figure 1.5). Cdc25 inactivation and p53 accumulation initiate signalling cascades that cause cell cycle arrest, DNA repair and apoptosis (Figure 1.5), (reviewed by Dai and Grant, 2010).

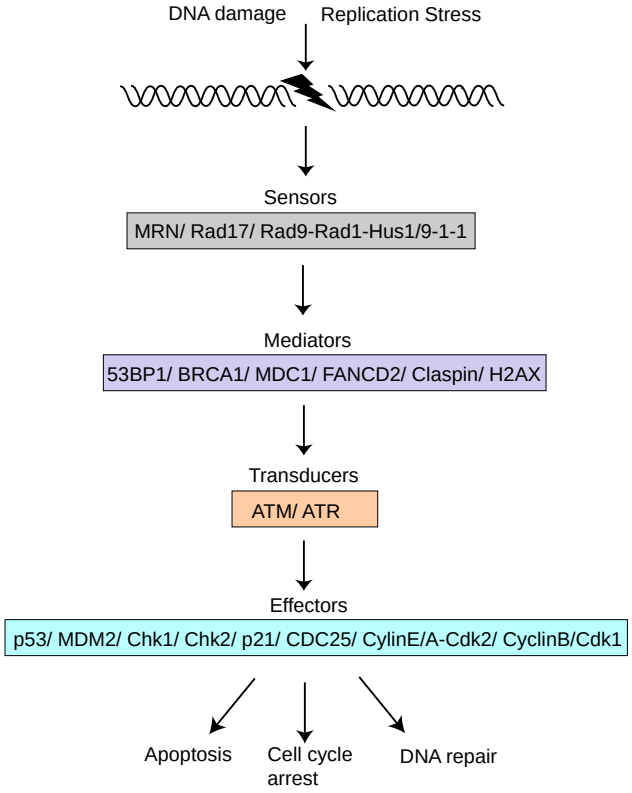

Figure 1.5 General outline of the DNA damage response signal-transduction pathway. (See text for details), (Adapted from Zhou and Elledge, 2000).

Following DNA damage, the MRN complex is recruited and H2AX (a variant H2A histone) is phosphorylated in the chromatin near the break. It has been shown that following exposure to ionizing radiation (IR), in a few minutes ATM is auto- or trans-phosphorylated on Ser1981 (Bakkenist and Kastan, 2003; Stiff et al., 2006). Activated ATM phosphorylates H2AX at Ser139 (γ-H2AX) around the DSBs (Burma et al., 2001). In a similar way, ATR phosphorylates H2AX in response to replicational stress (Ward and Chen, 2001). Following H2AX phosphorylation, many DNA damage proteins are recruited to the sites of DSBs and ATM directly phosphorylates 53BP1,

MDC1, BRCA1, and c-Abl (reviewed by Cann and Hicks, 2007). ATM is directly involved in the regulation of Rad51 recombinase function via c-Abl activation (Yuan et al., 2003). In addition, ATM indirectly activates BRCA1 via Chk2. The BRCT-containing proteins Nbs1, MDC1, 53BP1, and BRCA1 are mediator proteins that are involved in regulation of various repair and checkpoint proteins (Li and Zou, 2005). Nbs1 is directly involved in sensing DNA damage and activation of ATM through the MRN complex. Nbs1 appears to function in the intra-S-phase checkpoint and also in the G1–S checkpoint by promoting ATM-dependent phosphorylation events (Lee et al., 2007; Paull and Lee, 2005). MDC1 has a critical role in recognizing γ-H2AX and thereby amplifying the DSB signal through interaction with ATM (Lou et al., 2006). In addition, MDC1 functions in checkpoint control through interaction with the Rad51 recombinase (Zhang et al., 2005). BRCA1 interacts with both Rad51 and BRCA2 and functions in ATM-dependent phosphorylation events and checkpoint control. 53BP1 is also involved in promoting ATM activation following DSBs and functions in activating the G2/M checkpoint (reviewed by Cann and Hicks, 2007).

The central proteins in the DNA damage checkpoint are the phosphoinositide 3-kinase-related kinases (PIKKs), which are ATM (ataxia-telangiectasia (A-T), mutated), ATR (ataxia-telangiectasia- and Rad3-related), hSMG-1, mTOR and DNA-PK (DNA-dependent protein kinase). In general, the PIKKs possess serine/threonine kinase activity and respond to DNA damage by phosphorylating their substrates in the appropriate pathways (Abraham, 2004). ATM and DNA-PK mainly respond to DSBs whereas ATR responds to UV damage, stalled replication forks and replication inhibitors such as hydroxyurea (HU) and also to DSBs. The hSMG-1 kinase has a role both in UV damage and DSBs. ATM and ATR are central kinases in the DNA damage response that detects various forms of damaged DNA and activates DNA damage response cascades (reviewed by Shiloh, 2006).

In humans, hypomorphic mutations in the *ATR* gene results in a severe disease called ATR–Seckel syndrome. It is characterized by growth retardation, dwarfism, microcephaly, mental retardation and defects in various cellular DNA-damage responses. The hypomorphic phenotype of *ATR* in ATR–Seckel syndrome demonstrates the crucial role of ATR and indicates that there is no functional redundancy for this role (Alderton et al., 2004). In humans, mutations in *ATM* cause the disorder, ataxia-

telangiectasia, characterized by cerebellar degeneration, immunodeficiency, genome instability, radio sensitivity and predisposition to cancer. It has been shown that cells and mice lacking ATM are viable and that the kinase activity of ATM is minimal during the normal cell cycle, suggesting that ATM is not essential for normal cell cycle regulation (Shiloh and Kastan, 2001).

1.5.2 DNA damage-induced cell-cycle checkpoints

Following DNA damage cells need time for DNA repair. Therefore, cells initiate checkpoints responses to temporarily halt the cell cycle. There are three different checkpoints that can be activated in response to DNA damage: the G1–S checkpoint regulates transition into S phase, the intra-S-phase checkpoint regulates progression through S phase and the G2–M checkpoint regulates entry into mitosis (reviewed by Sancar et al., 2004). Although these checkpoints respond at different stages of the cell cycle in respond to DNA damage, they share many common proteins.

1.5.2.1 The G1/S and intra-S checkpoints

The G1-S checkpoint is mainly regulated via an ATM–p53–p21–Cdk2 pathway (Bartek and Lukas, 2001a; Bartek and Lukas, 2001b; Bartek et al., 2004). Following DSBs, the tumour suppressor p53 is directly phosphorylated on Ser15 and Chk2 is activated by ATM. Activated Chk2 further phosphorylates p53 on Ser20, thereby the association between p53 and its negative regulator MDM2 is interrupted resulting in the stabilization and accumulation of p53 (Bartek et al., 2004). ATM is also involved in the phosphorylation of MDM2, which prevents re-location of p53 to the cytoplasm for proteosomal degradation. Upon DNA damage, ATR is also involved in the phosphorylation of p53 through Chk1 phosphorylation and activation. Activated p53 induces transcription of several target genes. One of them is the critical G1–S regulator p21, which inhibits the Cdk2–cyclin E, Cdk2–cyclin A, and Cdk4(6)–cyclin D complexes. When inhibited, the Cdk2 and Cdk4 complexes cannot phosphorylate Rb, resulting in inhibition of E2F-dependent transcription. The target genes of E2F include the origin licensing factors Cdc6, Orc1, and Mcm proteins, Dbf4, DNA polymerases, and the G1–S regulators cyclin A, cyclin E, Cdk2, and Cdc25a (Bartek and Lukas, 2001a; Bartek and Lukas, 2001b; Bartek et al., 2004; reviewed by Cann and Hicks, 2007). It has been demonstrated that p53 can also function in the intra-S-phase checkpoint by suppression of replication fork progression after a low-dose of IR in a p21-independent manner (Shimura et al., 2006).

Cdk2 can also be inhibited by the phosphatase Cdc25a during the G1/S and intra-S checkpoints (Falck et al., 2001). DSB formation leads to activation of ATM which results in phosphorylation of Chk2, whereas single-strand gaps cause activation of Rad17–RFC, the 9–1–1 complex and ATR, resulting in phosphorylation of Chk1 (Cuadrado et al., 2006; Jazayeri et al., 2006; Myers and Cortez, 2006). Unphosphorylated Cdc25A, Cdc25B, and Cdc25C are involved in the G1/S and G2/M transition directly by dephosphorylating the cyclin-dependent kinases. Phosphorylation of Cdc25A–C by Chk1 or Chk2, targets them for ubiquitination and proteasomal degradation, which results in inactive Cdk2 (Falck et al., 2001).

In addition to the ATM/ATR-Chk1/Chk2-Cdc25A pathways, there is another pathway that can induce an intra-S-phase checkpoint, the ATM/NBS1/SMC1-SMC3 pathway (Falck et al., 2002). Following DNA damage, ATM or ATR phosphorylates the cohesin components SMC1 and SMC3, which inhibits DNA replication (Yazdi et al., 2002; Luo et al., 2008).

1.5.2.2 The G2–M checkpoint

The G2/M DNA damage checkpoint prevents cells from entering mitosis following DNA damage. The activity of Cdk1-cyclin B is very important in regulating the G2 phase transition and Cdk1 is kept in an inactive state by the tyrosine kinases Wee1 and Myt1. As in the G1-S checkpoint activated ATM or ATR phosphorylates Chk1, Chk2 and p53 following DNA damage. ATM also inactivates MDM2, the negative regulator of p53 (Sancar et al., 2004). After p53 is stabilized, it upregulates the transcription of p21 and 14-3-3 proteins (14-3-3s), and this results in the initiation of the G2–M checkpoint. (Niida and Nakanishi, 2006). 14-3-3s bind to the Cdk1-cyclin B1 complex and sequester it in the cytoplasm. p21 inhibits the Cdk2/cyclin A and Cdk4(6)/cyclin D complexes, resulting in transcriptional inhibition of target genes of E2F. These genes include G2-M regulators such as Cdk1 (Cdc2), cyclin A, cyclin B1, and cyclin B2 (DeGregori, 2002). p21 can also directly inhibit the Cdk1-cyclin B1 complex. In addition to p53 stabilization, Chk1 and Chk2 can also phosphorylate Cdc25 proteins, thereby ensuring that Cdk1/cyclin B1 remains phosphorylated and inactive (Niida and Nakanishi, 2006; Obaya and Sedivy, 2002).

Chk1 also functions in stabilising Wee1 kinase, which results in Cdk1 deactivation by its phosphorylation at the inhibitory site T14 (Raleigh and O'Connell, 2000). Therefore, all of the G2–M checkpoint pathways eventually cause the deactivation of Cdk1/cyclin B1. Deactived Cdk1/cyclin B complex cannot drive the cell to enter the division stage.

1.5.2.3 Spindle assembly checkpoint (SAC)

It is crucial to accurately segregate the duplicated chromosomes equally to the new daughter cells before division. This is achieved by proper attachment of sister kinetochores to microtubules extending from opposite spindle poles prior to anaphase onset. This state is called chromosome bi-orientation. If anaphase occurs in the presence of erroneous attachments, chromosomes separate unequally and aneuploid cells are generated. Therefore, cells have developed a surveillance mechanism called the Spindle Assembly Checkpoint (SAC) to ensure the proper attachment of microtubules to chromosomes. This checkpoint is conserved from yeast to human (reviewed by Holland and Cleveland, 2009).

The kinetochore is a protein assembly that links the chromosomes to the microtubules of the mitotic spindle. Misorientated or misattached kinetochores recruit SAC proteins. The main target of the spindle assembly checkpoint is APC/C. When the SAC is active, APC/C is inhibited by inactivation of its substrate-binding co-factor CDC20 (Hwang et al, 1998). By controlling the activity of CDC20, the SAC prolongs prometaphase until bipolar attachment and alignment of all chromosomes are achieved. Once chromosomes are biorienated, the spindle assembly checkpoint signal is inactivated allowing the cell to proceed to anaphase. The main targets of the APC/C are Securin and cyclin B, which are crucial for the onset of anaphase. Separase is a protease that is required to cleave the sister-chromatid cohesion at the metaphase to anaphase transition. Separase activity is essential to execute anaphase and it is inhibited until anaphase by two mechanisms: 1) Binding of the chaperone Securin and 2) phosphorylation-dependent binding of cyclin B associated with Cdk1. Once all the chromosomes are aligned and attached properly at the metaphase plate, the checkpoint signal is silenced, resulting in APC/C-mediated polyubiquitylation of Securin and cyclin B which leads to their destruction by the 26S proteasome. Following degradation of Securin and cyclin B, active Separase dissolves the cohesin subunits resulting in the loss of sister-chromatid cohesion and the separation of sister chromatids. Degradation of

cyclin B also results in the inactivation of Cdk1-cyclin B complex, which initiates cytokinesis and mitotic exit (reviewed by Peters, 2006; Musacchio and Salmon, 2007).

The main components of the SAC are called the mitotic checkpoint complex (MCC). The MCC includes the proteins MAD1, MAD2, BUBR1 and BUB3, as well as CDC20. Localization of this complex to unattached or misorientated kinetochores results in a diffusible signal that inhibits the ability of CDC20 to activate the APC/C (reviewed by Tanaka and Hirota, 2009). It has been shown that depletion of *MAD2* results in complete abrogation of the checkpoint signal, suggesting that MAD2 has a crucial role in SAC (Michel et al., 2004; reviewed by Peters, 2006). MAD2 accumulates on the kinetochores of unattached chromosomes and stably binds to MAD1, which is an essential protein for checkpoint function, forming a complex. This complex converts cytoplasmic-free MAD2 from an inactive conformation to an active form allowing binding to CDC20. The CDC20 -bound MAD2 activates more MAD2 molecules and therefore amplifies the checkpoint signal. This mechanism is called the `template model` and shows how a single unattached kinetochore can produce such a strong signal that can inhibit anaphase onset (reviewed by Tanaka and Hirota, 2009). The model suggested from the recent studies is that the formation of a MAD2-CDC20 subcomplex promotes the assembly of BUBR1-BUB3-CDC20 complex. In particular BUBR1 within the mitotic checkpoint complex inhibits APC/C activity by acting as a pseudosubstrate and by promoting the ubiquitination and degradation of CDC20 (Burton and Solomon, 2007; Nilsson et al., 2008).

1.5.3 DNA repair

The choice of which DNA repair pathway is activated depends on the type of DNA lesion and on the cell cycle timing. While damage on individual DNA bases activates base excision repair (BER) or nucleotide excision repair (NER) pathways, breaks in single (SSBs) or double (DSBs) DNA strands require repair mechanisms such as homologous recombination (HR), single strand annealing (SSA) or non-homologous end joining (NHEJ).

1.5.3.1 DNA double strand break mechanisms

DNA double strand breaks (DSBs) are the most dangerous form of DNA damage and can be introduced by external sources such as ionizing radiation (IR). IR damages

DNA directly by energy deposition or indirectly by ionization of water molecules to produce hydroxyl radicals that attack DNA (reviewed by Shrivastav et al., 2008; Mahaney et al., 2009). When two single strand breaks form on opposite DNA strands, double strand breaks occur that contain overhanging 3' and 5' ends. In mammalian cells, there are the two major repair pathways for the DSBs: non-homologous end joining and homologous recombination (Figure 1.6).

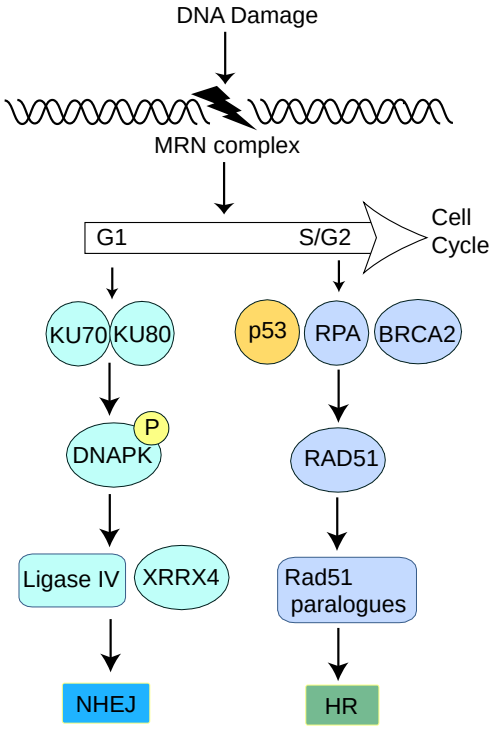

Figure 1.6 Schematic represantation of DSB-induced activation of DNA repair pathways (See text for details). (Adapted from Bolderson et al., 2009).

1.5.3.2 Non-homologous end joining (NHEJ)

NHEJ is active throughout the cell cycle and is the major pathway for the repair of double-strands breaks in the G0/G1 phases of the cell cycle in vertebrate cells (Takata et al., 1998; Rothkamm et al., 2003). Since NHEJ does not use the genetic information on the undamaged duplicate strand for the repair of damaged bases, it is more error-prone than repair through homologous recombination (reviewed by Warmerdam and Kanaar, 2010). In general, NHEJ involves the following steps: detection of the DBS, processing the DNA ends to remove damaged or nonligatable groups and the DNA ligation. The major proteins involved in NHEJ are the Ku70 /Ku80 (Ku) heterodimer, the catalytic subunit of the DNA-dependent protein kinase (DNA-PKcs), XRCC4, DNA ligase IV, Artemis, and XLF (XRCC4-like factor (also known as

Cernunnos). Mutations or deletions in these factors result in increased sensitivity to IR and other DSB inducing agents and defects in V(D)J recombination (reviewed by Bassing, et al., 2004; O'Driscoll and Jeggo, 2006; Meek et al., 2008; Meek et al., 2004).

The first step in this process is the detection of a DSB by the Ku heterodimer. Ku binds to the ends of a DSB and recruits DNA-dependent protein kinase (DNA-PKcs). DNA-PKcs prevents DNA end resection, regulates chromatin structure and facilitates DSB repair by protein phosphorylation (Meek et al., 2008). Together DNA-PKcs and DNA-bound Ku form a complex called the `synaptic complex`, which in turn triggers autophosphorylation of DNA-PKcs. This induces a conformational change that causes release of the DNA ends and/or release of phosphorylated DNA-PKcs from the complex (Mahaney et al., 2009). The XRCC4-DNA ligase IV complex and its associated factors, which are thought to be responsible for additional DNA end processing for ligation, are recruited to this site. Finally, XRCC4, DNA ligase IV and XLF/Cernunnos perform the ligation step resulting in the reannealing of the two broken ends (Meek et al., 2008; (Mahaney et al., 2009 493). Certain chemicals such as topoisomerase II inhibitors introduce DSBs that do not have directly ligatable DNA ends, because of the covalent attachment of topoisomerases. This type of repair also utilizes NHEJ and the nuclease Artemis, which localises to the sites of damage by interacting with DNS-PKcs and cleans up the DNA ends (Riballo et al., 2004; Ma et al., 2005; reviewed by Mahaney et al., 2009; Warmerdam and Kanaar, 2010).

1.5.3.3 Homologous recombination

Homologous recombination (HR) specifically occurs in late S and G2 phases of the cell cycle. HR is considered a more precise form of repair for double strand breaks since it requires an undamaged sister chromatid as a repair template and functions only after DNA replication (reviewed by Moynahan and Jasin, 2010). In eukaryotic cells, HR is initiated by 5'- 3' resection of the DNA ends at the damage site which results in the generation of 3' single stranded DNA (ssDNA) overhangs. Recruitment of the Mre11/Rad50/ NBS1 (MRN) complex to the break promotes DNA end resection, together with the endonuclease CtIP (reviewed by Bernstein & Rothstein, 2009). The product of the breast cancer susceptibility gene *BRCA1* interacts with both MRN and CtIP and may also be involved in the 5'- 3' end resection (Zhang and Powell, 2005). Following 5' to 3' resection, ssDNA is quickly covered with Replication Protein A (RPA), and subsequently Rad51 (Karagiannis and El-Osta, 2004; Thacker, 2005). It is

believed that Rad51 recruitment to the DSB is facilitated by the product of the breast cancer susceptibility gene, *BRCA2* (Pellegrini and Venkitaraman, 2004; Gudmundsdottir and Ashworth, 2006). Both *BRCA1* and *BRCA2* mutant cells are defective in HR. Once recruited to the DSB, Rad51 searches for the homologous site of the intact sister chromatid and mediates the strand exchange. During this process ssDNA invades the homologous duplex DNA and forms a displacement loop (D-loop). Using the undamaged chromatid as a template, DNA polymerases synthesize new DNA to span the break site (reviewed by Cann and Hicks, 2007). Other proteins are also involved in the repair including Rad51-like proteins (Rad51B, Rad51C, Rad51D, XRCC2, and XRCC3) and the Rad54 helicase (Karagiannis and El-Osta, 2004; Thacker, 2005). After DNA synthesis, Holliday junctions are cleaved and resolved by junction resolving complexes (BLM/TOPOIII) or nucleases GEN1, MUS81/EME1, SLX1/SLX4 (Andersen et al., 2009a; Ip et al., 2008a; Andersen et al., 2009b; Ciccia et al., 2008; Fekairi et al., 2009; Ip et al., 2008b; Muñoz et al., 2009; Svendsen et al., 2009). Holliday junction resolution can occur in different ways, resulting in crossover or non-crossover outcomes (reviewed by Moynahan and Jasin, 2010).

1.6 Centrosome amplification

Control of the structural and numerical integrity of centrosomes is crucial for the formation of a bipolar mitotic spindle. However, under certain conditions, abrogation of this control results in reduplication of centrosomes, which leads to centrosome amplification. Centrosome amplification can lead to formation of multiple (>2) spindle poles, which in turn may cause mitotic defects and thus promotes tumour progression. There are several mechanisms that can result in centrosome amplification: 1) DNA-damage induced centrosome overduplication; 2) De novo centriole biogenesis; 3) Division failure; 4) Cell fusion; 5) Centrosome fragmentation or premature splitting.

1.6.1 DNA-damage induced centrosome overduplication

Centrosome duplication occurs only once per cell cycle and is tightly regulated in coordination with DNA replication. However, in cells that are exposed to genotoxic agents, DNA replication and centrosome duplication cycles can become uncoupled, causing cells to go through one or more additional rounds of centrosome duplication (Lingle et al., 2005). Several studies have demonstrated that many cell cycle checkpoint proteins localize to centrosomes, indicating that centrosomes might play a role in the

DNA damage response. These proteins include Chk1, Chk2, p53, Cdc25, cyclin B/Cdk1, ATM, BRCA1, Nbs1 and Mcph1 (Dutertre et al., 2004; Jackman et al., 2003; Kramer et al., 2004; Takada et al., 2003; Tsvetkov and Stern, 2005; Jeffers et al., 2008; Oricchio et al., 2006; Zhang et al., 2007). Mutations or loss of these genes have been found to be related to centrosomal abnormalities, in addition to increased rates of genome instability and tumour development (reviewed by Shimada and Komatsu, 2009). Many groups have reported that following DNA damage, cell lines carrying mutations in those genes, including p53 (Fukasawa et al., 1996), the recombination repair genes *Xrcc2* and *Xrcc3* (Griffin et al., 2000), the recombinase *Rad51* (Dodson et al., 2004) and the tumor suppressor genes *BRCA1* (Deng, 2002) and *BRCA2* (Kraakman-van der Zwet et al., 2002) and *Mcph1*(Brown et al., 2010), exhibit a number of centrosomal responses including centrosome amplification.

Ionizing radiation treatment of tumor cells or cells with defective checkpoint or DNA repair genes results in an extended G2 arrest and centrosome amplification (Sato et al., 2000; Dodson et al., 2004). The checkpoint kinase Chk1 has also been implicated in radiation-induced centrosome amplification (Bourke et al., 2007; Loffler et al., 2007; Bourke et al., 2010). It has been reported that in addition to its nuclear localization, Chk1 also localizes to interphase centrosomes (Kramer et al., 2004). Its centrosomal localization is important for prevention of premature activation of cyclin B/Cdk1 through cytosolic Cdc25B, thereby avoiding premature entry to mitosis (Kramer et al., 2004; Jackman et al., 2003; Dutertre et al., 2004). Studies in our lab have shown that pharmacological inhibition or RNAi-mediated depletion of Chk1 in human cells result in suppression of centrosome amplification in response to ionizing radiation (Bourke et al., 2010). Loffler and colleagues have also shown that following DNA damage (UV radiation), accumulation of phosphorylated Chk1 on centrosomes causes G2/M cell cycle arrest and centrosome amplification (Loffler et al., 2007). These results also suggested that Chk1-mediated G2/M checkpoint arrest provides a backup mechanism for the elimination of cells with impaired S-phase checkpoints. Cdk2 activity is required for normal centrosome duplication. Studies in our lab have shown that Cdk2 activity is upregulated in IR-treated cells and is required for centrosome amplification after IR treatment (Bourke et al., 2010). Significantly, it has been demonstrated that IR-induced Cdk2 activation is dependent on Chk1 kinase through phosphorylation on threonine 160 (Bourke et al., 2010). Moreover, it has been shown that overexpression of cyclin E

restored the DNA damage-induced centrosome amplification in *Chk1* null DT40 cells, suggesting that the cyclin E-Cdk2 complex is involved in controlling centrosome numbers in response to DNA damage (Bourke et al, 2010).

In cells lacking checkpoint controls such as Chinese hamster ovary (CHO), U2OS cells, or *Tp53*-mutated cells including chicken DT40 cells, centrosome amplification occurs in response to drugs that inhibit S phase. For example, the drugs hydroxyurea (HU) or aphidicolin (Aph), which stall replication forks by inhibiting the enzyme ribonucleotide reductase (RNR), dysregulate the coordination of centrosome duplication and DNA synthesis (Balczon et al, 1995). Thus, while cells arrest in S phase, centrosome duplication continues and results in centrosome reduplication. Conversely, cells carrying wild-type p53 arrest both chromosome and centrosome cycle by stabilization and upregulation of the p53 protein in response to genotoxic stress such as HU (Fukasawa et al., 1996). p53 transactivates many proteins such as p21, and p21 blocks the initiation of centrosome duplication via continuous inhibition of Cdk2/cyclin E. However, in *Tp53* null cells, p21 does not become upregulated in response to cellular stress, and this allows continuous activation of Cdk2/cyclin E, which in turn results in centrosome reduplication (Fukasawa, 2005; Duensing et al., 2006; Meraldi et al., 1999).

Previous studies have shown that HU- and HPV-16 E7 oncogene-induced centrosome overduplication in mouse cells require Cdk2 activity (Duensing et al., 2006; Prosser et al., 2009). However, a recent study in our group has shown that in response to HU, centrosome amplification can occur in DT40 cells lacking either Cdk1 or Cdk2 activity, but not in DT40 cells lacking both Cdks (Bourke et al., 2010). These findings indicate that, in contrast to mouse cells, (Duensing et al., 2006; Prosser et al., 2009) in DT40 cells Cdk2 activity can be substituted by Cdk1 activity for the control of centrosome duplication. A recent study conducted in our lab has demonstrated that Chk1 deficiency in DT40 cells does not block HU-induced centrosome amplification suggesting that Chk1 is not involved in HU-induced centrosome reduplication in S-phase arrested cells (Bourke et al., 2010). Moreover, these results indicate that different mechanisms control IR-induced and HU-induced centrosome amplification. Consistent with this idea, the centrioles generated during G2 or S-phase arrest were found to be different in terms of maturity (Saladino et al., 2009). While centrioles generated after IR-mediated G2 arrest contain the mother centriole-specific protein, Cep170, centrioles

generated during an extended S phase arrest do not contain Cep170 (Saladino et al., 2009). These differences may indicate that different pathways are involved in S and G2 phase centrosome amplification. However, it appears that centrosome reduplication in both IR-induced G2/M arrest and HU-induced S phase arrest does not occur immediately, so that a prolonged arrest must be provided in both cases to allow sufficient time for centrosomes to reduplicate (Fukasawa, 2005).

1.6.2 Plk4-induced centriole overduplication

As explained in Section 1.4.3, the number of procentrioles that can form next to one parental centriole is limited and this is called copy number control. During centriole biogenesis, copy number control allows only one procentriole to form next to each pre-existing mother centriole. However, dysregulation of proteins involved in centriole biogenesis results in the formation of excessive numbers of procentrioles (Kleylein-Sohn et al., 2007). The polo kinase family member, Plk4, is a key regulator kinase of centriole biogenesis in both vertebrate and invertebrate cells. Sas-6 is another important protein in centriole biogenesis, and it is a structural component of the cartwheel (Hiraki et al., 2007; Kleylein-Sohn et al., 2007; Matsuura et al., 2004). It has been demonstrated that overexpression of Plk4/SAK in human and *Drosophila* cells, and Sas-6 in human cells, leads to the assembly of 'flower-like structures', a single mother centriole surrounded by several daughter centrioles (Habedanck et al., 2005; Strnad et al., 2007; Kleylein-Sohn et al., 2007; Cunha-Ferreira et al., 2009; Rogers et al., 2009). In addition, the absence of Plk4 impaires centriole duplication and causes severe anomalies in spindle formation (Habedanck et al., 2005). These observations are interesting because overexpression of a regulatory protein (Plk4), or a structural protein (Sas-6), results in dysregulation of the numerical control of centriole duplication. However, how Cdk2 and Plk4 and/or HsSas-6 act together to stimulate centriole overduplication is not known (reviewed by Duensing et al., 2009).

1.6.3 Viruses and centrosome amplification

Multiple rounds of centrosome amplification can also occur in tumour cells following viral infection. The high-risk human papillomavirus Type 16 (HPV-16) E6 and E7 oncoproteins are overexpressed in HPV-associated malignancies of the anogenital tract. E6 oncoprotein is known to cause centrosome amplification by triggering centrosome accumulation, whereas E7 oncoprotein cause centrosome

amplification through the formation of multiple daughters at a single maternal centriole (Duensing et al., 2008). Both oncoproteins disrupt host cell cycle checkpoints. While E6 oncoprotein induces proteasomal degradation of the p53, E7 binds and degrades RB leading to the inhibition of checkpoints and induction of centrosome amplification (Duensing et al., 2009; Saunders, 2005).

1.6.4 De novo centriole duplication

Another possible mechanism that can cause centrosome amplification is the generation of centrioles *de novo*. The *de novo* mode of centriole assembly exists in various organisms. For example, the mouse zygote initially does not contain centrioles, but at later stages of development each cell assembles the correct number of centrioles. Interestingly, the *de novo* centriole formation can be triggered in a cycling vertebrate somatic cell when all centrioles are removed by microsurgery or ablated by a laser microbeam. For example, in CHO cells, laser ablation of centrosomes during HU-induced S phase arrest results in *de novo* centriole formation (Khodjakov et al., 2002). Following activation of the *de novo* pathway, an aberrant number of centrioles was observed, suggesting that the numerical control over centriole formation is lost (Khodjakov et al., 2002; La Terra et al., 2005; Uetake et al., 2005; Uetake et al., 2007). The exact mechanism of the *de novo* pathway is not known; however, it may represent a mechanism of centrosome overduplication under certain conditions (reviewed by Nigg, 2006b). A recent study performed on *Xenopus* oocytes and egg extracts has provided some evidence on *de novo* centriole assembly regulation. Eckerdt and colleagues have shown that *de novo* centriole assembly requires Plx4 (homolog of human Plk4) activity, but not cyclinA/E/Cdk2 activity, in contrast to template-driven centrosome duplication, which requires cyclinA/E/Cdk2 activity (Eckerdt et al., 2011).

1.6.5 Cytokinesis failure and centrosome amplification

Cytokinesis failure can result in the formation of multinucleated cells that can accumulate abnormal numbers of centrosomes. Cells with wild-type p53 trigger checkpoint responses if cytokinesis fails, arrest their cycling and eventually undergo cell death. However, in the absence of intact p53-dependent checkpoint function, cells experience repeated cytokinesis block and induce tetraploidization and centrosome amplification (reviewed by Fukasawa, 2008). Several well-known oncogenes and tumour suppressor genes have been shown to induce tetraploidization. These include

mitotic progression genes such as Aurora-A , Plk1, SAC components and survivin and DNA response genes such as BRCA1, BRCA2, ATR, Rad51 and MDM2 (reviewed by Fukasawa, 2008). For example, overexpression of Aurora-A and other mitotic kinases in p53 defective cells may lead to the formation of extra centrosomes due to failed cytokinesis rather than deregulation of centrosome duplication (Meraldi, 2002; Anand et al., 2003). Similarly, overexpression of Plk1 in Hela and CHO cells results in an increase of cells with large and fragmented or multiple nuclei and centrosome amplification (Liu and Erikson, 2002; Meraldi et al., 2002). BRCA2 is an example of a tumor-suppressor protein that is involved in both DNA repair and cytokinesis. Loss of BRCA2 in murine embryonic fibroblasts and HeLa cells, results in centrosome amplification, possibly due to defects in DNA repair or in cytokinesis (Daniels et al., 2004; Tutt et al., 1999).

1.6.6 Cell fusion and centrosome overduplication

Cell fusion is another potential mechanism associated with overduplication of centrosomes and chromosomal aberrations in cells (reviewed by Zyss et al., 2009). Cell fusion during normal development such as in the placenta, muscle and bone, can result in centrosome amplification (reviewed by Ogle et al., 2005). Futhermore, centrosome amplification can occur in many tumor cells due to deregulation of physiological fusogenic proteins or viral infection (Pawelek, 2005). Fusogenic activity of certain viruses such as Sendai virus or abnormal expression of cellular proteins such as the ubiquitin-conjugating enzyme RAD6 may cause cell fusion, resulting in multinucleated cells, increased aneuploidy and centrosome amplification (Duelli et al., 2007; Shekhar et al., 2002). Therefore, although it is not very common, cell fusion-induced centrosome amplification, may be operative under certain circumstances.

1.6.7 Centrosome fragmentation and premature splitting

Another potential mechanism of centrosome amplification is improper splitting of centrioles and fragmentation of pericentriolar material (Date et al, 2006; Ehrhardt & Sluder, 2005; Hut et al, 2003). Centriole splitting occurs at the time of duplication during G1 phase. If premature centrosome splitting occurs, each of these split centrioles may form individual centrosomes (Hut et al., 2003). For example, following DNA damage centrosomes in CHO cells can split into individual centrioles (Hut et al., 2003), generating multipolar spindles. Human T cell leukemia virus type-1 (HTLV-1) is an

oncogenic virus and similar to human papillomavirus E7, it can also cause supernumerary centrosome formation. However, in contrast to HPV E7, HTLV-1 oncoprotein induce supernumerary centrosomes through centrosome fragmentation in mitosis, creating centrosomal abnormalities (Peloponese et al., 2005; Duensing et al., 2008). Studies have also shown that depletion of Kizuna (a centrosomal substrate of Plk1 and a structural component of centrosomes) may cause fragmentation and dissociation of the pericentriolar material from centrioles at prometaphase, resulting in multiple spindle poles (Oshimori et al., 2006).

In conclusion, structural or numerical centrosome abnormalities can arise through different mechanisms. In general, centrosome amplification can occur as a result of either failure of cytokinesis or deregulation of the centriole duplication cycle (Nigg, 2006b). Centrosome amplification could increase the frequency of multipolar mitosis and consequent chromosomal instability and finally aneuploidy, which will be discussed in the next section.

1.7 Centrosomes and cancer

Almost one hundred years ago, Theodor Boveri described centrosomal abnormalities in tumour cells. Since then, supernumerary centrosomes have been reported in almost all types of solid and hematological malignancies (Pihan et al., 1998; Lingle et al., 1998; Gustafson et al., 2000; Sato et al., 2000; Kuo et al., 2000; Piel et al., 2001; Kramer et al., 2003; Rajagopalan and Lengauer, 2004). Centrosomes in human tumour cells can display significant alterations compared to centrosomes in normal tissue. These alterations include supernumerary centrioles, excess PCM, unincorporated microtubule complexes, centrioles of unusual length, inappropriate phosphorylation of centrosomal proteins, and increased numbers of MTOCs nucleating unusually large arrays of microtubules (Lingle and Salisbury, 2001; Lingle et al., 2002).

Extra centrosomes may lead to the formation of multiple spindle poles during mitosis which may induce unequal distribution of chromosomes and the production of aneuploid daughter cells. Cells with amplified centrosomes have evolved at least three different mechanisms to minimize the possible harmful effects of centrosome amplification: 1) Cells can cluster centrosomes into two groups to allow division to occur in a bipolar fashion; 2) Extra centrosomes can be inactivated, thereby they can no

longer nucleate microtubules and contribute to spindle formation; 3) The mitotic checkpoint becomes activated in the presence of unstable or incorrect microtubule attachments that are formed in multipolar mitotic spindles and delays anaphase onset (reviewed by Holland and Cleveland, 2009).

Despite the recent advances in centrosome biology, there is still a debate over whether or not centrosome amplification is a cause of chromosomal instability and cancer development. A direct link between chromosomal instability and centrosome amplification came from recent studies carried out in fly and human cells (Basto et al., 2008; Ganem et al., 2009; Silkworth et al., 2009). In flies it has been demonstrated that experimental transplantation of larval brain cells containing extra centrosomes can initiate aggressive tumours in wild-type host flies. This study provided evidence that centrosome amplification can initiate tumourigenesis in fly cells (Basto et al., 2008). Live cell imaging studies in human cells have shown that human cells with extra centrosomes rarely undergo multipolar cell divisions, and that these daughter cells are typically inviable. However, it has also been observed that cells with extra centrosomes can undergo bipolar cell divisions, although these cells exhibit significantly elevated levels of lagging chromosomes during anaphase (Ganem et al., 2009; Silkworth et al., 2009). In the same studies, the mechanism behind this mitotic defect was explored and it has been found that extra centrosomes can promote chromosome missegregation during bipolar cell division. By promoting merotelic attachments where one kinetochore is attached to both mitotic spindle poles, extra centrosomes can alter spindle geometry. In addition, centrosome clustering may also cause syntelic attachments (both sister kinetochores attached to the same pole), which in turn can promote merotelic attachments. If the level of merotelic attachments exceeds the capacity of the spindle checkpoint machinery to efficiently repair them prior to anaphase onset, merotelic attachments are not resolved. Thus, this can result in lagging chromosomes at anaphase and eventually in the generation of aneuploid cells. The mechanism proposed in these studies could explain how extra centrosomes contribute to chromosomal instability in human cancer (Ganem et al., 2009; Silkworth et al., 2009).

1.8 Gene targeting

Gene targeting is a technique that allows the modification of endogenous genes in the genome using homologous recombination with a transgene (reviewed by Hudson

et al., 2002). It is a powerful tool used for studying gene function by the inactivation or modification of specific genes, for creating models for genetic diseases, for gene therapy and also for biotechnological improvement of crop plants. Gene targeting can be used both for generation of a knockout or a knock-in organism/cell. A knockout is achieved by inserting a construct with a null mutation in the targeted allelle, thereby eliminating the functional gene. In a knock-in organism, a mutation is introduced into the targeting sequence, thereby changing its function. The efficiency of gene targeting in a cell relies both on the design of the sequence homology between the donor DNA (exogenous transforming DNA molecule) and the target DNA (chromosomal DNA) and also on the DNA-repair system used by the target cell. Efficient gene targeting has been demonstrated in yeast, fungi and some cell lines, such as mouse embryonic stem cells (ES), chicken DT40 cells, and human Nalm-6 pre-B cells (Vasquez et al., 2001; Capecchi, 2005; Winding and Berchtold, 2001; Adachi et al., 2006).

First described in 1987 by Thomas and Capecchi, gene targeting via homologous recombination has become a standard technique in ES cells to determine gene function (Thomas and Capecchi, 1987). In summary, the production of a mutant mouse strain by homologous recombination requires an ES cell line, which is capable of contributing to the germ line, and a targeting construct. ES cell lines are derived from the inner cell mass of a blastocyst-stage embryo. During gene targeting, ES cells must be maintained in their undifferentiated state. Following electroporation or microinjection of ES cells with a targeting construct, homologous recombination occurs in a small number of cells. This results in the introduction of a mutation present in the targeting construct into the target gene. Following identification of mutant ES cell clones, they are microinjected to the blastocoel cavity of a pre-implantation mouse embryo. The resulting blastocyst is then transferred into a mouse uterus producing a chimeric embryo. Breeding germ-line chimeras yields animals that are heterozygous for the mutation introduced into the ES cell, and that can be interbred to produce homozygous mutant mice (Capecchi, 1989).

1.8.1 Gene targeting techniques

Foreign DNA is integrated into the genome by either a process of non-homologous or homologous recombination. The efficiency of cellular homologous recombination and the low frequency of nonhomologous recombination are the main

parameters for successful gene targeting (Vasquez et al., 2001). There are many factors to consider when designing a targeting vector in vertebrate cells. First of all, detailed information about the gene of interest is required, such as the predicted function of the gene and the full sequence of the target gene locus to obtain restriction and exon-intron maps. Depending on the size of the gene of interest, a targeting vector can be designed to delete entire open reading frames, various functional domains or to introduce point mutations. A targeting vector should contain the desired mutation and homologous flanking sequences up to 10 kb. One or two selectable markers can be introduced into the targeting vector to allow identification of cells that have undergone successful homologous recombination (reviewed by Volarevic et al., 1999). The positive selectable marker is used to enrich cells that have the integrated targeting vector, either by homologous or non-homologous recombination. A positive selectable marker is typically a resistance cassette, such as neomycin, that is flanked by the DNA sequence of the gene to be targeted. A negative selectable marker is used to eliminate the cells that have integrated the targeting vector by non-homologous recombination (Mansour et al., 1988). Following the recovery after positive and negative selection, the proper integration of targeted sequences in cells is confirmed by polymerase chain reaction (PCR) or by genomic Southern blotting and selected cells are expanded (reviewed by Volarevic et al., 1999; Gossen and Bujard, 2002).

Homozygous knockout of an essential gene can result in cell death and embryonic lethality or severe disruption of development in animals (Misra and Duncan, 2002). To overcome these problems, conditional strategies have been developed. Conditional knockout strategies allow activation or inactivation of a gene of interest in cell/tissue-specific or time controlled manner. The bacterial Cre/LoxP and yeast-derived FLP/Frt site-specific DNA recombination systems are the most commonly used cell/tissue-specific conditional knockout strategies (Dymecki, 1996; Gu et al., 1993). Cre and Flp recombinases recognise 34 bp sequences, called loxP and frt sites, respectively. When two recombinase recognition sequences are located in the same DNA strand in the same orientation, a recombination event causes deletion of the sequence between them. If the recombinase recognition sequences are located in the opposite orientation, a recombination event inverts the intervening sequence. For conditional gene deletion, two recombinase recognition sites should be introduced within intronic sequence such that they are floxing an essential part of the gene without

affecting its transcription, processing or function. The targeting construct is then integrated into cells by homologous recombination. In mice, this approach involves generation and breeding of two independent lines of mouse: a mouse carrying the floxed gene of interest and a mouse expressing *Cre* under a cell type specific promoter. In the DT40 cell line, the Cre/loxP system is also widely used, which facilitates the use of different vectors with the same drug resistance gene repeatedly for the selection of stable transfectants (Arakawa et al., 2001).

The major disadvantage of this system is the lack of control on the onset of recombinase expression, thus deletion of the gene can occur at all times. However development of a Cre/loxP recombinase system under the control of inducible promoters allows the deletion of the target gene at defined timepoints. There are several inducible systems that can be used in combination to Cre/loxP recombinase system: adenoviruses expressing Cre (Rohlmann et al., 1996; Akagi et al., 1997), tetracycline controlled *Cre* gene expression (Utomo et al., 1999) and interferon-inducible expression (Kuhn and Schwenk, 2003).

1.8.2 The DT40 model system

DT40 cells are derived from chicken B-lymphocytes immortalised by transformation with RAV-1, an avian leukosis virus (ALV) (Baba et al., 1985). The DT40 chicken B cell line is a widely used model system for gene targeting due to its ability to promote extraordinarily high rates of homologous chromosomal integration upon introduction of a targeting vector (Buerstedde and Takeda, 1991). Since many aspects of cellular function are conserved between DT40 and mammals, over the last two decades DT40 cells have been used in genetic studies of a wide range of cellular processes such as immunoglobulin diversification, the DNA damage response, DNA repair, chromosome segregation, RNA metabolism, and signalling (Winding and Berchtold, 2001).

Similar to ES cells, in DT40 cells site-specific homologous recombination occurs upon introduction of a targeting construct which carries genomic regions of the gene of interest interrupted by a selectable marker. Transfer of the targeting vector into DT40 cells by electroporation and selection of resistance cells under appropriate conditions results in a high percentage of stable clones, which will have one copy of the

gene of interest inactivated by homologous recombination. A second round of targeting with a different selectable marker yields high ratios of double knockout stable clones. The frequency of recombination in DT40 cells is even higher than in ES cells (Dhar et al., 2001) and efficient sequential inactivation of all alleles of any given gene is possible (Gossen and Bujard, 2002).

As is typical of lymphocytes, DT40 cells are small, approximately 10μm in diameter and have a high nucleus to cytoplasm ratio. DT40 cells have 80 chromosomes, which includes 11 macrochromosomes, 67 minichromosomes, and the ZW sex chromosomes. In addition, most chromosomes are disomic, except chromosome 2 and one of the minichromosomes, which are trisomic (Sonoda et al., 1998). The doubling time of DT40 cells is 8-10 hours under optimal conditions, thereby making them ideal tools for the process of gene targeting. A homozygous "knock-out" can be generated within one to three months. The high rates of recombination observed in DT40 cells is thought be linked to a mechanism by which chicken cells diversify their primary antibody repertoire. In chicken B cells, diversification of IgV (immunoglobulin variable) genes is achieved through Ig gene conversion, which occurs by HR (McCormack et al., 1991). In the same way, continuous Ig gene conversion in DT40 cells makes integration of exogenous DNA possible at the targeted locus (Buerstedde and Takeda, 1991).

DT40 cells lack functional p53 and thus lack a functional G1-S arrest and instead arrest in G2 phase in response to DNA damage. This permits longer cell survival in the presence of genotoxic insults and allows p53-independent features to be investigated (Takao et al., 1999).

1.8.3 Alternative methods for gene ablation

Although gene targeting by homologous recombination has provided a powerful means to analyse gene function, due to its low efficiency in some models, alternative methods can be applied to ablate gene activity. The molecules that mediate RNA interference (RNAi), are commonly-used tools to achieve targeted gene silencing in cells (Couzin, 2002). RNAi is a natural process through which expression of a targeted gene can be knocked down with high specificity and selectivity. RNAi utilises a double

stranded RNA (dsRNA) in which one strand is complementary to a segment of the gene's mRNA to disrupt a gene`s function (reviewed by Shan, 2010).

Upon introduction of dsRNAs into the cell, they are processed by an enzyme of the Dicer family into small interfering RNAs (siRNAs). In mammals, dsRNA molecules longer than 30 bp result in an interferon response, an antiviral defense mechanism, which causes the global shutdown of protein synthesis. RNAi can also be started by introducing siRNA molecules directly into cells. Once inside the cell, siRNA is assembled into an RNA-induced silencing complex (RISC). In mammals and fruitflies, the antisense strand is incorporated into RISC and guides the RISCs to complementary RNA molecules. Next, they cleave and destroy the cognate RNA, thereby suppressing gene expression (reviewed by Meister and Tuschl, 2004; Shan, 2010). Since siRNA is depleted at each cell division, DNA based vector systems have been developed to maintain stable suppression of gene expression (Paddison and Hannon, 2002). These vectors express short hairpin-like RNA (shRNA) transcripts with a dinucleotide 3' overhang that can act as siRNA molecules, using RNA polymerase III based promoters (e.g. U6 and HI RNA). Although gene knockdown techniques (either transiently by siRNA or stably by shRNA) may not result in complete ablation of the gene product of interest, as well as carrying the possibility of off-target effects, these techniques have some important advantages in the production of animal models and *in vitro* cell lines. These include studying the function of essential genes to a high degree of efficiency, specificity, and cost-effectiveness.

Aims of this study

Maintenance of proper centrosome number and duplication are critical factors for genetic stability. Following genotoxic stress, centrosome amplification can arise through mechanisms that deregulate centrosome duplication. The mechanism of how centrosome amplification arises after DNA damage is not clear. In the first part of this thesis, we analyzed the nature of the signal that leads to centrosome amplification following IR treatment and in the second part of the thesis, we explored various aspects of Cep135 function in centrosome integrity, centrosome duplication and also centrosome amplification following genotoxic stress.

In the first project, we tested if IR-induced centrosome amplification is allowed through a diffusible stimulatory signal or by the loss of a duplication-inhibiting signal. To further analyze the mechanism of this signal, we checked whether centriole disengagement acts as a control mechanism in DNA damage-induced centriole duplication. For this purpose, we studied the key molecules, Plk1 and Separase, in the control of centriole disengagement as a licensing signal after DNA damage.

Cep135 is a core centrosome protein that is believed to play an important role in organizing centrosome structure and function. Here, we aimed to dissect the role of Cep135 and further understand its involvement and requirement in centrosome duplication, centriole biogenesis, mitosis and microtubule nucleation. We generated a *Cep135*$^{-/-}$ chicken DT40 cell line and assessed centrosome structure in these cells using immunofluorescence and transmission electron microscopy. Finally, we examined changes in centrosomes of *Cep135* deficient cells in response to various genotoxic agents such as IR and hydroxyurea.

Chapter 2 Materials and Methods

2.1 Materials

2.1.1 Chemical Reagents

Chemicals used throughout this study were of analytical grade and were purchased from Sigma-Aldrich (St. Louis, MO), BDH (Hertfordshire, UK), Fisher (Leicestershire, UK) or Amersham Biosciences (Piscataway, NJ). Sigma-Aldrich, BDH or Fisher also supplied organic solvents, alcohols and acids. All solutions were prepared using Milli-Q purified water (Millipore, Billerica, MA). Buffers and reagents are listed in alphabetical order in Table 2.1.

Table 2.1 Common reagents and buffers

Name	Composition	Notes and references
Blocking solution	1X PBS, 0.05% Tween-20, 5% skimmed milk	To reduce antibody non-specific binding in immunoblotting
CLAP	1000 x stock solution of Chymostatin, Leupeptin, Antipain, Pepstatin A	Protease Inhibitors- To inhibit protease enzymes in sample preparation, each 1 mg/ml in DMSO
Incubation buffer 1	1X PBS, 0.05% Tween-20, 1% skimmed milk	To dilute antibodies in immunoblotting
Incubation buffer 2	1X PBS, 1% BSA	To dilute antibodies and wash cells in flow cytometry
LB Broth	1% tryptone, 0.5% yeast extract, 1% NaCl, pH adjusted to 7.0 with 4 M NaOH	To grow bacterial cultures
Lysis buffer	250 mM Tris, pH 7.6, 0.1% Triton-X-100	To lyse cells for protein analysis by SDS-PAGE
PBS (Phosphate buffered saline)	2.68 mM KCl, 1.47 mM KH_2PO_4, 136.9 mM NaCl, 8.1 mM Na_2HPO_4	10X stock solution was made up by dissolving tablets in distilled water. Solutions were autoclaved. Working dilution 1X.
Phosphatase inhibitors (50X)	2.5 mM NaF, 1.8 mM b-glycerophosphate, 0.5 mM Na_3VO_4, 2.5 mM EGTA, 12.5 mM sodium pyrophosphate	To inhibit phosphatase enzymes in immunoblotting for phosphorylation
PMSF	Protease Inhibitor, 250mM in ethanol	1000 x stock solution
Ponceau S. solution	0.5% Ponceau S, 5% acetic acid	To stain proteins on the nitrocellulose membrane
'Tail' buffer	50mM Tris pH 8.8, 100mM EDTA, 100mM NaCl, 1% SDS	For the preparation of genomic DNA
(Semi-dry) Transfer buffer	1X Tris-Glycine (TG), 20% Methanol, 0.037% SDS	For the semi-dry transfer of SDS-polyacrylamide gels onto nitrocellulose membranes
(Wet) Transfer buffer	72 mM Tris, 58.5 mM glycine, 15% methanol, 0.1% SDS	For the wet transfer of SDS-PAGE onto nitrocellulose membranes
Sodium cacodylate buffer	0.2 M, pH-7.2	Buffering agent for preparation and fixation of cells for transmission electron microscopy

2.1.2 Molecular biology reagents and equipment

All molecular biology reagents, such as as restriction enzymes and DNA ligase, were obtained from New England Biolabs (Ipswich, MA). The DNA polymerases TaKaRa LA Taq, KOD and SigmaTaq used in PCR were supplied by Takara Shizo Co, Ltd. (Osaka, Japan), Novagen (Darmstadt, Germany) and Sigma (Arklow, Ireland), respectively. Shrimp Alkaline Phosphatase (SAP) was from USB (Cleveland, OH). DNA and protein size markers were purchased from Fermentas (Glen Burnie, MD) or BioRad (Hercules, CA). Molecular biology kits used throughout this study are presented in Table 2.2.

Table 2.2 Molecular biology kits used

Name	Use	References
GenEluteTM Plasmid Miniprep Kit	Small scale plasmid DNA extraction	Sigma (Arklow, Ireland)
Midi/Maxi Prep Kit (Endotoxin-free)	Large scale plasmid DNA extraction	Qiagen (Crawley, UK)
QIAquick Gel Extraction Kit	Extraction and purification of DNA Fragments from the agarose gel	Qiagen (Crawley, UK)
Superscript First-Strand Synthesis for RT-PCR kit	cDNA synthesis	Invitrogen (Carlsbad, USA)
5'RACE System for Rapid Amplification of cDNA Ends (version 2.0)	Amplification of 5'cDNA ends	Roche (Mannheim, Germany)

Transformation of plasmid DNA during this study was performed into competent *Escherichia coli* Top10 cells, which have the following genotype: F^- *mcrA*Δ*(mrr-hsdRNS-mcrBC) ϕ80lacZ*Δ*M15* Δ*lacX74deoR recA1 araD139* Δ*(ara-leu)7697 galU galK rpsL(Str^R) endA1 nupG.* The cloning and expression plasmids used during the course of this project are shown in Table 2.3.

Table 2.3 Plasmids used in this study

Plasmid name	Use	Sources
pGEMT-Easy	General cloning	Promega (Southampton, UK)
pBlueScript(SK)		Stratagene (La Jolla, CA)
pEGFP-C1/N1	Expression in mammalian cells	Clontech (Palo Alto, CA)
pcDNA3.1(+)		Invitrogen (Carlsbad, CA)
pCMV-3TAG-2A/B/C	Mammalian expression vector carring 3 myc tags	Stratagene
pCS2-myc-securin	Myc tagged wild-type securin expression vector	Michael Brandeis (Zou et al., 1999)
pCS2-myc-securin-KAA-DM	Myc tagged nondegradable KAA-DM securin expression vector	Michael Brandeis (Zur and Brandeis, 2001)
pmRFP-N1-H2B	RFP tagged H2B expression vector	Helen Dodson (Bourke et al., 2007)
pPlk4-GFP-C1	GFP tagged chicken Plk4 expression vector	Loretta Breslin

2.1.3 Antibodies

The antibodies used throughout this study were applied in immunofluorescence microscopy (IF), immunoblotting (IB) detection and flow cytometry analyses (FACS). Tables 2.4 and 2.5 present the list of the antibodies used along with sources of each antibody, host species, clone serial number and the working dilutions for IB, IF and FACS.

Table 2.4 Antibodies used in this study

Reactivity	Clone/ Reference number	Host species	Working dilution for IF	Working dilution for IB	Working dilution for FACS	Source
Actin	A2066	Rabbit polyclonal		1:5000		Sigma-Aldrich (Arklow, Ireland)
α-tubulin	B512	Mouse monoclonal	1:2000	1:5000		Sigma-Aldrich
Aurora-A	35C1	Mouse polyclonal		1:1000 1:500*		Abcam (Cambridge, UK)
BrdU	B44/347580	Mouse monoclonal	1:100		1:50	BD Biosciences
BubR1	R895	Rabbit polyclonal	1:1000			Helen Dodson
C-Nap1	42	Mouse monoclonal	1:250	1:500		BD Transduction Laboratories (Franklin Lakes, NJ)
Cenp-F		Sheep polyclonal	1:800			Stephen Taylor (Hussein and Taylor, 2002)
Cdk2	sc163 g(M2)	Goat Polyclonal		1:1000		Santa Cruz (Santa Cruz, CA)
Centrin-2	poly6288	Rabbit polyclonal	1:250			BioLegend (San Diego, CA)
Centrin-2	sc-27793R (N17R)	Rabbit polyclonal	1:500	1:1000		Santa Cruz
Centrin-3	3E6	Mouse monoclonal	1:1000			Abnova (Taipei, Taiwan)
Centrobin	70448	Mouse polyclonal	1:500			Abcam
CEP76		Rabbit polyclonal	1:500 1:200*			Brian Dynlacht (Tsang et al., 2009)
CEP170		Rabbit polyclonal	1:1000	1:1000		Giulia Guarguaglini (Guarguaglini et al., 2005)
CEP135		Mouse polyclonal	1:2000			Ryoko Kuriyama (Ohta et al., 2002)
CEP135		Rabbit polyclonal	1:1000	1:2000		Ryoko Kuriyama (Ohta et al., 2002)
CHK1	DCS310	Mouse monoclonal		1:1000		Sigma-Aldrich
CP110	sc-136629	Rabbit polyclonal		1:500		Santa Cruz
γ-H2AX	JBW301	Mouse monoclonal	1:1000			Millipore (Carrigtwohill, Ireland)
γ-tubulin	GTU88	Mouse	1:500			Sigma-Aldrich

		monoclonal	1:200*			
γ-tubulin	T3559	Rabbit polyclonal	1:1000	1:2000		Sigma-Aldrich
γ-tubulin	sc-7396	Goat polyclonal	1:1000 1:200*	1:2000		Santa Cruz
Glutamylated tubulin	GT335	Mouse monoclonal	1:500			Carsten Janke (Wolff et al., 1992)
Kizuna		Rabbit polyclonal	1:500	1:1000		Naoki Oshimori (Oshimori et al., 2006)
Myc	9E10	Mouse monoclonal	1:1000	1:1000		Hybridoma cell line (ATCC)
NEDD1		Rabbit polyclonal	1:500			Andreas Merdes (Haren et al., 2006)
NEK2	20	Mouse monoclonal	1:250	1:250		BD Transduction Laboratories
Ninein	Ab4447	Rabbit polyclonal	1:100			Abcam
PCM-1		Rabbit polyclonal	1:5000			Andreas Merdes (Dammermann and Merdes, 2002)
Phospho Cdk2-T160	ab47330	Rabbit polyclonal		1:500		Abcam
Phospho-H3	06-570	Rabbit polyclonal			1:33	Upstate
Sas-6	BO1P	Mouse monoclonal	1:50			Abnova
Scc1		Rabbit polyclonal		1:500		Ciaran Morrison
Separase	ab16170	Mouse monoclonal		1:500		Abcam

(*) Dilution used for DT40 cells.

Table 2.5 Secondary antibodies

Antibody	Working dilution for IF	Working dilution for IB	Source
Texas Red and FITC (fluorescein isothiocyanate) conjugated Affini Pure F(ab')2 fragment, goat anti-mouse and anti-rabbit IgG (H+L) secondary antibodies (IF)	1:250		Jackson Labs (Bar Harbor, ME)
Alexa 594, Alexa 488 conjugated goat anti-rabbit IgG, donkey anti-rabbit IgG, goat anti-mouse IgG, and donkey anti-mouse IgG secondary antibodies (IF)	1:1000		Invitrogen
HRP (horseradish peroxide) conjugated Affini Pure goat anti-mouse and anti-rabbit IgG (H+L) secondary antibodies for ECL		1:10000	Amersham, Jackson Labs

2.1.4 Cell Culture

The work presented in chapter 3 was mainly performed on the human transformed cell line U2OS. Human-chicken fusion experiments were performed using chicken DU249 and human U2OS cells. The work presented in chapter 4 and 5 was performed on the chicken DT40 cell line. A brief description of each cell line used is listed in Table 2.6.

Table 2.6 Cell lines used in this study

Cell Type	Description	Source
Wild-type DT40	Chicken, B-cell lymphoma	Ciaran Morrison
Cep135$^{-/-}$ DT40	Chicken, *Cep135* mutant B-cell lymphoma	Fanni Gergely (University of Cambridge, UK)
DU249	Chicken hepatoma cells	W. C. Earnshaw (Wellcome Trust Centre for Cell Biology, Edinburgh, UK)
U2OS	Human, osteosarcoma cell line	ATCC (Middlesex, UK)
U2OS:: pGFP-NEDD1	Human, osteosarcoma cell line expressing GFP-NEDD1	Helen Dodson (NUI Galway)
U2OS:: pGFP-CENTRIN2	Human, osteosarcoma cell line expressing GFP-CENTRIN2	Helen Dodson (NUI Galway)

Transient transfections of chicken DT40 cells were carried out using a nucleofector (programme B-23), (Amaxa, Gaithersburg, MD). For the generation of stable chicken cell lines, a Gene Pulser apparatus from Bio-Rad (Hercules, CA) was used. Different drugs at varying concentrations were used as selection markers in the generation of stable chicken cell lines, as listed in Table 2.7.

Table 2.7 Drugs used for stable cell line selection

Name of the drug	Final Concentration
Blasticidin (Sigma)	25 μg/ml
G418-Geneticin (Invitrogen)	2 mg/ml
Histidinol (Sigma)	1 mg/ml

For transient transfection of U2OS cells, Lipofectamine 2000 (Invitrogen, Carlsbad, CA) and Oligofectamine (Invitrogen) were used for DNA and siRNA, respectively. Cells were frozen down for both -80^{o}C and liquid nitrogen storage in FBS with 10% DMSO. For the pharmacological treatments of chicken and human cells, the drugs listed in Table 2.8 were used.

Table 2.8 Drugs used in this study

Drug	Concentration	Application	Source
Hydroxyurea	4 mM	Reversible activation of S-phase checkpoint	Sigma-Aldrich
Nocodazole	100 µg/ml	Reversible activation of spindle assembly checkpoint (metaphase arrest)	Sigma-Aldrich
BI 2536	100 nM	Inhibition of Polo-like kinase 1(Plk1) (mitotic arrest)	JS Research Chemicals Trading (Schleswig Holstein, Germany)

2.1.4.1 Cell culture reagents and equipment

The sterile plasticware used for tissue culture was obtained from Sarstedt (Numbrecht, Germany), Corning (Riverfront Plaza, NY) and Sigma-Aldrich. DT40 and DU249 cells were cultured in Roswell Park Memorial Institute Media (RPMI) 1640 media (Lonza, Cologne, Germany) supplemented with 10% fetal calf serum (Lonza), 1% chicken serum (Sigma-Aldrich), and 1% penicillin/streptomycin (Sigma-Aldrich) at 39.5°C with 5% CO_2 (Takata et al., 1998). U2OS cells were cultured in DMEM (Lonza) supplemented with 10% FCS and 1% penicillin/streptomycin (Sigma-Aldrich) at 37°C in 5% CO_2. A variety of reagents used in cell culturing, such as trypsin, HEPES and Dimethyl sulfoxide (DMSO) were purchased from Sigma-Aldrich.

2.1.5 Computer software

Bioinformatic analyses were performed using ScanProSite (www.expasy.org/tools/scanprosite), BlastN, BlastP, BlastX (http://www.ncbi.nlm.nih.gov/BLAST), ClustalW (www.ebi.ac.uk/clustalw) and, dbEST (http://www.ncbi.nlm.nih.gov/dbEST/). DNA plasmid maps were created using pDRAW32 software (Acaclone, www.acaclone.com). Sequenced DNA samples were analysed using Chromas software (version 2.31, Digital River GmbH, Shannon, Ireland). Microscopy imaging was performed using an Olympus BX-51 microscope driven by OpenLab software version 5 (Improvision, Emeryville, USA). Deconvolved images were saved as Adobe Photoshop files (version 7; San Jose, USA). All live cell microscopy was carried out on a Deltavision microscope, controlled by SoftWorx software (Applied Precision, Issaquah, WA). Analysis of flow cytometry samples was carried out using CELLQuest version 3.3 (Becton Dickinson, Oxford, UK) or BD FACS Diva Software (version 6.1.2, Beckton Dickinson). Statistical analysis of microscopy data was performed by Prism 5 (GraphPad, La Jolla, CA).

2.2 Methods

2.2.1 Nucleic Acid Methods

2.2.1.1 RNA preparation

Approximately 2 x 10^6 suspension cells were harvested and resuspended in 1 ml of TRIzol (Total RNA Isolation Reagent; Invitrogen), according to the manufacturer's instructions. The RNA pellet was re-suspended in 20 µl of 0.1% DEPC treated water and incubated at 50^{o}C for 10 minutes for good re-suspension. The RNA yield was quantified using a spectrophotometer (A_{260}/A_{280}) and the RNA stored at –80 $^\circ$C.

2.2.1.2 Reverse Transcriptase-PCR

RNA extracted from cells, as described in section 2.2.1.1, was used in the generation of cDNA through reverse transcription. The Superscript II RT-PCR kit (Invitrogen) was used according to the manufacturer's instructions. The cDNA generated was then used as a PCR template as described below in section 2.2.1.4.

2.2.1.3 5' Rapid Amplification of cDNA Ends (5'RACE)

5' Rapid Amplification of cDNA Ends was carried out using a 5'RACE kit from Roche according to the manufacturer's instructions. The first step in 5'RACE was synthesis of first-strand cDNA using a gene specific primer - GSP1 and its purification. The next step was addition of homopolymeric A-tail using dATP and Terminal transferase, followed by preparation of a target cDNA for subsequent amplification by PCR using a nested, gene specific primer- GSP2 and an oligo-dT-anchor primer. For further characterization of 5'RACE products, an additional round of PCR using a progressively nested, gene specific primer- GSP3 and a PCR- anchor primer was performed. Oligo dT-anchor and PCR-anchor primers were provided with the 5'RACE System, whereas gene specific primers GSP1, GSP2 and GSP3 were designed by the user (see Appendix 2).

2.2.1.4 Polymerase Chain Reaction (PCR)

TaKaRa LA Taq polymerase or KOD enzyme was used for cloning purposes, while KOD enzyme was used for diagnostic PCR. PCR experiments were carried out on a T Gradient or T3 Thermocycler (Biometra, Göttingen, Germany). Table 2.9 gives an example of the PCR conditions used, including concentration of particular reagents (primers, dNTP's and enzyme) and programmes.

Table 2. 9 Example of typical PCR reaction conditions

		TaKaRa LA Taq Polymerase	KOD Polymerase
Reagent concentrations	**Buffer (10x)**	1X	1X
PCR steps	**Primers**	0.2 µM	0.2 µM
	dNTP's	200 µM	200 µM
	Mg^{2+}	2.5 mM	2 mM
	Enzyme	0.5 µl (5 U/µl)	0.5 µl (5 U/µl)
	'Hot start'	95°C - 2min	94°C - 2min
	Denaturation	95°C - 30sec	94°C - 30min
	Annealing	58-68°C - 2min	58-68°C- 2min
	Extension	72°C - 3min	72°C - 3min
	Final extension	72°C - 10min	72°C - 10min
No. of cycles		30	30

2.2.1.5 Plasmid DNA preparation

Mini and midi plasmid DNA preparations were carried out using HiYield Plasmid Mini kit from RBC Bioscience or GeneElute™ Plasmid MiniPrep Kit (Sigma) and Qiagen Midi Prep kit or Qiagen Endotoxin free MidiPrep kit, respectively. In both procedures, plasmid DNA was prepared according to the manufacturer's instructions. Bacterial cultures were grown overnight at 37°C on a shaking platform, in the presence of selective antibiotics. For minipreps, DNA was isolated from 2 ml of *E. coli* culture, and resuspended in 100 µl of deionised water. For midi prep, DNA was isolated from 50 ml of *E. coli* culture and resuspended in 160 µl of deionised water.

2.2.1.6 Restriction digestion of DNA

All restriction enzymes used for the digestion of plasmid DNA were purchased from New England Biolabs. The endonucleases were used with the 10x buffer provided and bovine serum albumin (BSA, 0.1 mg/ml) where required. Digestions were performed at the optimum temperature for 2-16 hours depending on the amount and type of DNA being digested. Where appropriate, the enzymes were heat inactivated at 65°C for 15 min.

2.2.1.7 Preparation of DNA for cloning

The general cloning methods used in this thesis were based on the molecular biology techniques described in Molecular Cloning (Sambrook and Russell, 2001). Digested plasmid DNA used for cloning was purified using SigmaSpin™ Sequencing Reaction Clean-Up columns (Sigma) to remove restriction endonuclease(s) and buffer. In order to reduce self-ligation, digested plasmid DNA was dephosphorylated on the 5' ends with shrimp alkaline phosphatese (SAP, 1U / pmol of DNA ends). The reaction was carried out in shrimp alkaline phosphatase buffer at 37°C for 1 hour and the SAP was heat inactivated prior to ligation by incubation at 65°C for 20 minutes. Prior to ligation, dephosphorylated plasmid and gel-extracted insert DNA (see section 2.2.1.9) were analysed by agarose gel electrophoresis. Once vectors and inserts were ready, ligations were performed using T4 DNA ligase in the 1X T4 ligase buffer overnight at 4°C or at room temperature for 3 hours prior to transformation into competent *E. coli* cells. Depending on the DNA concentration estimated by agarose gel electrophoresis, a vector:insert ratio of 1:3 to 1:6 was used. The reaction was incubated at room temperature for 3 hours or, at 4°C overnight.

2.2.1.8 Preparation of competent E. coli and transformation

E. coli cells were grown in LB broth (see Table 2.1) at 37°C to a A_{600nm} of 0.5 and then transferred to ice for 5 minutes. Cells were pelleted by centrifugation at 5000 *g* for 15 minutes and re-suspended in TfbI (40 ml per 100 ml culture, see Table 2.1). After that cells were pelleted, re-suspended in TfbII (4 ml per initial 100 ml culture, see Table 2.1) and incubated on ice for 15 minutes. Resuspension of bacterial cells in those solutions with high concentration of calcium creates small holes in the bacterial membranes (Sarkar et al., 2002). Those small holes in the bacterial membranes make cells competent to take up exogenous DNA. In order to make highly efficient competent cells, the final aliquoting was carried out in the cold room. The aliquoted cells were immediately transferred for storage at -80°C.

For transformations, 50 µl of competent *E. coli* cells were thawed on ice. After the addition of ligation mixture, the mixture was incubated on ice for 30 minutes. The mixture was then heat shocked at 42°C for 60 seconds and chilled on ice for 2 minutes. 1 ml of LB broth was then added and the cells incubated for 1 hour at 37°C with gentle shaking. The cells were then pelleted by centrifugation at 16000 *g* for 1 minute. The supernatant was removed and cells were resuspended in 100 µl of LB broth. This

solution was then spread on agar plates containing the appropriate antibiotic selection and incubated overnight at 37°C. The following morning single colonies were picked and incubated overnight for mini prep analysis.

2.2.1.9 Agarose gel electrophoresis and purification of DNA

Generally, 0.8% agarose gels were prepared using Sigma electrophoresis grade agarose in 1 x TAE buffer containing 0.5 μg/ml ethidium bromide. Gels were run in 1 x TAE buffer in Hoefer HE33 tanks (Mini Horizontal Submarine Unit, Amersham) until the required separation was achieved. DNA on the gel was analysed using a Multi Image Light Cabinet (ChemiImager 5500, Alpha Innotech, Medical Supply Company, Dublin, Ireland) and images were taken with a digital camera. When required, DNA bands were excised from gels under UV light with the help of a scalpel blade and purified using Qiaquik Gel Extraction kit (Qiagen) according to the manufacturer's protocol. The DNA was then eluted from the column with 20 μl of MilliQ water.

2.2.1.10 DNA sequencing

DNA samples were sent to Cogenics (Takeley, UK) or Agowa GmbH (Berlin, Germany) for commercial sequencing. In general, 250 ng of DNA and 5-10 pM primers were used per reaction. Analysed sequences were used to construct correct vector maps with the pDRAW32 (Acaclone, www.acaclone.com) software.

2.2.1.11 Preparation of genomic DNA from tissue culture cells

Genomic DNA was prepared from chicken DT40 cells in order to screen clones for potential targeting events by PCR (Sonoda et al., 1998). Colonies were picked from 96 well plates into 3 ml of medium and grown for 3-4 days. When cells became confluent, 1.5 ml was taken for freezing down and 1.5 ml for DNA preparation. Cells were harvested by centrifugation at 160 *g* for five minutes. The supernatant was removed and each pellet was resuspended in 500 μl Tail Buffer (see Table 2.1) containing 0.5 mg/ml proteinase K. This was incubated at 55°C for three hours, shaking for five minutes each hour in an Eppendorf shaker at maximum speed, or overnight at 37°C. Following this incubation, each sample was shaken vigorously for five minutes, 200 μl of 6M (saturated) NaCl was added and the sample vigorously shaken again for five minutes. Samples were then centrifuged at 16000 *g* for 10 minutes, and the supernatant was transferred to a new Eppendorf tube. 700 μl of isopropanol was added to the tube and mixed by slowly inverting. This mixture was centrifuged for ten minutes

at 16100 *g* at 4°C to pellet the DNA. The DNA pellet was washed with 300 µl 70% EtOH and spun down for five minutes at 16000 *g*. The pellet was then air dried, re-suspended in 70-100 µl of dH_20 and incubated at 37°C for 30 minutes for re-suspension. When the pellet had been resuspended, 2 µl was used for a PCR from genomic DNA.

2.2.2 Protein Methods

2.2.2.1 SDS – Polyacrylamide Gel Electrophoresis (SDS - PAGE)

The following equipment was used for running SDS-PAGE: mini gels (10x10 cm) – Hoefer mini VE (Amersham), wide gels (10x20 cm) – Vertical Maxi 2 Gel Device, Medical Supply Co. Ltd. (Dublin, Ireland). Gels were generally run at 200 V for 60 to 90 minutes in running buffer (see Table 2.1). Different SDS-Polyacrylamide gels were used in this study depending on the size of the proteins that were analyzed. 30% acrylamide: bisacrylamide (19:1 and 37.5:1) stock was purchased from Severn Biotech Ltd (Worcestershire, UK). Table 2.10 shows the final concentrations of components used to prepare 8% and 10% polyacrylamide gels.

Table 2.10 Example of 8% and 10% lower and upper gel mix

	8% gel	**10% gel**
Running Gel	375mM Tris pH 8.8	375 mM Tris pH 8.8
	8% acrylamide/bis (37.5:1)	10% acrylamide/bis (37.5:1)
	0.1% SDS	0.1% SDS
	-	1 mM EDTA*
	0.1% APS	0.1% APS*
	0.6% TEMED	0.4% TEMED*
Stacking Gel	78mM Tris pH 6.8	78mM Tris pH 6.8
	5% acrylamide/bis (37.5:1)	5% acrylamide/bis (37.5:1)
	0.1% SDS	0.1% SDS
	-	-
	0.05% APS	0.05% APS

(*) - See 'Abbreviations' for the fullname.

Protein samples for western blot analysis were prepared as follows: Cells were centrifuged at 160 *g* for 5 minutes, washed in 1X PBS and pelleted again. The cells were then lysed in Lysis Buffer (plus protease and phosphatase inhibitors), (see Table 2.1) for 20 min on ice and then centrifuged at 14000 *g* for 5 min at 4°C to pellet DNA and cell membranes. The supernatant, containing soluble proteins, was transferred to a new tube and the protein yield was measured by the Bradford dye binding assay (Bradford, 1976). The Bradford assay, a colorimetric protein assay, is based on an absorbance shift of the dye Coomassie Brilliant Blue G-250 from red to blue upon binding to proteins in a concentration-dependent manner. A standard curve was constructed by measuring the absorbance of bovine serum albumin standards of known concentration. 1 µl of supernatant was mixed with 0.5 ml dH_2O and with 0.5 ml of Bradford solution in a plastic cuvette and the absorbance at 595 nm was measured by spectrophotometry. Protein concentrations were then calculated using the BSA standard curve. In general, 30-40 µg of total proteins were loaded onto gels. Prior to electrophoresis or storage at -20°C, samples were boiled at 95°C for 5 minutes in 3x sample buffer containing β-mercaptoethanol (see Table 2.1) to completely denature proteins and facilitate their separation.

2.2.2.2 Western Blotting

For immunoblotting, proteins were transferred from the gel to a nitrocellulose membrane (GE Healthcare, Bucks, UK). Small proteins, up to 100 kDa, were transferred by a semidry transfer system for 90 min at constant amperage in semidry transfer buffer (see Table 2.1), using a Hoefer TE 22 Mighty Small Transfer apparatus (GE Healthcare). The amperage was dictated by the size of the membrane following the formula mA= 0.8 x membrane area (cm^2). Proteins larger than 100 kDa were transferred by a wet transfer system for 3 h at 350 in wet transfer buffer (see Table 2.1) at 4°C in cold room using a Hoefer TE 77 Semi Dry Transfer Unit (GE Healthcare).

Following transfer, membranes were then rinsed 3 times in dH_2O and proteins on the membrane were stained with Ponceau S solution (see Table 2.1) for 5 minutes, to assess transfer efficiency. To decrease non-specific antibody binding, the membrane was blocked by incubation with a 5% milk solution in 1X PBS-0.05% Tween-20 at room temperature with gentle agitation for 30 minutes. The blocked membrane was then incubated overnight in the primary antibody solution at 4°C. Optimal conditions for each western blot varied depending on the antibody used (Table 4). The next day, the

membrane was washed 3 times for 5 minutes in 1X PBS-0.05% Tween-20 and transferred to the secondary antibody solution (see Table 2.5) in 1% milk for 45 minutes at room temperature. After 3 x 5 minute washes in 1X PBS-0.05% Tween-20, the specific proteins on the membrane were detected with ECL detection kit (GE Healthcare or Milipore) and exposure to autoradiography film (Hartenstein, Wurzburg, Germany). The exposed film was then fixed and developed by passing it through a developing machine (CP 1000, AGFA, Brentford, UK).

2.2.3 Cell Biology Methods

2.2.3.1 Tissue culture techniques

The cells used in this study were cultured as described in section 2.1.4. Adherent cells reached confluency at a cell density of $7x10^6$ cells/75 cm^2 flask (80% confluency). When approaching confluency, cells were washed once in 1X PBS and trypsinized for 3 min at 37°C. Once the cells detached, prewarmed (37°C) medium was added to inhibit the trypsin. Cells were then diluted 1:10 ($6x10^5$ cells/flask) with prewarmed medium and replaced in the incubator. For freezing cell stocks, $2x10^6$ cells/vial were harvested and resuspended in 1 ml of freezing media (90% FBS, 10% DMSO) and transferred to cryo-vials. Vials were stored at -80°C for a week and then transferred to liquid nitrogen for long-term storage.

DT40 cells reached confluency at a cell density of $1x10^6$ cells/ml. Cells were counted using a haemocytometer as described in the manufacturer's protocol. Cultures were maintained at cell densities between $1x10^5$ cells/ml and $8x10^5$ cells/ml. For freezing cell stocks, $1x10^7$ cells were harvested by centrifugation at 1000 *g* for 5 minutes, resuspended in 500µl freezing media (10% DMSO in FBS) and transferred to cryo-vials. Vials were stored at -80°C for a week and then transferred to liquid nitrogen for long-term storage. To defrost frozen stocks, a frozen vial was thawed at room temperature, gently pipetted into 10 ml prewarmed media, and placed in the incubator.

Cells were irradiated using a ^{137}Cs irradiator (Mainance Engineering Ltd, Waterlooville, UK) at a dose rate of 1294 Gy/hour. Cells were exposed to various doses and analysed at various timepoints after irradiation, according to experimental requirements.

2.2.3.2 Transient transfections

DT40 cells were transiently transfected by endotoxin-free circular plasmids using the Amaxa nucleofection system (cell line nucleofection kit T (VCA-1002)). $5x10^6$cells were resuspended in Solution-T containing 5 µg of DNA and this mixture was transferred to an Amaxa transfection cuvette. Nucleofection was performed using Amaxa program B-23. 16 hours post transfection, cells were harvested and analysed either by immunofluorescence microscopy or SDS-PAGE and immunoblotting.

The day before transfection, U2OS cells were split and plated in 6 well plates or 60mm dishes containing antibiotic-free DMEM at an appropriate density to yield 40-50% confluent cells the next day. On the day of transfection, 2 µg of plasmid DNA were mixed with 100 µl serum-free Optimem, and 4 µl Lipofectamine 2000 mixed with 100µl serum-free Optimem. These mixtures were incubated separately for 5 minutes at room temperature. Next, the two solutions were mixed together and incubated for 20 more minutes to allow the formation of the lipofectamine-DNA complexes. The lipid-DNA mixture was added dropwise to the cells and the cells replaced in the 37°C incubator. Transiently transfected cells were then analysed at 24h, 48h and 72h post-transfection.

2.2.3.3 Stable transfections and gene targeting

Stably expressing DT40 cell lines were generated by electroporation of a linearised DNA construct using the Gene Pulser electroporation apparatus (Bio-Rad) (Sonoda et al., 1998; Takata et al., 1998; Morrison et al., 2000). $1x10^7$cells were pelleted at 160 *g* for 5 minutes. The cell pellet was then washed in 1X PBS, pelleted again and resuspended in 0.5 ml of 1X PBS. After addition of 25 µg of linearised DNA, the cell mixture was transferred to an electroporation cuvette (BioRad, 0.4 cm gap) and incubated on ice for 10 minutes. For targeted integration of DNA into DT40 genome, electroporation was carried out at 300 V/600 µF, while for random integration of DNA into the genome, the electroporation conditions were 550 V/25 µF. Following electroporation, the cell mixture was again incubated on ice for 10 minutes, and then pipetted into 20 ml of prewarmed media. After 16 to 18 hours, 20 ml of fresh media was added to the transfected cells. Selective antibiotics at the appropriate concentrations (Table 2.7) were added to the cultures and cells were pipetted into 4 x 96 well plates (100µl per well). Plates were incubated at 39.5°C until colonies were visible. Each single colony was then transferred to a well in a 24 well plate containing 3 ml of

medium and incubated at 39.5°C until confluent. 1.5 ml of this culture was then frozen at -80°C for temporary storage. The remaining 1.5 ml was used to analyze the clone by PCR or by immunofluorescence and western blot.

2.2.3.4 RNA Mediated Interference

ON-TARGET plus SMART pools of RNA duplexes (Dharmacon, Lafayette, CO) were used to knock down *ESPL1* (*Separase*) messenger RNA transcripts in U2OS cells (see Table 2.11). As a negative control, ON-TARGET plus non-targeting short interfering RNA pool was used. U2OS cells were seeded into 60 mm dishes the day before transfection such that they would be 20-30% confluent on the day of transfection. siRNAs were resuspended in 1X Dharmacon siRNA buffer to obtain the desired final stock concentration of 20 mM. The siRNA transfection protocol involved the preparation of two solutions. 25 nMol of siRNA (2.5 ml) were mixed with 355 ml serum-free OptiMEM and 12 µl Oligofectamine were mixed with 28 µl OptiMEM. These solutions were initially incubated separately for 5 minutes at room temperature, before mixing. Mixed solutions were incubated for 20 minutes at room temperature. Before addition of siRNA-Oligofectamine mixture, cells were washed 3 times with 1X PBS and, 1.5 ml of serum-free OptiMEM added to the dishes. After 4h, FBS in normal DMEM medium was added to 30% final concentration to restore normal levels of serum and other nutrients. 24 hours post-transfection, the medium was replaced. 24-96 hours after the transfection, the cells were analyzed by Western Blotting and immunofluorescence microscopy. Where indicated, cells were irradiated 48h after transfection with inhibitory RNAs for *ESPL1* and non-targeting siRNA.

Table 2.11 ON-TARGETplus SMART pool RNA duplex sequences

Gene	Target sequences (5`-3`)
ESPL1	CCGAGGAUCACUUGAAAUA GGAGAAGGCUCACAGUUAC GAUCGUUUCCUAUACAGUA GGAACGAAUUCUCUUUGUC

2.2.3.5 Synchronization of U2OS cells

U2OS cells were synchronized in G1 phase by a thymidine/mimosine double block procedure (Leinwand, 1997), and an enriched G2 population was obtained by releasing G1 cells into fresh growth medium for a defined time. U2OS cells were grown to 60% confluence and treated with 2 mM thymidine (Sigma) for 12 hours. Cells were then washed three times with warmed 1X PBS and released into fresh growth medium

for 10 h. A second block was induced with 0.4 mM mimosine (Sigma) treatment for 14 hours to arrest cells at the G1/S boundary. Cells were then washed three times with warmed 1X PBS and released into fresh medium for 11 h to obtain a cell population enriched in G2 phase cells. At various time points after release, the cells were harvested and the cell cycle profiles were analyzed by flow cytometry and immunofluorescence microscopy.

2.2.3.6 Cell staining and cell fusion

Wild-type U2OS cells were stained with the fluorochrome probe CellTracker™ Blue 7-amino-4-chloromethylcoumarin (CMAC; Invitrogen) before fusion. CellTracker™ Blue passes through cell membranes and once inside the cell it is transformed into a cell-impermeant fluorescent dye–thioether adduct (Gillis et al., 1994). The CellTracker Blue/ CMAC is not transferred to adjacent cells in a population. CellTracker Blue/ CMAC was prepared as a 10 mM stock solution in dimethyl sulfoxide. Cells were incubated at 37°C for 15 min in serum-free DMEM containing 3 µM of this dye. After washing with warmed 1X PBS, cells were resuspended in growth media and incubated for 30 min at 37°C. Where indicated, cells were irradiated just before fusion treatment.

For cell fusions, 1 x 10^6 wild-type U2OS cells stained with CellTracker Blue/ CMAC and GFP-NEDD1–expressing U2OS cells were trypsinized and washed with 10 ml of warmed growth media. The cells were then resuspended and incubated in 600 µl of 50 µM SDS in 1X PBS for 3 min at 37°C, as previously described (Wong and Stearns, 2003). Cells were then centrifuged and 0.5 ml of PEG-1450 solution Hybri-Max (Sigma) and 50 µl of serum-free DMEM mixture was added dropwise to the cells with gentle tapping for 2 min, after which 5 ml of serum-free DMEM medium was added to the mixture for 5 min at 37°C with continuous stirring. 5 ml of serum-free DMEM medium was then added, and the cell mixture was incubated at 37°C for 5 min before centrifugation. The cells were then washed twice with 10 ml serum-free media before being resuspended in growth media and seeded onto coverslips.

U2OS and DU249 cells were fused as described above without SDS-1X PBS incubation step using PEG-1500 (Roche, West Sussex, United Kingdom). U2OS-DU249 fusions were incubated in DMEM plus 10% FBS at 37°C in 5% CO_2.

2.2.4 Microscopy Methods

2.2.4.1 Immunofluorescence microscopy

Human and chicken cells were fixed and stained for immunofluorescence microscopy using a range of various antibodies (see Table 2.4). The appropriate fixation method was chosen depending on the nature of the antibody used. Below is a summary of the fixation and staining protocols involved. Images were taken using an Olympus BX51 microscope, 40x, 60x or 100x objective lenses, numerical aperture (NA) 1.35, using Openlab software (Improvision). Serial Z-sections (0.15 μm) were collected and the images then deconvolved, merged and saved as Abode Photoshop TIFF files. All cell/centrosome countings were performed blind.

To quantify the intensities of PCM1, all cells were treated identically during immunostaining and image acquisition. The images were analyzed using Image-Pro Plus 6.0 *(*Media Cybernetics Inc., MD). The minimum pixel value displayed was increased, until only the centrosome was labeled, so that only the centrosome spot was defined. The same setting was applied to all images. Next, the total pixel value of the marked region was measured in PCM1 channel. Total centrosome intensity was divided by the intensity of γ-tubulin measured in the same cell for normalization of the values.

2.2.4.2 Methanol fixation

Adherent human cells were seeded and cultured on glass coverslips in 3 or 6 cm dishes. After removing the medium, the cells were washed once with 1X PBS prior to fixation. DT40 cells were spun down at 160 *g* for 5 minutes, re-suspended in 1X PBS and adhered to poly-L-lysine slides (Menzer Glasser, Fisher Dublin Ireland) by gravity for 15 minutes at room temperature. The PBS was aspirated before fixation. For visualization of mitotic spindles and centrosomal proteins, cells were fixed and permeabilized for 3-10 minutes in cold 95% methanol at -20°C containing 5 mM EGTA. Certain antibodies against centrosomal proteins such as Ninein, Sas-6 and Aurora-A needed an additional permeabilization step to be visualized in DT40 cells. DT40 cells were extracted in PBS/1% Triton X-100/0.5% NP-40 for 5 min after methanol fixation. The cells were then washed 3 times for 5 minutes in 1X PBS, blocked in 1X PBS containing 1% BSA for 30 minutes at room temperature or overnight at 4°C and incubated with antibodies as described below in section 2.3.5.4.

2.2.4.3 Paraformaldehyde fixation

Certain antibodies and GFP fusion proteins were more readily visualised after paraformaldehyde fixation. Following medium removal and PBS washes, cells were fixed in 4% paraformaldehyde (PFA) diluted in 1X PBS for 10 min at room temperature. Cells were then washed 3 times in 1X PBS and permeabilised in 0.15% Triton X-100 in PBS for 2 min. Again the cells were washed 3 times in 1X PBS and then blocked in 1% BSA in 1X PBS for 30 minutes at room temperature or overnight at 4°C prior to staining with antibodies.

2.2.4.4 Immunofluorescence staining

After removing the blocking solution, incubation with primary antibodies diluted in blocking buffer (see Table 2.4 for dilutions) was performed in a dark humid chamber at 37°C for 1 hour. The specimens were then washed 3 times in 1X PBS for 5 minutes and incubated with the appropriate fluorescently-conjugated secondary antibody for 45 minutes at 37°C in a dark humid chamber. Following 3 washes in 1X PBS, the DNA was stained with DAPI (1μg/ml) in mounting media: 200 mM DABCO, (Sigma, Wicklow, Ireland) or Vectashield (Vector Laboratories, Burlingame, CA).

2.2.4.5 Microtubule regrowth in DT40 cells

For microtubule depolymerisation, DT40 cultures were treated with 1 μg/ml nocodazole for 3 h. Cells were washed three times in ice-cold 1X PBS (supplemented with 0.1% volume of DMSO) by centrifuging at 1100 *g* for 2 minutes. Cells were then adhered to poly-L-lysine slides for 10 min at 4°C on ice. Slides were submerged in growth media at 40°C for 1 min before methanol fixation. Fixed cells were immunostained with centrin-2 and α-tubulin antibodies to assess microtubule growth.

2.2.4.6 Live cell microscopy

For live cell imaging, DT40 cells were allowed to attach to poly-D-lysine–coated dishes (MatTek, Ashland, MA) for 2–3 hours in media supplemented with 12.5 mM Hepes, pH 7.5. To ensure that biological and physiological processes were not influenced or altered, all live cell imaging was performed under strictly controlled conditions of temperature, CO_2 concentration and humidity. Timing and light exposure were kept minimal by using reduced excitation light. Images were taken every 3 minutes for 3 hours on an integrated microscope system (DeltaVision) using a PlanApo

N60× oil objective (NA 1.42) and a 39.5°C environmental chamber (WeatherStation; Precision Control). A quick projection was made with SoftWorx software.

2.2.4.7 Fluorescence Recovery After Photobleaching (FRAP)

For FRAP analysis, GFP-Nedd1- or Centrin2-GFP expressing U2OS cells were grown on glass-bottomed 35-mm dishes (MatTek, Ashland, MA) in phenol-red free DMEM with 10% fetal calf serum and 25 mM HEPES (Invitrogen). During the FRAP experiment the lid of the dish was sealed with parafilm and images were taken in a 37°C environmental chamber on an integrated microscope system (DeltaVision). A small spot region (2.44 μm^2) of interest centered on centrosomes was bleached with 50% laser power (488-nm argon laser). Three images were captured before bleaching with a 1 second interval. An image was taken every 10 seconds (488-nm argon laser at 4% power) after bleaching over a 360 second period. The average signal intensity relative to the pre-bleached image was analyzed from 10 live cells by measuring the net intensity of the bleached area minus background relative to that of the whole cells in each frame by using ImageJ software (National Institutes of Health). The centrosomal GFP recovery in the bleached area was plotted as a function of time and fitted to a single exponential curve using Prism 5 (GraphPad, La Jolla, CA).

2.2.4.8 Transmission Electron Microscopy

DT40 cells were prepared for transmission electron microscopy (TEM) as previously described (Liptrot and Gull, 1992). 10 ml of confluent DT40 cells were pelleted at 250 g for 5 minutes and washed twice in 0.1 M sodium cacodylate buffer, pH 7.2 (see Table 2.1). Cells were pelleted at 250 *g* for 5 minutes and fixed as a clump in a mixture of 2% glutaraldehyde and 2% PFA in 0.1 M cacodylate buffer for an hour at room temperature. Following removal of fixation solution, cells were incubated in 2% osmium tetroxide in 0.1 M sodium cacodylate buffer pH 7.2 at room temperature at least for an hour until osmium tetroxide solution turned the pellets to dark brown. Pellets were then dehydrated in a graded series of ethanol washes (30, 60, 90, and 100%) and propylene oxide washes. The process of embedding pellets in resin was as follows: pellets were incubated in 50:50- propylene oxide:resin (Agar Scientific, Essex, UK) solution overnight, in 25:75- propylene oxide:resin solution for an hour, in pure resin for an hour and in pure resin for a day. Finally, pure resin was replaced with fresh resin and the pellet transferred to a 60°C incubator for 2 days to improve the quality of the sections. Sections were cut on a microtome (Reichert-Jung Ultracut E; Leica,

Wetzlar, Germany), stained with uranyl acetate and lead citrate, and then viewed on an electron microscope (H-7000; Hitachi, Tokyo, Japan). Images were taken with a camera (ORCA-HRL; Hamamatsu Photonics, Hamamatsu City, Japan) and processed using AMT version 6 (AMT Imaging, Woburn, MA).

2.2.5 Flow cytometry analysis

For flow cytometry analysis of U2OS and DT40 cells, cells were fixed in 70% ice-cold ethanol in phosphate-buffered saline (PBS) and stored overnight at 4°C. For cell cycle analysis by DNA content, cells were washed in 1X PBS, resuspended in 0.5 ml of 40µg/ml propidium iodide and 0.1 mg/ml RNase-A solution in 1X PBS. After incubation at room temperature for 1 hour, flow cytometry analysis was performed.

To quantitate cells in S phase, 5-bromo-2`-deoxyuridine (BrdU (Sigma)) was added to the cells to a final concentration of 20µM and incubated for 15 min at 37°C. After fixation in 70% ice-cold ethanol, cells were washed in 1X PBS with 1% BSA and treated with 2 M HCl/0.5% Triton X-100 for 30 min at 37°C. Cells were washed again in 1X PBS with 1% BSA and then incubated with anti-BrdU (BD Biosciences) (see Table 2.4 for dilution) for 1 h with shaking at 37°C. After washing in 1% BSA in 1X PBS, the cells were incubated with FITC-conjugated anti-mouse and incubated with propidium iodide/RNase A solution as described above.

To determine the mitotic index of DT40 cells, phosphorylated histone H3 (PH3) staining was employed. Cells were fixed and washed as described above. Cells were then resuspended in 1 ml of 1X PBS containing 0.25% Triton-X 100 and kept on ice for 15 minutes. Cells were pelleted and incubated with anti- phosphorylated histone H3 in1X PBS with 1% BSA (see Table 2.4 for dilution) for two hours at room temperature. After washing cells in 1% BSA in 1X PBS, cells were incubated with FITC-conjugated anti-mouse for 30 minutes at 37°C in the dark and then incubated with propidium iodide/RNase A solution as described above. Cells were analysed using a FACS Calibur or FACS Canto (Becton Dickinson, San Jose, CA) and Cell Quest (version 3.3, Becton Dickinson) or BD FACS Diva Software (version 6.1.2, Becton Dickinson), respectively.

Chapter 3
Testing the Licencing Model for DNA Damage-Induced Centrosome Amplification

3.1 Introduction

Centrosome amplification can occur in response to DNA damage (Dodson et al., 2004; Sato et al., 2000). Prevention of centrosome amplification is crucial for cells, since amplification leads to formation of abnormal spindles which can direct the unequal segregation of chromosomes during mitosis (Ganem et al., 2009). For this reason, centrosome duplication occurs only once per cell cycle and is tightly regulated in coordination with DNA replication. Two key mechanisms have been identified in controlling centrosome duplication: 1) activation of cyclin-dependent kinase (Cdk)-2-cyclin E in late G1 (Matsumoto et al., 1999; Bettencourt-Dias and Glover, 2007; Nigg, 2007) and 2) resolution of the centrosome intrinsic block to reduplication, in other words, disengagement of centrioles in mitosis (Wong and Stearns, 2003). The evidence for a centrosome-intrinsic block to reduplication came from cell fusion experiments which showed that G2 centrosomes were unable to reduplicate in S phase cytoplasm that supports centrosome duplication (Wong and Stearns, 2003). Recent studies have demonstrated that this centrosome-intrinsic block to reduplication is resolved by removing the physical engagement between the mother and daughter centrioles by the activity of Separase and Plk1 at the metaphase to anaphase transition and this process is called ‘licensing’ (Tsou and Stearns, 2006b; Tsou et al., 2009).

In this study, we aimed to investigate if the IR-induced centrosome amplification process is regulated by factors intrinsic to the centrosome, as is the case in the normal centrosome cycle. Therefore, we investigated the nature of the signal that allows centrosome amplification after genotoxic stress. We explored two hypotheses for how DNA damage-induced centrosome amplification can occur: activation and licensing. According to the activation model, an activating signal stimulates centriole overduplication, whereas in the licensing model an inhibitory signal, that normally limits the duplication of the centrosome to once per cell cycle is lost after DNA damage (Tsou and Stearns, 2006a; Nigg, 2006a). To test these hypotheses we first examined whether a G2 damage signal is permissive for centrosome overduplication. Then, we

used cell fusion assays to test these models with synchronized populations of U2OS cells at defined stages of the cell cycle. We also studied the relationship between centriole disengagement and centrosome amplification after DNA damage. In addition, we investigated the roles of Plk1 and Separase in licensing DNA damage-induced centrosome amplification.

3.2 IR-induced centrosome amplification in synchronized populations of U2OS cells

In several types of transformed and tumour-derived cell lines, centrosome amplification occurs in response to DNA damage (Balczon et al., 1995; Sato et al., 2000; Dodson et al., 2004). Previous studies conducted by our group have suggested that DNA damage-induced centrosome amplification requires an extended G2 arrest (Dodson et al., 2004; Bourke et al., 2007). To define the timing of centrosome overduplication after IR treatment, further studies were performed in our lab by Dr. Helen Dodson using the human U2OS osteosarcoma cell line, which has a defective p16/Rb pathway. Immunofluorescence microscopy analysis of irradiated U2OS cells revealed that majority of the cells with amplified centrosomes were carrying a Cenp-F signal which is an indicator of G2 phase (Holt et al., 2005). In addition to this analysis, examination of U2OS cells expressing both GFP-Nedd1 and RFP-PCNA by live cell imaging revealed that IR-induced centrosome amplification occurred outside S phase (Inanc et al., 2010). Taken together, these findings supported a model where IR-induced centrosome amplification occurs in G2 phase. According to this model, we would expect that IR-induced DNA damage incurred in G2 phase would permit high levels of centrosome amplification. On the other hand, another possibility is that irradiation of G1/S cells should allow higher levels of centrosome amplification than G2 cells, since G1/S centrosomes are already licensed for normal duplication (Tsou and Stearns, 2006b), but G2 centrosomes are not.

To investigate these models, we examined IR-induced centrosome amplification in synchronized populations of U2OS cells. As explained in Section 2.2.3.5, a thymidine/mimosine double block procedure was used to synchronize the cells (Leinwand, 1997). Flow cytometry analysis of Promidium Iodide (PI) stained cells showed that a highly enriched G1/S phase population was obtained following the double thymidine/mimosine block. Releasing G1/S cells into fresh medium for a period

of 11 hours allowed us to obtain a highly enriched G2 population (Figure 3.1A). Further confirmation of the initial flow cytometry analysis by BrdU incorporation showed that 75-80% of cells in the G1 population had the expected DNA content and almost no BrdU incorporation and 70-72% of cells in the G2 population had the expected DNA content with high Propidium Iodide but low BrdU-staining intensity (Figure 3.1B). Immunofluorescence microscopy was also used to verify the cell cycle status of synchronized cells by staining with antibodies to BrdU and CenpF. As shown in Figure 3.1 C and D, immunofluorescence microscopy and flow cytometry analyses demonstrated very similar levels of cell synchrony, indicating that high and reproducible synchrony was obtained using this approach.

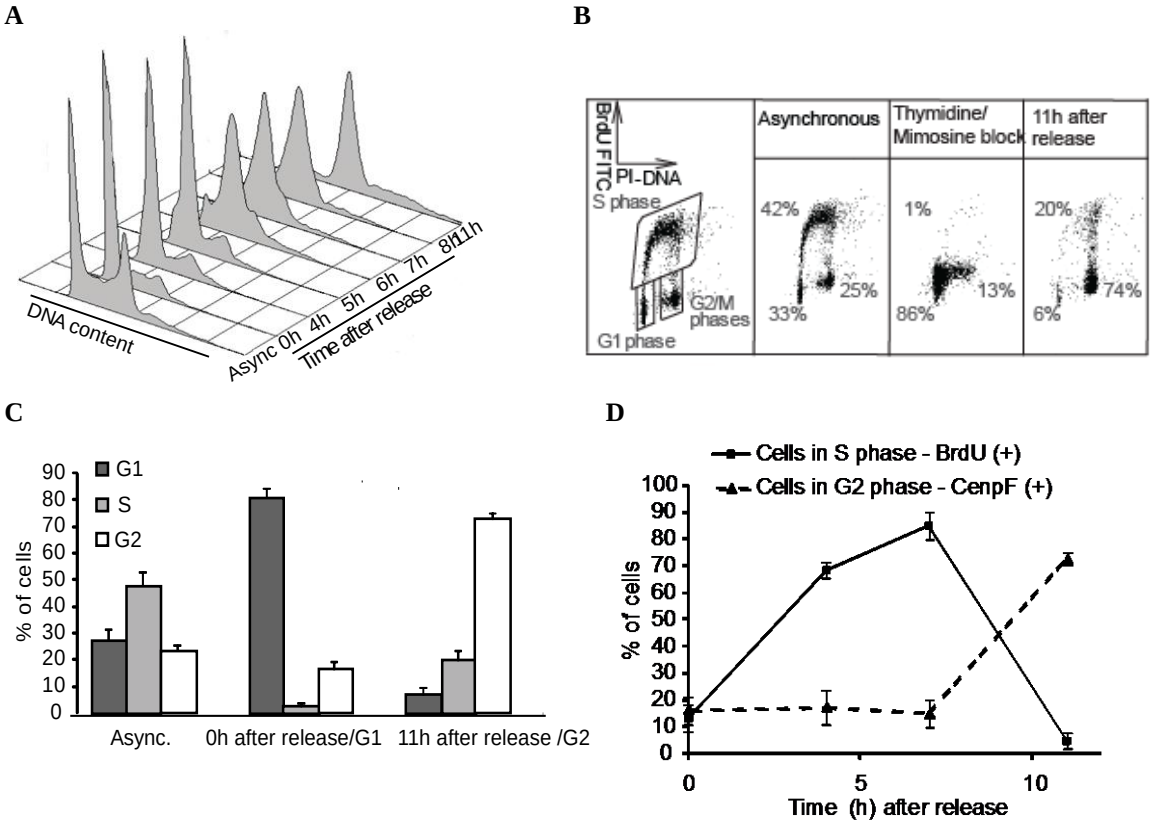

Figure 3.1 Cell cycle anaysis of U2OS cells by flow cytometry and microscopy following synchronization.

A. Cell cycle profile of cells stained with propidium iodide after synchronization and release from a thymidine/mimosine double block method. Async., asynchronous population.

B. Indicative cell cycle profile determination using flow cytometry to quantitate BrdU incorporation. Data shows a representative example of BrdU analysis after block and release. The percentage of cells in G1, S, and G2/M at each time point was calculated as shown.

C. Histogram showing population breakdown by cell cycle stage, based on the 2D flow cytometry analysis, in unsynchronized, G1-enriched and G2-enriched populations used for irradiation and fusion experiments. Data are expressed as the means ± SD of three independent experiments.

D. Microscopy analysis of cell cycle status of U2OS cells after thymidine/mimosine block and release. Cells in S phase were assayed by BrdU labeling, and cells in G2 phase were assayed by anti-CenpF antibody staining. Data show the mean ± SD of three separate experiments in which at least 100 cells were scored.

Having established that U2OS cells can be efficiently synchronized, we tested IR-induced centrosome amplification levels in asynchronous, highly enriched G1/S and G2 cell populations. Cells were treated with 5 Gy γ-irradiation and centrosome numbers were examined 24h, 48h and 72h following irradiation using γ-tubulin as a marker for immunofluorescence microscopy. As shown in Figure 3.2, we observed significantly higher levels of centrosome amplification after irradiation of G2-enriched cells compared with G1-enriched or asynchronous cells at 48h and 72h. This observation suggests that, although G2 phase centrosomes are not in a licenced state for a new round of duplication, DNA damage incurred in G2 phase allows centrosome amplification. This result, together with our previous findings, supports a model where IR-induced centrosome amplification occurs in G2 phase of the cell cycle (Dodson et al., 2004; (Bourke et al., 2007; Inanc et al., 2010). Consistent with our data, Loncarek et al. also found that U2OS and HeLa cells can reduplicate centrioles during RO3306-induced G2 arrest (Loncarek et al., 2010).

Irradiation in G1 phase also caused centrosome amplification, although as G1 centrosomes are already licensed for duplication, it is not clear whether DNA damage caused centrosome amplification directly or whether a prolonged G2 arrest after irradiation led to amplification.

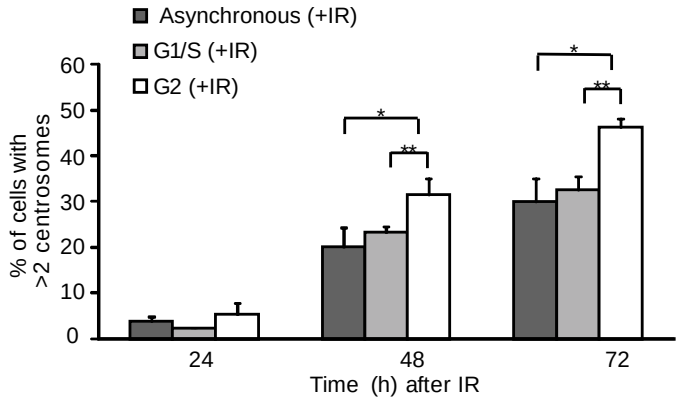

Figure 3.2 IR-induced centrosome amplification in synchronized populations of U2OS cells.
Graph showing the quantitation by γ-tubulin microscopy of centrosome amplification at the indicated times after 5 Gy IR treatment of differently synchronized populations. Data show the mean ± SD of three separate experiments in which at least 100 cells were scored. Statistical significances were calculated by Student's unpaired *t* test and are indicated on the histogram as *$p \leq 0.05$, **$p \leq 0.01$, and ***$p \leq 0.001$.

3.3 Fusion assay for IR irradiation of synchronised U2OS cells

Next, we investigated the nature of the signal that drives centrosome amplification in response to DNA damage. Fusion experiments have previously been used to demonstrate that the limitation on re-duplication of the centrosome in G2 phase is associated with the centrosome itself (Wong and Stearns, 2003). We explored two hypotheses for how DNA damage-induced centrosome amplification can occur: activation and licensing. According to the activation model, an activating signal that is transmissible in the cytoplasm stimulates centriole overduplication, whereas in the licensing model a centrosome specific inhibitory signal that normally limits the duplication of the centrosome to once per cell cycle is lost after DNA damage (Nigg, 2006a; Tsou and Stearns, 2006b).

To determine which model applies for IR-induced centrosome amplification, we used PEG-mediated cell fusion assays similar to previous work which demonstrated the intrinsic limitation to re-duplication in G2 centrosomes in an S phase cytoplasm that supports centrosome duplication (Wong and Stearns, 2003). To identify the fused cells, one population was marked with the cytoplasmic dye Cell Tracker Blue and the other population stably expressed GFP-Nedd1. Nedd1 is a centrosomal protein which functions in targeting the γ-TuRC to the centrosome and spindles (Haren et al., 2006; Luders et al., 2006) and it can be used as centrosome marker since it colocalizes with a range of centrosome markers including γ-tubulin (Inanc et al., 2010). The combination of these two coloured fluorophores allowed heterotypic fused cells to be distinguished from homotypic fused cells by microscopy (Figure 3.3).

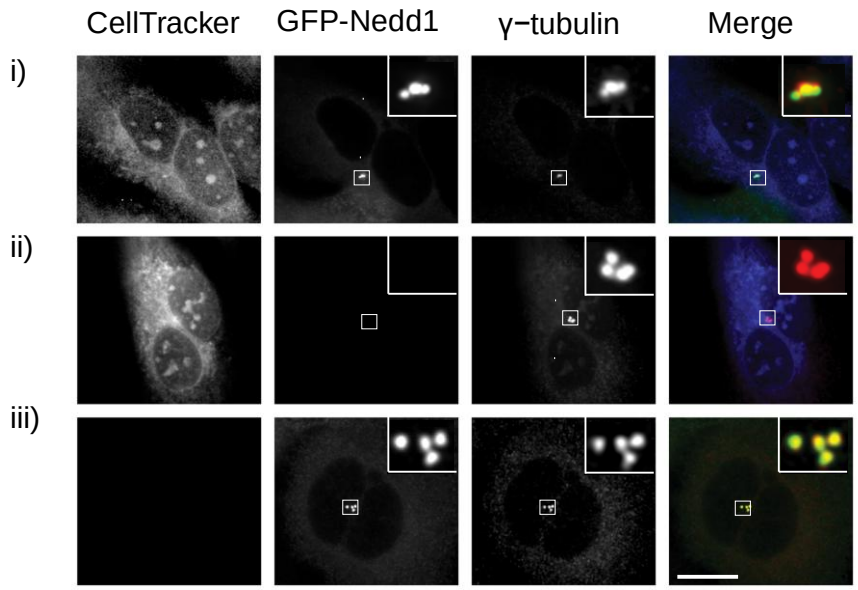

Figure 3.3 Fluorescence microscopy analysis of cell fusions.
Centrosome analysis in cell fusions. Wild-type U2OS cells were stained with CellTracker Blue and fused with GFP-Nedd1–expressing U2OS cells. Fused cells were fixed in methanol and stained for γ-tubulin (red). i) Heterotypic fused cells could be identified by blue and green cytoplasmic fluorescence, homotypic fusions showing ii) only blue or iii) only green fluorescence. The CellTracker Blue dye mixed in (the cytoplasm) fused cells but was not transferable between adjacent unfused cells. Staining with γ-tubulin antibodies revealed that GFP-Nedd1 incorporates into the centrosomes of the wild-type (nonexpressing) fusion partner.

It was important to establish that the GFP-Nedd1 expressing U2OS cells behaved in a manner similar to wild-type cells with regard to synchronization and IR-induced centrosome amplification. Therefore, we tested the level of synchronization of GFP-Nedd1 expressing cells in G2 phase after release from thymidine/mimosine block together with wild-type U2OS cells. Cell cycle analysis by BrdU/PI staining displayed the same level of synchronization in G2 phase in wild-type and GFP-Nedd1 U2OS cells (Figure 3.4A). In addition, GFP-Nedd1 expressing U2OS cells were irradiated with 5 Gy and the number of centrosomes was quantified. These cells showed centrosome amplification comparable to wild type U2OS following IR, and therefore we considered them to be a useful tool in the identification of fused cells (Figure 3.4B).

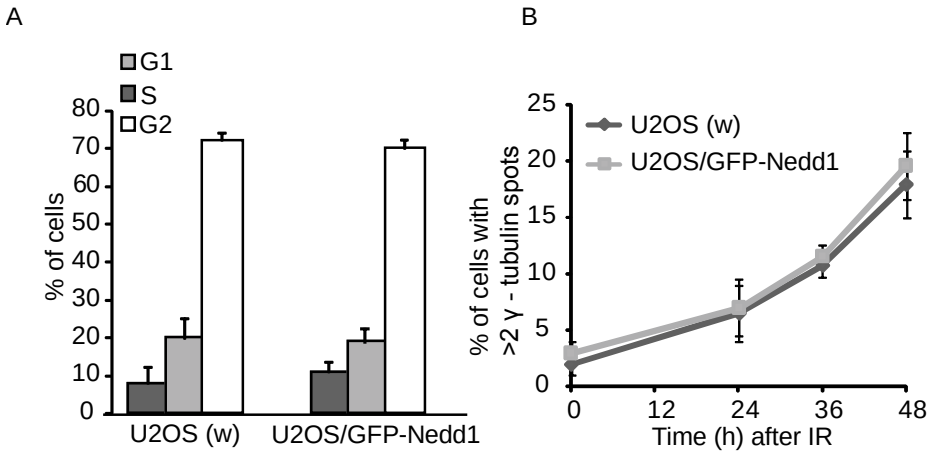

Figure 3.4 U2OS cells that express GFP-Nedd1 are a suitable model to analyse centrosome amplification.
A. G2 synchronization of GFP-NEDD1 cells. Histogram showing the cell cycle percentages of wild type and GFP-NEDD1-expressing U2OS cells, at the point after release from thymidine/mimosine block timed to yield G2-enriched populations, based on the 2D flow cytometry analysis. Data are expressed as the means ± SD of three independent experiments.
B. Centrosome amplification in wild type and GFP-Nedd1-expressing U2OS cells.
Graph showing centrosome amplification in wild type and GFP-Nedd1 expressing U2OS cells. Cells were exposed to 5 Gy IR and the number of centrosomes was quantified at the indicated times after IR. At least 200 cells were counted per timepoint and data are expressed as the means ± SD of three independent experiments.

To define the nature of the signal which causes IR-induced centrosome amplification, populations of wild-type U2OS cells stained with Cell Tracker Blue and GFP-Nedd1-expressing U2OS cells were enriched at defined cell cycle stages. Unirradiated wild-type cells were then fused with irradiated GFP-Nedd1-expressing U2OS cells. The number of centrosomes in unirradiated/ irradiated fused cells was then quantified and compared to unirradiated fusions (negative control) and fusions where both fusion partners were irradiated (positive control) following 24, 36 or 48 hours incubation. >4 centrosomes was considered centrosome amplification in fused cells. Figure 3.5A shows an example of a fusion between irradiated wild-type U2OS cells stained with Cell Tracker Blue and unirradiated GFP-Nedd1-expressing U2OS cells where centrosome amplification had occurred. As shown in Figure 3.5B, we found that in negative control experiments, less than 15% of fused, unirradiated cells had >4 centrosomes, indicating that the fusion process itself did not cause high levels of centrosome amplification. The level of centrosome amplification in unirradiated G2-irradiated G2 fusions was significantly higher than in unirradiated-G2 (negative control) fusions at 36 and 48 h post-IR and the level of centrosome amplification in unirradiated G2- irradiated G2 fusions was significantly lower than the irradiated-G2 (positive control) fusions at all time points post-IR (Figure 3.5B).

Similarly, analysis of centrosome numbers in irradiated G1/S-irradiated G1/S fusions showed significantly higher levels of centrosome amplification than did irradiated G1/S-unirradiated G1/S cell fusions at 48 h post-IR. The level of centrosome amplification (p=0.0625) was very close to significance (p=0.05) at 36 h post-IR (Figure 3.6C). These results allowed us to differentiate between the two models, as we had predicted that if there were a diffusible activating signal, then the same level of centrosome amplification would be seen if one or both of the fusion partners were irradiated. However, if the signal was a centrosome-intrinsic inhibitory one lost upon irradiation, then the prediction would be that only the centrosomes in the irradiated cell would be able to amplify. Therefore, these data suggested that a centrosome-autonomous inhibitory signal is lost upon irradiation, which allows only the irradiated centrosomes to duplicate, in other words licensing the centrosome for further duplication.

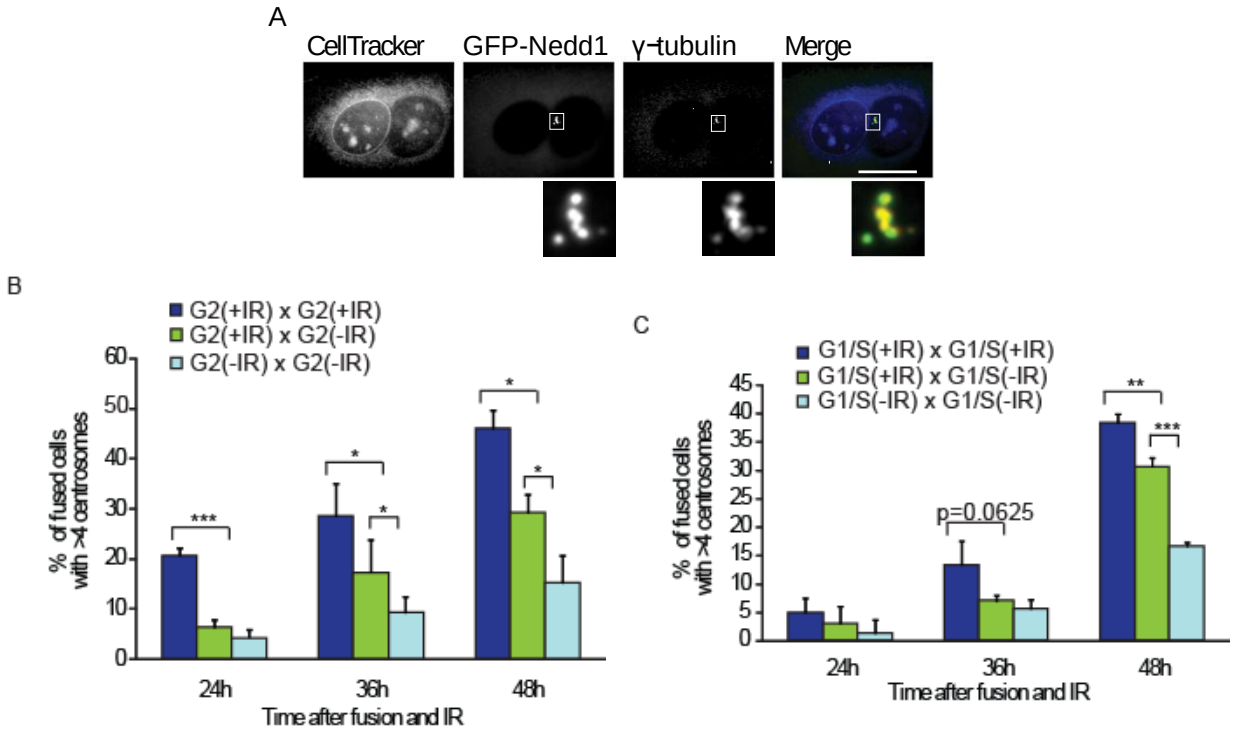

Figure 3.5 IR-induced centrosome amplification in fused cells.
A. Micrograph of centrosome amplification in fused cells. Fused binucleate cells 36h after treatment with 5 Gy irradiation, containing multiple centrosomes. GFP-Nedd1 (green) and anti γ-tubulin antibody staining (red) were used as markers of IR-induced centrosome amplification.
B. Histogram showing the percentage of fused, G2-enriched populations with more than four centrosomes at the indicated times after treatment, where indicated, with 5 Gy of IR. Data show the mean ± SD of three separate experiments in which at least 35 cells were scored. Statistical significances were calculated by Student's unpaired *t* test and are indicated on the histogram as *p ≤ 0.05, **p ≤ 0.01, and ***p ≤ 0.001.
C. Histogram showing the percentage of fused, G1/S-enriched populations with more than four centrosomes at the indicated times after treatment, where indicated, with 5 Gy of IR. Quantitation and statistical analysis were as described in B.

We also analyzed the transferability of the IR-induced DNA damage signal between the nuclei of irradiated-unirradiated cell fusions. DNA double-strand breaks (DSBs) are formed after IR exposure in cells and they can be detected by the appearance of γ-H2AX, a phosphorylated form of the histone H2A variant H2AX, at sites of DNA DSBs (Redon et al., 2002; Pilch et al., 2003; Sedelnikova et al., 2003). U2OS cells were untreated or irradiated with 5 Gy and then fused and stained with an antibody to γ-H2AX at 2h post-IR. As shown in Figure 3.6, more than 90% of the irradiated/ irradiated fused cells had 2 γ-H2AX positive nuclei and 80% of the irradiated/unirradiated fused cells have only 1 γ-H2AX positive nucleus, indicating that DNA damage signal was limited to the irradiated fusion partner.

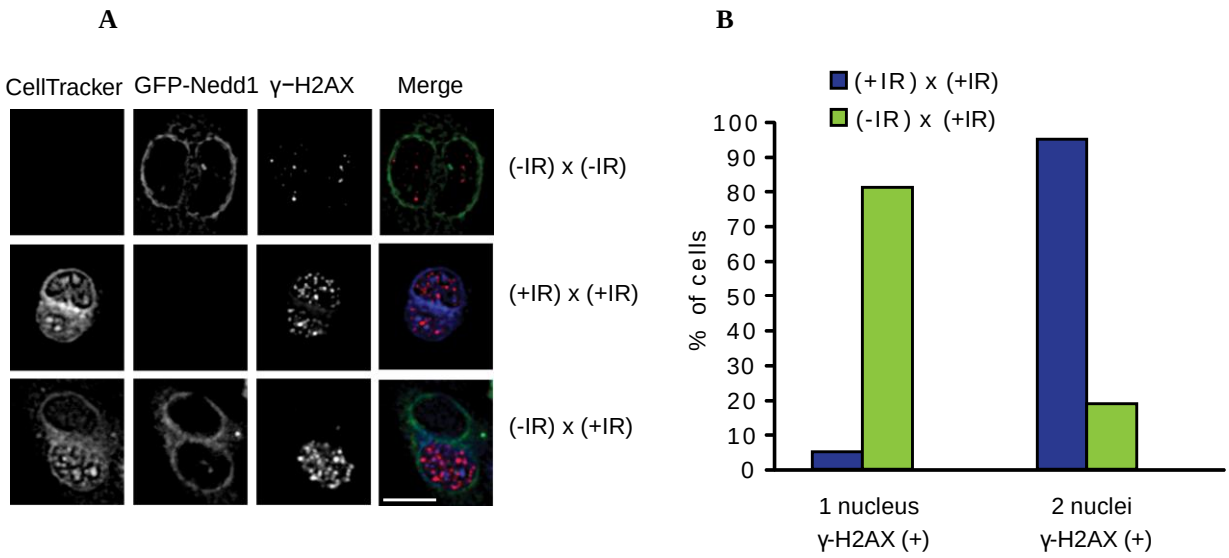

Figure 3.6 Limitation of DNA damage signal to the irradiated fusion partners.
A. Cells were untreated or irradiated with 5 Gy and then fused with the indicated partners. Fused cells were fixed in methanol and stained with antibodies to γ-H2AX (red).
B. Quantitation of γ-H2AX signal in nuclei of untreated and 5 Gy treated cells fused to irradiated partners. Representative example of experiment in which at least 100 cells were scored.

To confirm that centrosome amplification is centrosome-autonomous, in other words, that licensing occurs only at irradiated centrosomes, we needed to show which centrosome in the fused cell undergoes duplication. To identify the origin of the amplified centrosomes in fused cells we tried several different approaches. Our initial experimental design planned to use GFP-Nedd1 to follow the irradiated centrosome over time after fusion. We hoped that the source of the amplified centrosomes would be traceable. However, GFP-Nedd1 was detected in the centrosomes of both fusion partners (Figure 3.3). In the example shown in 3.3i, the heterotypic fusion was Cell Tracker Blue positive and GFP-Nedd1 positive, although the centrosomes of the fused

cell were all GFP-Nedd1 positive, indicating that the GFP-Nedd1 becomes incorporated into the centrosomes of non-expressing cells. These observations suggested that GFP-Nedd1 was highly mobile within cytoplasm of fused cells. We also tested Centrin1-GFP expressing U2OS cells for fusion experiments and similarly to GFP-Nedd1, Centrin1-GFP also become incorporated into the centrosomes of the wild-type fusion partner, indicating that tagging only the irradiated centrosome over time after fusion was not possible using this method. These findings were consistent with our preliminary fluorescence recovery after photobleaching (FRAP) analysis of GFP-Nedd1. This analysis showed the rapid recovery of the GFP-Nedd1 signal after bleaching, indicating the rapid recruitment of GFP-Nedd1 to the centrosome (Figure 3.7).

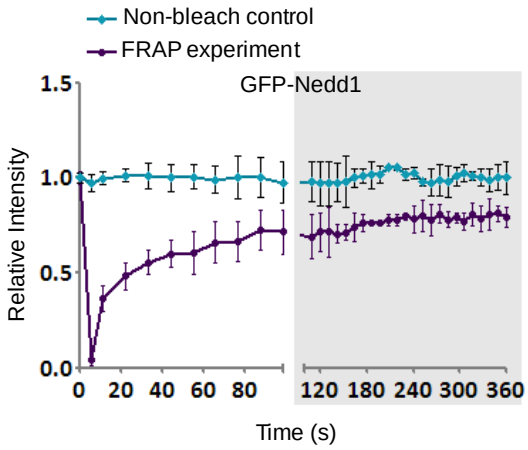

Figure 3.7 Fluorescence recovery after photobleaching (FRAP) analysis reveals rapid recruitment of GFP-Nedd1 to the centrosome. FRAP data were analyzed using ImageJ software, and the centrosomal GFP recovery within the bleached area was recorded as a measure of time, and fitted to a single exponential curve using Prism 5, each data point represents the average intensity from 35 cells.

We tested the possible changes in the localization of several centrosomal proteins such as Aurora-A, Kizuna, C-NAP1, Nek2 and Rootletin following IR treatment using immunofluorescence. However, we saw that these proteins were highly mobile between the centrosomes in fused cells after irradiation. It has been shown that proteins involved in the DNA damage response, such as Chk1, Chk2, p53, Cdc25, Cyclin B/Cdk1 and ATM, are localized to the centrosomes (Takada et al., 2003; Tsvetkov et al., 2003; Dutertre et al., 2004; Jackman et al., 2003; Oricchio et al., 2006; Kramer et al., 2004). For this reason, we tested possible changes in the centrosomal localization of total Chk1, total ATM and phospho ATM (S1981) following IR treatment. Unfortunately, we failed to find any alteration in the localization pattern or expression of these proteins that could allow us to distinguish between irradiated and unirradiated centrosomes (data not shown).

3.4 Chicken-human cell fusions demonstrate that only the irradiated centrosomes amplify

As an alternative strategy to monitor the origin of irradiated centrosomes, we took advantage of the fact that certain antibodies to centrosome components are specific for the human proteins and not for their chicken orthologues. Anti-centrobin was one such human-specific antibody in our hands. Centrobin is a core component of the centrosomes and asymmetrically localizes to daughter centrioles (Zou et al., 2005). Immunofluorescence microscopy analysis in human cells showed that centrobin staining exhibits one or two dots in interphase cells depending on the cell cycle stage, similar to γ-tubulin staining pattern (Zou et al., 2005). Therefore, we performed interspecies fusions between GFP-Nedd1-expressing U2OS cells and DU249 chicken hepatoma cells stained with Cell Tracker Blue. As shown in Figure 3.8, in the same field, all centrosomes in the nonfused U2OS cells and homokaryons were stained both with anti-γ-tubulin and anti-centrobin antibodies (Figure 3.8i, ii-1-5), whereas centrosomes of nonfused DU249 cells or homokaryons were only stained with anti-γ-tubulin but not with anti-centrobin antibodies (Figure 3.8i, ii-6-8). In DU249/U2OS heterokaryons, only 2 centrosomes were positive for centrobin staining out of 4 centrosomes stained with anti-γ-tubulin antibody (Figure 3.10A). This indicates that the centrobin from one species does not become incorporated into the centrosome from the other species in fused cells over the experimental period.

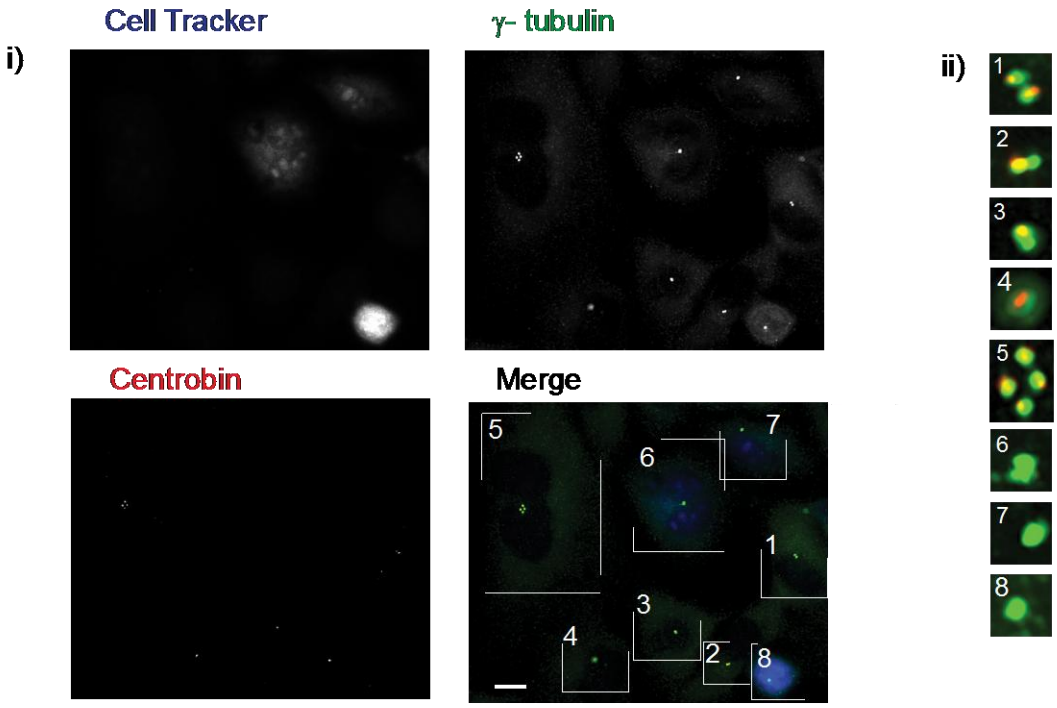

Figure 3.8 Centrosome analysis in U2OS and DU249 cell fusions. DU249 cells were stained with CellTracker Blue and fused with wild-type U2OS cells. Fused cells were fixed in methanol and stained for γ-tubulin (green) and centrobin (red). U2OS cells were recognized by both centrobin and γ-tubulin antibodies, whereas DU249 cells were only stained with γ-tubulin antibody. i) DU249 cells could be distinguished from U2OS cells by blue cytoplasmic fluorescence. U2OS cells could be distinguished from DU249 cells by coimmunostaining for centrosomes with antibodies to γ-tubulin and centrobin. ii) Blowups of the boxed insets in i showing (1–5) U2OS and (6–8) DU249 centrosomes. Note that images 5 and 6 are from homokaryotic DU249 and U2OS fusions, respectively. Scale bar, 10 μm.

Before proceeding with chicken-human fusion experiments to identify the origin of amplified centrosomes, we tested if DU249 cells amplified their centrosomes when irradiated in a manner similar to U2OS cells. Since the efficiency of chicken-human cell fusions was quite low (~1%), and the doubling time of chicken cells is around 8 hours, we analysed centrosome amplification at 24h post-5Gy IR treatment. As visualized by γ-tubulin staining, the level of centrosome amplification was 12% in DU249 cells and 8% in U2OS cells (Figure 3.9). This indicated that DU249 cells would be a suitable cell line in which to perform our experiment.

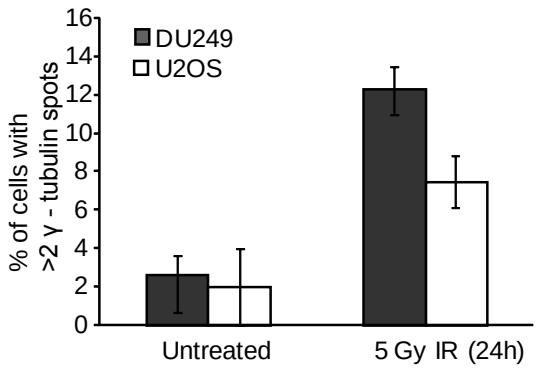

Figure 3.9 Centrosome amplification in wild type DU249 and U2OS cells. Graph showing centrosome amplification in wild type DU249 and U2OS cells. Cells were untreated or exposed to 5 Gy IR. Cells were fixed and stained with γ-tubulin and the number of centrosomes was quantified at 24h after IR. Data show the mean ± S.D. of three separate experiments in which at least 200 cells were scored.

Using the γ-tubulin:centrobin ratio in U2OS-DU249 fusions allowed us to analyse the centrosomes in each population. As shown in Figure 3.10, immunofluorescence microscopy analysis of U2OS-DU249 fusions, where one population was irradiated and the other not, revealed that only the irradiated population displayed centrosome amplification. In addition to this, when both populations were irradiated and fused, centrosome amplification was observed in both populations, indicating no inhibitory effect of the interspecies fusion on centrosome amplification. These results clearly showed that amplified centrosomes were derived from DNA-damaged cells, but not from non-damaged cells. Even though we cannot exclude the possibility that a putative diffusible signal from chicken cells may not induce centrosome amplification in human cells, and vice versa, we can conclude that the centrosome amplification was limited to the irradiated partner. Taken together, our findings suggest that permission for centrosome amplification is a centrosome-autonomous activity and not the consequence of a diffusible signal.

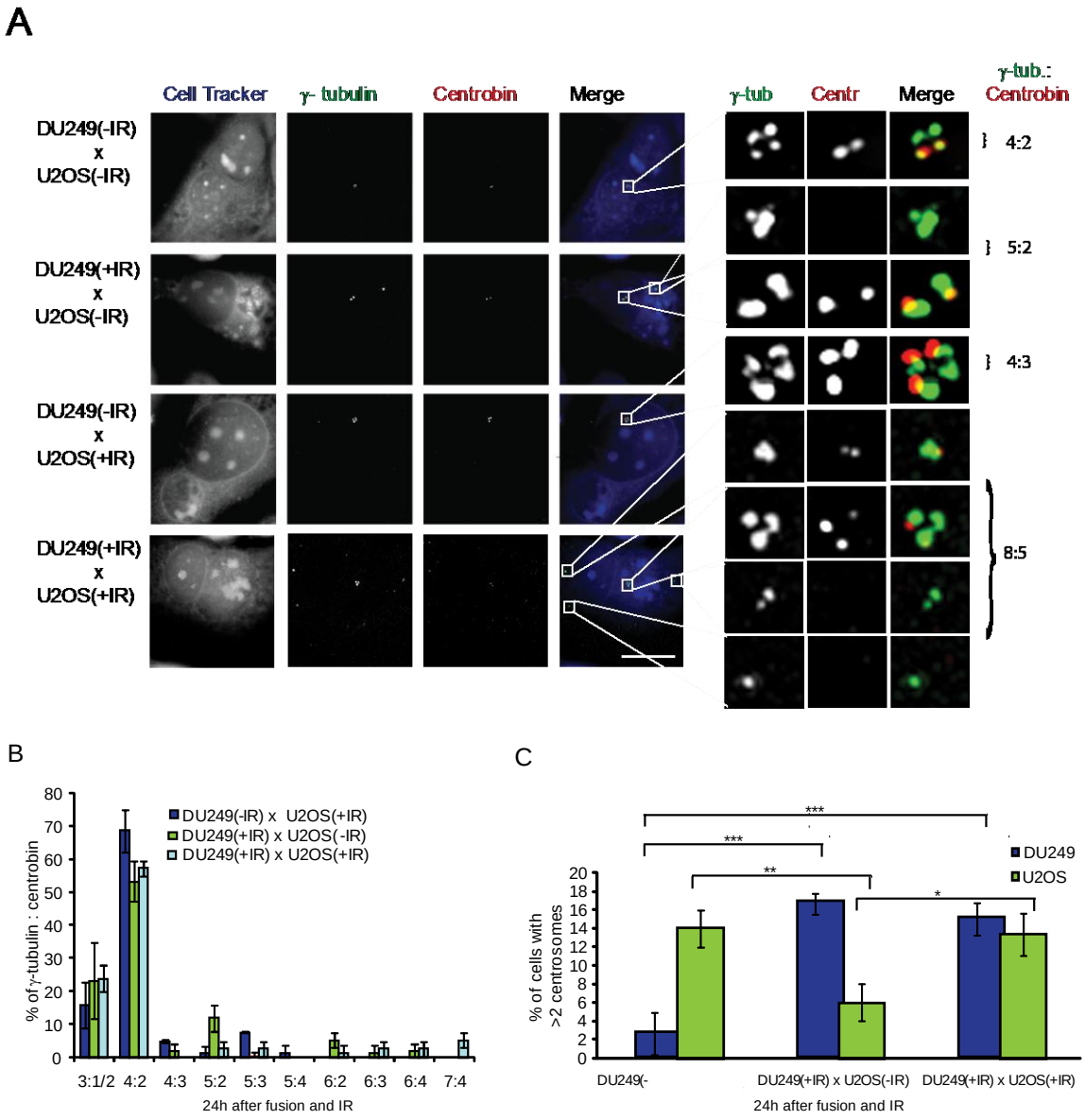

Figure 3.10 Amplified centrosomes were derived from DNA-damaged cells, but not from non-damaged cells.

A. Micrographs of fusions between U2OS and DU249 cells. Cells were untreated or irradiated with 5 Gy and then fused with the indicated partners. Fused cells were fixed in methanol and stained for γ-tubulin (green) and centrobin (red). Boxed insets are shown at right along with the ratio of γ-tubulin stained centrosomes (green, U2OS and DU249) to centrobin stained centrosomes (red, U2OS only). Scale bar, 10 μm.

B. Quantitation of centrosome numbers by γ-tubulin:centrobin ratio in U2OS-DU249 fusions following treatment, where indicated, with 5 Gy of IR. For example, a ratio of 3:1 means that there were three γ-tubulin spots and one centrobin spot, indicating a G2 DU249 fused with a G1 U2OS cell; 6:2 indicates four DU249 centrosomes and two U2OS centrosomes. Data show the mean ± SD of three separate experiments in which 25 cells were scored.

C. Histogram showing the percentage of DU249 and U2OS cells with more than two centrosomes in U2OS-DU249 heterokaryons after treatment, where indicated, with 5 Gy of IR. Fixation, staining, and scoring were performed as described in A. Data show the mean ± SD of three separate experiments in which 25 cells were scored. Statistical significances were calculated by Student's unpaired *t* test (two-tailed) and are indicated on the histogram as *p ≤0.05, **p ≤0.01, and ***p ≤0.001.

3.5 Testing the impact of DNA damage on centriole disengagement

Studies based on *in vitro* assays using *Xenopus* egg extracts and purified centrosomes have shown that the centriole-intrinsic block to reduplication is the close physical association of the centrioles, which is termed as `centriole engagement` (Tsou and Stearns, 2006a; Tsou and Stearns, 2006b). Disengagement of mother from daughter centrioles to allow growth of new centrioles requires the activity of Separase, a protease which is also required for sister-chromatid separation at anaphase onset (Tsou and Stearns, 2006b; Tsou et al., 2009). In addition, the activity of Plk1, a centrosomally-localised mitotic kinase, is also required and acts upstream of Separase activation (Tsou et al., 2009).

Since disengagement events license centrosome duplication, we wondered if centriole disengagement has any impact on DNA damage-induced centrosome amplification. As previously shown (Tsou and Stearns, 2006b), the ratio of the distal centriolar protein Centrin2 to the centriole linker protein C-NAP1 can be used to distinguish engaged centrioles from disengaged centrioles. When centrioles are engaged, each centriole pair has two foci of Centrin with one focus of C-NAP1 (2:1 ratio of centrin2:C-NAP1), whereas when the centriole pairs have lost their tight orthogonal association, each disengaged centriole has one Centrin focus with one or no C-NAP1 focus (1:1 or 1:0 ratio of centrin2:C-NAP1), (Tsou and Stearns, 2006b).

Therefore, we examined the levels of engaged and disengaged centrioles in unirradiated, irradiated and unirradiated/unirradiated fused cells using Centrin2-GFP–expressing U2OS cells (generated by Dr. Helen Dodson) and a C-NAP1 antibody in immunofluorescence microscopy. As shown in Figure 3.11 A (i) and B, in fusions of untreated cells, around 85% of centrioles were found to be engaged. A small number of disengaged centrioles were also observed, which we considered likely to reflect the cell cycle stage at which fusions were performed. However, when one or both of the fusion partners was irradiated we found that the level of cells with disengaged centrioles increased almost two-fold compared to the number of cells with engaged centrioles (Figure 3.11 A (ii, iii), B). This result suggests that irradiation induces centriole disengagement and that IR-induced disengagement could be a control mechanism for IR-induced centrosome amplification.

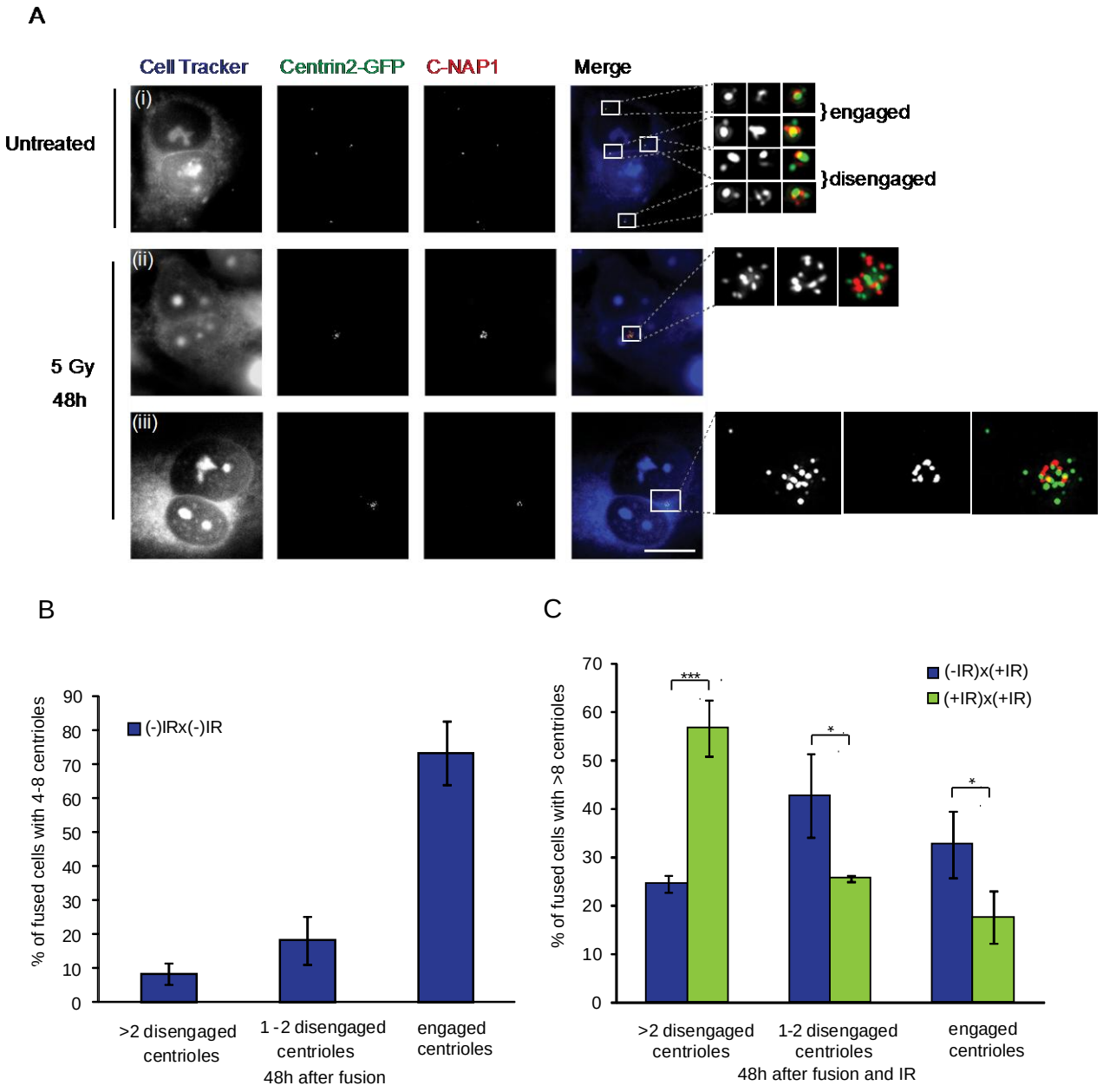

Figure 3.11 IR induces centriole disengagement.

ngagement in cell fusions. Wild-type U2OS cells were stained with CellTracker Blue and fused with Centrin2-GFP–expressing U2OS cells. Cells were fixed in methanol and stained for C-NAP1 (red). Centriole engagement was determined with Centrin2-GFP and anti-C-NAP1 antibody. i) Micrograph of untreated, fused cell with engaged and disengaged centrioles, as indicated. Micrographs of fused binucleate cells with amplified ii) engaged and iii) disengaged centrioles at 48h after treatment with 5 Gy of irradiation. Boxed insets are shown at right. Scale bar, 10 µm.

B. Histogram showing the percentages of 5 Gy-treated fused cells with more than eight Centrin2 spots. Data show the mean ± SD of three separate experiments in which 40 cells were scored. Statistical significances were calculated by Student's unpaired *t* test (two-tailed) and are indicated on the histogram as *$p \leq 0.05$, **$p \leq 0.01$, and ***$p \leq 0.001$.

C. Histogram showing centriole engagement in untreated fused cells with four to eight Centrin2 spots. Quantitation and analysis were as described in B.

3.6 Impact of wild-type or nondegradable Securin overexpression and Plk1 inhibition on IR-induced centrosome amplification

It has been shown that Separase has a major function in stimulating cleavage of cohesin on centrioles and together with Plk1, induces centriole disengagement (Tsou et al., 2009; Schockel et al., 2011). We saw a notable increase in centriole disengagement in irradiated, fused cells compared to unirradiated/irradiated fused cells (Figure 3.11). In agreement with this result, previous studies have shown that DNA damage causes centriole splitting, providing support for the model of DNA damage-induced centriole disengagement and centrosome overduplication (Saladino et al., 2009). We therefore tested whether centriole disengagement is the permissive signal for centrosome amplification after DNA damage. To do this we disrupted Separase function by overexpressing a nondegradable form of its regulator, Securin (Zur and Brandeis, 2001). The anaphase-promoting complex/cyclosome targets Securin for proteolysis, thus releasing Separase from inhibition. It has been shown that expression of mutant Securin causes incomplete chromatid separation, giving rise to daughter cells connected by a thin chromatin fiber (Zur and Brandeis, 2001). We transiently overexpressed myc-tagged forms of wild-type and nondegradable form of Securin (DM-KAA Securin) in U2OS cells and then treated cells with 5 Gy IR 24h after transfection. As shown in Figure 3.12A, the expression of myc-Securin and myc-DM-KAA-Securin was confirmed 72 hours after transfection by western blot analysis. Centrosome numbers in untreated and IR-treated myc positive cells were examined by counting γ-tubulin spots using immunofluorescence microscopy. As shown in Figure 3.12B, overexpression of either form of Securin led to a notable increase in centrosome amplification. In addition, we observed many binucleated cells due to failed cytokinesis. However, after the irradiation of transfected cells, we saw a small increase in centrosome amplification compared to irradiated cells and unirradiated transfected cells, although we had expected to see reduced levels of centrosome amplification. Taken together, these results did not provide clear support for the role of Separase in DNA damage-induced centrosome amplification.

To inhibit the other known pathway of centriole disengagement, we inactivated Plk1, using a specific pharmacological inhibitor called BI2536, (Johnson et al., 2007; Steegmaier et al., 2007). As shown in Figure 3.12C, inhibition of Plk1 in U2OS cells resulted in a high level of cells with more than two centrosomes, possibly due to the

failure of cytokinesis, as reported in previous studies (Brennan et al., 2007; Burkard et al., 2007; Santamaria et al., 2007; Petronczki et al., 2008; Tsou et al., 2009). Next, we treated wild-type or nondegradable Securin-expressing cells with BI2536. Tsou and colleagues have shown previously that *Separase* depletion and Plk1 inhibition in HCT116 cells caused centriole disengagement and duplication to fail (Tsou et al., 2009). As expected, combined inactivation of both Separase and Plk1 caused a significant decrease in the levels of cells with more than two centrosomes (Figure 3.12C). This is in agreement with the previous study (Tsou et al., 2009). Next, we treated Securin-overexpressing U2OS cells with BI2536 and 5 Gy IR. As shown in Figure 3.12C, Plk1 inhibition caused significant reduction in IR-induced centrosome overduplication in U2OS cells. However, no further reduction in IR-induced centrosome amplification was observed when cells were both transfected with Securin and treated with BI2536. Overall, these data provide support for the idea that DNA damage and DNA damage-induced centriole disengagement licences centrosome reduplication and that Plk1 has a role in centriole disengagement in IR-induced centrosome amplification.

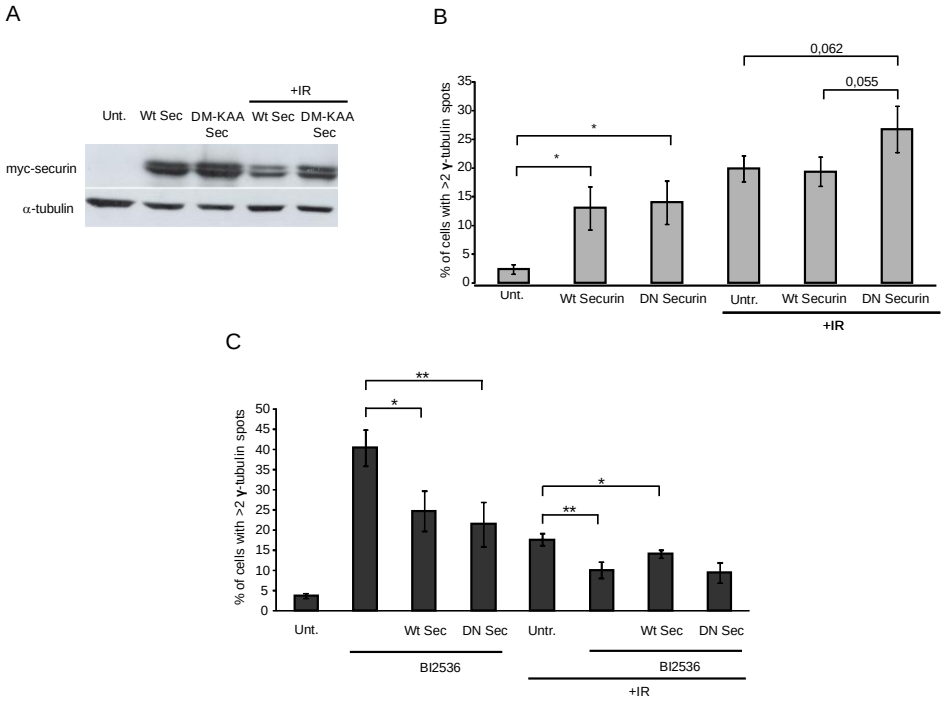

Figure 3.12 Impact of Securin overexpression and Plk1 inhibition on centrosome amplification.
A. Immunoblot of cell lysates from cells transfected with expression vectors for myc-Securin or myc-DMKAA-Securin at 72h after transfection. Where indicated, cells were irradiated at 24h after transfection with 5 Gy of IR.
B. Effects of Securin overexpression on IR-induced centrosome amplification. Cells were treated as described in A, and centrosome numbers were assessed by scoring γ-tubulin in myc-positive cells. Data show the mean ± SD of three separate experiments in which at least 100 cells were scored. Statistical significances were calculated by Student's unpaired *t* test (two-tailed) and are indicated on the histogram as the p value or as*$p \leq 0.05$, **$p \leq 0.01$, and ***$p \leq 0.001$.
C. Impact of Plk1 inhibition and of combined Plk1 inhibition and Securin overexpression on centrosome amplification. Where indicated, cells were transfected with the Securin expression construct and then irradiated 8h after transfection. BI2536 was added to the cells 1h before irradiation with 5 Gy. All cells were analyzed 38h after irradiation as described in B.

3.7 Effects of *Separase* knockdown by RNA interference on IR-induced centrosome amplification

Since overexpression of wild-type and non-degradable Securin in U2OS cells did not provide a clear result for the involvement of Separase in IR-induced centrosome amplification, we followed another approach. We knocked down *ESPL1 (Separase)* expression by interference with small, specific RNA duplexes. Knockdown efficiency was analyzed by western blot analysis. Cells were transfected with 25 nM siRNA and collected and analysed at 48, 60 and 72h after transfection. As shown in Figure 3.13, Separase levels were significantly reduced to ~15% of wild-type levels 48h after transfection. We analysed cell cycle progression in *Separase*-depleted cells at 48, 60h, 72h timepoints, by flow cytometry analysis. As shown in Figure 3.14, depletion of *Separase* increased the fraction of cells in G2/M from around 20% to 34% compared to

untreated and control siRNA-treated cells at 48h following transfection. These results, in agreement with the previous studies, showed that *Separase* depletion leads to a delay or arrest at G2/M (Gimenez-Abian et al., 2005; Sak et al., 2008). At 60h and 72h following transfection, the fraction of cells in G2/M went back to normal levels (20%). In addition, the fraction of dead cells, which was found to be around 15% in untreated or control siRNA treated samples, increased to around 25% in *Separase*-depleted cells at 72h after transfection, indicating that *Separase* depletion eventually caused cell death. These results were in agreement with the previous studies which showed that Separase depletion leads to G2/M arrest and cell death (Gimenez-Abian et al., 2005; Sak et al., 2008).

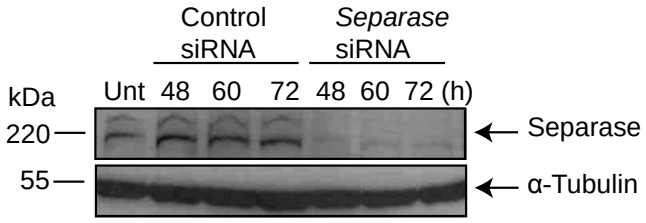

Figure 3.13 Separase depletion by RNA interference in U2OS cells.
Immunoblot of cell lysates from U2OS cells showing Separase levels after treatment with 25nM selective siRNA and with a control siRNA at different timepoints. α-tubulin serves as the loading control.

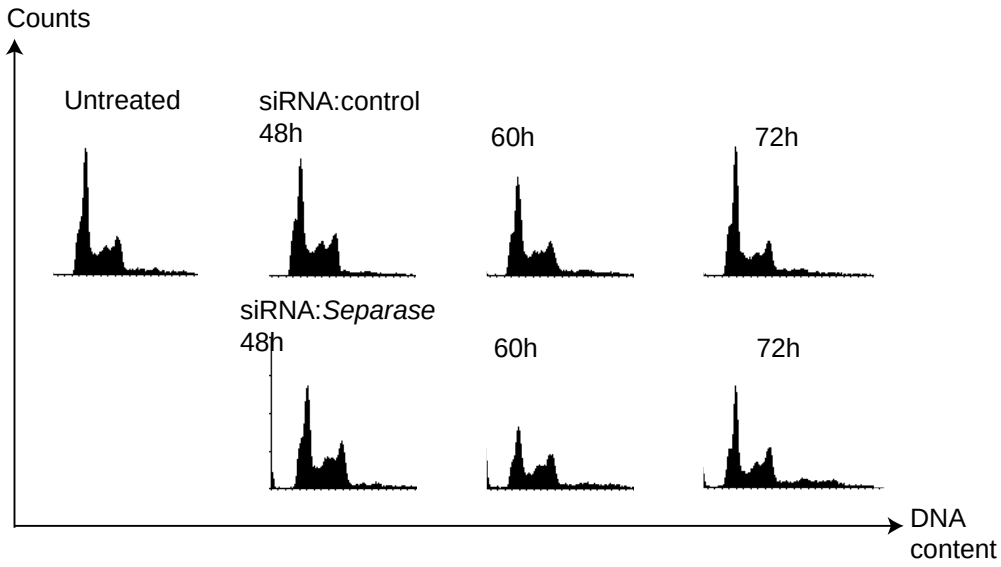

Figure 3.14 Influence of Separase depletion on cell cycle progression.
Cell cycle profile of U2OS cells stained with propidium iodide after transfection with control or *Separase*-specific targeting siRNAs at 48h, 60h, and 72h.

To study the involvement of Separase in IR-induced centrosome amplification, cells were irradiated 48h after siRNA transfection and centrosome numbers were analysed by immunofluorescence microscopy using γ-tubulin as a centrosome marker. Similar to our previous result (Figure 3.13B) with non-degradable Securin, inhibition of *Separase* by RNAi led to a notable increase in the number of cells with more than 2 centrosomes (Figure 3.15B). In addition, IR treatment of *Separase*-depleted cells resulted in similar levels of centrosome amplification as in IR treated Securin overexpressing cells (Figure 3.15B, 3.13B). Unexpectedly, combined treatment with Plk1 inhibitor and IR in *Separase*-depleted cells led to a small increase in the level of centrosome amplification compared to *Separase*-depleted cells that were either untreated or only treated with Plk1 inhibitor. This result contrasted with our previous result, where we saw a decrease in the levels of centrosome amplification in Securin-overexpressing, BI2536 and IR treated cells. However, this could be due the differences in active Separase levels in each system. Although our experimental approaches did not allow us to evaluate directly the effects of Separase in IR-induced centrosome amplification, pharmacological inhibition of Plk1 clearly showed that Plk1 has a role on centriole disengagement in IR-induced centrosome amplification.

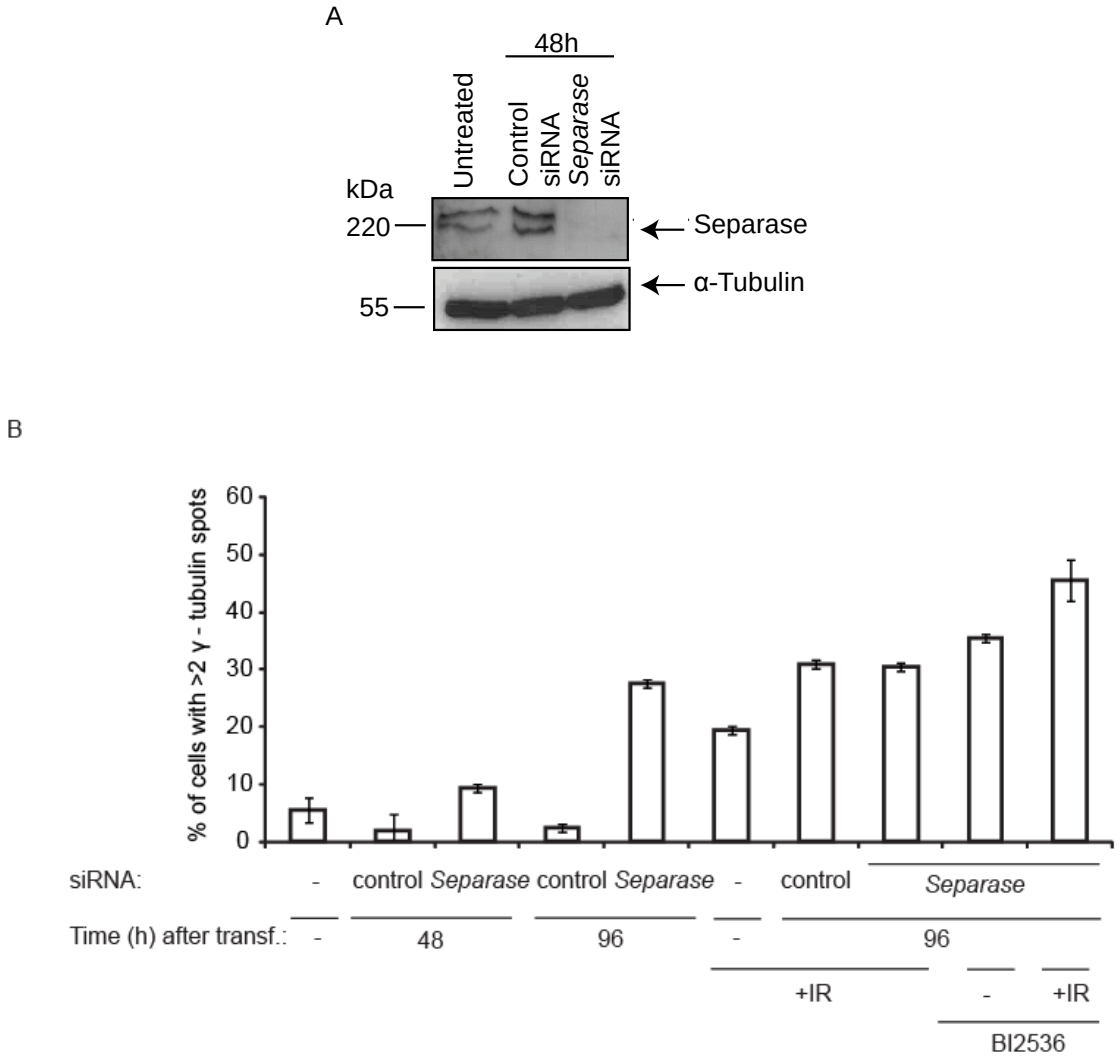

Figure 3.15 Impact of *Separase* knockdown and Plk1 inhibition on centrosome amplification.
A. Immunoblot of cell lysates from U2OS cells showing Separase levels after 48h treatment with 25nM selective siRNA and with a control siRNA. α-tubulin serves as the loading control.
B. Impact of *Separase* depletion and of combined Plk1 inhibition and *Separase* depletion on centrosome amplification. Where indicated, cells were transfected with *Separase* or control siRNAs and treated with 10Gy IR, 48h after transfection. 100 nM of BI2536 was added to the cells 1h before irradiation. All cells were analyzed 96h after siRNA treatment and 48h after irradiation. Centrosome numbers were assessed by scoring γ-tubulin spots in immunofluorescence microscopy. Data show the mean ± SD of two separate experiments in which at least 100 cells were scored.

3.8 Discussion

During the normal cell cycle, centrosome duplication is tightly coupled to DNA replication and its occurrence is restricted to once per cell cycle. Similar to DNA replication, centrosome duplication requires the kinase activities of cyclin E/Cdk2 and/or cyclin A/Cdk2 during the S phase of cell cycle (Lacey et al., 1999; Meraldi et al., 1999). The second requirement for centrosome duplication is the licensing event that occurs via disengagement of centrioles in mitosis (Tsou and Stearns, 2006b). Disengagement of the mother from the daughter centriole is mediated by the activities of Separase and Plk1 during the metaphase-to-anaphase transition (Tsou et al., 2009). In transformed cells after DNA damage, the centrosome duplication cycle is decoupled from the DNA replication cycle and centrosomes can reduplicate. Cdk2 activity is required for centrosome reduplication, in addition to enough time being provided by the cell cycle arrest before the next cell division (Balczon et al., 1995; Lacey et al., 1999; Hinchcliffe et al., 1999; Duensing et al., 2006; Dodson et al., 2004; Bourke et al., 2007), Prosser et al., 2009; Bourke et al., 2010).

Two hypotheses have been proposed for the mechanism of centrosome amplification: 1) overduplicated centrioles arise from multiple disengagement and procentriole formation steps during prolonged S phase (Guarguaglini et al., 2005; Duensing et al., 2007) and 2) already-duplicated centrosomes undergo an additional disengagement and procentriole formation during a prolonged G2 phase (Dodson et al., 2004; Bourke et al., 2007). The mechanism of the first hypothesis fits well with the overduplication of centrosomes in S-phase arrested cells as seen in response to HU (Guarguaglini et al., 2005; Duensing et al., 2007), but cannot explain the mechanism involved in IR-induced centrosome amplification. Our group has demonstrated that Chk1-mediated G2/M checkpoint arrest causes a prolonged G2 phase arrest, which could provide enough time for centrosomes to reduplicate (Dodson et al., 2004). Further studies in our lab by live cell imaging on cell cycle timing of centrosome amplification have also shown that IR-induced centrosome reduplication occurs outside S-phase and that the majority of the cells with amplified centrosomes carried the G2-phase marker Cenp-F (Inanc et al., 2010). Here, we investigated the duplication capacity of G2 phase centrosomes after IR, using sychronized populations of G2 phase U2OS cells. Our analysis has clearly shown that G2 cells are more permissive to reduplicate their centrosomes than asychronous cells or cells sychronized at G1/S. Together with the

previous data from our group, these results further support the notion of G2 phase centrosome amplification after IR.

Recent studies have clearly shown that the centrosome-intrinsic block that is present in G2 centrosomes does not allow G2 cells to undergo an additional round of duplication when fused to G1 or S phase cells (Wong and Stearns, 2003). Our findings suggest that the centrosome-intrinsic block to reduplication in G2 centrosomes is removed in response to IR, thus licensing centrosomes to reduplicate. Based on the licensing requirement for centriole duplication, using PEG-mediated cell fusion assays, we investigated the nature of the centrosome amplification signal in IR treated cells. We asked whether an activating signal, such as a mobile enzyme activity, causes irradiated/unirradiated G2 centrioles to reduplicate in the same cytosolic environment, or whether a signal inhibiting duplication/disengagement is lost only at the irradiated G2 centrioles (Tsou and Stearns, 2006a; Nigg, 2006a). Examination of centrosome numbers in irradiated G2-irradiated G2 cell fusions showed significantly higher levels of centrosome amplification than in irradiated G2-unirradiated G2 fusions. Further investigation of the source of the centrosomes that amplified in fusions between irradiated human-unirradiated chicken cells and vice versa, using a species-specific centrobin antibody led us to conclude that they were derived from the irradiated cells (Inanc et al., 2010). Taken together, our findings support a model in which centrosome amplification is centrosome-autonomous and centrosome-limited duplication licensing in G2 centrosomes occurs in response DNA damage.

The current model for the control of centrosome duplication is that Separase- and Plk1-dependent centriole disengagement licenses the centrosome for duplication in the following cell cycle (Tsou et al., 2009). Considering that disengagement is the licensing signal for normal centrosome duplication, it is possible that centriole disengagement can also be a permissive signal for IR-induced centrosome amplification. Our fusion experiments showed that levels of disengagement were increased in amplified centrioles when one or both fusion partners were irradiated in fused cells compared unirradiated fusions, suggesting a link between IR-induced centriole disengagement and centrosome amplification. These results were in agreement with previous findings showing that increased levels of centriole separation and

fragmentation occurred after DNA damage in Chinese hamster ovary and hTERT-RPE1 cells (Hut et al., 2003; Saladino et al., 2009).

Separase activity is regulated via its inhibition by Securin and Cyclin B1. These are both targeted for degradation by the anaphase promoting complex/cyclosome (APC/C), thereby activating Separase at anaphase (Zou et al., 1999; Holland and Taylor, 2006; Gorr et al., 2005). Since Separase activity is essential for centriole disengagement, we tested the role of Separase activity in IR-induced centriole amplification by overexpression of nondegradable Securin (Zou et al., 1999; Tsou and Stearns, 2006a). Unfortunately, this analysis did not provide any clear support for Separase`s involvement in IR-induced centriole disengagement. However, our experimental approach may not have been suitable for the inhibition of Separase activation after DNA damage, since there is another mechanism involved in Separase inactivation through Cdk/Cyclin B (Gorr et al., 2005). We also attempted to study the role of Separase in IR-induced centriole amplification by *Separase* depletion using RNAi. This approach also did not allow us to obtain clear results either. An alternative experimental approach to study Separase`s involvement in IR-induced centriole disengagement could be to use a cell line which has conditional null alleles of *Separase* (Tsou et al., 2009).

It is known that centrioles can still disengage in Separase-deficient cells via Separase-independent mechanisms (Tsou et al., 2009). Therefore, we tested the involvement of Plk1 in IR-induced centrosome amplification. Inhibition of Plk1 by BI2536 prevented centrosome overduplication in irradiated U2OS cells, suggesting that Plk1 might be involved as a licensing factor in IR-induced centrosome amplification. As shown in Figure 3.16, we propose a model for IR-induced centrosome amplification that involves Plk1 and possibly Separase. Similarly, it was reported that in HU treated U2OS cells, Plk1 depletion caused a significant reduction in centrosome amplification (Liu and Erikson, 2002). Previous studies have suggested that the kinase activity of Plk1 decreases in an ATM-dependent manner in DNA damaged cells (Smits et al., 2000; van Vugt et al., 2001). Although our findings regarding the role of Plk1 on IR-induced centrosome amplification do not agree with this model, upregulation of cell cycle regulatory kinases such as Cdk2 in transformed cells after IR could act as coregulatory signal to induce centrosome amplification (Bourke et al., 2010). In addition to its role in

bipolar spindle formation, activation of the anaphase-promoting complex, centrosome separation and disengagement, Plk1 has also been implicated in centrosome maturation which occurs late in G2 (Haren et al., 2009; Wang et al., 2011). Previous studies have shown that IR-induced amplified centrosomes contain maturation markers such as CEP170 and Ninein, further indicating the involvement of Plk1 in IR-induced centrosome amplification (Saladino et al., 2009; Inanc et al., 2010).

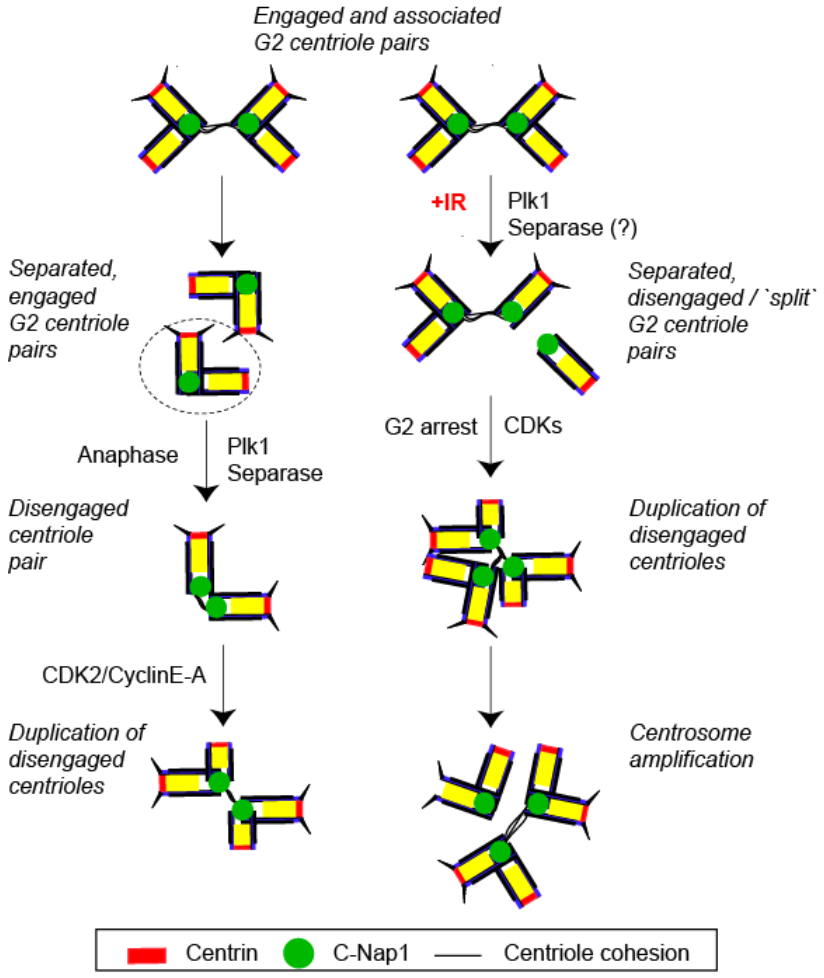

Figure 3.16 Model for how IR-induced centrosome amplification occurs.
Tightly associated (engaged) centriole pairs in an orthogonal arrangement, are attached by centrosomal cohesion in G2 phase. Each G2 centriole pair contains one fully mature centriole (mother) and daughter centriole and in late G2 centrosomal cohesion is lost. Disengagement, mediated by Separase and Plk1in anaphase, licences centrioles for duplication in the next cell cycle. Following IR treatment, centrioles disengage in an extended G2 arrest in a process that involves Plk1 and possibly Separase. This allows the reduplication of the disengaged centrioles and centrosome amplification. C-Nap1 and centrin are used as indicators of engagement and disengagement (Tsou and Stearns, 2006b; Inanc et al., 2010). Adapted from (Inanc and Morrison, 2011).

The identities of the Plk1 and Separase substrates that mediate centriole disengagement are just beginning to be unravelled. Studies have indicated that the members of the cohesin ring complex, in addition to their role in regulating the separation of sister chromatids during mitosis, act as centriole-engagement factors.

Moreover it was demonstrated that the members of cohesin complex such as Scc1, Smc3 and Rad21 localize to the centrosomes and are cleaved by Separase at anaphase, coincidentally with their chromosomal partners (Wang et al., 2008; Schockel et al., 2011; Gimenez-Abian et al., 2010). Recent studies have also provided evidence that sSgo1, a variant of Sgo1, which has a protective role in sister chromatid cohesion, is also required for holding paired centrioles together in an engaged state in early mitosis. Plk1 is involved in phosphorylation of sSgo1 resulting in its targeting to the centrosomes where it functions as a protector of centriole cohesion at the spindle poles (Wang et al., 2008; Schockel et al., 2011). Our findings suggest a model where a centrosome-autonomous inhibitory signal is lost upon irradiation of centrioles and where this centrosome-autonomous inhibitory signal is the engagement of the centrioles. Although our Plk1 inhibition using BI2536 clearly provided support for DNA damage-induced centriole disengagement leading to centrosome amplification, the targets of Plk1 and Separase still remained to be discovered. In future experiments it would be interesting to assess the precise roles of the members of the centrosome cohesion complex and understand their regulation by Separase and Plk1, as well as to identify possible additional regulators in DNA damage-induced centrosome amplification.

Chapter 4
Cloning of chicken *Cep135* and generation of *Cep135* null chicken DT40 cells

4.1 Introduction

Cep135 is a centrosomal protein first identified in centrosomes of *Spisula* oocytes (Vogel et al., 1997; Kuriyama et al., 2001). Orthologues of Cep135 have been found in a wide range of organisms from protozoa to mammals (Ryu et al., 2000; Matsuura et al., 2004; Mottier-Pavie and Megraw, 2009). Cep135 is a highly coiled-coil protein with no distinctive domains and is an essential component of centrioles that is required for centriole formation (Ohta et al., 2002; Kleylein-Sohn et al., 2007). It has been shown that Bld10, the orthologue of human Cep135 in *Chlamydomonas* and *Drosophila*, is a structural component of the cartwheel and is involved in the formation of nine-fold symmetry of the centrioles (Hiraki et al., 2007; Nakazawa et al., 2007; Mottier-Pavie and Megraw, 2009). Cep135 also localises to the surface of the parental centriolar cyclinder and to the proximal lumen of the centrioles (Ohta et al., 2002; Kleylein-Sohn et al., 2007). Previous reports have suggested that when *Cep135* is depleted via RNAi or overexpressed, microtubule organization is altered both in interphase and mitotic cells (Ohta et al., 2002). In addition, it has been proposed that Cep135 functions as a platform protein by holding C-NAP1 at the proximal ends of the centrioles (Kim et al., 2008).

Due to the important functions that have been attributed to Cep135 in microtubule organization and in organising centrosomes and their functions, we decided to focus our genetic analysis on chicken *Cep135*. We used reverse genetics in the chicken B-cell line, DT40, to disrupt the *Cep135* locus. DT40 cells exhibit a high ratio of homologous versus non-homologous targeting events, thus making them an ideal system to carry out gene knockouts (Buerstedde and Takeda, 1991). The work presented in this chapter describes the bioinformatic analysis of *cCep135 (chicken Cep135)*, cloning of *cCep135* cDNA, targeting of *cCep135* locus, generation of *cCep135*$^{-/-}$ knockout clones, and basic phenotypic characterization of the selected clones for viability and mitosis. In this study we found that Cep135-deficient DT40 cells are viable and do not exhibit any mitotic abnormalities.

4.2 Cloning and analysis of chicken *Cep135* cDNA

We searched for the *Cep135* chicken (*cCep135*) orthologues in the NCBI and Ensembl databases. We found gene level information associated with chicken *Cep135* gene in Ensembl (accession no: ENSGALG00000013776). According to Ensembl, there were 2 transcripts of this gene (accession no: ENSGALT00000022372, ENSGALT00000037552). The first is transcribed as a 3441 bp mRNA which encodes a protein of 1147 amino acids and the second is transcribed as a 3465 bp mRNA which encodes a protein of 1155 amino acids. To confirm that the predicted *cCep135* mRNAs are expressed in chicken cells, we searched the expression sequence tag (EST) database (dbEST, NCBI). We found that there were multiple EST clones that cover the first 1734 nucleotides (39 nucleotides were missing in both transcripts in the middle of this region) and the last 600 nucleotides of the *Cep135* sequence. Around 1000 nucleotides in the middle of the mRNA were not covered by any EST clones, suggesting that these were low quality sequences. An EST database search did not provide any information for tissue-specific *Cep135* expression. A BLAST search against the entire nucleotide collection revealed that there is no similar gene in the *G. gallus* genome.

For cloning of the *cCep135* cDNA, we needed to ensure that the *cCep135* cDNA sequence shown in Ensembl was annotated correctly. So, we examined the sequence of the 5`-most end of the *cCep135* gene. 5`RACE (5` Rapid Amplification of cDNA Ends) was carried out on chicken cDNA. Primers were designed on the basis of the predicted *cCep135* sequence in the Ensembl database (see Fig. 4.1A). The amplified RACE product (700 bp) was cloned into pGEMT-easy and sequenced (see Fig.4.1B). Alignment of the sequenced chicken, mouse and human *Cep135* 5`*UTRs* (5` untranslated regions) revealed significant similarities in this region (see Figure 4.1C). The Kozak sequence, which lies within a short 5' untranslated region and directs translation of mRNA, was analyzed and found to be G/UUUACAAUGA in chicken *Cep135* sequence. The nucleotide at the -3 position of ATG is crucial for the efficient initiation of translation and is usually A in a Kozak sequence (Kozak, 1986). From the data shown in Fig 4.1C, it can be seen that A at position -3 is conserved between the sequences in chicken and mouse. Also, G at position +4 is conserved and this shows a strong consensus.

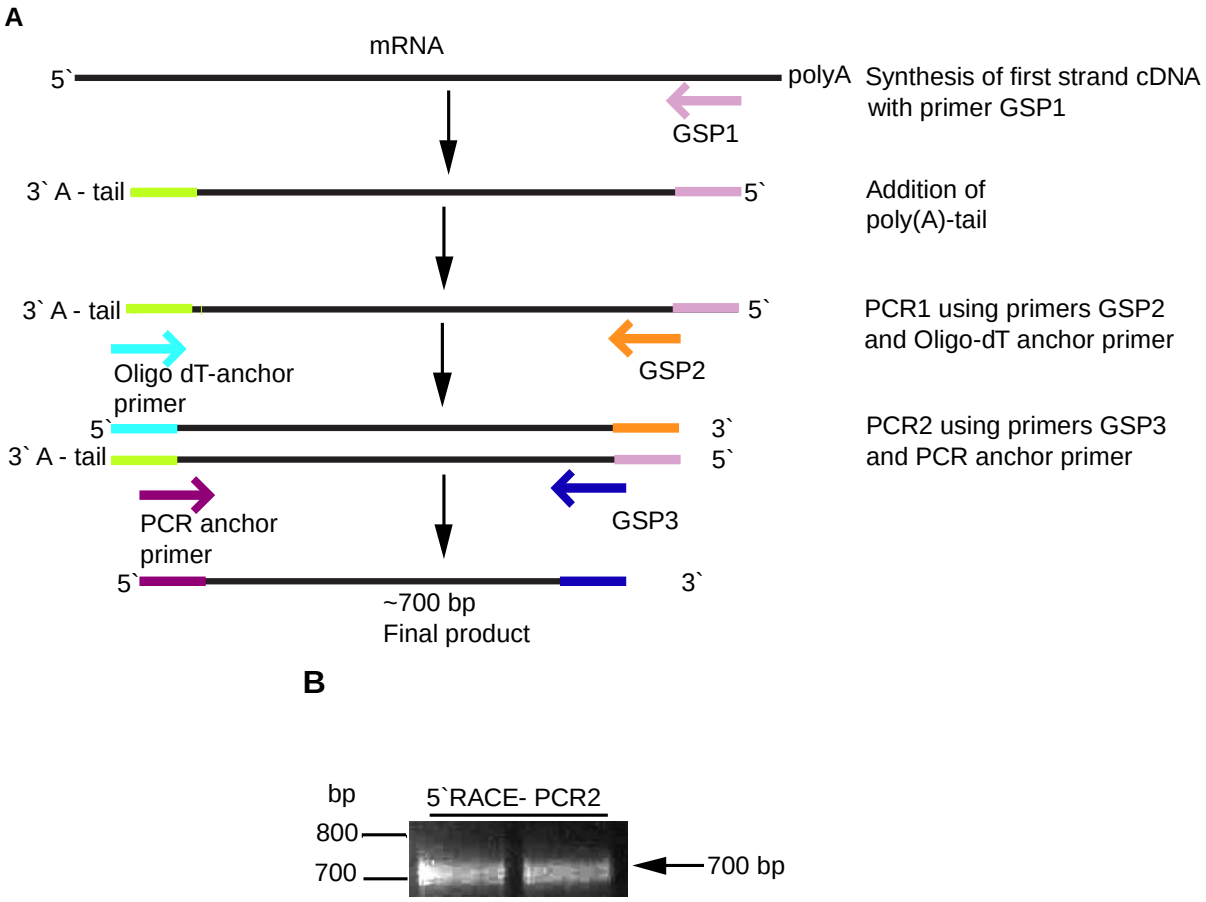

C

Chicken Cep135 TACAAAAGCCACTTTGGATCTGTGTTTACAATGACGACAACAGCGGAGCGGAAGTTTGTTAACCTCAGGAAACGTCTGGA
Human Cep135 ATAAAACTTGTTTTAGAAGACGAGATGACTACAGCTGTAGAGAGAAAGTATATTAATATTAGGAAAAGGCTGGATCAGCTG
Mouse Cep135 GGCCTTTAAGTTGGGAGTGTGACTAAAACTGGTTTTGGAAGCAAGATGACTACAGCTGCAGAGAGAAAGTATATTAACATT

Figure 4.1 Rapid Amplification of cDNA Ends (5`RACE) and identification of the ATG of chicken *Cep135*.
A. Schematic representation of 5'RACE procedure. The first-strand cDNA is synthesised from mRNA using reverse transcriptase (RT) from a gene specific primer (GSP1). This cDNA is then tailed using dATP and terminal transferase and purified. Two rounds of amplification are then performed; the first PCR with GSP2 and an oligo dT-anchor primer, and the second PCR with a nested gene specific primer-GSP3 and a PCR- anchor primer.
B. Image of DNA agarose gel showing amplified 5'RACE product (~700 bp), obtained with two different sets of primers as described in A.
C. Sequence comparison between the 5'UTR sequence of chicken, human and mouse is shown, with the Kozak sequence underlined and ATG in red, and the crucial nucleotides in the consensus at positions -3 and +4 indicated in blue.

The c*Cep135* cDNA sequence was used to design specific primers for cDNA amplification. First, we generated cDNA through reverse transcription from total RNA isolated from DT40 cells, to be used as a template for PCR. The full-length *cCep135* cDNA was then amplified by PCR with gene-specific primers. The chicken *Cep135* cDNA was cloned into pEGMT-easy and subsequently to pCMV-3TAG-2C. Analysis

of the amplified candidate *Cep135* cDNA product by agarose gel electrophoresis revealed a size (3500bp) consistent with the sequence predicted in the Ensembl database (Figure 4.2). Also, PCR amplification of *Cep135* cDNA in this way confirmed that Cep135 is expressed in DT40 cells. The sequenced full length *cCep135* cDNA was analysed and found to be 3453 bp in length with the ATG at position 112 in the sequence. *cCep135* cDNA encodes a protein of 1151 aa with a predicted size of 135 kDa. The human mRNA and protein have a similar size of 3423 bp and 1141 amino acids (135 kDa), respectively. Sequencing of the PCR products revealed that the 39 nucleotides missing from the Ensembl *Cep135* mRNA sequences were present in our *cCep135* transcripts, as in EST database sequences. This sequence information is shown in Appendix 1.

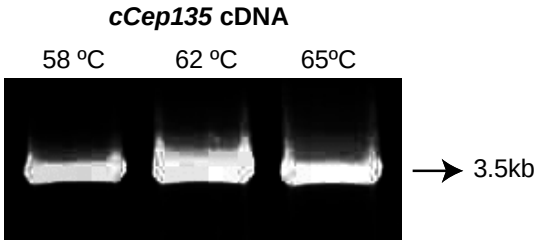

Figure 4.2 Cloning of full-length *cCep135* cDNA. Image of DNA agarose gel showing PCR amplification of full-length *cCep135* cDNA carried out at three different annealing temperatures.

Orthologues of *Cep135* have been identified in several organisms, including human, *Xenopus,* mouse, *Paramecium, Chlamydomonas* and *Drosophila.* A ClustalW alignment of chicken and human *Cep135* sequence showed 65% identity with a similar level of identity with other organisms, as shown in Table 4.1. Analysis performed using the COILS program (Lupas et al., 1991) revealed that chicken Cep135 contains extensive coiled-coil and α-helical regions (Figure 4.3), similar to human Cep135 and many centrosome proteins characterized so far (Kimble and Kuriyama, 1992; Stearns and Winey, 1997).

Table 4.1 Results of ClustalW alignment of chicken Cep135 sequence to other vertebrate Cep135 proteins

Organism	**NCBI Protein Accession code**	**Length (aa)**	**Identity** **Score with chicken Cep135**
Homo sapiens	NP_079285.2	1140	65%
Pan troglodytes	XP_517281.2	1140	65%
Canis lupus familiaris	XP_539276.2	919	62%
Mus musculus	NP_950197.1	1140	62%
Rattus norvegicus	XP_223341.4	1140	62%
Drosophila melanogaster	NP_648749.3	1059	23%
Xenopus tropicalis	XP_002934717.1	1174	65%

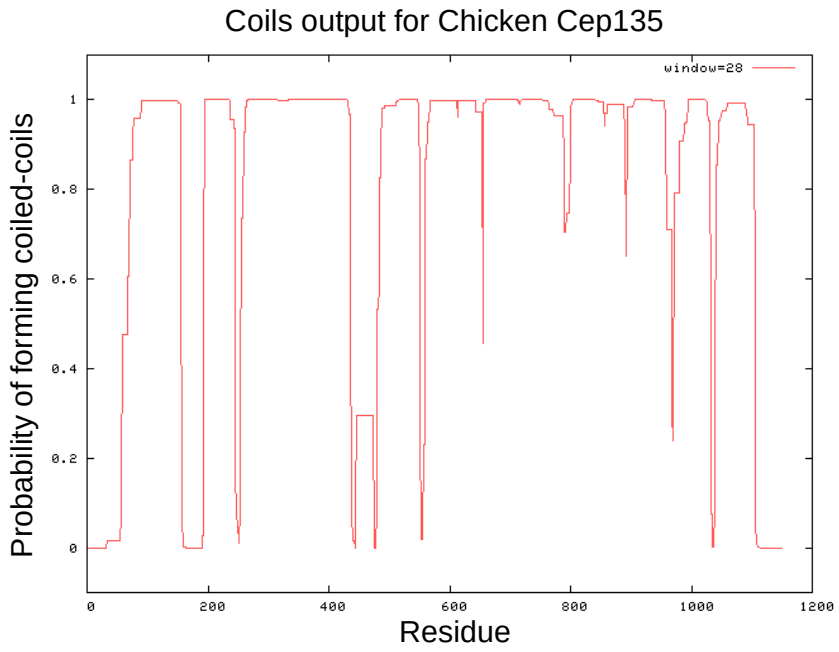

Figure 4.3 Prediction of coiled-coil regions in chicken Cep135 using the COILS program.

Human Cep135 contains two repeats with a hypothetical leucine zipper motif, suggesting that Cep135 is involved in protein-protein interactions. It also contains three putative tyrosine phosphorylation motifs, which shows that Cep135 might be a phosphoprotein (Ohta et al., 2002). Further analysis of domain structure revealed that hypothetical leucine zipper motifs and three putative tyrosine phosphorylation motifs found in human Cep135 were also conserved in chicken Cep135 as well as in mouse and *Xenopus* (Figure 4.4).

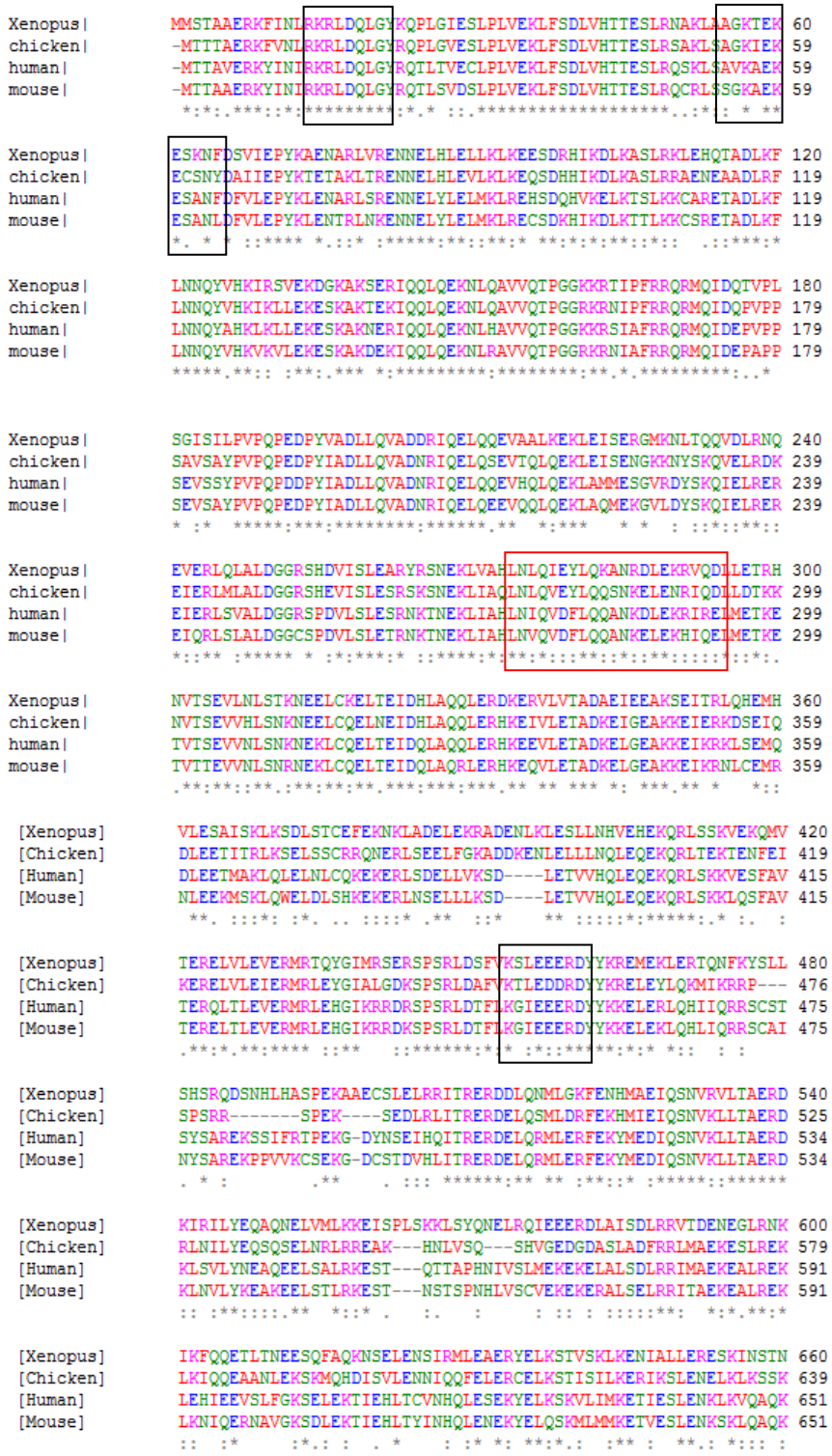
Xenopus| MMSTAAERKFINLRKRLDQLGYKQPLGIESLPLVEKLFSDLVHTTESLRNAKLAAGKTEK 60
chicken| -MTTTAERKFVNLRKRLDQLGYRQPLGVESLPLVEKLFSDLVHTTESLRSAKLSAGKIEK 59
human| -MTTAVERKYINIRKRLDQLGYRQTLTVECLPLVEKLFSDLVHTTESLRQSKLSAVKAEK 59
mouse| -MTTAAERKYINIRKRLDQLGYRQTLSVDSLPLVEKLFSDLVHTTESLRQCRLSSGKAEK 59
Xenopus| ESKNFQSVIEPYKAENARLVRENNELHLELLKLKEESDRHIKDLKASLRKLEHQTADLKF 120
chicken| ECSNYQAIIEPYKTETAKLTRENNELHLEVLKLKEQSDHHIKDLKASLRRAENEAADLRF 119
human| ESANFQFVLEPYKLENARLSRENNELYLELMKLREHSDQHVKELKTSLKKCARETADLKF 119
mouse| ESANLQFVLEPYKLENTRLNKENNELYLELMKLRECSDKHIKDLKTTLKKCSRETADLKF 119
Xenopus| LNNQYVHKIRSVEKDGKAKSERIQQLQEKNLQAVVQTPGGKKRTIPFRRQRMQIDQTVPL 180
chicken| LNNQYVHKIKLLEKESKAKTEKIQQLQEKNLQAVVQTPGGRKRNIPFRRQRMQIDQPVPP 179
human| LNNQYAHKLKLLEKESKAKNERIQQLQEKNLHAVVQTPGGKKRSIAFRRQRMQIDEPVPP 179
mouse| LNNQYVHKVKVLEKESKAKDEKIQQLQEKNLRAVVQTPGGRKRNIAFRRQRMQIDEPAPP 179
Xenopus| SGISILPVPQPEDPYVADLLQVADDRIQELQQEVAALKEKLEISERGMKNLTQQVDLRNQ 240
chicken| SAVSAYPVPQPEDPYIADLLQVADNRIQELQSEVTQLQEKLEISENGKKNYSKQVELRDK 239
human| SEVSSYPVPQPDDPYIADLLQVADNRIQELQQEVHQLQEKLAMMESGVRDYSKQIELRER 239
mouse| SEVSAYPVPQPEDPYIADLLQVADNRIQELQEEVQQLQEKLAQMEKGVLDYSKQIELRER 239
Xenopus| EVERLQLALDGGRSHDVISLEARYRSNEKLVAHLNLQIEYLQKANRDLEKRVQDLLETRH 300
chicken| EIERLMLALDGGRSHEVISLESRSKSNEKLIAQLNLQVEYLQQSNKELENRIQDLLDTKK 299
human| EIERLSVALDGGRSPDVLSLESRNKTNEKLIAHLNIQVDFLQQANKDLEKRIRELMETKE 299
mouse| EIQRLSLALDGGCSPDVLSLETRNKTNEKLIAHLNVQVDFLQQANKELEKHIQELMETKE 299
Xenopus| NVTSEVLNLSTKNEELCKELTEIDHLAQQLERDKERVLVTADAEIEEAKSEITRLQHEMH 360
chicken| NVTSEVVHLSNKNEELCQELNEIDHLAQQLERHKEIVLETADKEIGEAKKEIERKDSEIQ 359
human| TVTSEVVNLSNKNEKLCQELTEIDQLAQQLERHKEEVLETADKELGEAKKEIKRKLSEMQ 359
mouse| TVTTEVVNLSNRNEKLCQELTEIDQLAQRLERHKEQVLETADKELGEAKKEIKRNLCEMR 359
[Xenopus] VLESAISKLKSDLSTCEFEKNKLADELEKRADENLKLESLLNHVEHEKQRLSSKVEKQMV 420
[Chicken] DLEETITRLKSELSSCRRQNERLSEELFGKADDKENLELLLNQLEQEKQRLTEKTENFEI 419
[Human] DLEETMAKLQLELNLCQKEKERLSDELLVKSD----LETVVHQLEQEKQRLSKKVESFAV 415
[Mouse] NLEEKMSKLQWELDLSHKEKERLNSELLLKSD----LETVVHQLEQEKQRLSKKLQSFAV 415
[Xenopus] TERELVLEVERMRTQYGIMRSERSPSRLDSFVKSLEEERDYYKREMEKLERTQNFKYSLL 480
[Chicken] KERELVLEIERMRLEYGIALGDKSPSRLDAFVKTLEDDRDYYKRELEYLQKMIKRRP--- 476
[Human] TERQLTLEVERMRLEHGIKRRDRSPSRLDTFLKGIEEERDYYKKELERLQHIIQRRSCST 475
[Mouse] TERELTLEVERMRLEHGIKRRDKSPSRLDTFLKGIEEERDYYKKELEKLQHLIQRRSCAI 475
[Xenopus] SHSRQDSNHLHASPEKAAECSLELRRITRERDDLQNMLGKFENHMAEIQSNVRVLTAERD 540
[Chicken] SPSRR-------SPEK----SEDLRLITRERDELQSMLDRFEKHMIEIQSNVKLLTAERD 525
[Human] SYSAREKSSIFRTPEKG-DYNSEIHQITRERDELQRMLERFEKYMEDIQSNVKLLTAERD 534
[Mouse] NYSAREKPPVVKCSEKG-DCSTDVHLITRERDELQRMLERFEKYMEDIQSNVKLLTAERD 534
[Xenopus] KIRILYEQAQNELVMLKKEISPLSKKLSYQNELRQIEEERDLAISDLRRVTDENEGLRNK 600
[Chicken] RLNILYEQSQSELNRLRREAK---HNLVSQ---SHVGEDGDASLADFRRLMAEKESLREK 579
[Human] KLSVLYNEAQEELSALRKEST---QTTAPHNIVSLMEKEKELALSDLRRIMAEKEALREK 591
[Mouse] KLNVLYKEAKEELSTLRKEST---NSTSPNHLVSCVEKEKERALSELRRITAEKEALREK 591
[Xenopus] IKFQQETLTNEESQFAQKNSELENSIRMLEAERYELKSTVSKLKENIALLERESKINSTN 660
[Chicken] LKIQQEAANLEKSKMQHDISVLENNIQQFELERCELKSTISILKERIKSLENELKLKSSK 639
[Human] LEHIEEVSLFGKSELEKTIEHLTCVNHQLESEKYELKSKVLIMKETIESLENKLKVQAQK 651
[Mouse] LKNIQERNAVGKSDLEKTIEHLTYINHQLENEKYELQSKMLMMKETVESLENKSKLQAQK 651

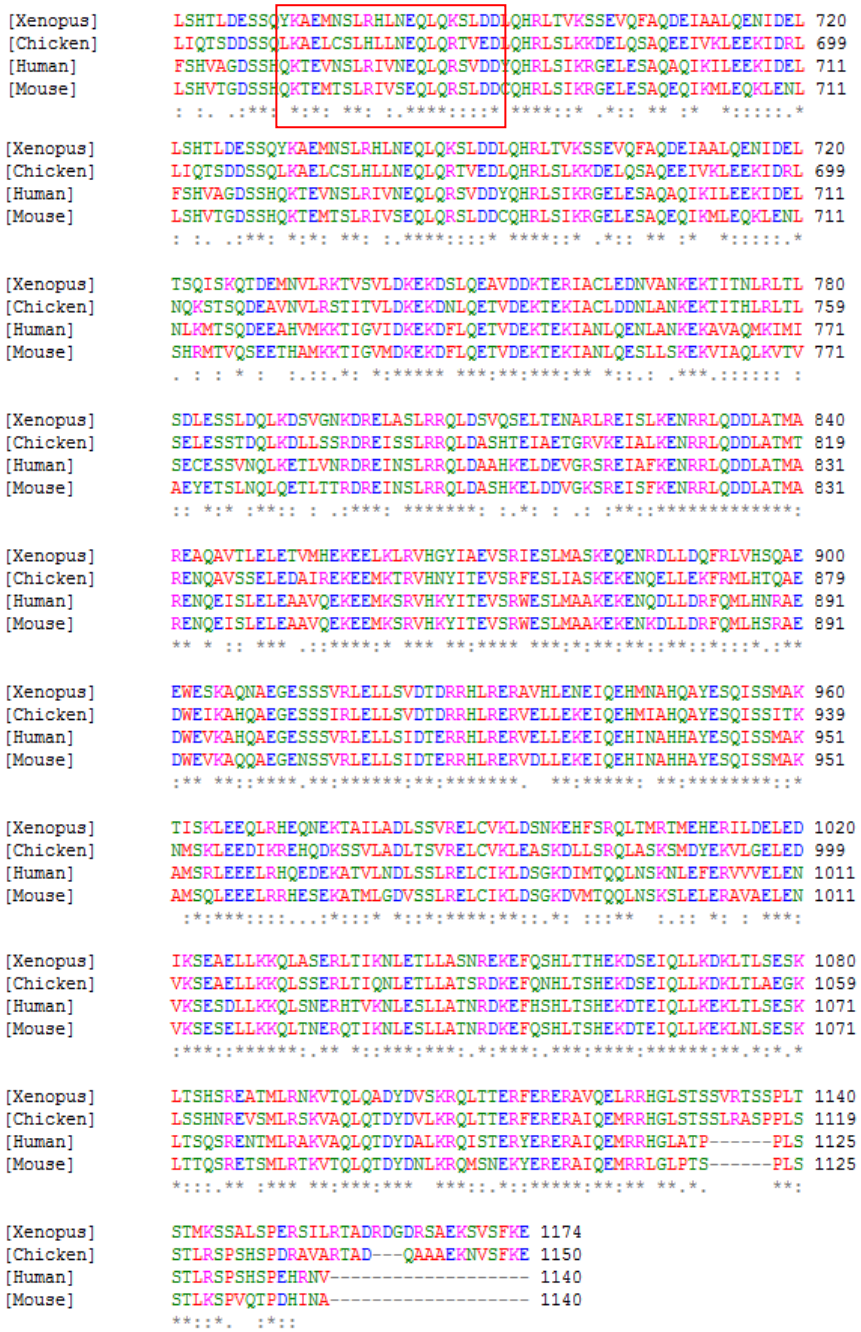

Fig. 4.4 ClustalW analysis of vertebrate Cep135 sequences. A ClustalW alignment of Cep135 proteins is shown. The black boxes show the highly conserved putative tyrosine phosphorylation motifs between species. The red boxes show conserved leucine zipper motifs between species. Key to the Clustal consensus: *****amino acid fully conserved,: strong group fully conserved, weaker group fully conserved; Colouring of ClustalW alignment, red: AFILMPVW, green: CGHNTQSY, blue: DE, pink: KR.

In a detailed bioinformatic analysis of Cep135, Carvalho-Santos and colleagues found that Cep135 and its orthologue Bld10 contain two conserved regions (Carvalho-Santos et al., 2010), (Bld10/Cep135 CR1: residues 6-147 and Bld10/Cep135 CR2: residues 678-1021), apart from the highly coiled-coil regions. They identified a paralog of Cep135, `Tsga10`, by sequence similarity. Tsga10 is shorter than Cep135/ Bld10 and shares a high degree of similarity with Cep135/ Bld10 in the CR2 region. Tsga10 is the

testis-specific protein 10 and it is expressed in several human tissues such as testis, peripheral blood mononuclear cells, skin, isolated lymphocytes, keratinocytes and fibroblasts (Theinert et al., 2005). According to the EST database, chicken *Tsga10* (NCBI accession number XP_416892.2) is expressed only in testis tissue. BlastP analysis of chicken Cep135 and Tsga10 protein sequences displayed only 39% identity, indicating a low degree of similarity between these proteins.

In human Cep135 protein, three centrosome targeting domains were identified which cover the entire length of the protein (Ohta et al., 2002). In addition, it was reported that the C-terminal region of Cep135 binds to a 50-kDa subunit of the dynactin complex (Echeverri et al., 1996; Uetake et al., 2004) and interacts with C-NAP1 (Kim et al., 2008). However, the exact amino acid sequences in the C terminus of Cep135 responsible for these interactions are not known. Analysis of sequence homology at the C termini of human and chicken Cep135 showed that they share significant homology (71% overall identity). The similarities observed between chicken and human Cep135 on the protein and gene levels indicate that we have identified and cloned the chicken orthologue of human Cep135.

4.3 Cloning and mapping of the chicken *Cep135* genomic locus

To investigate the cellular functions of *Cep135*, we decided to use targeted gene disruption in the chicken B-cell line, DT40. Hyper-recombinogenic DT40 cell lines offer a more convenient system to deliver gene-targeted mutations than human cell lines (Buerstedde and Takeda, 1991).

Before designing a targeting vector to disrupt *cCep135*, more information was needed about this locus. Therefore, the full-length chicken *Cep135* cDNA sequence (as described in Section 4.2) was aligned with *cCep135* genomic sequence using Spidey (NCBI) to analyze the exon and intron structure of the *cCep135* locus. We found that *cCep135* lies on chromosome 4, therefore there are 2 copies of *Cep135* gene in DT40 cells. *cCep135* is a large gene with 25 exons that spans 30.039 kb. As shown in Table 4.2, comparison of the human exons with those identified in chicken reveals that there is a high level of synteny between these genes. Exons in both species are very similar in size, with the only major differences being the size of the exon 10 and the total number of exons. In addition, the exon 25 of *cCep135* (including the stop codon) consists of a

shorter sequence than the last exon of *hCep135*. We also looked at similarities in the genomic regions around human and chicken *Cep135*. We found *EXOC1* (encoding for exocyst complex component 1) upstream of *Cep135* in both human and chicken, further confirming the chicken sequence as the orthologue of *hCep135*.

Table 4.2 Analysis of synteny between human and chicken *Cep135*

Human exon	Exon length (bp)	Chicken exon	Exon length (bp)	Human exon	Exon length (bp)	Chicken exon	Exon length (bp)
1	113	**I**	113	**13**	78	**XIII**	78
2	191	**II**	191	**14**	152	**XIV**	152
3	168	**III**	168	**15**	116	**XV**	116
4	142	**IV**	142	**16**	155	**XVI**	155
5	85	**V**	85	**17**	56	**XVII**	56
6	129	**VI**	129	**18**	169	**XVIII**	169
7	216	**VII**	216	**19**	111	**XIX**	111
8	67	**VIII**	66	**20**	186	**XX**	186
9	138	**IX**	151	**21**	210	**XXI**	210
10	225	**X**	194	**22**	203	**XXII**	203
11	152	**XI**	144	**23**	105	**XXIII**	105
12	153	**XII**	144	**24**	102	**XXIV**	147
				-	-	**XXV**	22

4.4 Targeting of the chicken *Cep135* locus

As mentioned, the *cCep135* locus covers 30 kb in the chicken genome. Since recombination events become less efficient when the size of the targeted region is over 5 kb, we did not attempt to disrupt the entire *cCep135* locus. Little is known about the functional domains of Cep135, as explained in Section 4.3. Therefore we decided to delete as much of the coding region as possible, by targeting the 5` end of the *cCep135* locus including the start codon. The gene-targeting strategy that we used is shown in Figure 4.5. The targeted region contains the first 4 exons (including the start codon) that spread over 4.5 kb.

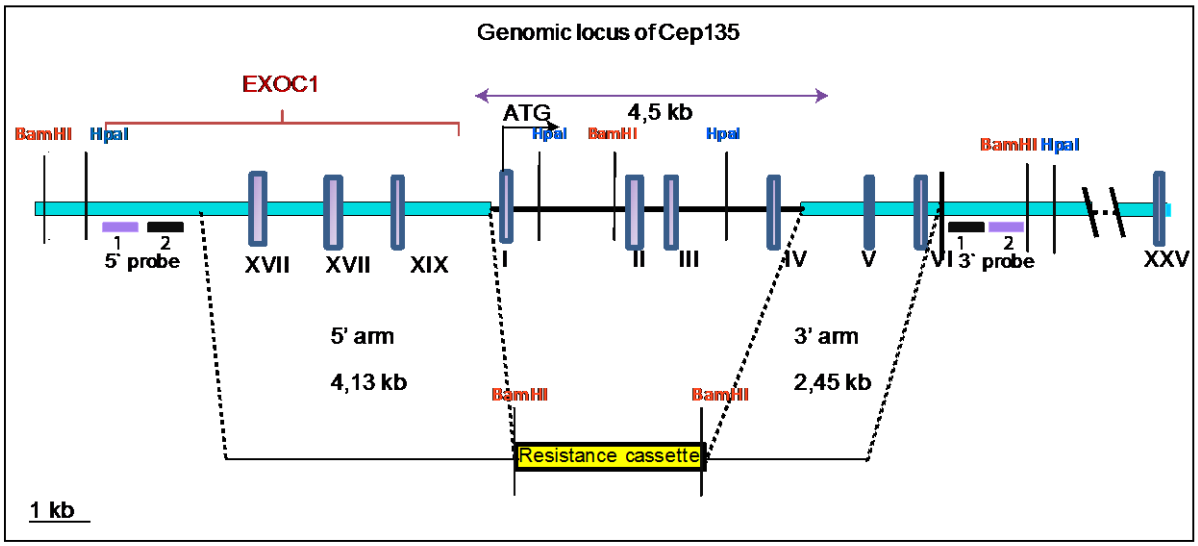

Figure 4.5 Gene-targeting strategy to disrupt the chicken *Cep135* genomic locus. Schematic representation of the *cCep135* genomic locus and the disruption construct. Boxes shown in Roman numerals represent the position of exons. HpaI and BamHI recognition sites are shown. Positions of the probes that were planned to be used in Southern blot analysis are indicated. In the targeting construct antibiotic resistance cassettes were flanked by 5` and 3` homology arms.

Gene disruption was to be mediated by replacement of the 5` end of the *cCep135* gene with antibiotic resistance cassettes under the control of the chicken *β-actin* promoter. Furthermore, the resistance cassette was flanked by homology arms (5'– 4.1kb and 3'– 2.4 kb). Firstly, to clone the targeting vectors, 5` and 3` homology arms were amplified by PCR using DT40 genomic DNA as template (section 2.2.1.4), then cloned into pBluescript and sequenced. The 5`arm contains intronic sequence of as well as the last three exons (exons #17, 18, 19) of *cExoc1*. To prevent any disruption of the *cExoc1* gene, the sequence of the 5` arm was verified before it was cloned into the targeting vector.

Since gene targeting efficiency may change with the resistance cassette used as a selection marker, four different targeting vectors were generated by subcloning the resistance cassettes (puromycin, blastocidin, histidinol and hygromycin) between the 5' and 3' homology arms using BamHI restriction sites. These vectors were named pPuro-Cep135, pBsr-Cep135, pHis-Cep135 and pHygro-Cep135, respectively. Before DT40 wild-type cells were transfected with the targeting vectors, 2 different 5' and 2 different 3' probes (Figure 4.5) were tested by cold and radioactive Southern Blot. We found that none of the probes tested by both methods recognised the predicted bands after genomic DNA digestions with BamHI or HpaI. This may be due to errors or polymorphisms in the genomic *Cep135* sequence in the database, or in other words the predicted

restriction sites on the genomic DNA may not exist. Another explanation is that due to the low annealing temperature of our probes, they may have been easily washed off the target DNA. An alternative approach to Southern blot for screening of the clones was to use a PCR-based strategy.

As shown in Figure 4.6A, a primer located downstream of the 3` arm (primer R) and a primer (primer C) located at the 3` end of the resistance cassette were used for screening by PCR-CR. Primer C was designed to be universal for all the resistance cassettes used in the targeting vectors. With PCR-CR, it was confirmed that the targeting construct was integrated in the correct genomic locus and not randomly inserted into the genome. The same reverse primers were used for positive control PCR for homozygous knockout screening. The deletion of the targeted region in homozygous knockout clones was confirmed by PCR-GR using primer R, and primer G, which is located within the targeted region. Both alleles of the *cCep135* gene were disrupted by sequential gene targeting and confirmed by PCR-CR and PCR-GR on genomic DNA as shown in Figure 4.6 A and B.

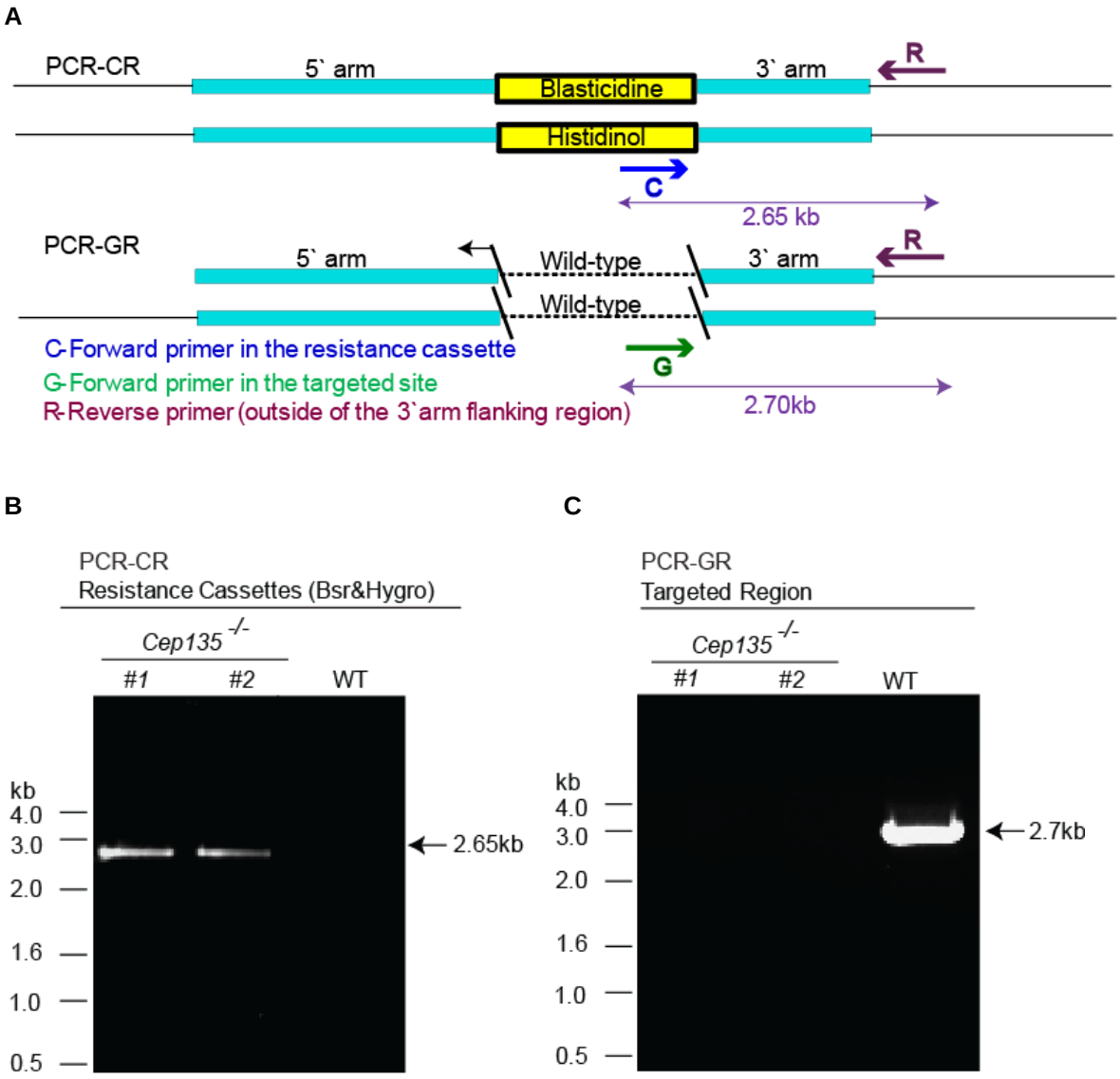

Figure 4.6 PCR analysis confirming targeted integration of the c*Cep135* knockout construct.
A. Schematic representation of two PCR sets to confirm gene disruption in *cCep135* locus. Insertion of the resistance cassettes to the *cCep135* locus were confirmed by PCR-CR using primers from areas outside the 3`arm (R) and in the resistance cassettes (C) Deletion of the targeted region was confirmed by PCR-GR using primers from the areas outside the 3`arm (R) and the targeted genomic region (G). Expected band sizes are 2700 bp for the wild-type allele and 2650bp for the null allele.
B. Genomic DNA from wild-type and the indicated clones were isolated and used for PCR analysis. With PCR-CR, targeted mutants were expected to yield a 2.65 kb DNA fragment, corresponding to the resistance cassettes.
C. In PCR-GR the wild type was expected to amplify a 2.7 kb DNA fragment corresponding to the targeted region. Knockout clones were not expected to produce any product, confirming the generation of double *Cep135* $^{-/-}$ knockout cell lines.

In the first round of targeting, 157 clones were screened. Targeting vectors with blasticidin and histidinol resistance cassettes showed roughly similar targeting efficiencies of 11% and 15%, respectively (Table 4.3). For the second round of targeting, one clone was chosen from the histidinol- or blasticidin- resistant heterozygotes and targeted with other vector to increase the possibility of obtaining a

knockout cell line. In total, 250 clones were screened and 5 clones were identified as targeted. Although the targeting efficiencies of the histidinol vector and blasticidin vector were similar in the first round of targeting, the efficiency was lower with the histidinol-resistance vector (0.7%) than with the blasticidin vector (3.7%) in the second round of targeting (Table 4.3).

Table 4.3 Targeting frequencies of the targeting vectors to generate *Cep135* heterozygous/ homozygous knockout

Background	Resistance	Number of clones screened	Number of targeted clones	Targeting efficiency
Wildtype	Histidinol	85	13	15%
Wildtype	Blasticidin	72	8	11%
Cep135 $^{+/-}$ **His**	Histidinol	142	1	0.7%
Cep135$^{+/-}$ **Bsr**	Blasticidin	106	4	3.7%

4.5 Characterisation of *Cep135* null DT40 cells

To confirm the PCR results, *cCep135* knockout DT40 cell lines were verified by reverse transcriptase-polymerase chain reaction (RT-PCR), Western blot and immunofluorescence microscopy. First, we performed RT-PCR analysis with mRNA isolated from wild type and *Cep135*-targeted cells using two different sets of primers (Figure 4.7A). *β-actin* primers were used as a positive control in RT-PCR experiments. We found that the full-length *cCep135* mRNA is transcribed in wild-type cells but not in knockout clones. To investigate if transcription had reinitiated downstream of the gene disruption, we performed another RT-PCR using the primers from the undisrupted region. This RT-PCR revealed that a truncated form of the *Cep135* gene is still transcribed at very low levels in the knockout clones (Figure 4.7B).

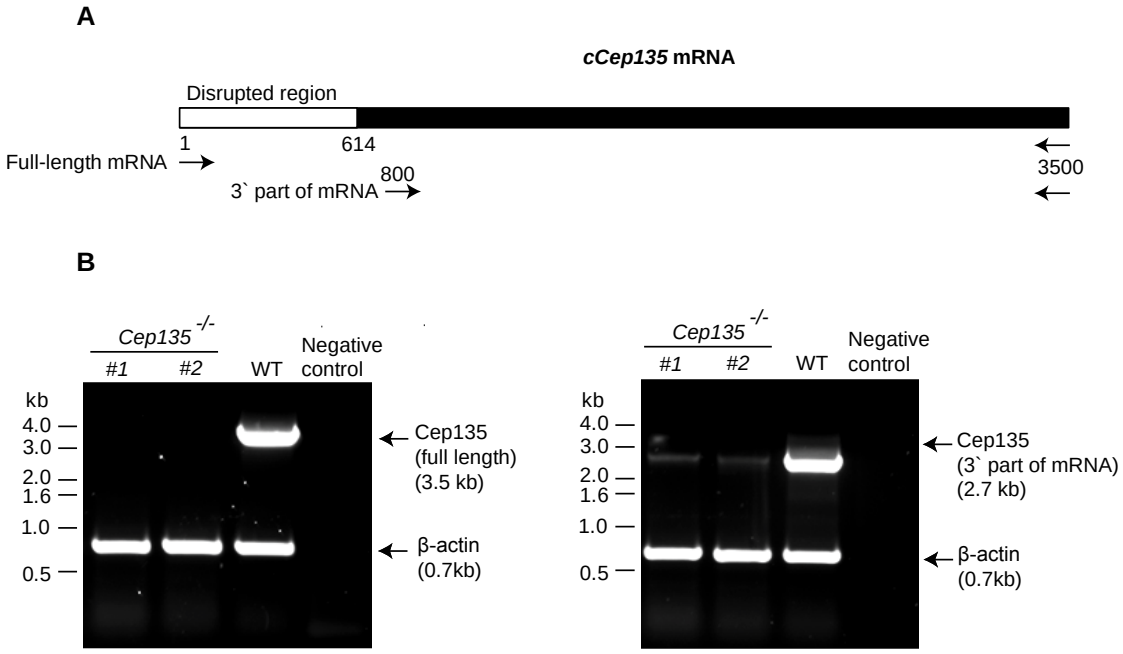

Figure 4.7 RT-PCR analysis of expression of the *Cep135* gene in wild-type and Cep135-deficient DT40 cells.
A. Schematic representation of *cCep135* mRNA showing the disrupted region of *Cep135* gene and the positions of the primers used in RT-PCR to test expression of *Cep135* mRNA.
B. Image of agarose gels showing RT-PCR amplification of full-length and 3`part of *Cep135* mRNA in wild-type DT40 cells and two *Cep135* targeted clones.

Next, to investigate whether the *cCep135*$^{-/-}$ cell lines were indeed deficient in Cep135 expression, we examined Cep135 protein levels by immunofluorescence microscopy and Western blotting. Cep135 antibodies were kindly provided by Ryoko Kuriyama (University of Minnesota, MN, USA), (Ohta et al., 2002). As shown in Figure 4.8A, Cep135 was present at centrosomes in wild-type cells, colocalising with γ-tubulin but was absent in knockout cells.

In wild-type DT40 cells, the Cep135 antibody recognised a protein of approximately 135 kDa on Western blots, similar to the band detected in the human cell line U2OS (Figure 4.8B). In *Cep135*$^{-/-}$ cells, no band corresponding to Cep135 protein was detectable by Western blot. We also did not detect any extra lower band (which was expected to be approximately 80kDa) on the blot that could represent a truncated form of the protein remaining from the undisrupted region of the *cCep135*. Since the Cep135 antibody that we used for Western blot analysis was raised against the C-terminal end of Cep135, any truncated form of this protein should have been detected by this antibody.

Together, our PCR, RT-PCR, Western blot and immunofluorescence analysis demonstrate that we have successfully generated *Cep135* knockout cell lines.

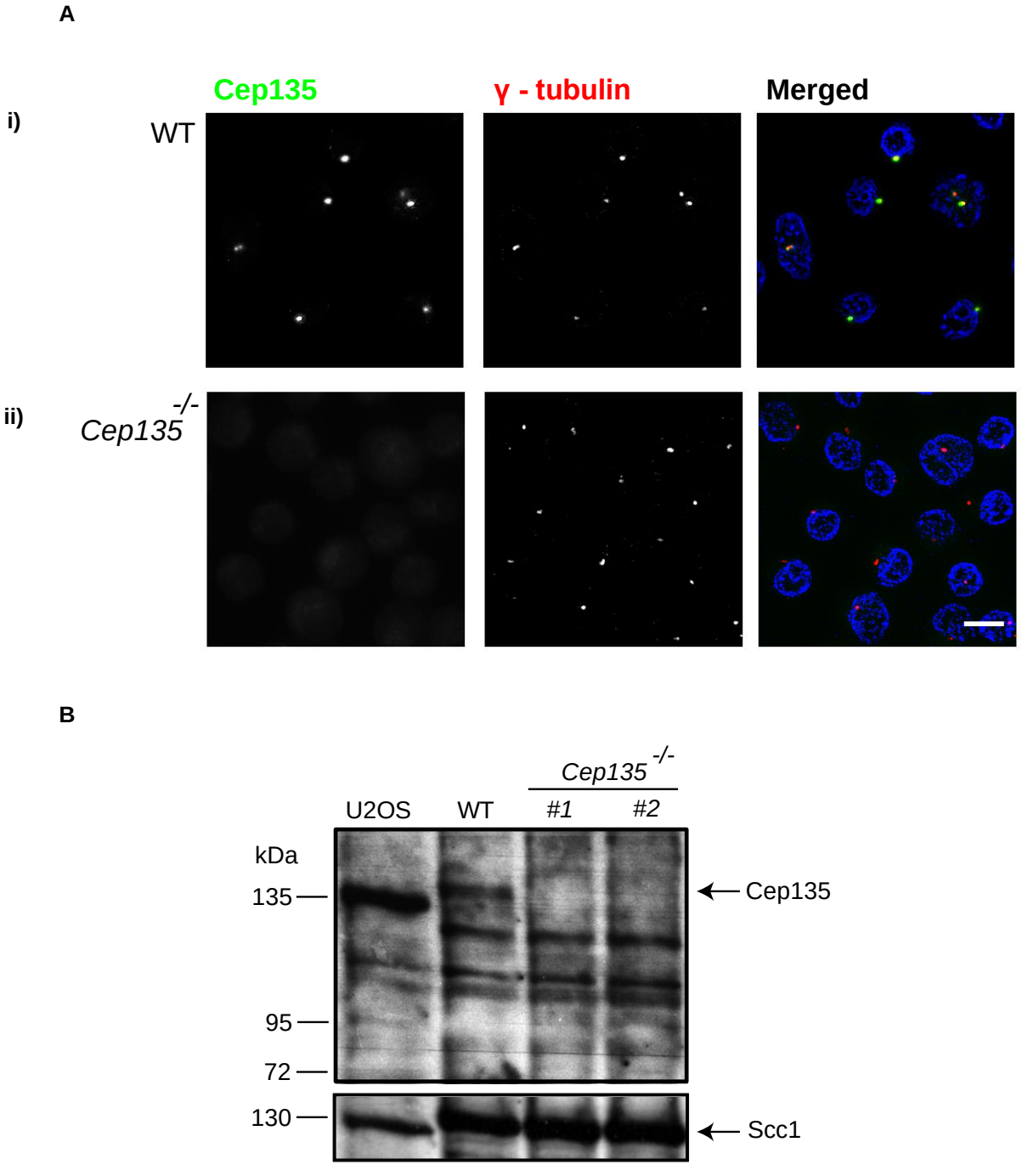

Figure 4.8 Analysis of Cep135-deficient cells at protein level.
A. Immunofluorescence microscopy analysis of (i) wild-type DT40 cells, (ii) *Cep135*-targeted clone. Cells stained with antibodies to Cep135 (anti-mouse) and γ-tubulin as a reference marker. DNA is blue, Cep135 is green and γ-tubulin is red in the merged images. Bar, 10 μm.
B. Western blots of total protein from human U2OS, wild-type DT40 cells and clone *Cep135*$^{-/-}$ #1 and #2 with Cep135 antibody (anti-rabbit). Scc1 serves as the loading control.

4.6 Basic phenotypic characterisation of *Cep135*$^{-/-}$ cell lines

Mutations in the *Cep135* orthologue *Bld10* gene in *Drosophila* produce viable but male sterile flies (Mottier-Pavie and Megraw, 2009). Depletion of *Cep135* by siRNA in Chinese hamster ovary (CHO) cells resulted in very slow growth rates (Ohta et al., 2002), suggesting that Cep135 could be required for viability. However, the chicken *Cep135* knockouts were viable, indicating that *Cep135* is not an essential gene in DT40 cells. To examine whether disruption of *cCep135* affected cell growth, we analysed proliferation rates in wild-type cells and 2 *Cep135*$^{-/-}$ clones every 24h over a 72h time period. As plotted in Figure 4.9, the proliferative kinetics of *Cep135* knockout clones and wild-type cells were indistinguishable. Thus, we conclude that Cep135 is not required for the proliferation of DT40 cells.

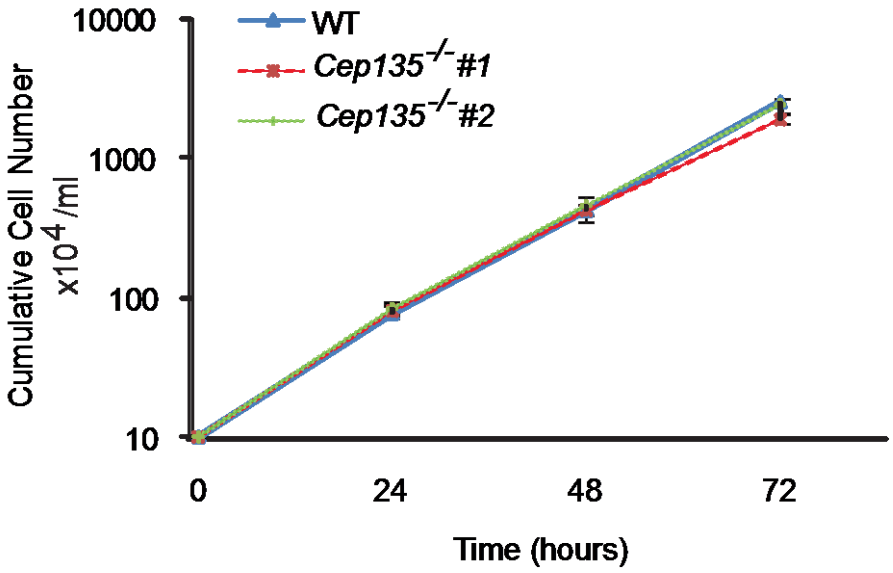

Figure 4.9 Proliferation analysis of *Cep135* knockout DT40 cells. Cells were seeded at 10^5/ml and cell numbers were counted over 72h. Data show the mean ± SD of three separate experiments.

Flow cytometry was performed to analyse the cell cycle profile of Cep135-deficient cells in detail. Cell cycle analysis with PI displayed the same distribution of DNA content in different phases of the cell cycle in wild-type and *Cep135* knockout cells (Figure 4.10A). Quantitative analysis of stages in the cell cycle was performed in exponentially growing wild-type and Cep135-deficient cells, stained for incorporated BrdU and total DNA levels. Both wild-type and Cep135-deficient cells have similar number of cells in G1, S and G2/M phases of cell cycle (Figure 4.10B). This analysis revealed that Cep135-deficient cell lines appear to be cycling normally without any

delay at any of the cell cycle stages. To assess whether there were any changes in the mitotic index of Cep135-deficient cells, we performed flow cytometry for histone H3 phosphorylation, which is an indicator of late G2 and mitotic cells (Zeitlin et al., 2001). As expected, wild-type and Cep135-deficient cells displayed similar levels of PH3 positive cells, which shows that *Cep135*$^{-/-}$ cells do not show any delay or arrest during mitosis (Figure 4.10C).

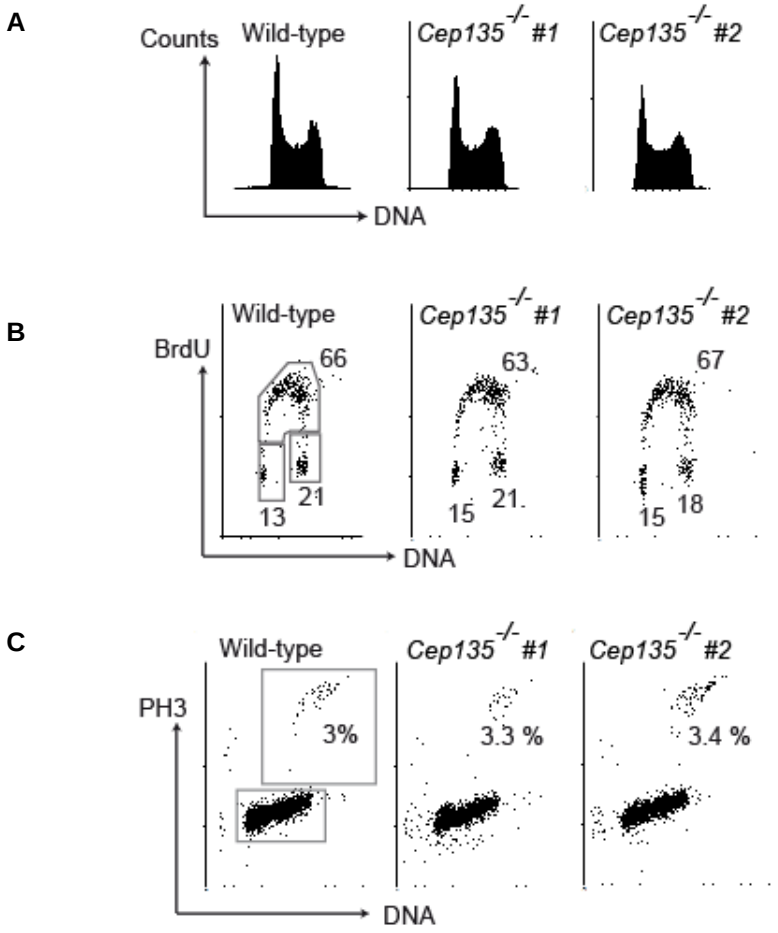

Figure 4.10 Cell cycle analysis of *Cep135* knockout DT40 cells by flow cytometry.
A. Cell cycle profile of wild-type cells and two *Cep135*$^{-/-}$ clones stained with propidium iodide.
B. Quantitative cell cycle analysis of asynchronous cells of the indicated genotype stained for incorporated BrdU and total DNA levels. BrdU incorporation was monitored with an FITC-anti-BrdU antibody (vertical axis) and DNA content by propidium iodide staining (horizontal axis). The G1 (bottom left), S (top), and G2/M (bottom right) gates are indicated in boxes, and the numbers refer to the percentage of cells detected in each of the gates averaged from three separate experiments.
C. Mitotic indices for wild-type, and two *Cep135*$^{-/-}$ clones were determined by the late G2/M-phase marker phosphorylated histone H3 (PH3). The numbers refer to the percentage of cells in M-phase averaged from three separate experiments.

Overall the growth curve and flow cytometry analyses indicate that Cep135 function is not necessary for normal cell proliferation and mitosis. From these results, we concluded that Cep135 is dispensable for the viability of DT40 cells.

4.7 Cep135-deficient centrosomes are fully functional during mitosis

It has been demonstrated previously that changes in Cep135 protein levels in CHO cells caused disorganized, unfocused microtubule arrays, resulting in abnormal mitotic spindles with multipolarity in some cells (Ohta et al., 2002). The same authors have also shown that Cep135 has an important role in the recruitment of dynamitin (a 50-kDa subunit of the dynactin complex) to the centrosomes and that Cep135 interacts with dynamitin in centrosomes (Uetake et al., 2004). Dynactin has an important role in anchoring microtubules at the centrosome (Echeverri et al., 1996) and the p50 dynactin subunit is involved in assembly and maintenance of the functional MTOCs at the centrosomes (Quintyne et al., 1999). Although we did not see any changes in the mitotic index and cell cycle distribution of *Cep135*$^{-/-}$ cells, because of the important roles attributed to Cep135 in organizing microtubules, we decided to further explore the effects of Cep135 deficiency on microtubule formation and the establishment of the mitotic spindle.

First, we examined the organization of mitotic spindles at different stages of mitosis by immunofluorescence microscopy. Centrosomes and microtubules were stained for γ-tubulin and α-tubulin, respectively. DNA was visualized by DAPI staining. As shown in Figure 4.11A, we did not observe any abnormalities in mitotic microtubules or mitotic chromosomes at any phase of mitosis. We next analyzed the percentage of cells in each phase of mitosis. As shown in Figure 4.11B, we observed wild-type distribution of cells in the different phases of mitosis in the absence of Cep135. We also saw similar level of multipolarity in Cep135-deficient cells as in wild-type cells.

A

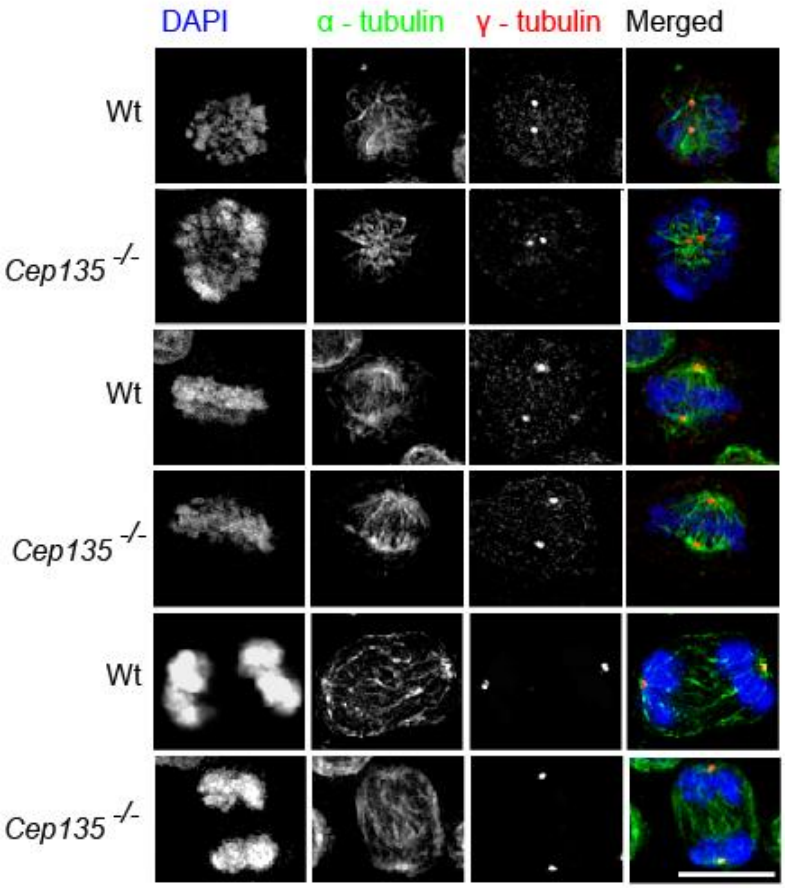

B

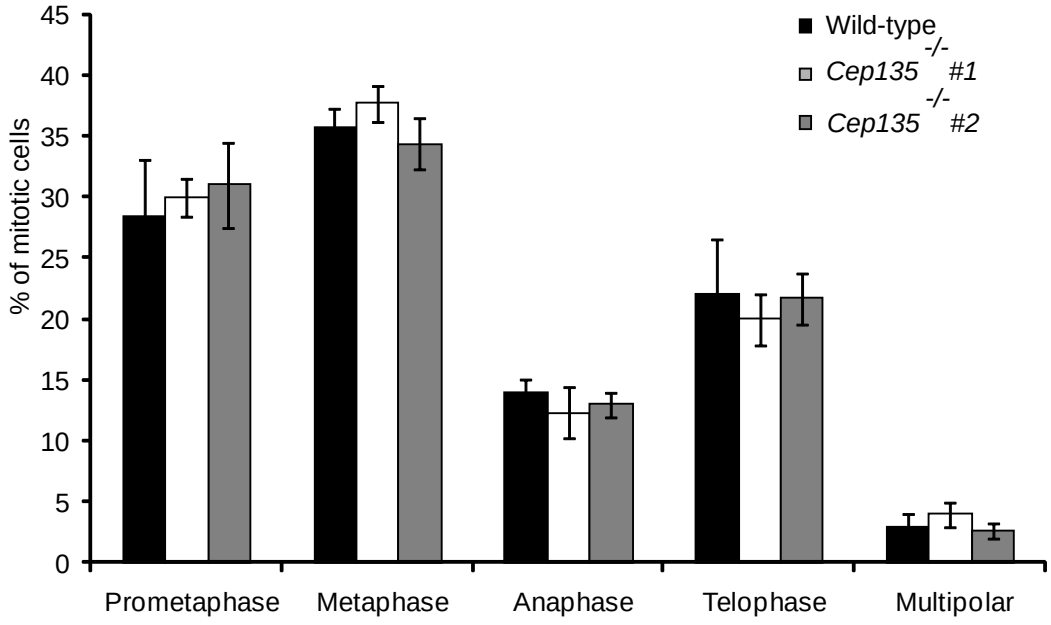

Figure 4.11 Microscopy analysis of mitotic phases in wild-type and *Cep135*$^{-/-}$ cells.
A. Immunofluorescence images of mitotic cells of the indicated genotype stained with antibodies to α-tubulin (red) and γ-tubulin (green). Scale bar, 10 μm.
B. Number of cells in prometaphase, metaphase, anaphase, telophase and multipolar cells were assayed by anti-α-tubulin, anti-γ-tubulin and DAPI staining. Data show the mean ± SD of three separate experiments in which at least 100 cells were scored.

We found that mitotic spindles in Cep135-deficient cells were bipolar, with γ-tubulin localized exclusively at the spindle poles and the chromosomes aligned at the metaphase plate as in wild-type cells (reviewed by Karsenti and Vernos, 2001). To examine if there was a change in metaphase spindle length in *Cep135* null cells, we determined the metaphase spindle length by measuring the distance between the 2 Centrin spots in metaphase cells defined by BubRI localization (Zhang et al., 2007) (figure 4.12A). Spindle lengths in Cep135-deficient cells were found to be 7.66±0.84μm and in wild-type cells, 7.40±0.97μm, showing no significant difference.

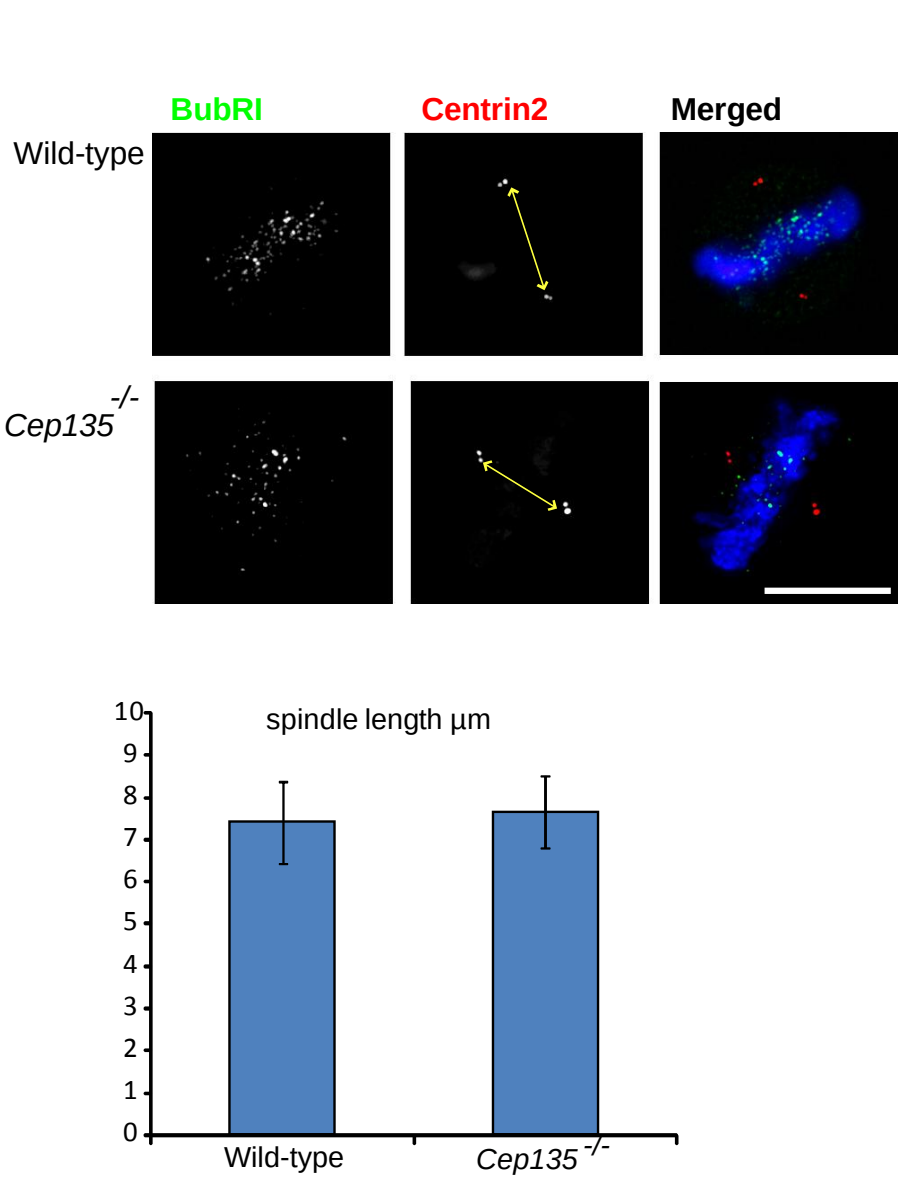

Figure 4.12 Spindle length at metaphase is normal in *Cep135*$^{-/-}$ cells. A. Centrin2 antibody (red) was used to define the spindle pole and BubRI antibody (green) was used to define the metaphase plate with *DAPI* (blue) staining. Bar 10 μm. Metaphase spindle length was measured by the distance (yellow arrow) defined by 2 Centrin spots in metaphase cells. **B.** Graph showing the spindle length measurement in wild-type and *Cep135*$^{-/-}$ DT40 cell lines. Data show the mean ± SD of measurements in 50 metaphase cells for each cell line.

To extend our analysis of mitosis in Cep135-deficient cells, we measured the duration of mitosis by live cell imaging. In order to perform live cell imaging experiments, we generated wild-type and Cep135-deficient cells that stably express histone H2B-RFP. These cells were imaged every 3 minutes for a total of 3 hours (Figure 4.13). The mean time taken from chromosome condensation to decondensation was found to be 42.98 min in wild-type cells and 42.97 min in Cep135-deficient cells (Figures 4.13, 4.14A). Furthermore, the mean time from the beginning of prometaphase to the end of metaphase and the mean time from the beginning of anaphase to the end of telophase were almost same in both cell lines (Figure 4.14B). Live imaging of mitosis revealed that the duration of mitosis in wild-type and Cep135-deficient cells is the same and confirmed that mitotic progression is normal in cells lacking Cep135.

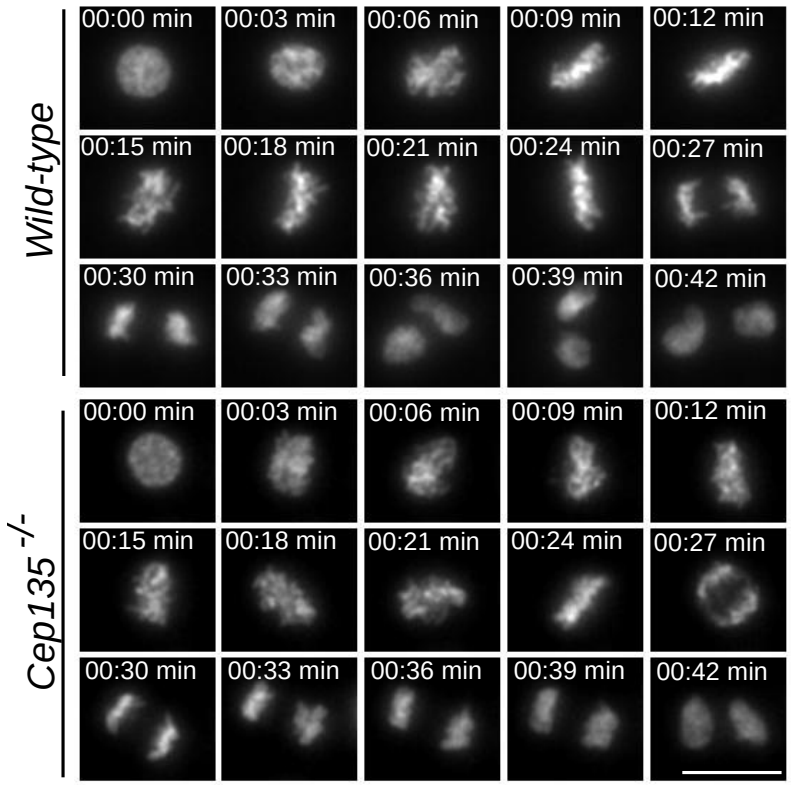

Figure 4.13 Live-cell imaging of mitosis in wild-type and *Cep135*$^{-/-}$ DT40 cells. Wild-type and *Cep135*$^{-/-}$ cells that stably expressed histone H2B-RFP were imaged by time-lapse microscopy. Frames from time-lapse experiments following wild-type and *Cep135*$^{-/-}$ cells.

A

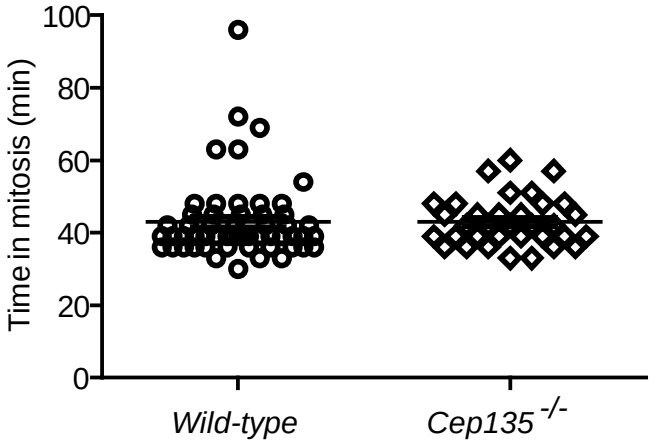

B

Genotype	Prometaphase –Metaphase (Mean)	Anaphase –Telophase (Mean)	Total time in mitosis (min)
Wild-type-H2B-RFP	29.34 ± 11.13	13.63 ± 2.14	42.98 ± 11.12
Cep135$^{-/-}$ -H2B-RFP	29.02 ± 6.70	13.94 ± 1.45	42.97 ± 6.757

Figure 4.14 Duration of mitosis in Cep135-deficient cells.
A. Graph shows time in mitosis in minutes, each data point represents one cell.
B. Table summarizes the mean of time in mitosis and the mean time from the beginning of prometaphase to the end of metaphase and the mean time from the beginning of anaphase to the end of telophase. Data show mean ± SD for the 50 individual cells analyzed in 3 different experiments. (Live cell imaging experiments of wild-type-H2B-RFP cells were performed in collaboration with Tiago J. Dantas).

4.8 Microtubule nucleation is normal in Cep135-deficient cells

γ-tubulin is a key factor in centrosomal microtubule nucleation (Moritz and Agard, 2001; reviewed by Raynaud- Messina and Merdes, 2007). Although we could not detect any abnormalities in α-tubulin or γ-tubulin localisation at the centrosomes of mitotic *Cep135*$^{-/-}$ cells (see figures 4.8A, 4.11A), we wanted to examine if Cep135 deficiency had any effect on microtubule nucleation. Therefore, we assessed microtubule nucleation using Centrin2 to locate centrosomes, DAPI for DNA and α-tubulin for microtubule asters. We counted the cells with aster nucleation after microtubule regrowth for 1 min at 39.5°C (Figure 4.15A). We found that microtubule recovery from nocodazole-induced depolymerisation was indistinguishable between mitotic wild-type and *Cep135*$^{-/-}$ centrosomes (Figure 4.15B). This indicates that Cep135 deficient centrosomes are competent in microtubule nucleation.

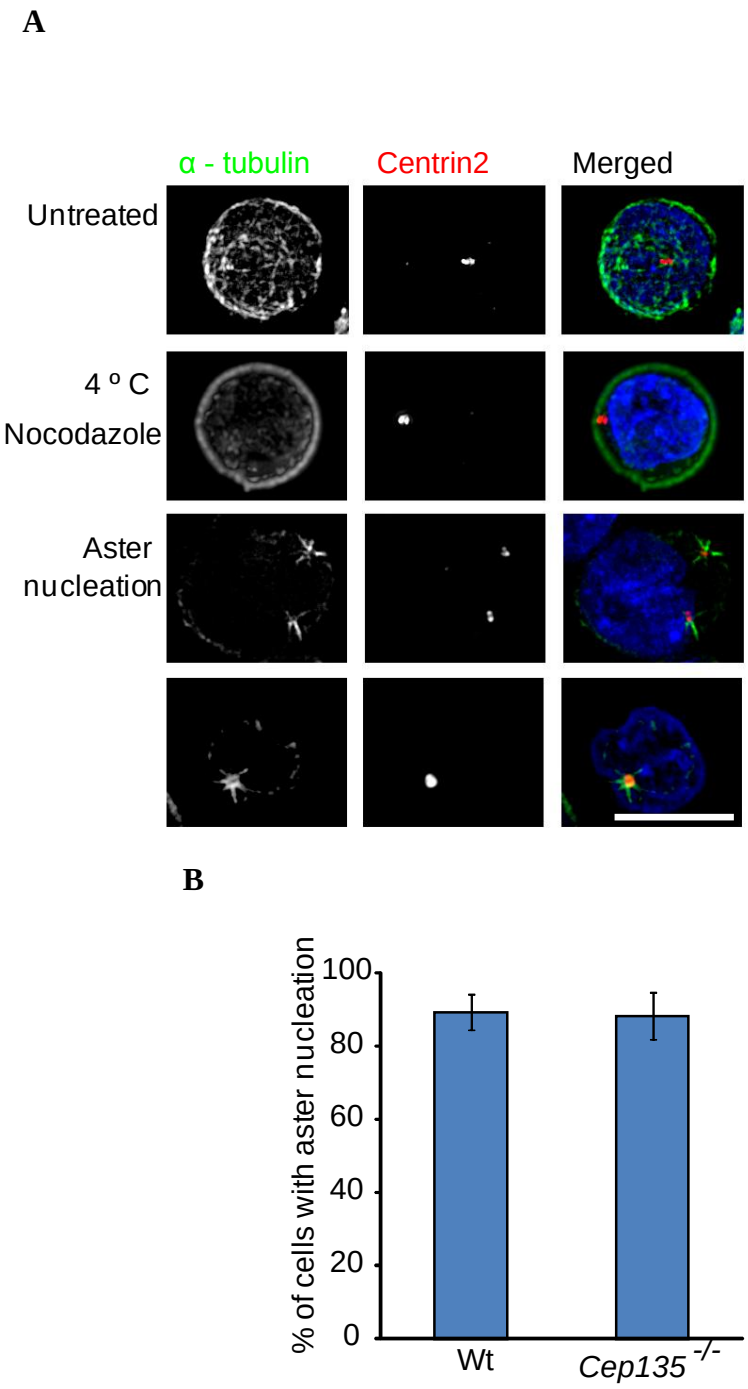

Figure 4.15 Microtubule regrowth is normal in Cep135-deficient cells.
A. Immunofluorescence microscopy analysis of microtubule nucleation in DT40 cells before and after release from 3-h arrest in 1 μg/ml nocodazole at 4°C. Cells were stained with antibodies to α-tubulin (green) and Centrin2 (red). DNA (blue) visualized with DAPI staining before imaging. Bar, 10 μm.
B. Graph shows the quantitation of the percentage of cells with aster nucleation after microtubule regrowth for 1 min at 39.5°C. Histogram shows mean ± SD of three separate experiments in which at least 200 cells per experiment were counted.

4.9 Discussion

4.9.1 Cloning and analysis of chicken *Cep135* cDNA

Since our main aim was the targeted disruption of *Cep135* locus in DT40 cells, we carried out an extensive bioinformatic analysis to characterise the *cCep135* genomic locus and *cCep135* cDNA in detail. First we determined the 5` end of *cCep135* cDNA by RACE PCR using primers from the predicted *cCep135* sequence in the Ensembl database. A Kozak sequence and an ATG codon that is in frame with the rest of the sequence were successfully determined and this information led us to design a forward primer for the cloning of the *Cep135* cDNA. The full-length chicken c*Cep135* cDNA was successfully cloned and the predicted sequence information in the Ensembl database was found to be correct with the exception of lacking 39 nucleotides in the sequence. We found that the chicken Cep135 protein is very similar to vertebrate as well as *Drosophila* and *Xenopus* orthologues. Many centrosome protein clusters contain multiple coiled-coil domains (Rose et al., 2005). As expected, we found that chicken Cep135 comprises extensive alpha-helical and coiled-coil domains, similar to its orthologues and to other centrosome proteins. The hypothetical leucine zipper and the putative tyrosine phopshorylation motifs, that has been shown in human Cep135 (Ohta et al., 2002), were also found to be conserved in all organisms examined, suggesting that Cep135 structure has been conserved throughout the evolution. Our detailed bioinformatic analysis of *cCep135* cDNA verified that we have successfully cloned the chicken homologue of Cep135 protein.

4.9.2 Generation of *Cep135* null cell lines and basic phenotypic characterization

With the information obtained from the analysis of chicken Cep135 at the mRNA and protein level we were able to design and generate a targeting construct to disrupt the chicken *Cep135* locus. Comparison of Cep135 sequence with the available genomic sequence for the *Cep135* locus in the NCBI database led us to identify the intronic and exonic regions in chicken *Cep135*. The *cCep135* locus was found to comprise 30039 bb in length and to contain 25 exons. Further comparison of the chicken and human *Cep135* loci showed that there is high level of synteny between these genes, with similar numbers and length of exons. In addition, we noticed that in both species the 3`end of *EXOC1* gene overlaps with the 5` end of the *Cep135* gene.

A *Cep135* targeting construct was designed to target the 5`end of *Cep135* disrupting the first 4 exons of the gene including the ATG. Since *Cep135* is on chromosome 4, two rounds of targeting were performed. In the first round of targeting we obtained many clones and these clones were screened successfully by a PCR strategy that confirmed the targeted integration of the blastocidin or histidinol resistance cassette and the deletion of the targeted site in the *Cep135* genomic locus.

It was shown previously that *Chlamydomonas reinhardtii* cells carrying mutations in *Bld10* (orthologue of *cCep135*) displayed mitotic defects and slower growth rates than wild-type cells (Matsuura et al., 2004). Mutations in *Drosophila/ Bld10* resulted in viable but infertile male flies, with shorter centrioles and basal bodies compared to wild-type cells (Mottier-Pavie and Megraw, 2009). Similarly, RNAi-mediated *Cep135* knockdown studies in *CHO cells* revealed that cells grow slowly in the absence of Cep135 (Ohta et al., 2002). Since these studies showed that *Cep135* is an important gene for cell viability, we initially thought that *Cep135* would be an essential gene in DT40 cells. Therefore, in case of any failure in the second round of targeting we decided to use a conditional expression system in which DT40 cells express the tetracycline-regulated *cCep135* transgene. However, in the second round of targeting we obtained 5 clones that were successfully targeted in both *Cep135* alleles. Further characterization of the 2 selected clones confirmed that we successfully generated *Cep135* knockout cell lines.

A detailed bioinformatic study performed by Carvalho-Santos and colleagues revealed that together with Bld10/Cep135, several components of centriole and basal body (CBB) structure such as Sas-6, Sas-4/CPAP are evolutionarily conserved throughout eukaryotes (Carvalho-Santos et al., 2010). Given the evolutionary conservation of Cep135 and its requirement for maintaining the CBB structure, the viability of *Cep135*$^{-/-}$ cells was unexpected. However, contrary to our expectations, we found that *Cep135*$^{-/-}$ cells were viable without any obvious growth defects and we also established that *Cep135*$^{-/-}$ cells were morphologically normal. Growth curve analysis confirmed this observation and showed that growth rate of *Cep135*$^{-/-}$ cells was indistinguishable from that of wild type. Cell cycle analysis in *Cep135* null cells revealed that Cep135 is not required for normal cell cycle progression or normal mitosis.

We do not know why *Cep135* null DT40 cells are viable and why the absence of this protein does not cause any defects in growth or mitosis. One possible explanation for this is the existence of an unknown/known centrosomal protein that is functionally redundant with Cep135 in chicken DT40 cells. A second possible explanation is that the absence of p53 could allow to DT40 cells to respond in different ways to overcome the absence of Cep135 than did *Drosophila* and *Chlamydomona* cells. Also, since DT40 cells cannot grow cilia (Alieva and Vorobjev, 2004) and mutant *Cep135* causes defects during basal body/flagella formation in *Drosophila*,and *Chlamydomonas* cells (Mottier-Pavie and Megraw, 2009; Carvalho-Santos et al., 2010; Dobbelaere et al., 2008; Matsuura et al., 2004; Nakazawa et al., 2007), it is possible that the extent of Cep135 requirement for cell viability and function may be cell-type specific. Similar to Cep135, Centrin function is important in ensuring centriole/basal body assembly and its function is conserved throughout evolution in eukaryotes (Salisbury, 2007). It has been shown that *Centrin* depletion by RNAi in hTERT-RPE1 cells results in slow growth and cell cycle delay or death (Salisbury et al., 2002; Kleylein-Sohn et al., 2007; Mikule et al., 2007). Contrary to expectation the observed phenotype of *Cep135* knockout in DT40 cells was similar to that of *Centrin*-deficient DT40 cells: no effect on cell viability and cell cycle progression (Dantas et al., 2011). In another knockout study in DT40 cells, it has been shown that loss of the telomere repeat-binding protein Trf1 resulted in viable cells although it had been shown that it is required for embryonic viability and for embryonic stem cell proliferation in mouse (Cooley et al., 2009). These observations, together with our results, raise the possibility that the effects of Cep135 loss would vary in different systems and the dispensable character of Cep135 is peculiar to a transformed cell line such as DT40.

4.9.3 Mitosis and microtubule nucleation is normal in Cep135-deficient cells

Centrosomes are responsible for nucleating and organizing microtubules in animal cells (Schnackenberg and Palazzo, 1999). Specifically, γ-tubulin, which is a component of the γ-tubulin ring complex, nucleates microtubules from their minus ends towards the (+) direction (Moritz et al., 1995). The microtubule motor protein, dynein, and its activator dynactin are involved in focusing the minus ends of microtubules at centrosomes (Quintyne et al., 1999). Previous studies suggested that Cep135 is involved in the recruitment of dynamitin to the centrosomes and through their interaction with dynamitin, microtubule minus ends are connected to Cep135 (Uetake et al., 2004). The

authors showed that in CHO cells in which *Cep135* or *p50* was depleted via RNAi, microtubule renucleation was inhibited after release from nocodazole treatment. In addition, Cep135 has been implicated in the organization of functional mitotic spindles and completion of cytokinesis. RNAi-mediated depletion of *Cep135* in CHO cells caused abnormal mitotic spindles: some cells had monopolar or multipolar spindles and some cells showed disorganized microtubule arrangements (Ohta et al., 2002). Therefore, we predicted that disruption of *Cep135* in DT40 cells would cause abnormalities in the organization and nucleation of microtubules, as well as in mitotic spindles.

However, our detailed analysis of Cep135 involvement in mitosis and microtubule formation in *Cep135*$^{-/-}$ background in DT40 cells did not provide any support for this prediction. In *Cep135*$^{-/-}$ DT40 cells, several lines of evidence have indicated that cell-cycle progression occurs in mitotic cells with normal spindles and Cep135-deficient centrosomes are fully functional during mitosis: 1) No difference was observed in mitotic index and the distribution of cells in mitotic phases between wild-type and *Cep135* null cells. 2) The duration of mitosis was very similar to that of wild type cells. 3) Metaphase spindle lengths of *Cep135* null cells showed no difference from those of wild-type cells. 4) Microtubule formation and organization of mitotic spindles at different phases of mitosis was found to be normal in *Cep135* null cells. 5) We did not observe any increase or decrease in the level of cells with monopolar or multipolar spindles. 6) The kinetics of microtubule recovery from nocodazole-induced depolymerisation were normal in Cep135-deficient centrosomes.

These findings, together with our cell proliferation assays, confirm that *Cep135*$^{-/-}$ cells show no obvious phenotypic differences in terms of viability, mitosis and microtubule nucleation from the parental DT40 line. We cannot explain why Cep135 is not required for microtubule formation and mitotic centrosome function in DT40 cells. However we cannot exclude the possibility that undetectable levels of truncated Cep135 expression in these cells could have been rescued the expected phenotype. Nevertheless, performing a more sensitive assay for the microtubule organization could provide more insight into roles of Cep135 in microtubule organization (Ohta et al., 2002).

Chapter 5
Characterisation of *Cep135* $^{-/-}$ DT40 cells

5.1 Introduction

Previous studies have shown that down-regulation of *Cep135/Bld10* by RNAi or mutations causes changes in centrosome structure and composition in human, mouse, *Chlamydomonas*, *Paramecium* and *Drosophila* cells (Kleylein-Sohn et al., 2007; Ohta et al., 2002; Uetake et al., 2004; Jerka-Dziadosz et al., 2010; Kim et al., 2008). Studies in human cells have implicated Cep135 in Plk4-induced centriole biogenesis (Kim et al., 2008). Therefore, we sought to further assess the role of Cep135 in centrosome structure and biogenesis in DT40 cells. In this study we found that ablation of chicken Cep135 had no detectable effect on centriole composition and centriole duplication. However, ultrastructural analysis of *Cep135*$^{-/-}$ cells revealed a novel electron-dense structure in the centriolar lumen.

In addition to its critical role in formation of bipolar mitotic spindles, the centrosome is involved in the cellular response to DNA damage (Sato et al., 2000). Centrosome amplification occurs in DT40 cells in response to ionizing radiation (IR) through a mechanism that requires an extended G2 arrest (Dodson et al., 2004) and the kinase activities of several cell cycle regulatory and DNA damage response proteins such as ATM, ATR, Chk1 and Cdk2 (Dodson et al., 2004; Bourke et al., 2007). Centrosome amplification can also occur during an extended S-phase induced by DNA synthesis inhibitors such as hydroxyurea (HU) in p53-deficient cells and it requires Cdk2-cyclin E activity (Balczon et al., 1995; Lacey et al., 1999; Hinchcliffe et al., 1999; Duensing et al., 2006; Prosser et al., 2009). To investigate whether Cep135 has any role in DNA damage-induced centrosome amplification we used *Cep135*$^{-/-}$ DT40 cell lines. Here we report that DT40 cells lacking Cep135 exhibit a significant increase in HU-induced centrosome overduplication.

5.2 Cep135 deficiency has no detectable impact on centrosome composition

To investigate the consequences of Cep135 deficiency on DT40 centrosomes, we first analysed the centrosome composition both in wild-type and Cep135-deficient DT40 cells by immunofluorescence microscopy using antibodies specific to the various centrosome components (Figure 5.1). Since it had been proposed that Cep135 is a scaffolding protein and important for the maintenance of the structural integrity of the pericentriolar material (Ohta et al., 2002), we examined the localization of PCM components such as PCM-1, γ-tubulin, Aurora-A and glutamylated tubulin (Prigent et al., 1996) in these cells. Our analysis revealed that Cep135-deficient centrosomes contained PCM-1, γ-tubulin, glutamylated tubulin and Aurora-A. Since PCM-1 is a major component of pericentriolar satellites which is required for targeting many centrosomal proteins to the centrosomes and microtubule anchoring (Dammermann and Merdes, 2002), PCM-1 staining indicated that centrosomal integrity was not perturbed in *Cep135* null cells. In addition, glutamylated tubulin staining showed that Cep135-deficient centrioles contained polyglutamylated, stabilized microtubules. Centrosome maturation requires recruitment of pericentriolar proteins such as Aurora-A to increase the microtubule nucleation activity in G2 and mitosis (reviewed by Barr and Gergely, 2007). We observed that Aurora-A localization was intact in *Cep135* null cells during G2 phase and mitosis, suggesting that centrosome maturation was normal (Figure 5.1).

We also analyzed the localization of Centrin and Cep76 in these cells. Centrin2 and Cep76 are structural centriolar components that localizes to centrioles throughout the cell cycle (Salisbury et al., 1988; Salisbury, 1995; White et al., 2000; Tsang et al., 2009). Centrin2 and Cep76 displayed a typical centriolar localization in interphase cells, also confirming that Cep135-deficient centrioles were structurally intact. Ninein is a component of the subdistal appendages of mature centrioles and is important not only in microtubule anchoring but also in microtubule nucleation (Mogensen et al., 2000; Delgehyr et al., 2005). Immunofluorescence examination of Cep135-deficient centrioles using an anti-ninein antibody revealed that ninein localizes normally to the Cep135-deficient centrosomes, as did pericentriolar and centriolar markers (Figure 5.1).

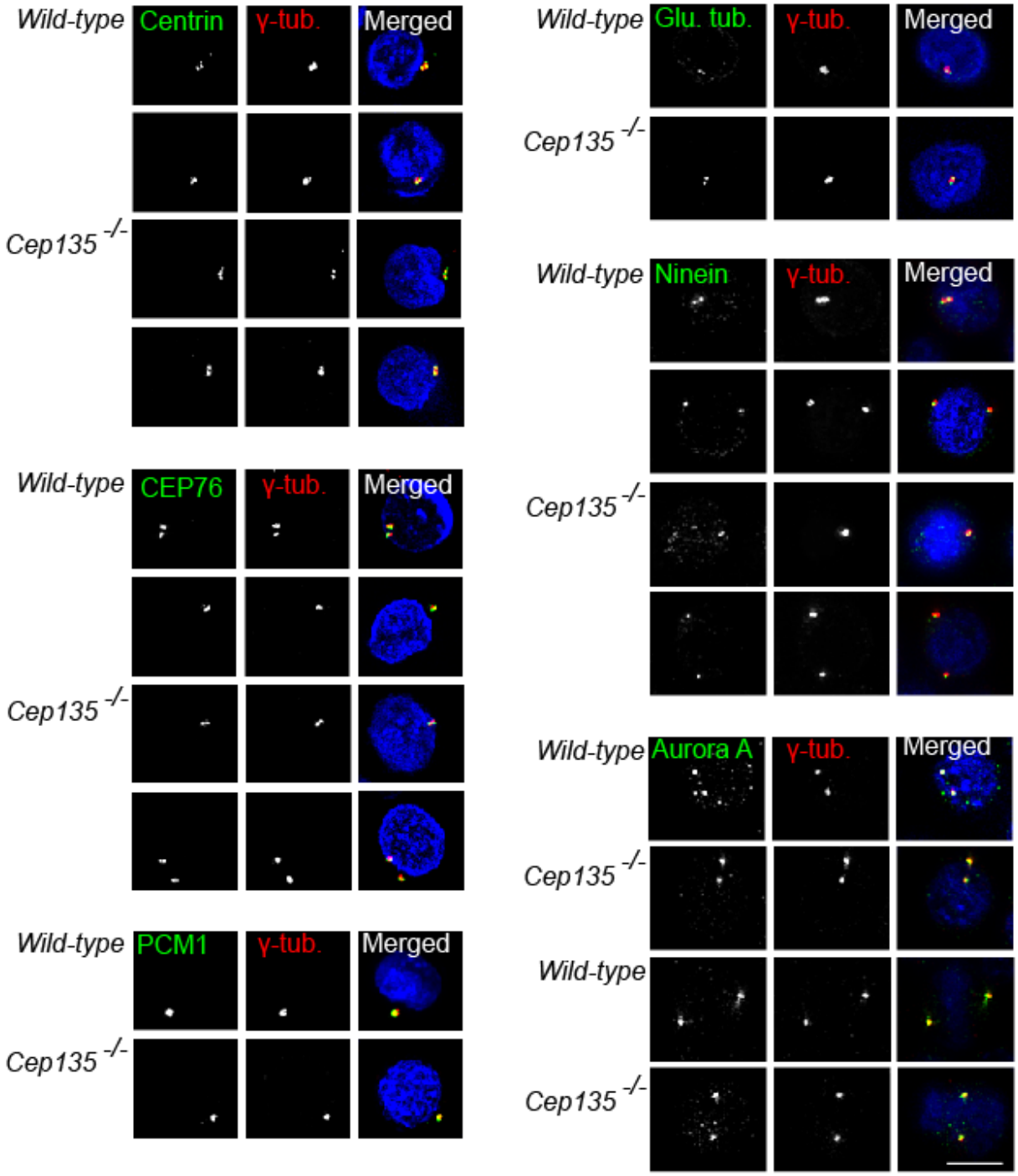

Figure 5.1 Immunofluorescence microscopy analysis of wild-type and *Cep135*$^{-/-}$ DT40 cells. Cells were fixed in methanol and stained with the following antibodies to centrosomal or centrosome-associated proteins: γ-tubulin (red), Centrin2, Cep76, PCM-1, glutamylated tubulin, Ninein and Aurora-A (green). Cells were then counterstained with DAPI (blue). Scale bar, 5μm.

It has been shown that siRNA depletion of *Bld10* causes PCM maturation defects in *Drosophila* cells (Dobbelaere et al., 2008). To further investigate the effects of Cep135 deficiency on PCM components, we measured the intensity levels of the pericentriolar components PCM-1 and CDK5RAP2 (Fong et al., 2008) in wild-type and *Cep135*$^{-/-}$ DT40 cells. Cells were stained with anti-PCM-1 or anti-CDK5RAP2 and anti-

γ-tubulin antibodies. The average of total γ-tubulin intensity for each cell line was used as a normalization factor, as described in Section 2.2.4.1. The relative intensities of both PCM-1 and CDK5RAP2 were slightly decreased in Cep135-deficient cells compared to wild-type cells, but this decrease was not significant for either PCM-1 or CDK5RAP2 levels, indicating that PCM integrity was normal in *Cep135* null cells (Figure 5.2).

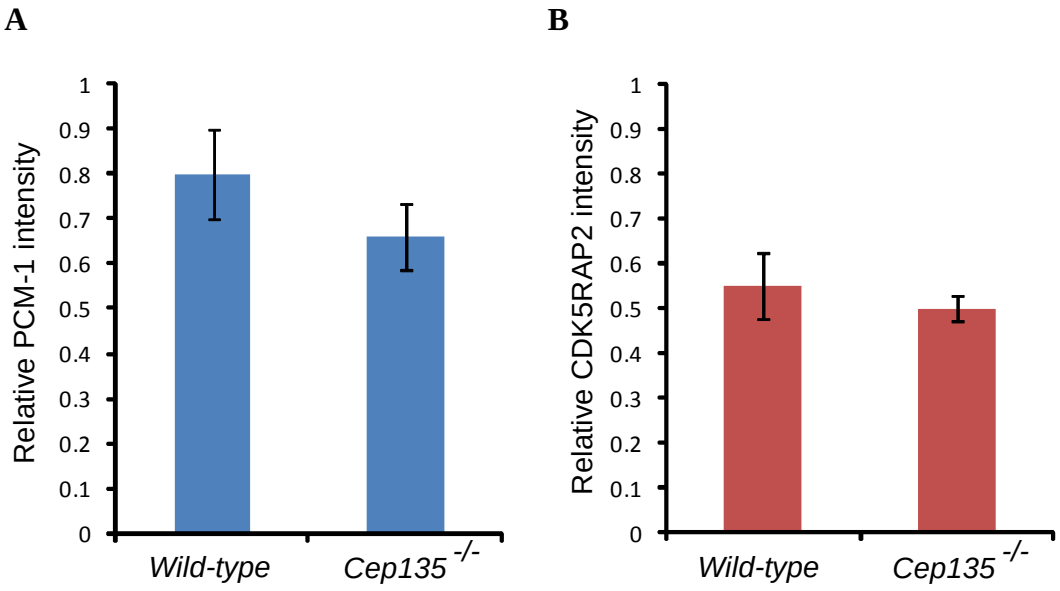

Figure 5.2 PCM integrity is normal in *Cep135* null cells.
A. Graph showing the quantification of relative PCM-1 intensity centrioles- associated in wild-type and *Cep135*$^{-/-}$ cells.
B. Graph showing the quantification of relative CDK5RAP2 intensity centrioles- associated in wild-type and *Cep135*$^{-/-}$ cells. At least 50 centrosomes were counted per experiment for each cell line. Data show the mean ± SD of three separate experiments. Statistical significances were calculated by Student's unpaired *t* test.

Cep135 has been implicated as a scaffold protein that holds C-NAP1 at the proximal ends of the centrioles (Kim et al., 2008). The same authors also reported that Cep135 suppression induces centrosome separation in 293T cells. Therefore, we analysed centrosome separation in wild-type and *Cep135*$^{-/-}$ DT40 cells. Centrin2 was used as a marker, and centrosomes were counted as separated whenever the distance between the two centrioles was >2 μm. As shown in figure 5.3A, we did not observe any significant difference between the number of wild-type and *Cep135* null cells with separated centrioles. Furthermore, we did not observe any abnormalities in terms of the number of the cells containing more than 4 centrioles in *Cep135* null cells (Figure 5.3B).

In summary, our observations show that Cep135 deficiency has no obvious impact on centrosome composition during interphase and mitosis. In addition, we found no evidence that Cep135 functions in maintaining centrosome cohesion in DT40 cells.

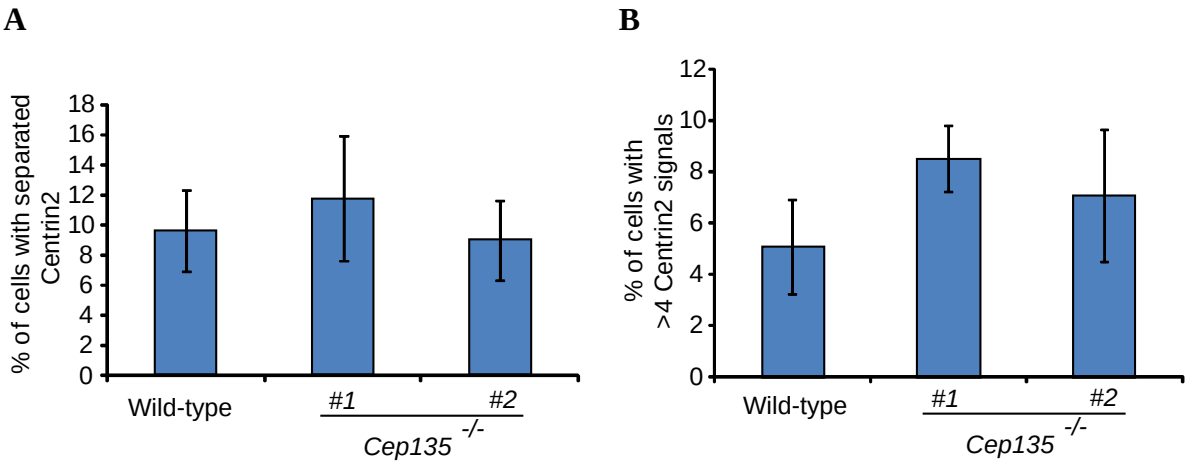

Figure 5.3 *Cep135* deficiency has no impact on centriole number or centriole separation.
A. Graph showing the number of cells with separated centrioles. The level of centriole separation was quantified by immunofluorescence microscopy using Centrin2 antibody in wild-type and *Cep135*$^{-/-}$ #1 and #2 cell lines.
B. Graph showing the number of cells with more than 4 centrioles. Percentage of cells with more than 4 centrioles was quantified by immunofluorescence microscopy a using Centrin2 antibody in wild-type and *Cep135*$^{-/-}$ #1 and #2 cell lines. Data are expressed as the means ± SD of three independent experiments, in which at least 200 cells were counted.

5.3 Ultrastructural analysis of Cep135-deficient centrosomes reveals an unusual centriole structure

Together with Sas-6, *Chlamydomonas* and human Bld10/Cep135 have been shown to be an important structural element in cartwheel formation during the early steps of procentriole and basal body assembly (Hiraki et al., 2007; Kleylein-Sohn et al., 2007; Matsuura et al., 2004). As a component of the cartwheel, immunoelectron microscopy of Cep135 revealed that it localises around the centrioles (Ohta et al., 2002), being specifically concentrated in the proximal lumen of both parental centrioles and procentrioles, as well as along the centriolar surface (Kleylein-Sohn et al., 2007). We investigated centriolar ultrastructure by transmission electron microscopy (TEM) in *Cep135* null cells to see if there was a change in the overall centriole structure. The significance of the cartwheel comes from its role in establishing the nine-fold symmetrical structure of centrioles and therefore its involvement in interphase and mitotic spindle microtubule nucleation and elongation. It has been demonstrated that when a C-terminal mutant form of *Bld10* was introduced into *Chlamydomonas* cells, the cartwheel spoke was shortened and centrioles with 8-fold symmetry were formed.

(Hiraki et al., 2007; Jerka-Dziadosz et al., 2010). However, in contrast to observations in *Chlamydomonas*, RNAi depletion studies in *Paramecium* indicated no role for Bld10 for determining the ninefold symmetry of the microtubule triplets (Jerka-Dziadosz et al., 2010). TEM of *Cep135* null DT40 cells revealed that centrioles were composed of nine triplet microtubules, showing no impact of Cep135 deficiency on centriolar triplet symmetry (Figure 5.4-i, ii) as was seen in basal bodies of *Bld10*-depleted *Paramecium* cells.

Like wild-type cells, Cep135-deficient cells have orthogonally-arranged centrioles surrounded by electron-dense pericentriolar material with procentriole elongating orthogonally from the mother centriole (Figure 5.4-ii, iii). These observations indicate that PCM is recruited by *Cep135*$^{-/-}$ centrioles, confirming the findings we made with immunofluorescence microscopy and that Cep135-deficient centrioles are capable of promoting normal centriole duplication. In addition, Cep135-deficient centrioles have normal subdistal appendages that are capable of anchoring microtubules (Figure 5.4-iv) and of normal microtubule nucleation (Figure 5.4-v).

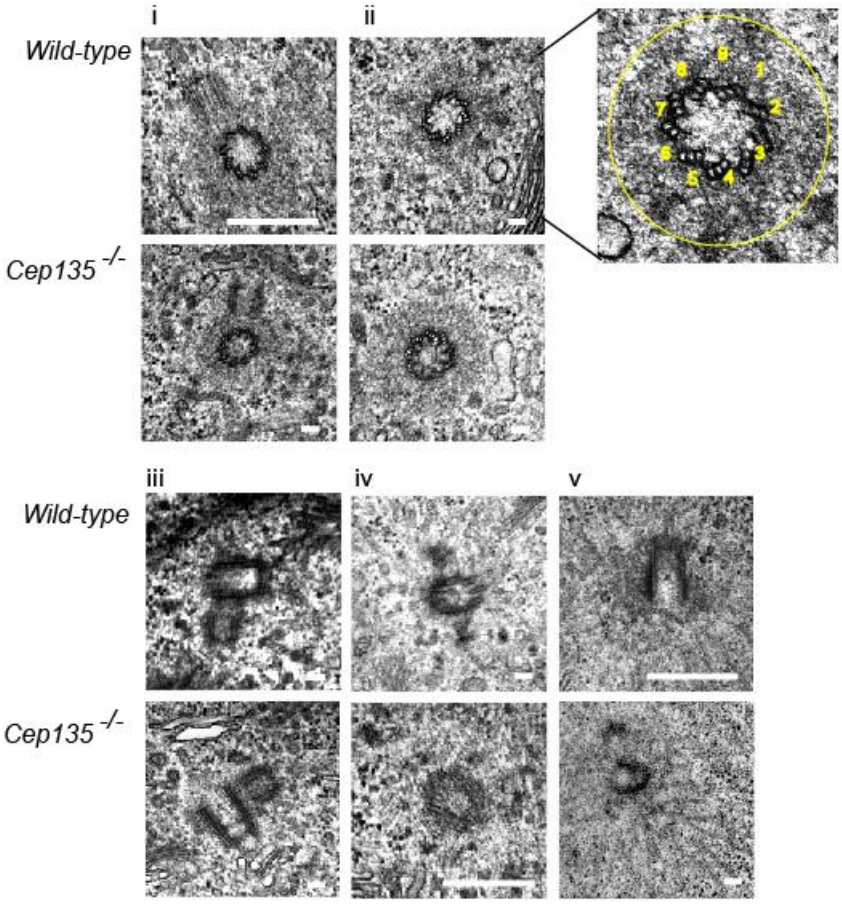

Figure 5.4 Wild-type and *Cep135*$^{-/-}$ centrosome ultrastructure. Transmission electron micrographs of wild-type and Cep135-deficient cells showing i) composition of nine triplet microtubules, ii) PCM integrity, iii) centriole duplication, iv) subdistal appendages and, v) microtubule anchoring on centrosomes. On the inset, numbers indicate nine-triplet microtubules, yellow circle indicates PCM. Short scale bar 100nm, long scale bar 500nm. (Micrographs iv and v from wild-type DT40 cells were kindly provided by Tiago J. Dantas).

Although overall nine-fold symmetry, centriole duplication, PCM integrity, subdistal appendages and microtubule anchoring seemed normal at the ultrastructural level in Cep135-deficient centrioles, during our analysis we observed an unusual structure in the longitudinal sections of these centrioles. As shown in Figure 5.5, an electron-dense dark band was visible within the barrels of Cep135-deficient centrioles, but not in wild-type centrioles. We detected this structure in 20/22 *Cep135*$^{-/-}$ cells analyzed, but not in any of 47 wild-type cells. In collaboration with Fanni Gergely`s laboratory at the University of Cambridge in the UK, where separate *Cep135* null cell lines has been generated by deleting exons 5-9, we analyzed the centriolar ultra-structure in the B11 *Cep135*$^{-/-}$ cell line. Similarly to our *Cep135*$^{-/-}$ cell lines, the overall ultrastructure appeared to be normal in B11 cells. However, in 14/18 cells, we observed the unusual structure in the longitudinal sections of their centrioles.

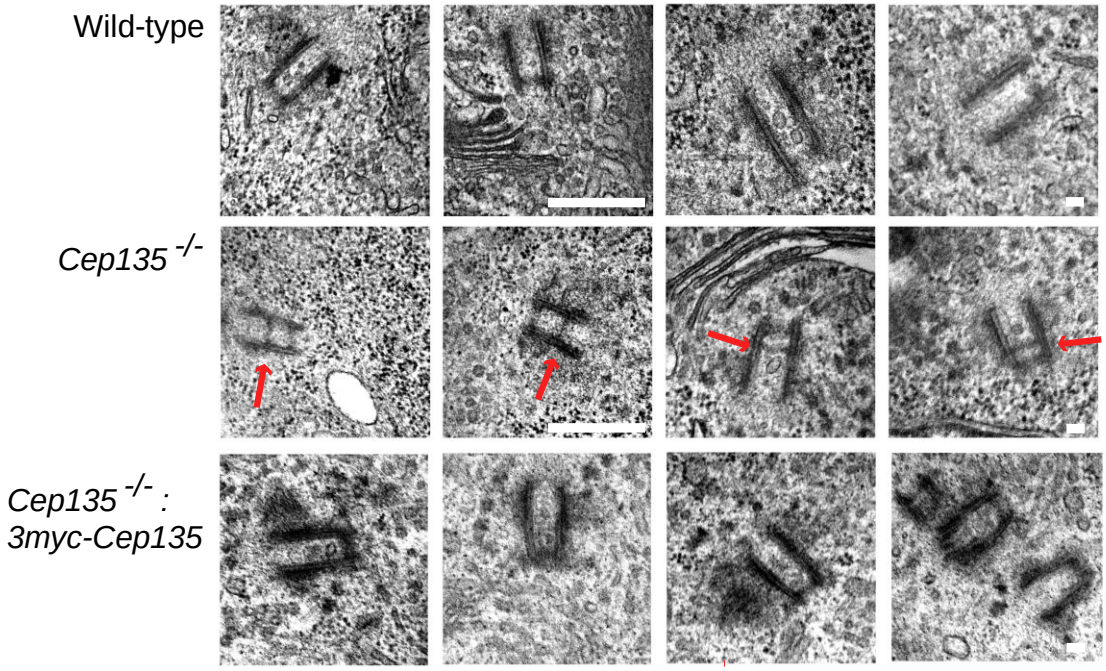

Figure 5.5 An unusual structure on the longitudinal sections of *Cep135*$^{-/-}$ centrioles. Transmission electron micrographs of wild-type, *Cep135*$^{-/-}$ cells and *Cep135*$^{-/-}$ rescue cell line (*Cep135*$^{-/-}$:3myc-Cep135) showing longitudinal parts of centrioles. Note that the electro-dense structure (indicated by the red arrow) is only observed in *Cep135*$^{-/-}$ cells but not in wild-type and rescued cells. Short scale bar 100nm, long scale bar 500nm.

To be certain that the formation of the unusual electron-dense structure was due to loss of Cep135 function, we generated stable *Cep135*$^{-/-}$ cell lines expressing 3myc-Cep135. The *Cep135* cDNA (as described in Section 4.2) was cloned into pCMV-3TAG-2C and this construct was stably expressed in *Cep135*$^{-/-}$ cells. As shown in Figure 5.6A-B, stable expression of 3myc-Cep135 in *Cep135*$^{-/-}$ cells was confirmed by immunofluorescence microscopy and western blot analysis. As shown in Figure 5.5, we did not observe the unusual structure in any of 15 *Cep135*$^{-/-}$ cells that stably express 3-myc-Cep135.

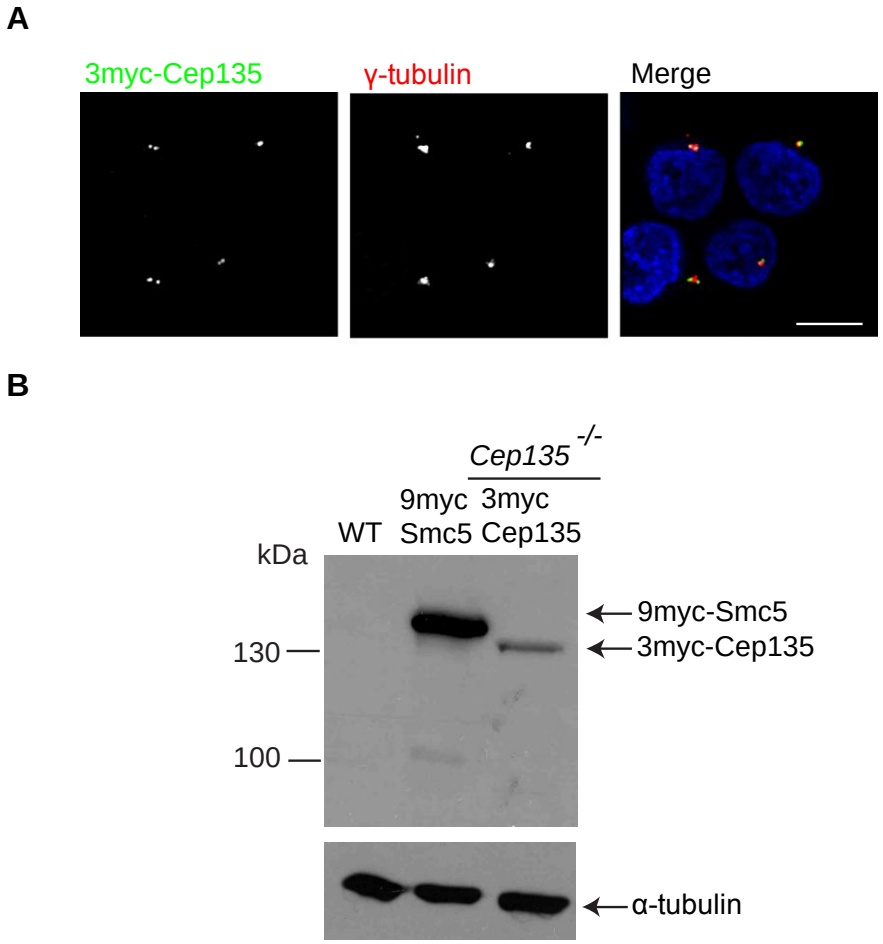

Figure 5.6 Generation of rescued *Cep135*$^{-/-}$ (*Cep135*$^{-/-}$: 3myc-Cep135) cell lines.
A. Immunofluorescence microscopy analysis of rescued *Cep135*$^{-/-}$ cells. Cells were stained with anti-myc and with anti-γ-tubulin as a reference marker. DNA is blue, myc is green and γ-tubulin is red in merged images. Scale bar, 10 μm.
B. Western blot analysis of total proteins from the representative *Cep135*$^{-/-}$ cell line expressing 3myc-Cep135 with myc antibody. Wild-type DT40 and DT40 cells expressing 9myc-Smc5 serve as the negative and positive control, respectively. α-tubulin serves as the loading control.

Observation of the unusual structure in two different, independently-generated *Cep135* null cell lines but not in *Cep135*$^{-/-}$ rescue cell lines confirms that this unknown structure was formed due to the loss of Cep135 in these cells. We have found no other example of this structure, despite extensive literature searching. Serial electron microscopy sections of centrosomes might provide better insight into this unusual structure in *Cep135* null cells.

The mean length of wild-type centrioles was 370 ± 28 nm whereas the *Cep135* null centrioles averaged 350 ± 30 nm, showing no impact of Cep135 deficiency on centriole elongation. This result indicates that the unusual structure does not affect the centriole length or centriole elongation. Although the nine-fold symmetrical structure

was found intact in Cep135-deficient centrioles, we could not analyze the cartwheel structure directly. In *Bld10* mutant *Chlamydomonas* cells, centrioles with eight symmetrically arranged triplets formed cartwheels with a smaller diameter (Hiraki et al., 2007). Therefore, if there were a defect in the cartwheels of Cep135-deficient centrioles, measurement of centriole diameter would provide some information. Centriole diameters were 183 ±23 nm in wild-type cells and 173 ± 18 nm in *Cep135* null cells, indicating no impact of Cep135 deficiency on cartwheel and centriole ultrastructure. This result also indicates that the observed abnormal ultrastructure does not have any obvious impact on cartwheel formation.

5.4 Plk4-induced assembly of procentrioles is not suppressed in *Cep135*$^{-/-}$ cells

An ordered cascade composed of Plk4, Sas-6, Cep135, CPAP, γ-tubulin and CP110 regulates centriole duplication (Leidel et al., 2005; Kleylein-Sohn et al., 2007; Peel et al., 2007). Plk4 in mammalian cells, SAK in *Drosophila* and ZYG-1 in *Caenorhabditis elegans*, is a key protein kinase necessary for centriole biogenesis (Bettencourt-Dias et al., 2005; Kleylein-Sohn et al., 2007; Peel et al., 2007). It has been demonstrated that overexpression of Plk4/SAK in human and *Drosophila* and Sas-6 in human cells has been lead to assembly of 'flower-like structures', a single mother centriole surrounded by several daughter centrioles (Strnad et al., 2007; Kleylein-Sohn et al., 2007; Cunha-Ferreira et al., 2009; Rogers et al., 2009). Kleylein-Sohn and colleagues have shown that Plk4-induced multiple centrioles were positively stained by Cep135 along with the other components involved in centriole biogenesis listed above (Kleylein-Sohn et al., 2007). In the same study it was reported that *Cep135* depletion by siRNA suppressed Plk4-induced centriole biogenesis.

To see if *Cep135* disruption affected Plk4-induced centriole biogenesis in DT40 cells, cells were transiently transfected with a GFP-tagged version of chicken Plk4 (cloned from DT40 cells in our laboratory by Loretta Breslin, Steere et al., 2011). Cells were examined for the presence of supernumerary centrosomes after Plk4 expression using immunoflorescence microscopy. In this experiment we compared two different *Cep135*$^{-/-}$ cell lines from our lab and one from Fanni Gergely`s lab (B11) with wild-type DT40 cells from our lab and wild-type DT40 cells (Wt*) from the Gergely lab as controls. 24h and 48h after transfection, Plk4 localization was analyzed and the number of centrioles per cell was quantified using an anti-Centrin2 antibody. Following

successful GFP-Plk4 transfection, we observed that in both wild-type and *Cep135* null cells Plk4 localized around the centrioles (Figure 5.7A), consistent with previous reports of Plk4-induced centrosome amplification (Kleylein-Sohn et al., 2007).

We had expected that the absence of Cep135 would cause a defect in Plk4-induced centriole biogenesis, and that cells would be unable to form supernumerary centrioles. However we observed robust levels of centriole biogenesis and supernumerary centriole formation in *Cep135*$^{-/-}$ cells (Figure 5.7B). Although there was a small decrease in the percentage of cells with multiple centrioles in the *Cep135*$^{-/-}$ cell lines, these values did not differ significantly from those seen wild-type cells at either 24h or 48h after Plk4 transfection. Overall, our results suggest that Cep135 is not required for Plk4-induced centriole duplication, as it is not required for the normal centrosome duplication cycle.

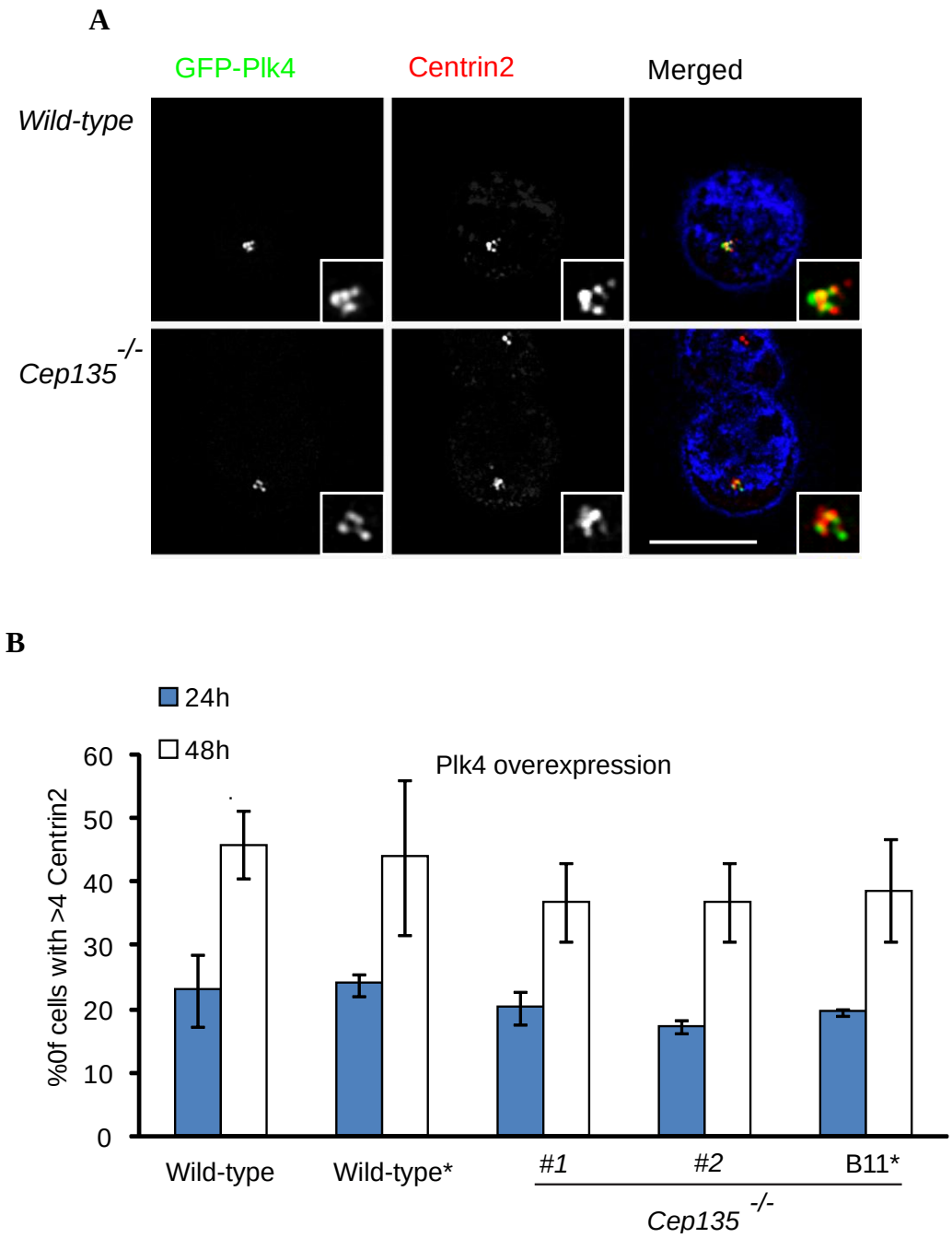

Figure 5.7 Plk4-induced multiple centriole formation occurs in *Cep135*$^{-/-}$ cells.
Wild-type, wild-type* and *Cep135*$^{-/-}$ #1, #2, B11* cell lines were transiently transfected with GFP-Plk4 and fixed 24h and 48h after treatment.
A. Micrographs showing the expression and impact of GFP-Plk4 transfection after 48h. Cells were stained with an antibody against Centrin2 (red) and counterstained with DAPI. Blowups show supernumerary centrosomes. Scale bar, 5µm.
B. Levels of centrosome amplification were quantified by immunofluorescence microscopy using Centrin2 antibodies in cells positive for GFP-Plk4. Data represent the mean ± SD of three separate experiments in which at least 200 cells were counted for each time point. (* DT40 cell lines from Fanni Gergely`s lab).

5.5 Localization of CP110, Sas-6 and Cenp-J is normal in *Cep135*$^{-/-}$ cells

After Plk4 activation, *Sas-6*, Cep135, CENPJ (CPAP), and CP110 are recruited to the nascent procentrioles at different times and are involved in different stages of centriole formation. Therefore, we decided to look at the localisation of these proteins, to see whether the absence of Cep135 in DT40 cells had any effect on them. In several studies in human, *Chlamydomonas*, *Paramecium* and *Drosophila* (Strnad and Gonczy, 2008; Nakazawa et al., 2007; Rodrigues-Martins et al., 2007), it has been shown that Sas-6 has an essential role for the initial steps of centriole assembly. Together with Cep135 which localises at the tip of the spokes, Sas-6 is another known cartwheel component which localises to the cartwheel hub. In *Paramecium*, it has been shown that Bld10 depletion by siRNA caused the disappearance of Sas-6 from the basal bodies (Jerka-Dziadosz et al., 2010). Therefore, we predicted that Sas-6 recruitment could be perturbed in *Cep135*$^{-/-}$ centrosomes and that such perturbation might be related to the unusual structure in the *Cep135*$^{-/-}$ centrioles. We immunostained wild-type and *Cep135*$^{-/-}$ DT40 cells with antibodies against Sas-6 and γ-tubulin. However, our immunofluorescence analysis revealed that Sas-6 antibody co-localised with γ-tubulin in *Cep135*$^{-/-}$ centrosomes, as in wild-type centrosomes (Figure 5.8A). We also checked Sas-6 expression levels by western blot and, as shown in Figure 5.8B, Sas-6 levels appeared similar in both wild-type and *Cep135*$^{-/-}$ cells. These results suggest that Sas-6 expression is normal and is not perturbed in the absence of Cep135 in DT40 cells and the formation of unusual ultrastructure in the longitudinal sections of *Cep135*$^{-/-}$ centrioles is not related to Sas-6 protein.

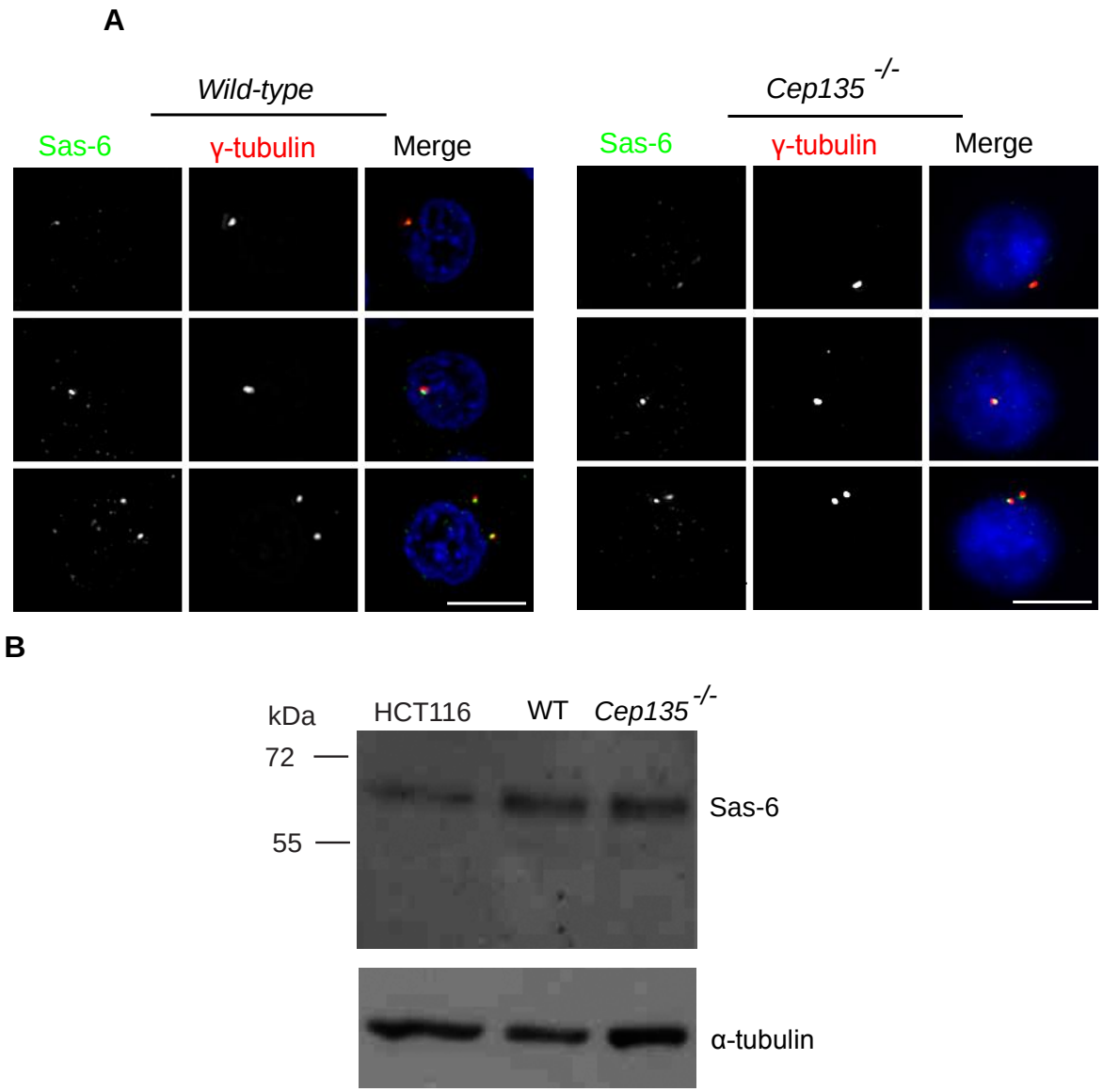

Figure 5.8 Sas-6 localisation and expression level is normal in *Cep135*$^{-/-}$ DT40 cells.
A. Micrographs showing the subcellular localisation of the Sas-6 protein in wild-type and *Cep135*$^{-/-}$ cells. Cells were stained with antibodies against Sas-6 (green), γ-tubulin (red) and counterstained with DAPI. Scale bar, 5μm.
B. Western blots of total proteins from human HCT116, wild-type and *Cep135*$^{-/-}$ DT40 cells with Sas-6 antibody. α-tubulin serves as the loading control.

CenpJ (CPAP) is another important protein in the centriole assembly cascade. CenpJ was shown to trigger the recruitment of the γ-tubulin ring complex at the proximal end of the cartwheel and to be involved in centriole elongation by the addition of tubulin subunits to the growing centrioles (Kohlmaier et al., 2009; Schmidt et al., 2009; Tang et al., 2009). To test if *Cep135* disruption affected CenpJ localisation and stability in DT40 cells, we transiently transfected wild-type and *Cep135*$^{-/-}$ cells with a GFP-tagged version of chicken CenpJ (cloned from DT40 cells in our laboratory by Dr. Barry Coull). 24h after transfection, cells were stained with γ-tubulin and CenpJ-GFP

analyzed by immunofluorescence microscopy. As shown in Figure 5.9, this analysis did not reveal any difference between wild-type and *Cep135*$^{-/-}$ cells in terms of expression and localisation of CenpJ. In human cells it was shown that both the depletion of CP110 and the overexpression of CPAP lead to the generation of elongated centrioles (Spektor et al., 2007; Schmidt et al., 2009). We did not observe centriole elongation in wild-type or *Cep135*$^{-/-}$ DT40 cells after 24h and 48h CenpJ overexpression. However, DT40 cells are a B lymphocyte cell line and do not grow primary cilia (Alieva and Vorobjev, 2004), which may explain the absence of any impact on centriole length.

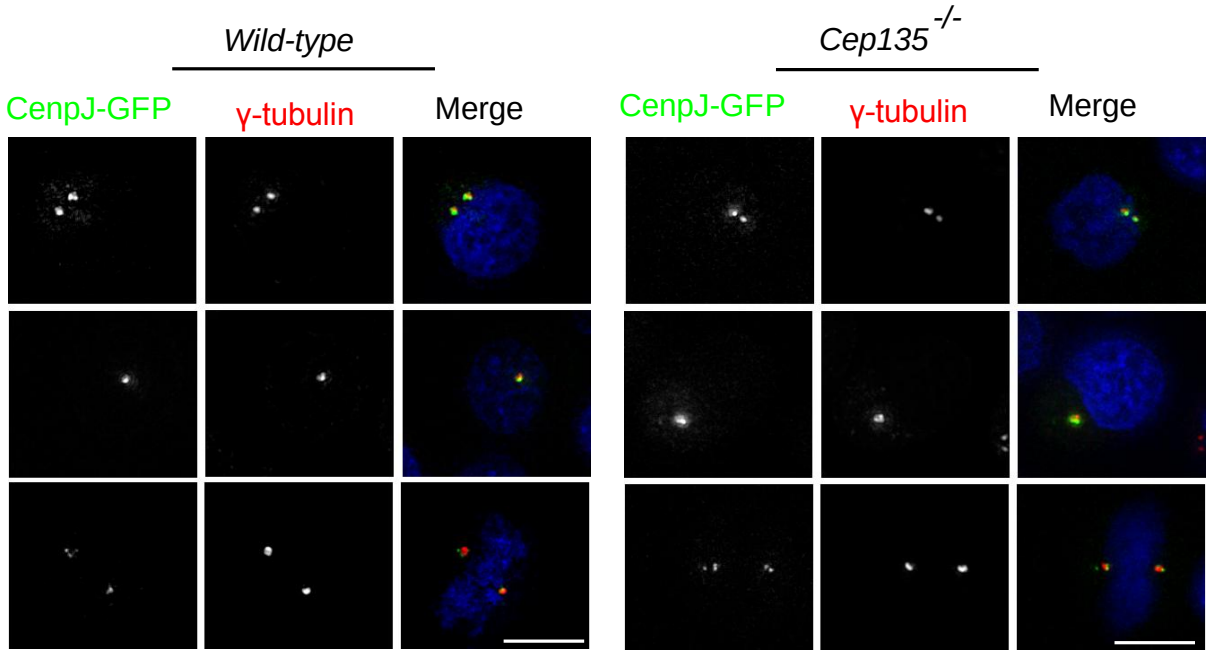

Figure 5.9 CenpJ localisation is normal in *Cep135*$^{-/-}$ DT40 cells.
Wild-type and *Cep135*$^{-/-}$ DT40 cells transiently transfected with CenpJ-GFP and fixed 24h after treatment. Micrographs show the expression and localisation of the CenpJ protein in wild-type and *Cep135*$^{-/-}$ cells. Cells were stained with an antibody against γ-tubulin (red) and counterstained with DAPI. Scale bar, 5μm.

By high resolution fluorescence and immunoelectron microscopy studies it has been shown that CP110 is recruited to the growing distal tips of the procentriole seed and forms a cap structure with Cep97 to control procentriolar microtubule growth (Kleylein-Sohn et al., 2007; Schmidt et al., 2009). We hypothesised that the unusual structure we observed in *Cep135*$^{-/-}$ centrioles could be an additional cap structure on the centriole barrel. This could be formed due to accumulation of CP110 at this site in the absence of Cep135. In other words, this unusual structure could be a second cap structure in the centriole. Therefore we tested the CP110 localization in *Cep135*$^{-/-}$ cells by immunofluorescence microscopy. We tested a commercially-available CP110

antibody in combination with a variety of fixation conditions on chicken DT40 cells but unfortunately we could not detect the chicken CP110 despite the moderate homology between chicken and human CP110 proteins (56% identical). Therefore, we decided to clone chicken CP110 in a 3myc vector.

We searched for a *CP110* chicken orthologue in the NCBI database. We found gene level information associated with the chicken *CP110* gene in NCBI website (accession no: XM_414915.2). According to the NCBI and Ensembl databases, there exists only 1 transcript of this gene, transcribed as a 2961 bp mRNA and encoding a predicted protein of 987 amino acids. To confirm that the predicted *CP110* mRNA entry is expressed in chicken cells, we searched the expression sequence tag (EST) database (dbEST, NCBI). We found that there were multiple EST clones that cover all of the nucleotides in the *CP110* sequence. Furthermore, there were extra 57 nucleotides in the EST sequence at the 3`end of the CP110 gene. A BLAST search against the entire nucleotide collection revealed that there is no similar gene in *Gallus gallus* genome. We then used the *cCP110* cDNA sequence to design specific primers for cDNA amplification. Full-length *cCP110* cDNA was amplified from total RNA isolated from DT40 cells by PCR using gene-specific primers. Analysis of the amplified candidate *cCP110* cDNA product by agarose gel electrophoresis revealed a size (3000bp) consistent with the sequence predicted in the NCBI database (data not shown). The chicken *cCP110* cDNA was cloned into pEGMT-easy and sequenced. The full length *cCP110* cDNA was found to be 3018bp in length and the cDNA encodes a protein of 1006 aa. The human CP110 protein has a similar size of 991 and 1012 amino acids. Sequencing of the PCR products revealed that the 57 missing nucleotides in the NCBI *cCP110* mRNA sequence were present in our *cCP110* transcript, as in the EST database. Once the sequence information was confirmed, *cCP110* cDNA was cloned into pCMV-3TAG-2C from pEGMT-easy. Sequence information is shown in Appendix 3.

Our 3myc-CP110 construct was then used for expression studies in chicken DT40 cells. Wild-type and *Cep135*$^{-/-}$ cells were transiently transfected with 3myc-CP110 and analyzed 24h after transfection. Cells were stained with myc and γ-tubulin antibodies and analyzed by immunofluorescence microscopy. As shown in Fig. 5.9, 3myc-CP110 was successfully expressed and localized with γ-tubulin at the

centrosomes. However, we observed no difference between wild-type and *Cep135*$^{-/-}$ cells in terms of CP110 expression or localization.

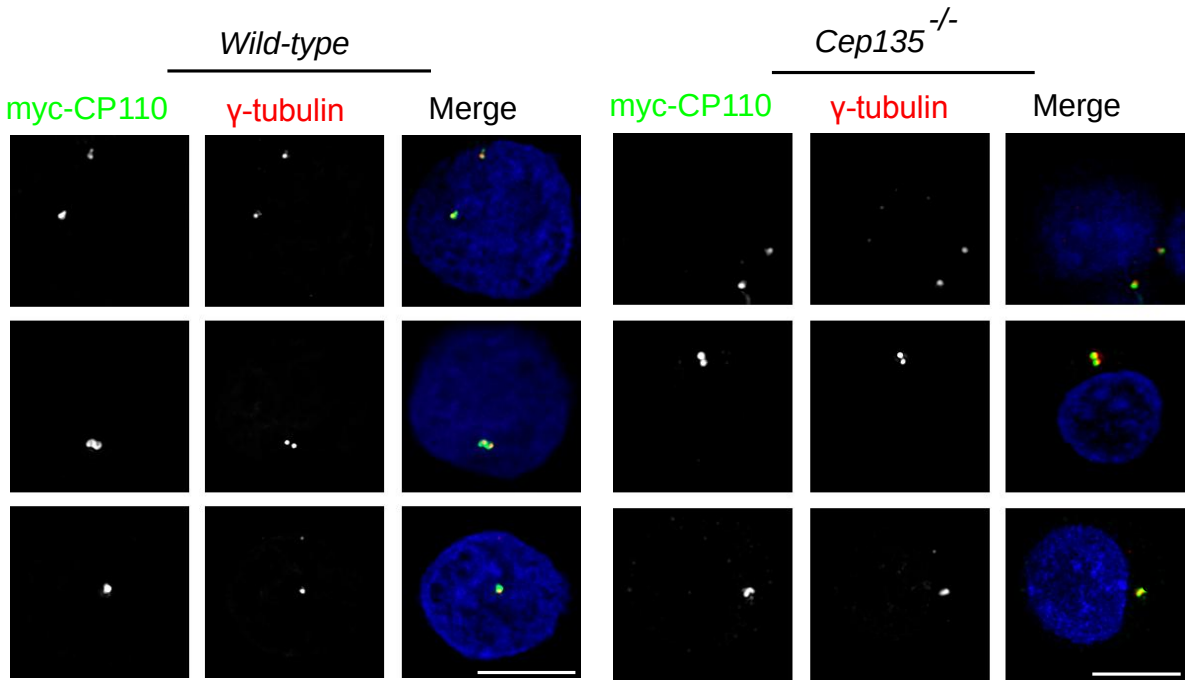

Figure 5.10 CP110 localisation is normal in *Cep135*$^{-/-}$ DT40 cells.
Wild-type and *Cep135*$^{-/-}$ DT40 cells transiently transfected with 3myc-CP110 and fixed 24h after treatment. Micrographs showing the expression and localisation of the CP110 protein in wild-type and *Cep135*$^{-/-}$ cells. Cells were stained with antibodies against myc, γ-tubulin and counterstained with DAPI. DNA is blue, CP110 is green and γ-tubulin is red in the merged images. Scale bar, 5μm.

This analysis did not provide any clear information regarding potential changes in CP110 in the absence of Cep135 and its possible involvement in the unusual electron-dense structure in *Cep135*$^{-/-}$ centrosomes. To further analyze CP110 in *Cep135*$^{-/-}$ cells, we need to study its localization by high resolution fluorescence microscopy or immunoelectron microscopy.

5.6 Ionizing radiation (IR) induced centrosome amplification in *Cep135* $^{-/-}$ cells

Since DT40 cells are deficient for p53, after DNA damage they are able to cycle through S phase and arrest in G2 phase in a Chk1-dependent manner (Takao et al., 1999; Zachos et al., 2003). Previous studies conducted in our lab have shown that in response to IR and the subsequent G2 arrest, DT40 cells overduplicate their centrosomes (Dodson et al., 2004; Bourke et al., 2007). It is known that several cell cycle regulatory and DNA damage response proteins localize to centrosomes (Tsvetkov et al., 2003; Kramer et al., 2004; Starita et al., 2004; Oricchio et al., 2006; Loffler et al.,

2006; Fukasawa, 2008). For these reasons and to explore on the potential role of Cep135 in centrosome duplication, based on the Plk4-induced centriole biogenesis experiments in human cells (Kleylein-Sohn et al., 2007), we investigated if Cep135 has any role in IR-induced centrosome amplification in DT40 cells. To address this question we treated wild-type and *Cep135*$^{-/-}$ DT40 cells with 5Gy and analyzed centrosome numbers 24h after irradiation using Centrin2 or γ-tubulin as markers in immunofluorescence microscopy. As shown in Figure 5.11, IR-induced centrosome amplification to a similar extent in both wild-type and *Cep135*$^{-/-}$ cells. Our data suggest that Cep135 does not have a role in IR-induced centrosome amplification.

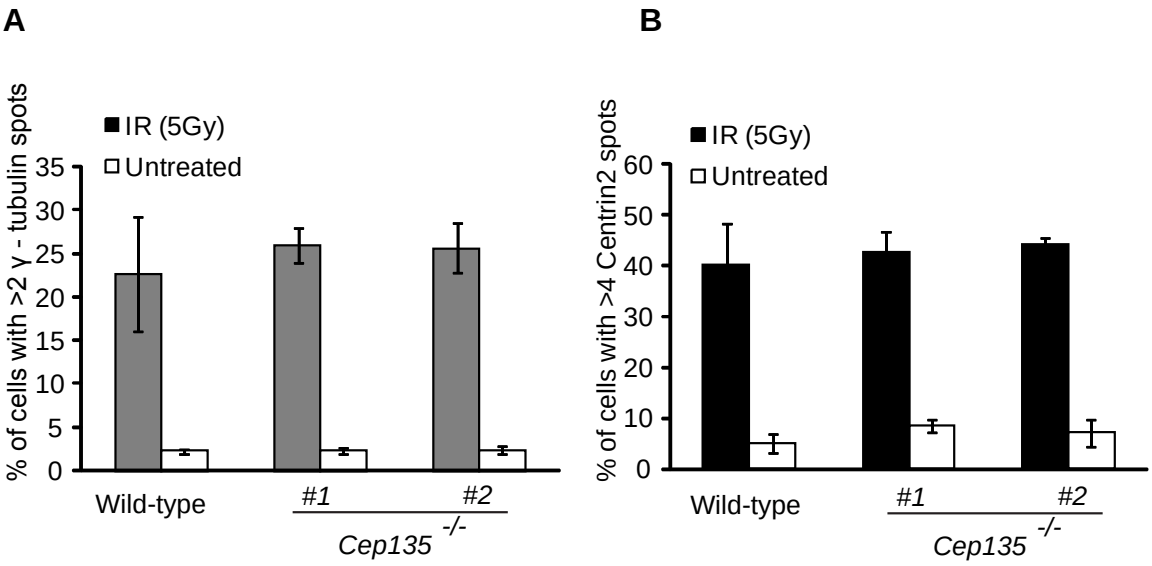

Figure 5.11 Centrosome amplification occurs in Cep135-/- DT40 cells in response to IR. Graphs showing centrosome amplification in wild type and *Cep135*$^{-/-}$ DT40 cells. Cells were untreated or exposed to 5 Gy IR. Cells were fixed and stained with γ-tubulin and Centrin2 and the number of centrosomes was quantified at 24h after IR.
A. Quantitation of cells with more than 2 centrosomes using γ-tubulin as a marker.
B. Quantitation of cells with more than 4 centrioles using Centrin2 as a marker. Data show the mean ± SD of three separate experiments in which at least 200 cells were scored.

5.7 The capacity of *Cep135*$^{-/-}$ cells to overduplicate centrosomes in response to hydroxyurea (HU)

Hydroxyurea (HU) is a DNA replication fork-stalling agent that causes centrosome aberrations in several types of cancer cells during a prolonged S phase arrest (Balczon et al., 1995; Wong and Stearns, 2003). HU works by inhibiting the enzyme ribonucleotide reductase (RNR) and therefore starves the DNA polymerase at the replication forks of dNTPs (Huberman, 1981). DT40 cells amplify their centrosomes in response to prolonged (>12 hour) hydroxyurea (HU) treatment (Dodson et al., 2004). To test whether Cep135 plays a role in the centrosomal response to HU, we treated cells with 4mM hydroxyurea for 24 hours. We analyzed two *Cep135*$^{-/-}$ cell lines from our lab as well as the *Cep135*$^{-/-}$ cell line from Fanni Gergely`s lab and wild-type DT40 cell lines from both labs for controls. After 24 hour HU treatment, we fixed the cells and analysed centrosome numbers by γ-tubulin staining. As shown in Figure 5.12A, the pattern of amplified centrosomes in *Cep135*$^{-/-}$ cells was similar to that of wild-type cells; in both cell lines amplified centrioles were labelled with γ-tubulin and Centrin2. As shown in Figure 5.12B, significantly higher levels of centrosome amplification were observed after HU treatment in all *Cep135*$^{-/-}$ cell lines compared with wild-type populations. These data suggested that Cep135 may have a role in centrosome overduplication in response to HU treatment.

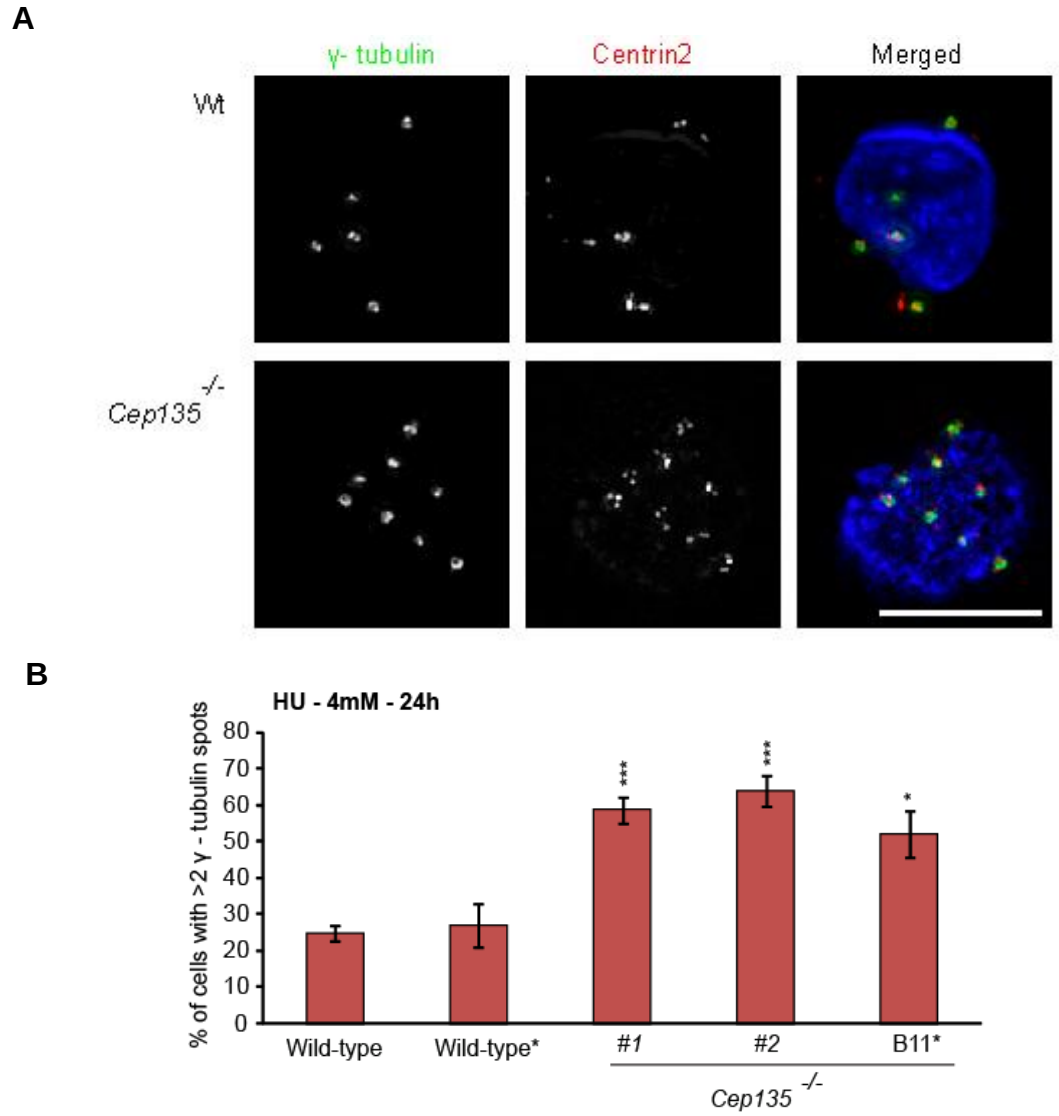

Figure 5.12 Increased HU-induced centrosome amplification in *Cep135* $^{-/-}$ cells. Immunofluorescence microscopy analysis of wild-type, wild-type* and *Cep135*$^{-/-}$ #1, #2, B11 (*Cep135*$^{-/-}$)* DT40 cell lines 24h after treatment with 4mM HU.
A. Micrograph showing HU treated wild-type and *Cep135*$^{-/-}$ cells with multiple centrosomes. Cells were stained with antibodies against Centrin2 (red), γ-tubulin (green) and counterstained with DAPI. Scale bar 5μm.
B. Graph shows quantitation of HU-induced centrosome amplification using γ-tubulin as a marker. Data show the mean ± SD of three separate experiments in which at least 200 cells were scored). Statistical significances were calculated by Student's unpaired t test and are indicated on the histogram as *$p \leq 0.05$, **$p \leq 0.01$, and ***$p \leq 0.001$. (* DT40 cell lines from Fanni Gergely`s lab).

It has been shown that centrosome overduplication in response to HU treatment requires cyclin E-Cdk2 activity during prolonged S phase arrest in CHO cells and frog embryos (Matsumoto et al., 1999; Hinchcliffe et al., 1999). Studies conducted by our group have shown that Cdk2 is a downstream target of Chk1 signalling and that Cdk2 activation through Chk-1 dependent phosphorylation on T160 was associated with IR-induced centrosome amplification in DT40 cells (Bourke et al., 2010). Therefore, we

examined the total Cdk2 and phospho-T160 Cdk2 levels in *Cep135*$^{-/-}$ cells at various timepoints after 4mM HU treatment by western blot. As shown in Figure 5.13, immunoblot analysis revealed that there was no difference in T160 phosphorylation levels between wild-type and *Cep135*$^{-/-}$ cells at any timepoints analyzed. Therefore, higher levels of centrosome amplification in HU treated *Cep135*$^{-/-}$ cells did not result from elevated phosphorylation of T160 on Cdk2.

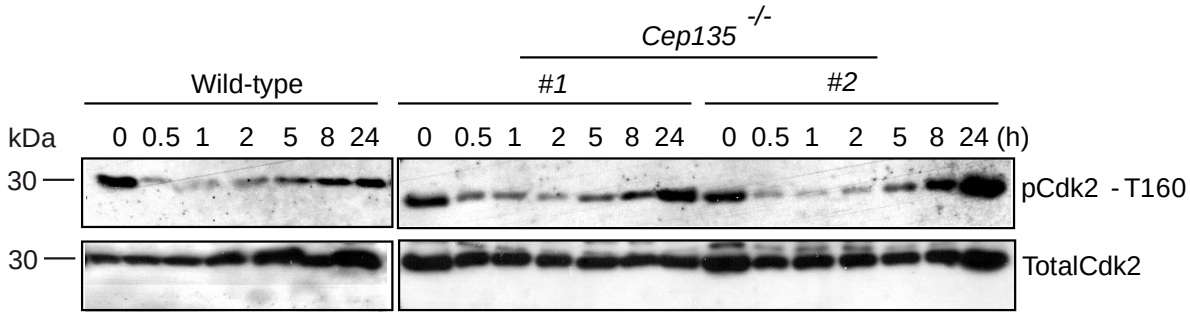

Figure 5.13 Total Cdk2 and pCdk2-T160 levels in *Cep135*$^{-/-}$ cells are similar to wild-type DT40 cells after HU treatment. Immunoblot analysis of Cdk2 and pCdk2-T160 levels in wild-type and *Cep135*$^{-/-}$ #1 and *Cep135*$^{-/-}$ #2 cells before and at the indicated times following 4mM HU treatment.

To be certain that the effect on HU-induced centrosome amplification was due to loss of Cep135 function, we treated *Cep135*$^{-/-}$ rescue cell line (*Cep135*$^{-/-}$:3myc-Cep135) with 4mM hydroxyurea for 24 hours together with wild-type and *Cep135*$^{-/-}$ cell lines. As shown in Figure 5.14, reintroduction of the Cep135 protein within the Cep135-deficient cells restored centrosome amplification levels after HU treatment to wild-type levels. Therefore, increased levels of HU-induced centrosome amplification are specifically due to loss of the *Cep135* gene and not a result of additional factors. Taken together, these results demonstrate that Cep135 plays a role in inhibiting centrosome amplification during prolonged S-phase arrest DT40 cells.

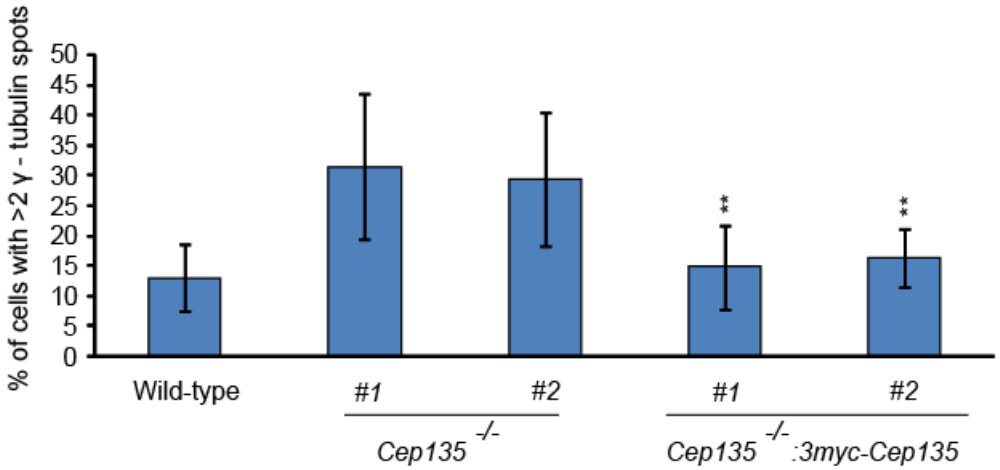

Figure 5.14 Restoration of Cep135 rescues the HU-induced centrosome amplification phenotype in *Cep135*$^{-/-}$ cells. Immunofluorescence microscopy analysis of wild-type, *Cep135*$^{-/-}$ DT40 and rescued *Cep135*$^{-/-}$ #1, #2 cell lines (Cep135$^{-/-}$:3myc-Cep135) cell lines 24h after treatment with 4mM HU. Graph shows quantitation of HU-induced centrosome amplification using γ-tubulin as a marker. Data show the mean ± SD of three separate experiments in which at least 200 cells were scored. Statistical significances were calculated by Student's unpaired t test and are indicated on the histogram as *$p \leq 0.05$, **$p \leq 0.01$, and ***$p \leq 0.001$.

5.8 Discussion

Despite the identification of many of the key centrosomal proteins in a wide range of organisms (reviewed by Bettencourt-Dias and Glover, 2007), the mechanisms of how centrosome regulation occurs and the functions of centrosome proteins are just starting to be unravelled. Here we have extensively investigated the role of the core centrosome protein Cep135 in centrosome duplication and its involvement in establishing the centrosome structure in chicken DT40 cells using gene targeting.

5.8.1 Structure and composition of centrioles in *Cep135*$^{-/-}$ DT40 cells

Cep135 has been shown to be an important protein for the assembly and maintenance of functional centrosomes (Ohta et al., 2002; Kleylein-Sohn et al., 2007). When *Cep135* was depleted by RNAi in CHO cells, core centrosome proteins such as γ-tubulin, Centrin2 and PCM-1 were displaced from the centrosomes. In addition, Cep135 depletion resulted in detachment of C-NAP1 from centrioles, which in turn caused premature centrosome separation (Uetake et al., 2004; Kim et al., 2008). Using several antibodies specific to centrosome components, we tested if loss of Cep135 cause any change in the overall centrosome composition and configuration. Chicken DT40 cells with disrupted Cep135 gene behaved the same as wild-type. Major centrosome components such as γ-tubulin, Centrin2, Cep76, ninein, PCM-1, CDK5RAP2, and Aurora-A were intact in Cep135-deficient centrosomes and the intensities of pericentriolar components such as PCM-1 and CDK5RAP2 were similar to those in wild-type cells. In addition, contrary to our predictions we did not observe any abnormalities in the centrosome duplication cycle, such as premature centriole separation.

It has been suggested that the cascade composed of Plk4, Sas-6, Cep135, CPAP, γ-tubulin and CP110 regulates centriole duplication (Leidel et al., 2005; Kleylein-Sohn et al., 2007; Peel et al., 2007) and RNAi depletion of *Cep135* in U2OS cells blocked Plk4-induced centriole biogenesis (Kleylein-Sohn et al., 2007). However, our results clearly demonstrated that Cep135, contrary to the current view, is not required for Plk4-induced centriole biogenesis and is not an essential structural and functional component of centrioles, at least in DT40 cells. The difference between our results in chicken cells and previous findings in human cells is difficult to explain. Based on the Kleylein-Sohn data, we expected a significant reduction in Plk4-induced centriole overduplication in

Cep135$^{-/-}$ cells. In contrast to what was found in human cells, it was shown that the initiation of centriole assembly was not affected in mutant fruit flies lacking Bld10 (Blachon et al., 2009; Mottier-Pavie and Megraw, 2009; reviewed by Azimzadeh and Marshall, 2010). However, another study in *Drosophila* demonstrated that depletion of *Bld10* by RNAi in S2 cells causes a reduction in the number of centrioles, indicating that Bld10/Cep135 could be required for centriole biogenesis under some conditions (Dobbelaere et al., 2008). These discrepancies could be due to the differences between human, mouse, *Drosophila* and chicken functions of Cep135 in different cell types. Similarly, in a recent knockout study of chicken Centrin, it has been shown that Centrin is not required for centriole assembly and duplication in DT40 cells (Dantas et al., 2011), even though it was found to be essential for centriole duplication in Hela cells (Salisbury et al., 2002) .

In addition to its scaffolding role in centrosomes, ultrastructural studies in diverse organisms have revealed that Cep135 is an essential component of the cartwheel. As well as the immunofluorescence microscopy analysis mentioned above, we also examined the centrosomes of *Cep135*$^{-/-}$ cells at an ultrastructural level by EM. Although the overall ultrastructure of centrioles in *Cep135*$^{-/-}$ cells appeared normal for nine-fold symmetry, centriole duplication, centriole configuration, PCM integrity, appendages and microtubule nucleation, our analysis revealed a presence of an unusual structure in the longitudinal sections of the centrioles. It is clear that this structure is peculiar to Cep135 loss, since it was not detected in any of the wild-type cells analyzed. In previous studies where Cep135-depleted centrioles have been examined in several organisms from *Paramecium* to human, no such structure has been reported (Ohta et al., 2002; Kleylein-Sohn et al., 2007; Jerka-Dziadosz et al., 2010; Matsuura et al., 2004; Mottier-Pavie and Megraw, 2009). We do not know if the electron-dense structure continues inside the barrel or if it is a hollow structure. Further investigation by serial section electron microscopy of centrosomes should provide better insight on the inner arrangement of this structure.

While the significance of this observation is unclear, we have two hypotheses for what this electron-dense structure could be:

1) We speculate that in the absence of Cep135, microtubule triplet formation may have been destabilized and a defect in the transition from triplet to doublet

microtubules around the centriolar wall could have caused the formation of the electron-dense structure. From our observations, we did not detect any abnormalities in microtubule nucleation and organization in *Cep135*$^{-/-}$ cells, as explained in Chapter 4. However, such a problem in transition from triplet to doublet microtubules might have an effect on cilia formation. As DT40 cells do not bear primary cilia (Alieva and Vorobjev, 2004), we are unable to test this hypothesis. Nevertheless, future work by cryo-electron tomography of purified centrioles from *Cep135*$^{-/-}$ cells would be useful to investigate the electron-dense structure in detail.

2) As explained in Section 5.5, considering the similarity in appearance between the distal cap of centrioles and the unusual structure, we speculate that the structure could be a second cap structure formed by accumulation of CP110. As depicted in Figure 5.15A, in wild-type cells an ordered cascade of several proteins is required during centriole assembly after Plk4 induction. At the distal end of the procentriole, CP110 and Cep97 form a cap structure that is required to stabilize the procentriole and to control procentriole microtubule growth (Kleylein-Sohn et al., 2007; Azimzadeh and Marshall, 2010). In *Cep135*$^{-/-}$ cells, defective ordering of centriole assembly may have led to a second cap forming not only at the distal end, but also in the centriolar barrel (Figure 5.15B). Future work on immuno-EM localization of CP110 would be useful to test this hypothesis.

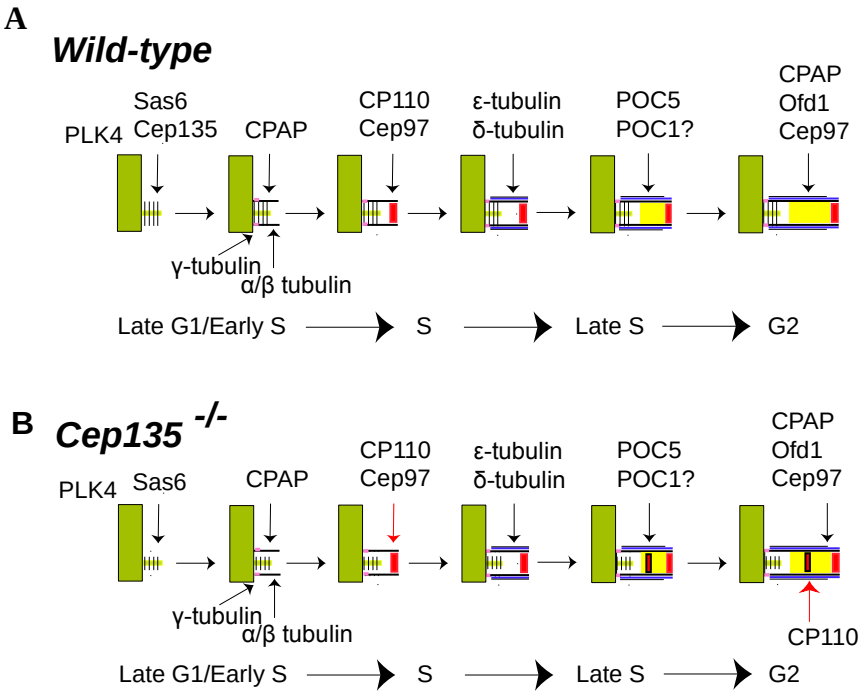

Figure 5.15 Current model for centriole assembly in A. wild-type cells and B. proposed model for centriole assembly in *Cep135*$^{-/-}$ cells after Plk4 induction (Adapted from Azimzadeh and Marshall, 2010).

5.8.2 Hydroxyurea-induced centrosome amplification is increased in *Cep135*$^{-/-}$ cells

During the course of this study, the second phenotype we observed in *Cep135*$^{-/-}$ cells was high levels of HU-induced centrosome amplification in comparison to wild-type DT40 cells. Cdk2-cyclin E activation activity is required for normal centrosome duplication (Matsumoto et al., 1999; Meraldi et al., 1999; Lacey et al., 1999). It has been shown that HU-induced centrosome amplification also requires Cdk2 activity during prolonged S phase arrest (Duensing et al., 2006; Prosser et al., 2009) and Chk1-dependent phosphorylation of Cdk2 on T160 is required for IR-induced centrosome amplification (Bourke et al., 2010). Loffler and colleagues have also shown that Chk1 accumulates at centrosomes after treatment with HU (Loffler et al., 2007). Therefore, we checked the levels of total and T160 phosphorylated Cdk2 levels in HU treated *Cep135*$^{-/-}$ cells and wild-type cells. No difference in Cdk2 levels between two cell lines indicated that centrosome amplification response in HU treated *Cep135*$^{-/-}$ cells was mediated by different mechanisms. These data are consistent with the recent work conducted in our lab. Our colleagues have shown that centrosome amplification can still occur in *Chk1*$^{-/-}$ DT40 cells after HU treatment (Bourke et al., 2010).

Among the proteins (CP110, Cep97, CPAP and OFD1) implicated both in procentriole assembly and centriole elongation (Schmidt et al., 2009; Spektor et al.,

2007; Singla et al., 2010; Kleylein-Sohn et al., 2007), CP110 has also been shown to be involved in centrosome duplication. CP110 is a substrate of Cdk2 and mutations in phosphoacceptor sites in CP110 cause polyploid cells with reduced levels of centrosome amplification and premature centrosome separation (Chen et al., 2002). In addition, it has been reported that RNAi-mediated *CP110* depletion prevents HU-induced centrosome overduplication in S-phase arrested cells and inhibits Plk4-induced centriole biogenesis (Chen et al., 2002; Spektor et al., 2007; Kleylein-Sohn et al., 2007). It has also been shown that overexpression of CP110 causes a modest increase in HU-induced centrosome amplification (Tsang et al., 2009), further indicating that CP110 activity is required for HU-induced centrosome amplification. Therefore we speculated that if the unusual electron-dense structure on the centriole barrels of *Cep135*$^{-/-}$ cells forms due to CP110 accumulation, then the high levels of centrosome amplification in HU-induced cells could result from increased levels of CP110, since it would provide more phosphoacceptor sites for Cdk2 on centrioles (Figure 5.16). To prove this hypothesis it would be necessary to generate *Cep135*$^{-/-}$ DT40 cell lines that express a mutant version of CP110 that cannot undergo Cdk phosphorylation or to disrupt CP110 in *Cep135*$^{-/-}$ DT40 cell lines.

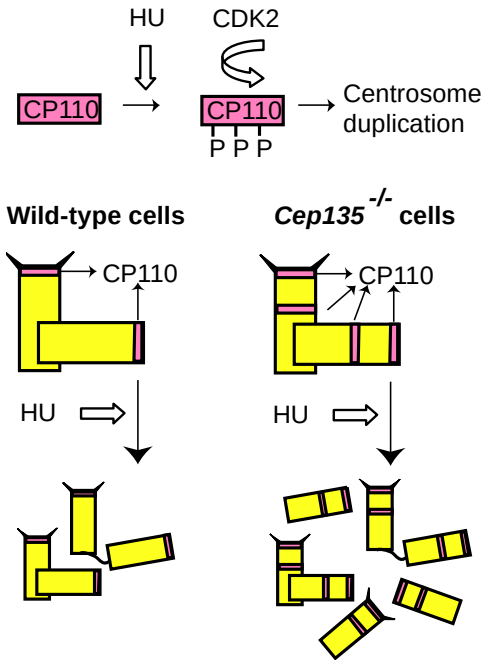

Figure 5.16 Hypothetical model for how Cep135 depletion causes increased levels of HU-induced centrosome amplification. Loss of Cep135 cause changes in localisation of CP110 in centriole barrels. Over accumulation of CP110 on centrosomes provides more phosphoacceptor sites for Cdk2. Thereby phosphorylation of CP110 by Cdk2 in response to hydroxyurea treatment results in high levels of centrosome amplification in *Cep135*$^{-/-}$ cells.

Our electron microscopy findings have clearly demonstrated that loss of Cep135 results in formation of an unusual structure within the barrel of DT40 centrioles. While we have not been able to clearly define any effects of this uncharacterised structure on centrosome organization and duplication, the overduplication phenotype after HU treatment observed in *Cep135*$^{-/-}$ cells may be related to this structure.

All together, our findings suggest that although Cep135 deficiency causes DT40 cells to become more permissive to multiple rounds of centriole duplication, loss of Cep135 does not have any impact on normal centrosome duplication and IR- and Plk4-induced centrosome overduplication. It has been suggested that Plk4- and HU- induced centrosome amplification are mechanistically different from each other, since assembly of `flower-like structures` are only observed in Plk4-induced cells (Loncarek et al., 2008). In addition, it has been suggested that centrosome amplification mechanisms are different in IR- and HU- treated DT40 cells, since IR-induced centrosome amplification is Chk1 dependent (Bourke et al., 2007) and HU-induced centrosome amplification is Chk1 independent in DT40 cells (Bourke et al., 2010). Different mechanisms suggested for HU-, Plk4- and IR-induced centrosome overduplication might explain the differences observed in the kinetics of centrosome overduplication after either treatment in Cep135-deficient DT40 cells.

Chapter 6
Conclusion and future perspectives

In this thesis, two main topics have been addressed. In the first part of the thesis, we investigated the nature of the signal that leads to centrosome amplification following DNA damage using cell fusion assays. In second part of the thesis, we investigated the requirement of Cep135 in maintaining centrosome structure, centrosome duplication, mitotic centrosome function and also in controlling the centrosome duplication response after DNA damage using a *Cep135* null chicken DT40 cell line.

Centrosome duplication, in a manner similar to DNA replication, occurs once and only once during each cell cycle. Centrosome duplication requires CDK activities at late G1/ early S phase (Matsumoto et al., 1999; Bettencourt-Dias and Glover, 2007; Nigg, 2007), and also centriole disengagement in mitosis that releases the centrosome-intrinsic block to duplication (Tsou and Stearns, 2006b; Tsou et al., 2009). Centriole engagement is a safeguard mechanism to ensure that centrosomes do not reduplicate until they have passed through the cell cycle. However, this intrinsic control to centrosome duplication could be lost in cells exposed to genotoxic stress such as gamma-irradiation and this can result in aberrant centrosome duplication, which can lead to genome instability and multipolar mitosis. Our group has demonstrated that IR-induced centrosome amplification requires Chk1 mediated G2-to-M checkpoint function and a prolonged G2 arrest (Dodson et al., 2004; Bourke et al., 2007). Here, we asked whether the IR-induced centrosome amplification process is regulated by factors intrinsic to the centrosome, as is the case in the normal centrosome cycle, or stimulated by an activating signal that causes centrosome overduplication (Tsou and Stearns, 2006a; Nigg, 2006a).

Our findings indicated that irradiation of G2-enriched cells are more permissive to duplicate their centrosomes compared with G1-enriched or asynchronous cells (Inanc et al., 2010), consistent with the model where IR-induced centrosome amplification occurs in G2 phase of the cell cycle (Dodson et al., 2004; Bourke et al., 2007). Moreover, our cell fusion analysis showed that the levels of cells with amplified centrosomes in irradiated G2-irradiated G2 cell fusions were significantly higher than in

irradiated G2-unirradiated G2 fusions, suggesting that licensing occurs only at irradiated centrosomes. Further investigation of the source of the centrosomes that amplified in fusions between irradiated human-unirradiated chicken cells and vice versa revealed that amplified centrosomes were derived from the irradiated cells (Inanc et al., 2010). In addition to this, we saw a notable increase of centriole disengagement after irradiation of one or both fusion partners in cells with amplified centrosomes. Taken together, our findings support a model in which centrosome amplification is centrosome-autonomous, and this centrosome-autonomous activity could be the disengagement of centrioles which licences centrosome reduplication following IR treatment.

Considering that disengagement could be the licensing signal for IR-induced centrosome amplification, we tested the involvement of known regulators of centrosome disengagement, Plk1 and Separase, in IR-induced centrosome amplification (Tsou et al., 2009). Although our experiments with the overexpression of nondegradable Securin or siRNA mediated Separase depletion did not indicate a clear role for Separase in DNA damage-induced centrosome amplification, pharmacological inhibition of Plk1 prevented centrosome overduplication in irradiated U2OS cells, suggesting that Plk1 might be involved as a licensing factor in IR-induced centrosome amplification.

Recent studies have indicated that members of the cohesin complex act as centriole-engagement factors (Wang et al., 2008; Schockel et al., 2011; Gimenez-Abian et al., 2010). Therefore, an interesting extension of this study may involve the characterization of centriole engagement factors before or after irradiation. Generation of human or DT40 cell lines that have conditional null alleles of *Separase* could also be useful to investigate Separase's involvement in IR-induced centriole disengagement.

In the second part of the thesis, we changed our focus from the mechanisms of IR-induced centrosome amplification to the analysis of Cep135 in centrosome structure and function. Given that Cep135 has been implicated in the maintenance of centriole structure, in microtubule nucleation and the organization of functional mitotic spindles in mammalian cells and in some model organisms (Ohta et al., 2002; Kleylein-Sohn et al., 2007; Ryu et al., 2000; Matsuura et al., 2004; Hiraki et al., 2007; Nakazawa et al., 2007; Mottier-Pavie and Megraw, 2009), we anticipated that disruption of *Cep135* in DT40 cells would provide more information about its functions. We cloned full-length

chicken *Cep135* cDNA and its 5' UTR and then generated *Cep135* null chicken DT40 cell lines. Growth curve and flow cytometry analysis of Cep135 deficient DT40 cells demonstrated that Cep135 is dispensable for cell viability and is not required for normal cell cycle progression. Also, we found Cep135 is not required for microtubule formation and mitotic centrosome functions in DT40 cells. Additionally, we showed that Cep135, contrary to the current view, is not an essential structural and functional component of centrioles, at least in DT40 cells.

In addition to its scaffolding role in centrosomes, ultrastructural studies in diverse organisms have revealed that Cep135 is an essential component of the cartwheel together with Sas6 (Matsuura et al., 2004; Hiraki et al., 2007; Kleylein-Sohn et al., 2007). Although the loss of Cep135 does not have any detectable effect on the overall centrosome ultrastructure in DT40 cells, we observed a novel electron-dense structure in the centriolar lumen of Cep135 deficient centrioles. Further studies will be necessary to determine the molecular composition of this structure and also its significance in centrosome organization and function.

We have shown that Cep135 deficiency does not have any detectable impact on normal centrosome duplication, Plk4-induced centriole biogenesis or IR-induced centrosome amplification. However, our analysis indicates that loss of Cep135 makes DT40 cells more permissive to multiple rounds of centriole duplication following HU treatment. This observation suggests that Cep135 might have an inhibitory role in centrosome reduplication during S phase arrest. Taken together, in agreement with the current literature, the work presented here suggests that there are different mechanisms in HU-, Plk4- and IR-induced centrosome overduplication. Further work to characterize the unusual ultrastructure and its possible contribution to the increased levels of HU-induced centrosome overduplication will further our understanding of Cep135 in centrosome biology. Our hypotheses related to the unusual structure, as detailed in Section 5.8, will be tested by generating a *Cep135* null cell line that expresses a mutant version of *CP110* or a double *Cep135*/ *CP110* knockout DT40 cell line.

Overall the work presented here provides evidence that centriole disengagement could be the licensing signal for DNA damage-induced centrosome amplification. Also we have shown a role for Cep135 in centrosome reduplication during S phase arrest, although its ablation has no detectable effect on centrosome function or cell cycle

progression in the chicken DT40 cells. Together, these findings provide novel insight into the mechanisms that control centrosome duplication and thus, cell division in vertebrates.

References

Abraham, R.T. (2004). PI 3-kinase related kinases: 'big' players in stress-induced signaling pathways. DNA Repair (Amst) 3, 883-887.

Adachi, N., So, S., Iiizumi, S., Nomura, Y., Murai, K., Yamakawa, C., Miyagawa, K., and Koyama, H. (2006). The human pre-B cell line Nalm-6 is highly proficient in gene targeting by homologous recombination. DNA Cell Biol 25, 19-24.

Akagi, K., Sandig, V., Vooijs, M., Van der Valk, M., Giovannini, M., Strauss, M., and Berns, A. (1997). Cre-mediated somatic site-specific recombination in mice. Nucleic Acids Res 25, 1766-1773.

Albanese, C., D'Amico, M., Reutens, A.T., Fu, M., Watanabe, G., Lee, R.J., Kitsis, R.N., Henglein, B., Avantaggiati, M., Somasundaram, K., et al. (1999). Activation of the cyclin D1 gene by the E1A-associated protein p300 through AP-1 inhibits cellular apoptosis. J Biol Chem 274, 34186-34195.

Alderton, G.K., Joenje, H., Varon, R., Borglum, A.D., Jeggo, P.A., and O'Driscoll, M. (2004). Seckel syndrome exhibits cellular features demonstrating defects in the ATR-signalling pathway. Hum Mol Genet 13, 3127-3138.

Alieva, I.B., and Vorobjev, I.A. (2004). Vertebrate primary cilia: a sensory part of centrosomal complex in tissue cells, but a "sleeping beauty" in cultured cells? Cell Biol Int 28, 139-150.

Amos, L.A., and J. Lowe. (1999). How Taxol stabilises microtubule structure. Chem Biol 6, 65-9.

Anand, S., Penrhyn-Lowe, S., and Venkitaraman, A.R. (2003). AURORA-A amplification overrides the mitotic spindle assembly checkpoint, inducing resistance to Taxol. Cancer Cell 3, 51-62.

Andersen, J.S., Wilkinson, C.J., Mayor, T., Mortensen, P., Nigg, E.A., and Mann, M. (2003). Proteomic characterization of the human centrosome by protein correlation profiling. Nature 426, 570-574.

Andersen, S.L., Bergstralh, D.T., Kohl, K.P., LaRocque, J.R., Moore, C.B., and Sekelsky, J. (2009a). Drosophila MUS312 and the vertebrate ortholog BTBD12 interact with DNA structure-specific endonucleases in DNA repair and recombination. Mol Cell 35, 128-135.

Arakawa, H., Lodygin, D., and Buerstedde, J.M. (2001). Mutant loxP vectors for selectable marker recycle and conditional knock-outs. BMC Biotechnol 1, 7.

Askham, J.M., Vaughan, K.T., Goodson, H.V., and Morrison, E.E. (2002). Evidence that an interaction between EB1 and p150(Glued) is required for the formation and maintenance of a radial microtubule array anchored at the centrosome. Mol Biol Cell 13, 3627-3645.

Azimzadeh, J., and Bornens, M. (2007). Structure and duplication of the centrosome. J Cell Sci 120, 2139-2142.

Azimzadeh, J., Hergert, P., Delouvee, A., Euteneuer, U., Formstecher, E., Khodjakov, A., and Bornens, M. (2009). hPOC5 is a centrin-binding protein required for assembly of full-length centrioles. J Cell Biol 185, 101-114.

Azimzadeh, J., and Marshall, W.F. (2010). Building the centriole. Curr Biol 20, R816-825.

Baba, T.W., Giroir, B.P., and Humphries, E.H. (1985). Cell lines derived from avian lymphomas exhibit two distinct phenotypes. Virology 144, 139-151.

Bahe, S., Stierhof, Y.D., Wilkinson, C.J., Leiss, F., and Nigg, E.A. (2005). Rootletin forms centriole-associated filaments and functions in centrosome cohesion. J Cell Biol 171, 27-33.

Bahmanyar, S., Kaplan, D.D., Deluca, J.G., Giddings, T.H., Jr., O'Toole, E.T., Winey, M., Salmon, E.D., Casey, P.J., Nelson, W.J., and Barth, A.I. (2008). beta-Catenin is a Nek2 substrate involved in centrosome separation. Genes Dev 22, 91-105.

Bakkenist, C.J., and Kastan, M.B. (2003). DNA damage activates ATM through intermolecular autophosphorylation and dimer dissociation. Nature 421, 499-506.

Balczon, R., Bao, L., Zimmer, W.E., Brown, K., Zinkowski, R.P., and Brinkley, B.R. (1995). Dissociation of centrosome replication events from cycles of DNA synthesis and mitotic division in hydroxyurea-arrested Chinese hamster ovary cells. J Cell Biol 130, 105-115.

Barr, A.R., and Gergely, F. (2007). Aurora-A: the maker and breaker of spindle poles. J Cell Sci 120, 2987-2996.

Bartek, J., Lukas, C., and Lukas, J. (2004). Checking on DNA damage in S phase. Nat Rev Mol Cell Biol 5, 792-804.

Bartek, J., and Lukas, J. (2001a). Mammalian G1- and S-phase checkpoints in response to DNA damage. Curr Opin Cell Biol 13, 738-747.

Bartek, J., and Lukas, J. (2001b). Pathways governing G1/S transition and their response to DNA damage. FEBS Lett 490, 117-122.

Basto, R., Brunk, K., Vinadogrova, T., Peel, N., Franz, A., Khodjakov, A., and Raff, J.W. (2008). Centrosome amplification can initiate tumorigenesis in flies. Cell 133, 1032-1042.

Bernstein, K.A., and Rothstein, R. (2009). At loose ends: resecting a double-strand break. Cell 137, 807-810.

Berthet, C., and Kaldis, P. (2007). Cell-specific responses to loss of cyclin-dependent kinases. Oncogene 26, 4469-4477.

Bettencourt-Dias, M., and Glover, D.M. (2007). Centrosome biogenesis and function: centrosomics brings new understanding. Nat Rev Mol Cell Biol 8, 451-463.

Bettencourt-Dias, M., Rodrigues-Martins, A., Carpenter, L., Riparbelli, M., Lehmann, L., Gatt, M.K., Carmo, N., Balloux, F., Callaini, G., and Glover, D.M. (2005). SAK/PLK4 is required for centriole duplication and flagella development. Curr Biol 15, 2199-2207.

Blachon, S., Cai, X., Roberts, K.A., Yang, K., Polyanovsky, A., Church, A., and Avidor-Reiss, T. (2009). A proximal centriole-like structure is present in Drosophila spermatids and can serve as a model to study centriole duplication. Genetics 182, 133-144.

Blagden, S.P., and Glover, D.M. (2003). Polar expeditions--provisioning the centrosome for mitosis. Nat Cell Biol 5, 505-511.

Bolderson, E., Richard, D.J., Zhou, B.B., and Khanna, K.K. (2009). Recent advances in cancer therapy targeting proteins involved in DNA double-strand break repair. Clin Cancer Res 15, 6314-6320.

Bornens, M. (2002). Centrosome composition and microtubule anchoring mechanisms. Curr Opin Cell Biol 14, 25-34.

Bourke, E., Brown, J.A., Takeda, S., Hochegger, H., and Morrison, C.G. (2010). DNA damage induces Chk1-dependent threonine-160 phosphorylation and activation of Cdk2. Oncogene 29, 616-624.

Bourke, E., Dodson, H., Merdes, A., Cuffe, L., Zachos, G., Walker, M., Gillespie, D., and Morrison, C.G. (2007). DNA damage induces Chk1-dependent centrosome amplification. EMBO Rep 8, 603-609.

Boutros, R., Lobjois, V., and Ducommun, B. (2007). CDC25 phosphatases in cancer cells: key players? Good targets? Nat Rev Cancer 7, 495-507.

Bradford, M.M. (1976). A rapid and sensitive method for the quantitation of microgram quantities of protein utilizing the principle of protein-dye binding. Anal Biochem 72, 248-254.

Brehm, A., Miska, E., Reid, J., Bannister, A., and Kouzarides, T. (1999). The cell cycle-regulating transcription factors E2F-RB. Br J Cancer 80 Suppl 1, 38-41.

Brennan, I.M., Peters, U., Kapoor, T.M., and Straight, A.F. (2007). Polo-like kinase controls vertebrate spindle elongation and cytokinesis. PLoS One 2, e409.

Brown, J.A., Bourke, E., Liptrot, C., Dockery, P., and Morrison, C.G. (2010). MCPH1/BRIT1 limits ionizing radiation-induced centrosome amplification. Oncogene 29, 5537-5544.

Brown, J.R., Nigh, E., Lee, R.J., Ye, H., Thompson, M.A., Saudou, F., Pestell, R.G., and Greenberg, M.E. (1998). Fos family members induce cell cycle entry by activating cyclin D1. Mol Cell Biol 18, 5609-5619.

Buerstedde, J.M., and Takeda, S. (1991). Increased ratio of targeted to random integration after transfection of chicken B cell lines. Cell 67, 179-188.

Burkard, M.E., Randall, C.L., Larochelle, S., Zhang, C., Shokat, K.M., Fisher, R.P., and Jallepalli, P.V. (2007). Chemical genetics reveals the requirement for Polo-like kinase 1 activity in positioning RhoA and triggering cytokinesis in human cells. Proc Natl Acad Sci U S A 104, 4383-4388.

Burma, S., Chen, B.P., Murphy, M., Kurimasa, A., and Chen, D.J. (2001). ATM phosphorylates histone H2AX in response to DNA double-strand breaks. J Biol Chem 276, 42462-42467.

Burton, J.L., and Solomon, M.J. (2007). Mad3p, a pseudosubstrate inhibitor of APCCdc20 in the spindle assembly checkpoint. Genes Dev 21, 655-667.

Cann, K.L., and Hicks, G.G. (2007). Regulation of the cellular DNA double-strand break response. Biochem Cell Biol 85, 663-674.

Capecchi, M.R. (1989). Altering the genome by homologous recombination. Science 244, 1288-1292.

Capecchi, M.R. (2005). Gene targeting in mice: functional analysis of the mammalian genome for the twenty-first century. Nat Rev Genet 6, 507-512.

Carvalho-Santos, Z., Machado, P., Branco, P., Tavares-Cadete, F., Rodrigues-Martins, A., Pereira-Leal, J.B., and Bettencourt-Dias, M. (2010). Stepwise evolution of the centriole-assembly pathway. J Cell Sci 123, 1414-1426.

Cazales, M., Boutros, R., Brezak, M.C., Chaumeron, S., Prevost, G., and Ducommun, B. (2007). Pharmacologic inhibition of CDC25 phosphatases impairs interphase microtubule dynamics and mitotic spindle assembly. Mol Cancer Ther 6, 318-325
.
Chang, P., Giddings, T.H., Jr., Winey, M., and Stearns, T. (2003). Epsilon-tubulin is required for centriole duplication and microtubule organization. Nat Cell Biol 5, 71-76.

Chen, Z., Indjeian, V.B., McManus, M., Wang, L., and Dynlacht, B.D. (2002). CP110, a cell cycle-dependent CDK substrate, regulates centrosome duplication in human cells. Dev Cell 3, 339-350.

Ciccia, A., McDonald, N., and West, S.C. (2008). Structural and Functional Relationships of the XPF/MUS81 Family of Proteins. Annual Review of Biochemistry 77, 259-287.

Cooley, C., Baird, K.M., Faure, V., Wenner, T., Stewart, J.L., Modino, S., Slijepcevic, P., Farr, C.J., and Morrison, C.G. (2009). Trf1 is not required for proliferation or functional telomere maintenance in chicken DT40 cells. Mol Biol Cell 20, 2563-2571.

Couzin, J. (2002). Breakthrough of the year. Small RNAs make big splash. Science 298, 2296-2297.

Cuadrado, M., Martinez-Pastor, B., Murga, M., Toledo, L.I., Gutierrez-Martinez, P., Lopez, E., and Fernandez-Capetillo, O. (2006). ATM regulates ATR chromatin loading in response to DNA double-strand breaks. J Exp Med 203, 297-303.

Cunha-Ferreira, I., Rodrigues-Martins, A., Bento, I., Riparbelli, M., Zhang, W., Laue, E., Callaini, G., Glover, D.M., and Bettencourt-Dias, M. (2009). The SCF/Slimb ubiquitin ligase limits centrosome amplification through degradation of SAK/PLK4. Curr Biol 19, 43-49.

Dai, Y., and Grant, S. (2010). New insights into checkpoint kinase 1 in the DNA damage response signaling network. Clin Cancer Res 16, 376-383.

Dammermann, A., Maddox, P.S., Desai, A., and Oegema, K. (2008). SAS-4 is recruited to a dynamic structure in newly forming centrioles that is stabilized by the gamma-tubulin-mediated addition of centriolar microtubules. J Cell Biol 180, 771-785.

Dammermann, A., and Merdes, A. (2002). Assembly of centrosomal proteins and microtubule organization depends on PCM-1. J Cell Biol 159, 255-266.

Daniels, M.J., Wang, Y., Lee, M., and Venkitaraman, A.R. (2004). Abnormal cytokinesis in cells deficient in the breast cancer susceptibility protein BRCA2. Science 306, 876-879.

Dantas, T.J., Wang, Y., Lalor, P., Dockery, P., and Morrison, C.G. (2011). Defective nucleotide excision repair with normal centrosome structures and functions in the absence of all vertebrate centrins. J Cell Biol 193, 307-318.

David O. Morgan (2007). The Cell Cycle, Principles of Control, New Science Press.

De Luca, M., Lavia, P., and Guarguaglini, G. (2006). A functional interplay between Aurora-A, Plk1 and TPX2 at spindle poles: Plk1 controls centrosomal localization of Aurora-A and TPX2 spindle association. Cell Cycle 5, 296-303.

Debec, A., Sullivan, W., and Bettencourt-Dias, M. (2010). Centrioles: active players or passengers during mitosis? Cell Mol Life Sci 67, 2173-2194.

DeGregori, J. (2002). The genetics of the E2F family of transcription factors: shared functions and unique roles. Biochim Biophys Acta 1602, 131-150.

Delgehyr, N., Sillibourne, J., and Bornens, M. (2005). Microtubule nucleation and anchoring at the centrosome are independent processes linked by ninein function. J Cell Sci 118, 1565-1575.

Deng, C.X. (2002). Roles of BRCA1 in centrosome duplication. Oncogene 21, 6222-6227.

Desai, D., Wessling, H.C., Fisher, R.P., and Morgan, D.O. (1995). Effects of phosphorylation by CAK on cyclin binding by CDC2 and CDK2. Mol Cell Biol 15, 345-350.

Dhar, P.K., Sonoda, E., Fujimori, A., Yamashita, Y.M., and Takeda, S. (2001). DNA repair studies: experimental evidence in support of chicken DT40 cell line as a unique model. J Environ Pathol Toxicol Oncol 20, 273-283.

Dobbelaere, J., Josue, F., Suijkerbuijk, S., Baum, B., Tapon, N., and Raff, J. (2008). A genome-wide RNAi screen to dissect centriole duplication and centrosome maturation in Drosophila. PLoS Biol 6, e224.

Dodson, H., Bourke, E., Jeffers, L.J., Vagnarelli, P., Sonoda, E., Takeda, S., Earnshaw, W.C., Merdes, A., and Morrison, C. (2004). Centrosome amplification induced by DNA damage occurs during a prolonged G2 phase and involves ATM. EMBO J 23, 3864-3873.

Doxsey, S. (2001). Re-evaluating centrosome function. Nat Rev Mol Cell Biol 2, 688-698.

Duelli, D.M., Padilla-Nash, H.M., Berman, D., Murphy, K.M., Ried, T., and Lazebnik, Y. (2007). A virus causes cancer by inducing massive chromosomal instability through cell fusion. Curr Biol 17, 431-437.

Duensing, A., Chin, A., Wang, L., Kuan, S.F., and Duensing, S. (2008). Analysis of centrosome overduplication in correlation to cell division errors in high-risk human papillomavirus (HPV)-associated anal neoplasms. Virology 372, 157-164.

Duensing, A., Liu, Y., Perdreau, S.A., Kleylein-Sohn, J., Nigg, E.A., and Duensing, S. (2007). Centriole overduplication through the concurrent formation of multiple daughter centrioles at single maternal templates. Oncogene 26, 6280-6288.

Duensing, A., Liu, Y., Tseng, M., Malumbres, M., Barbacid, M., and Duensing, S. (2006). Cyclin-dependent kinase 2 is dispensable for normal centrosome duplication but required for oncogene-induced centrosome overduplication. Oncogene 25, 2943-2949.

Duensing, A., Spardy, N., Chatterjee, P., Zheng, L., Parry, J., Cuevas, R., Korzeniewski, N., and Duensing, S. (2009). Centrosome overduplication, chromosomal instability, and human papillomavirus oncoproteins. Environ Mol Mutagen 50, 741-747.

Dutertre, S., Cazales, M., Quaranta, M., Froment, C., Trabut, V., Dozier, C., Mirey, G., Bouche, J.P., Theis-Febvre, N., Schmitt, E., et al. (2004). Phosphorylation of CDC25B by Aurora-A at the centrosome contributes to the G2-M transition. J Cell Sci 117, 2523-2531.

Dymecki, S.M. (1996). Flp recombinase promotes site-specific DNA recombination in embryonic stem cells and transgenic mice. Proc Natl Acad Sci U S A 93, 6191-6196.

Echeverri, C.J., Paschal, B.M., Vaughan, K.T., and Vallee, R.B. (1996). Molecular characterization of the 50-kD subunit of dynactin reveals function for the complex in chromosome alignment and spindle organization during mitosis. J Cell Biol 132, 617-633.

Eckerdt, F., Yamamoto, T.M., Lewellyn, A.L., and Maller, J.L. (2011). Identification of a polo-like kinase 4-dependent pathway for de novo centriole formation. Curr Biol 21, 428-432.

Etienne-Manneville, S. (2010). From signaling pathways to microtubule dynamics: the key players. Curr Opin Cell Biol 22, 104-111.

Falck, J., Mailand, N., Syljuasen, R.G., Bartek, J., and Lukas, J. (2001). The ATM-Chk2-Cdc25A checkpoint pathway guards against radioresistant DNA synthesis. Nature 410, 842-847.

Falck, J., Petrini, J.H., Williams, B.R., Lukas, J., and Bartek, J. (2002). The DNA damage-dependent intra-S phase checkpoint is regulated by parallel pathways. Nat Genet 30, 290-294.

Fekairi, S., Scaglione, S., Chahwan, C., Taylor, E.R., Tissier, A., Coulon, S., Dong, M.-Q., Ruse, C., Yates Iii, J.R., Russell, P., et al. (2009). Human SLX4 Is a Holliday Junction Resolvase Subunit that Binds Multiple DNA Repair/Recombination Endonucleases. Cell 138, 78-89.

Fisher, R.P., and Morgan, D.O. (1994). A novel cyclin associates with MO15/CDK7 to form the CDK-activating kinase. Cell 78, 713-724.

Fisk, H.A., Mattison, C.P., and Winey, M. (2003). Human Mps1 protein kinase is required for centrosome duplication and normal mitotic progression. Proc Natl Acad Sci U S A 100, 14875-14880.

Fisk, H.A., and Winey, M. (2001). The mouse Mps1p-like kinase regulates centrosome duplication. Cell 106, 95-104.

Fong, K.W., Choi, Y.K., Rattner, J.B., and Qi, R.Z. (2008). CDK5RAP2 is a pericentriolar protein that functions in centrosomal attachment of the gamma-tubulin ring complex. Mol Biol Cell 19, 115-125.

Fry, A.M., Mayor, T., Meraldi, P., Stierhof, Y.D., Tanaka, K., and Nigg, E.A. (1998). C-Nap1, a novel centrosomal coiled-coil protein and candidate substrate of the cell cycle-regulated protein kinase Nek2. J Cell Biol 141, 1563-1574.

Fukasawa, K. (2005). Centrosome amplification, chromosome instability and cancer development. Cancer Lett 230, 6-19.

Fukasawa, K. (2008). P53, cyclin-dependent kinase and abnormal amplification of centrosomes. Biochim Biophys Acta 1786, 15-23.

Fukasawa, K., Choi, T., Kuriyama, R., Rulong, S., and Vande Woude, G.F. (1996). Abnormal centrosome amplification in the absence of p53. Science 271, 1744-1747.

Ganem, N.J., Godinho, S.A., and Pellman, D. (2009). A mechanism linking extra centrosomes to chromosomal instability. Nature 460, 278-282.

Gillis, C., Haegerstrand, A., Ragnarson, B., and Bengtsson, L. (1994). Rapid visualization of viable and nonviable endothelium on cardiovascular prosthetic surfaces by means of fluorescent dyes. J Thorac Cardiovasc Surg 108, 1043-1048.

Gimenez-Abian, J.F., Diaz-Martinez, L.A., Beauchene, N.A., Hsu, W.S., Tsai, H.J., and Clarke, D.J. (2010). Determinants of Rad21 localization at the centrosome in human cells. Cell Cycle 9, 1759-1763.

Gimenez-Abian, J.F., Diaz-Martinez, L.A., Waizenegger, I.C., Gimenez-Martin, G., and Clarke, D.J. (2005). Separase is required at multiple pre-anaphase cell cycle stages in human cells. Cell Cycle 4, 1576-1584.

Glotzer, M., Murray, A.W., and Kirschner, M.W. (1991). Cyclin is degraded by the ubiquitin pathway. Nature 349, 132-138.

Gorr, I.H., Boos, D., and Stemmann, O. (2005). Mutual inhibition of separase and Cdk1 by two-step complex formation. Mol Cell 19, 135-141.

Gossen, M., and Bujard, H. (2002). Studying gene function in eukaryotes by conditional gene inactivation. Annu Rev Genet 36, 153-173.

Graser, S., Stierhof, Y.D., Lavoie, S.B., Gassner, O.S., Lamla, S., Le Clech, M., and Nigg, E.A. (2007). Cep164, a novel centriole appendage protein required for primary cilium formation. J Cell Biol 179, 321-330.

Griffin, C.S., Simpson, P.J., Wilson, C.R., and Thacker, J. (2000). Mammalian recombination-repair genes XRCC2 and XRCC3 promote correct chromosome segregation. Nat Cell Biol 2, 757-761.

Gruber, S., Haering, C.H., and Nasmyth, K. (2003). Chromosomal cohesin forms a ring. Cell 112, 765-777.

Gu, H., Zou, Y.R., and Rajewsky, K. (1993). Independent control of immunoglobulin switch recombination at individual switch regions evidenced through Cre-loxP-mediated gene targeting. Cell 73, 1155-1164.

Guarguaglini, G., Duncan, P.I., Stierhof, Y.D., Holmstrom, T., Duensing, S., and Nigg, E.A. (2005). The forkhead-associated domain protein Cep170 interacts with Polo-like kinase 1 and serves as a marker for mature centrioles. Mol Biol Cell 16, 1095-1107.

Gudmundsdottir, K., and Ashworth, A. (2006). The roles of BRCA1 and BRCA2 and associated proteins in the maintenance of genomic stability. Oncogene 25, 5864-5874.

Guichard, P., Chretien, D., Marco, S., and Tassin, A.M. (2010). Procentriole assembly revealed by cryo-electron tomography. EMBO J 29, 1565-1572.

Gustafson, L.M., Gleich, L.L., Fukasawa, K., Chadwell, J., Miller, M.A., Stambrook, P.J., and Gluckman, J.L. (2000). Centrosome hyperamplification in head and neck squamous cell carcinoma: a potential phenotypic marker of tumor aggressiveness. Laryngoscope 110, 1798-1801.

Habedanck, R., Stierhof, Y.D., Wilkinson, C.J., and Nigg, E.A. (2005). The Polo kinase Plk4 functions in centriole duplication. Nat Cell Biol 7, 1140-1146.

Haering, C.H., Farcas, A.M., Arumugam, P., Metson, J., and Nasmyth, K. (2008). The cohesin ring concatenates sister DNA molecules. Nature 454, 297-301.

Halazonetis, T. D., Gorgoulis, V. G., and Bartek, J. (2008). An oncogene-induced DNA damage model for cancer development. Science 319,1352-1355.

Harbour, J.W., and Dean, D.C. (2000). Rb function in cell-cycle regulation and apoptosis. Nat Cell Biol 2, E65-67.

Haren, L., Remy, M.H., Bazin, I., Callebaut, I., Wright, M., and Merdes, A. (2006). NEDD1-dependent recruitment of the gamma-tubulin ring complex to the centrosome is necessary for centriole duplication and spindle assembly. J Cell Biol 172, 505-515.

Haren, L., Stearns, T., and Luders, J. (2009). Plk1-dependent recruitment of gamma-tubulin complexes to mitotic centrosomes involves multiple PCM components. PLoS One 4, e5976.

Hatch, E., and Stearns, T. (2010). The life cycle of centrioles. Cold Spring Harb Symp Quant Biol 75, 425-431.

Hayward, D.G., Clarke, R.B., Faragher, A.J., Pillai, M.R., Hagan, I.M., and Fry, A.M. (2004). The centrosomal kinase Nek2 displays elevated levels of protein expression in human breast cancer. Cancer Res 64, 7370-7376.

Helps, N.R., Luo, X., Barker, H.M., and Cohen, P.T. (2000). NIMA-related kinase 2 (Nek2), a cell-cycle-regulated protein kinase localized to centrosomes, is complexed to protein phosphatase 1. Biochem J 349, 509-518.

Hinchcliffe, E.H., Li, C., Thompson, E.A., Maller, J.L., and Sluder, G. (1999). Requirement of Cdk2-cyclin E activity for repeated centrosome reproduction in Xenopus egg extracts. Science 283, 851-854.

Hinchcliffe, E.H., Miller, F.J., Cham, M., Khodjakov, A., and Sluder, G. (2001). Requirement of a centrosomal activity for cell cycle progression through G1 into S phase. Science 291, 1547-1550.

Hiraki, M., Nakazawa, Y., Kamiya, R., and Hirono, M. (2007). Bld10p constitutes the cartwheel-spoke tip and stabilizes the 9-fold symmetry of the centriole. Curr Biol 17, 1778-1783.

Hirota, T., Kunitoku, N., Sasayama, T., Marumoto, T., Zhang, D., Nitta, M., Hatakeyama, K., and Saya, H. (2003). Aurora-A and an interacting activator, the LIM protein Ajuba, are required for mitotic commitment in human cells. Cell 114, 585-598.

Hochegger, H., Dejsuphong, D., Sonoda, E., Saberi, A., Rajendra, E., Kirk, J., Hunt, T., and Takeda, S. (2007). An essential role for Cdk1 in S phase control is revealed via chemical genetics in vertebrate cells. J Cell Biol 178, 257-268.

Hochegger, H., Takeda, S., and Hunt, T. (2008). Cyclin-dependent kinases and cell-cycle transitions: does one fit all? Nat Rev Mol Cell Biol 9, 910-916.

Holland, A.J., and Cleveland, D.W. (2009). Boveri revisited: chromosomal instability, aneuploidy and tumorigenesis. Nat Rev Mol Cell Biol 10, 478-487.

Holland, A.J., and Taylor, S.S. (2006). Cyclin-B1-mediated inhibition of excess separase is required for timely chromosome disjunction. J Cell Sci 119, 3325-3336.

Holt, S.V., Vergnolle, M.A., Hussein, D., Wozniak, M.J., Allan, V.J., and Taylor, S.S. (2005). Silencing Cenp-F weakens centromeric cohesion, prevents chromosome alignment and activates the spindle checkpoint. J Cell Sci 118, 4889-4900.

Huberman, J.A. (1981). New views of the biochemistry of eucaryotic DNA replication revealed by aphidicolin, an unusual inhibitor of DNA polymerase alpha. Cell 23, 647-648.

Hudson, D.F., Morrison, C., Ruchaud, S., and Earnshaw, W.C. (2002). Reverse genetics of essential genes in tissue-culture cells: 'dead cells talking'. Trends Cell Biol 12, 281-287.

Hussein, D., and Taylor, S.S. (2002). Farnesylation of Cenp-F is required for G2/M progression and degradation after mitosis. J Cell Sci 115, 3403-3414.

Hut, H.M., Lemstra, W., Blaauw, E.H., Van Cappellen, G.W., Kampinga, H.H., and Sibon, O.C. (2003). Centrosomes split in the presence of impaired DNA integrity during mitosis. Mol Biol Cell 14, 1993-2004.

Hutterer, A., Berdnik, D., Wirtz-Peitz, F., Zigman, M., Schleiffer, A., and Knoblich, J.A. (2006). Mitotic activation of the kinase Aurora-A requires its binding partner Bora. Dev Cell 11, 147-157.

Inanc, B., Dodson, H., and Morrison, C.G. (2010). A centrosome-autonomous signal that involves centriole disengagement permits centrosome duplication in G2 phase after DNA damage. Mol Biol Cell 21, 3866-3877.

Inanc, B., and Morrison, C.G. (2011). Getting permission: How DNA damage causes centrosome amplification. Cell Cycle 10, 1890-1891.

Ip, S.C., Rass, U., Blanco, M.G., Flynn, H.R., Skehel, J.M., and West, S.C. (2008a). Identification of Holliday junction resolvases from humans and yeast. Nature 456, 357-361.

Ishikawa, H., Kubo, A., and Tsukita, S. (2005). Odf2-deficient mother centrioles lack distal/subdistal appendages and the ability to generate primary cilia. Nat Cell Biol 7, 517-524.

Jackman, M., Lindon, C., Nigg, E.A., and Pines, J. (2003). Active cyclin B1-Cdk1 first appears on centrosomes in prophase. Nat Cell Biol 5, 143-148.

Jazayeri, A., Falck, J., Lukas, C., Bartek, J., Smith, G.C., Lukas, J., and Jackson, S.P. (2006). ATM- and cell cycle-dependent regulation of ATR in response to DNA double-strand breaks. Nat Cell Biol 8, 37-45.

Jeffers, L.J., Coull, B.J., Stack, S.J., and Morrison, C.G. (2008). Distinct BRCT domains in Mcph1/Brit1 mediate ionizing radiation-induced focus formation and centrosomal localization. Oncogene 27, 139-144.

Jerka-Dziadosz, M., Gogendeau, D., Klotz, C., Cohen, J., Beisson, J., and Koll, F. (2010). Basal body duplication in Paramecium: the key role of Bld10 in assembly and stability of the cartwheel. Cytoskeleton (Hoboken) 67, 161-171.

Johnson, E.F., Stewart, K.D., Woods, K.W., Giranda, V.L., and Luo, Y. (2007). Pharmacological and functional comparison of the polo-like kinase family: insight into inhibitor and substrate specificity. Biochemistry 46, 9551-9563.

Karagiannis, T.C., and El-Osta, A. (2004). Double-strand breaks: signaling pathways and repair mechanisms. Cell Mol Life Sci 61, 2137-2147.

Karsenti, E., and Vernos, I. (2001). The mitotic spindle: a self-made machine. Science 294, 543-547.

Kasbek, C., Yang, C.H., Yusof, A.M., Chapman, H.M., Winey, M., and Fisk, H.A. (2007). Preventing the degradation of mps1 at centrosomes is sufficient to cause centrosome reduplication in human cells. Mol Biol Cell 18, 4457-4469.

Kaye, F.J. (2002). RB and cyclin dependent kinase pathways: defining a distinction between RB and p16 loss in lung cancer. Oncogene 21, 6908-6914.

Keller, L.C., Geimer, S., Romijn, E., Yates, J., 3rd, Zamora, I., and Marshall, W.F. (2009). Molecular architecture of the centriole proteome: the conserved WD40 domain protein POC1 is required for centriole duplication and length control. Mol Biol Cell 20, 1150-1166.

Khodjakov, A., Rieder, C.L., Sluder, G., Cassels, G., Sibon, O., and Wang, C.L. (2002). De novo formation of centrosomes in vertebrate cells arrested during S phase. J Cell Biol 158, 1171-1181.

Kim, K., Lee, S., Chang, J., and Rhee, K. (2008). A novel function of CEP135 as a platform protein of C-NAP1 for its centriolar localization. Exp Cell Res 314, 3692-3700.

Kimble, M., and Kuriyama, R. (1992). Functional components of microtubule-organizing centers. Int Rev Cytol 136, 1-50.

Kirkham, M., Muller-Reichert, T., Oegema, K., Grill, S., and Hyman, A.A. (2003). SAS-4 is a C. elegans centriolar protein that controls centrosome size. Cell 112, 575-587.

Kitagawa, D., Busso, C., Fluckiger, I., and Gonczy, P. (2009). Phosphorylation of SAS-6 by ZYG-1 is critical for centriole formation in C. elegans embryos. Dev Cell 17, 900-907.

Kitajima, T.S., Sakuno, T., Ishiguro, K., Iemura, S., Natsume, T., Kawashima, S.A., and Watanabe, Y. (2006). Shugoshin collaborates with protein phosphatase 2A to protect cohesin. Nature 441, 46-52.

Kleylein-Sohn, J., Westendorf, J., Le Clech, M., Habedanck, R., Stierhof, Y.D., and Nigg, E.A. (2007). Plk4-induced centriole biogenesis in human cells. Dev Cell 13, 190-202.

Kline-Smith, S.L., and Walczak, C.E. (2004). Mitotic spindle assembly and chromosome segregation: refocusing on microtubule dynamics. Mol Cell 15, 317-327.

Kohlmaier, G., Loncarek, J., Meng, X., McEwen, B.F., Mogensen, M.M., Spektor, A., Dynlacht, B.D., Khodjakov, A., and Gonczy, P. (2009). Overly long centrioles and defective cell division upon excess of the SAS-4-related protein CPAP. Curr Biol 19, 1012-1018.

Kozak, M. (1986). Point mutations define a sequence flanking the AUG initiator codon that modulates translation by eukaryotic ribosomes. Cell 44, 283-292.

Kraakman-van der Zwet, M., Overkamp, W.J., van Lange, R.E., Essers, J., van Duijn-Goedhart, A., Wiggers, I., Swaminathan, S., van Buul, P.P., Errami, A., Tan, R.T., et al. (2002). Brca2 (XRCC11) deficiency results in radioresistant DNA synthesis and a higher frequency of spontaneous deletions. Mol Cell Biol 22, 669-679.

Kramer, A., Mailand, N., Lukas, C., Syljuasen, R.G., Wilkinson, C.J., Nigg, E.A., Bartek, J., and Lukas, J. (2004). Centrosome-associated Chk1 prevents premature activation of cyclin-B-Cdk1 kinase. Nat Cell Biol 6, 884-891.

Kramer, A., Schweizer, S., Neben, K., Giesecke, C., Kalla, J., Katzenberger, T., Benner, A., Muller-Hermelink, H.K., Ho, A.D., and Ott, G. (2003). Centrosome aberrations as a possible mechanism for chromosomal instability in non-Hodgkin's lymphoma. Leukemia 17, 2207-2213.

Kuhn, R., and Schwenk, F. (2003). Conditional knockout mice. Methods Mol Biol 209, 159-185.

Kuo, K.K., Sato, N., Mizumoto, K., Maehara, N., Yonemasu, H., Ker, C.G., Sheen, P.C., and Tanaka, M. (2000). Centrosome abnormalities in human carcinomas of the gallbladder and intrahepatic and extrahepatic bile ducts. Hepatology 31, 59-64.

La Terra, S., English, C.N., Hergert, P., McEwen, B.F., Sluder, G., and Khodjakov, A. (2005). The de novo centriole assembly pathway in HeLa cells: cell cycle progression and centriole assembly/maturation. J Cell Biol 168, 713-722.

Lacey, K.R., Jackson, P.K., and Stearns, T. (1999). Cyclin-dependent kinase control of centrosome duplication. Proc Natl Acad Sci U S A 96, 2817-2822.

Lane, H.A., and Nigg, E.A. (1996). Antibody microinjection reveals an essential role for human polo-like kinase 1 (Plk1) in the functional maturation of mitotic centrosomes. J Cell Biol 135, 1701-1713.

Lee, A.Y., Liu, E., and Wu, X. (2007). The Mre11/Rad50/Nbs1 complex plays an important role in the prevention of DNA rereplication in mammalian cells. J Biol Chem 282, 32243-32255.

Leidel, S., Delattre, M., Cerutti, L., Baumer, K., and Gonczy, P. (2005). SAS-6 defines a protein family required for centrosome duplication in C. elegans and in human cells. Nat Cell Biol 7, 115-125.

Leidel, S., and Gonczy, P. (2003). SAS-4 is essential for centrosome duplication in C elegans and is recruited to daughter centrioles once per cell cycle. Dev Cell 4, 431-439.

Li, L., and Zou, L. (2005). Sensing, signaling, and responding to DNA damage: organization of the checkpoint pathways in mammalian cells. J Cell Biochem 94, 298-306.

Lieber, M.R. (2010). The mechanism of double-strand DNA break repair by the nonhomologous DNA end-joining pathway. Annual review of biochemistry 79, 181-211.

Lingle, W.L., Barrett, S.L., Negron, V.C., D'Assoro, A.B., Boeneman, K., Liu, W., Whitehead, C.M., Reynolds, C., and Salisbury, J.L. (2002). Centrosome amplification drives chromosomal instability in breast tumor development. Proc Natl Acad Sci U S A 99, 1978-1983.

Lingle, W.L., Lukasiewicz, K., and Salisbury, J.L. (2005). Deregulation of the centrosome cycle and the origin of chromosomal instability in cancer. Adv Exp Med Biol 570, 393-421.

Lingle, W.L., Lutz, W.H., Ingle, J.N., Maihle, N.J., and Salisbury, J.L. (1998). Centrosome hypertrophy in human breast tumors: implications for genomic stability and cell polarity. Proc Natl Acad Sci U S A 95, 2950-2955.

Lingle, W.L., and Salisbury, J.L. (2001). Methods for the analysis of centrosome reproduction in cancer cells. Methods Cell Biol 67, 325-336.

Liu, X., and Erikson, R.L. (2002). Activation of Cdc2/cyclin B and inhibition of centrosome amplification in cells depleted of Plk1 by siRNA. Proc Natl Acad Sci U S A 99, 8672-8676.

Loffler, H., Bochtler, T., Fritz, B., Tews, B., Ho, A.D., Lukas, J., Bartek, J., and Kramer, A. (2007). DNA damage-induced accumulation of centrosomal Chk1 contributes to its checkpoint function. Cell Cycle 6, 2541-2548.

Loffler, H., Lukas, J., Bartek, J., and Kramer, A. (2006). Structure meets function--centrosomes, genome maintenance and the DNA damage response. Exp Cell Res 312, 2633-2640.

Loncarek, J., Hergert, P., and Khodjakov, A. (2010). Centriole reduplication during prolonged interphase requires procentriole maturation governed by Plk1. Curr Biol 20, 1277-1282.

Loncarek, J., Hergert, P., Magidson, V., and Khodjakov, A. (2008). Control of daughter centriole formation by the pericentriolar material. Nat Cell Biol 10, 322-328.

Loncarek, J., and Khodjakov, A. (2009). Ab ovo or de novo? Mechanisms of centriole duplication. Mol Cells 27, 135-142.

Lou, Z., Minter-Dykhouse, K., Franco, S., Gostissa, M., Rivera, M.A., Celeste, A., Manis, J.P., van Deursen, J., Nussenzweig, A., Paull, T.T., et al. (2006). MDC1 maintains genomic stability by participating in the amplification of ATM-dependent DNA damage signals. Mol Cell 21, 187-200.

Lucibello, F.C., Sewing, A., Brusselbach, S., Burger, C., and Muller, R. (1993). Deregulation of cyclins D1 and E and suppression of cdk2 and cdk4 in senescent human fibroblasts. J Cell Sci 105 (Pt 1), 123-133.

Luders, J., Patel, U.K., and Stearns, T. (2006). GCP-WD is a gamma-tubulin targeting factor required for centrosomal and chromatin-mediated microtubule nucleation. Nat Cell Biol 8, 137-147.

Luders, J., and Stearns, T. (2007). Microtubule-organizing centres: a re-evaluation. Nat Rev Mol Cell Biol 8, 161-167.

Lukas, J., Lukas, C., and Bartek, J. (2004). Mammalian cell cycle checkpoints: signalling pathways and their organization in space and time. DNA Repair (Amst) 3, 997-1007.

Lukasiewicz, K.B., and Lingle, W.L. (2009). Aurora A, centrosome structure, and the centrosome cycle. Environ Mol Mutagen 50, 602-619.

Luo, H., Li, Y., Mu, J.J., Zhang, J., Tonaka, T., Hamamori, Y., Jung, S.Y., Wang, Y., and Qin, J. (2008). Regulation of intra-S phase checkpoint by ionizing radiation (IR)-dependent and IR-independent phosphorylation of SMC3. J Biol Chem 283, 19176-19183.

Lupas, A., Van Dyke, M., and Stock, J. (1991). Predicting coiled coils from protein sequences. Science 252, 1162-1164.

Ma, Y., Schwarz, K., and Lieber, M.R. (2005). The Artemis:DNA-PKcs endonuclease cleaves DNA loops, flaps, and gaps. DNA Repair (Amst) 4, 845-851.

Macurek, L., Lindqvist, A., Lim, D., Lampson, M.A., Klompmaker, R., Freire, R., Clouin, C., Taylor, S.S., Yaffe, M.B., and Medema, R.H. (2008). Polo-like kinase-1 is activated by aurora A to promote checkpoint recovery. Nature 455, 119-123.

Mahaney, B.L., Meek, K., and Lees-Miller, S.P. (2009). Repair of ionizing radiation-induced DNA double-strand breaks by non-homologous end-joining. Biochem J 417, 639-650.

Marshall, W.F. (2009). Centriole evolution. Curr Opin Cell Biol 21, 14-19.

Matsumoto, Y., Hayashi, K., and Nishida, E. (1999). Cyclin-dependent kinase 2 (Cdk2) is required for centrosome duplication in mammalian cells. Curr Biol 9, 429-432.

Matsumoto, Y., and Maller, J.L. (2004). A centrosomal localization signal in cyclin E required for Cdk2-independent S phase entry. Science 306, 885-888.

Matsuura, K., Lefebvre, P.A., Kamiya, R., and Hirono, M. (2004). Bld10p, a novel protein essential for basal body assembly in Chlamydomonas: localization to the cartwheel, the first ninefold symmetrical structure appearing during assembly. J Cell Biol 165, 663-671.

Mayor, T., Stierhof, Y.D., Tanaka, K., Fry, A.M., and Nigg, E.A. (2000). The centrosomal protein C-Nap1 is required for cell cycle-regulated centrosome cohesion. J Cell Biol 151, 837-846.

McCormack, W.T., Tjoelker, L.W., Stella, G., Postema, C.E., and Thompson, C.B. (1991). Chicken T-cell receptor beta-chain diversity: an evolutionarily conserved D beta-encoded glycine turn within the hypervariable CDR3 domain. Proc Natl Acad Sci U S A 88, 7699-7703.

Meek, K., Dang, V., and Lees-Miller, S.P. (2008). DNA-PK: the means to justify the ends? Adv Immunol 99, 33-58.

Meek, K., Gupta, S., Ramsden, D.A., and Lees-Miller, S.P. (2004). The DNA-dependent protein kinase: the director at the end. Immunol Rev 200, 132-141.

Meister, G., and Tuschl, T. (2004). Mechanisms of gene silencing by double-stranded RNA. Nature 431, 343-349.

Meraldi, P., Honda, R., and Nigg, E.A. (2002). Aurora-A overexpression reveals tetraploidization as a major route to centrosome amplification in p53-/- cells. EMBO J 21, 483-492.

Meraldi, P., Lukas, J., Fry, A.M., Bartek, J., and Nigg, E.A. (1999). Centrosome duplication in mammalian somatic cells requires E2F and Cdk2-cyclin A. Nat Cell Biol 1, 88-93.

Meraldi, P., and Nigg, E.A. (2002). The centrosome cycle. FEBS Lett 521, 9-13.

Michel, L., Diaz-Rodriguez, E., Narayan, G., Hernando, E., Murty, V.V., and Benezra, R. (2004). Complete loss of the tumor suppressor MAD2 causes premature cyclin B degradation and mitotic failure in human somatic cells. Proc Natl Acad Sci U S A 101, 4459-4464.

Mikule, K., Delaval, B., Kaldis, P., Jurcyzk, A., Hergert, P., and Doxsey, S. (2007). Loss of centrosome integrity induces p38-p53-p21-dependent G1-S arrest. Nat Cell Biol 9, 160-170.

Misra, R.P., and Duncan, S.A. (2002). Gene targeting in the mouse: advances in introduction of transgenes into the genome by homologous recombination. Endocrine 19, 229-238.

Mogensen, M.M., Malik, A., Piel, M., Bouckson-Castaing, V., and Bornens, M. (2000). Microtubule minus-end anchorage at centrosomal and non-centrosomal sites: the role of ninein. J Cell Sci 113 (Pt 17), 3013-3023.

Morgan, D.O. (1997). Cyclin-dependent kinases: engines, clocks, and microprocessors. Annu Rev Cell Dev Biol 13, 261-291.

Mori, D., Yano, Y., Toyo-oka, K., Yoshida, N., Yamada, M., Muramatsu, M., Zhang, D., Saya, H., Toyoshima, Y.Y., Kinoshita, K., et al. (2007). NDEL1 phosphorylation by Aurora-A kinase is essential for centrosomal maturation, separation, and TACC3 recruitment. Mol Cell Biol 27, 352-367.

Moritz, M., and Agard, D.A. (2001). Gamma-tubulin complexes and microtubule nucleation.Curr Opin Struct Biol. 11, 174-181.

Moritz, M., Braunfeld, M.B., Sedat, J.W., Alberts, B., and Agard, D.A. (1995). Microtubule nucleation by gamma-tubulin-containing rings in the centrosome. Nature 378, 638-640.

Morrison, C., Sonoda, E., Takao, N., Shinohara, A., Yamamoto, K., and Takeda, S. (2000). The controlling role of ATM in homologous recombinational repair of DNA damage. EMBO J 19, 463-471.

Mottier-Pavie, V., and Megraw, T.L. (2009). Drosophila bld10 is a centriolar protein that regulates centriole, basal body, and motile cilium assembly. Mol Biol Cell 20, 2605-2614.

Moynahan, M.E., and Jasin, M. (2010). Mitotic homologous recombination maintains genomic stability and suppresses tumorigenesis. Nat Rev Mol Cell Biol 11, 196-207.

Muñoz, I.M., Hain, K., Déclais, A.-C., Gardiner, M., Toh, G.W., Sanchez-Pulido, L., Heuckmann, J.M., Toth, R., Macartney, T., Eppink, B., et al. (2009). Coordination of Structure-Specific Nucleases by Human SLX4/BTBD12 Is Required for DNA Repair. Molecular Cell 35, 116-127.

Musacchio, A., and Salmon, E.D. (2007). The spindle-assembly checkpoint in space and time. Nat Rev Mol Cell Biol 8, 379-393.

Myers, J.S., and Cortez, D. (2006). Rapid activation of ATR by ionizing radiation requires ATM and Mre11. J Biol Chem 281, 9346-9350.

Nakamura, A., Arai, H., and Fujita, N. (2009). Centrosomal Aki1 and cohesin function in separase-regulated centriole disengagement. J Cell Biol 187, 607-614.

Nakazawa, Y., Hiraki, M., Kamiya, R., and Hirono, M. (2007). SAS-6 is a cartwheel protein that establishes the 9-fold symmetry of the centriole. Curr Biol 17, 2169-2174.

Nevins, J.R., Leone, G., DeGregori, J., and Jakoi, L. (1997). Role of the Rb/E2F pathway in cell growth control. J Cell Physiol 173, 233-236.

Nigg, E.A. (2006a). Cell biology: a licence for duplication. Nature 442, 874-875.

Nigg, E.A. (2006b). Origins and consequences of centrosome aberrations in human cancers. Int J Cancer 119, 2717-2723.

Nigg, E.A. (2007). Centrosome duplication: of rules and licenses. Trends Cell Biol 17, 215-221.

Nigg, E.A., and Raff, J.W. (2009). Centrioles, centrosomes, and cilia in health and disease. Cell 139, 663-678.

Niida, H., and Nakanishi, M. (2006). DNA damage checkpoints in mammals. Mutagenesis 21, 3-9.

Nilsson, J., Yekezare, M., Minshull, J., and Pines, J. (2008). The APC/C maintains the spindle assembly checkpoint by targeting Cdc20 for destruction. Nat Cell Biol 10, 1411-1420.

Nogales, E., S.G. Wolf, I.A. Khan, R.F. Luduena, and K.H. Downing. (1995). Structure of tubulin at 6.5 A and location of the taxol-binding site. Nature 375, 424-7.

O'Driscoll, M., and Jeggo, P.A. (2006). The role of double-strand break repair - insights from human genetics. Nat Rev Genet 7, 45-54.

Obaya, A.J., and Sedivy, J.M. (2002). Regulation of cyclin-Cdk activity in mammalian cells. Cell Mol Life Sci 59, 126-142.

Ogle, B.M., Cascalho, M., and Platt, J.L. (2005). Biological implications of cell fusion. Nat Rev Mol Cell Biol 6, 567-575.

Ohta, T., Essner, R., Ryu, J.H., Palazzo, R.E., Uetake, Y., and Kuriyama, R. (2002). Characterization of Cep135, a novel coiled-coil centrosomal protein involved in microtubule organization in mammalian cells. J Cell Biol 156, 87-99.

Okuda, M., Horn, H.F., Tarapore, P., Tokuyama, Y., Smulian, A.G., Chan, P.K., Knudsen, E.S., Hofmann, I.A., Snyder, J.D., Bove, K.E., et al. (2000). Nucleophosmin/B23 is a target of CDK2/cyclin E in centrosome duplication. Cell 103, 127-140.

Oricchio, E., Saladino, C., Iacovelli, S., Soddu, S., and Cundari, E. (2006). ATM is activated by default in mitosis, localizes at centrosomes and monitors mitotic spindle integrity. Cell Cycle 5, 88-92.

Ortega, S., Prieto, I., Odajima, J., Martin, A., Dubus, P., Sotillo, R., Barbero, J.L., Malumbres, M., and Barbacid, M. (2003). Cyclin-dependent kinase 2 is essential for meiosis but not for mitotic cell division in mice. Nat Genet 35, 25-31.

Oshimori, N., Ohsugi, M., and Yamamoto, T. (2006). The Plk1 target Kizuna stabilizes mitotic centrosomes to ensure spindle bipolarity. Nat Cell Biol 8, 1095-1101.

Ou, Y.Y., Mack, G.J., Zhang, M., and Rattner, J.B. (2002). CEP110 and ninein are located in a specific domain of the centrosome associated with centrosome maturation. J Cell Sci 115, 1825-1835.

Paddison, P.J., and Hannon, G.J. (2002). RNA interference: the new somatic cell genetics? Cancer Cell 2, 17-23.

Paull, T.T., and Lee, J.H. (2005). The Mre11/Rad50/Nbs1 complex and its role as a DNA double-strand break sensor for ATM. Cell Cycle 4, 737-740.

Pawelek, J.M. (2005). Tumour-cell fusion as a source of myeloid traits in cancer. Lancet Oncol 6, 988-993.

Pedersen, L.B., and Rosenbaum, J.L. (2008). Intraflagellar transport (IFT) role in ciliary assembly, resorption and signalling. Curr Top Dev Biol 85, 23-61.

Peel, N., Stevens, N.R., Basto, R., and Raff, J.W. (2007). Overexpressing centriole-replication proteins in vivo induces centriole overduplication and de novo formation. Curr Biol 17, 834-843.

Pellegrini, L., and Venkitaraman, A. (2004). Emerging functions of BRCA2 in DNA recombination. Trends Biochem Sci 29, 310-316.

Peloponese, J.M., Jr., Haller, K., Miyazato, A., and Jeang, K.T. (2005). Abnormal centrosome amplification in cells through the targeting of Ran-binding protein-1 by the human T cell leukemia virus type-1 Tax oncoprotein. Proc Natl Acad Sci U S A 102, 18974-18979.

Peters, J.M. (2006). The anaphase promoting complex/cyclosome: a machine designed to destroy. Nat Rev Mol Cell Biol 7, 644-656.

Petronczki, M., Lenart, P., and Peters, J.M. (2008). Polo on the Rise-from Mitotic Entry to Cytokinesis with Plk1. Dev Cell 14, 646-659.

Piel, M., Nordberg, J., Euteneuer, U., and Bornens, M. (2001). Centrosome-dependent exit of cytokinesis in animal cells. Science 291, 1550-1553.

Pihan, G.A., Purohit, A., Wallace, J., Knecht, H., Woda, B., Quesenberry, P., and Doxsey, S.J. (1998). Centrosome defects and genetic instability in malignant tumors. Cancer Res 58, 3974-3985.

Pilch, D.R., Sedelnikova, O.A., Redon, C., Celeste, A., Nussenzweig, A., and Bonner, W.M. (2003). Characteristics of gamma-H2AX foci at DNA double-strand breaks sites. Biochem Cell Biol 81, 123-129.

Pines, J., and Hunter, T. (1991). Cyclin-dependent kinases: a new cell cycle motif? Trends Cell Biol 1, 117-121.

Pinhero, R., Liaw, P., Bertens, K., and Yankulov, K. (2004). Three cyclin-dependent kinases preferentially phosphorylate different parts of the C-terminal domain of the large subunit of RNA polymerase II. Eur J Biochem 271, 1004-1014.

Prigent, C., Glover, D.M., and Giet, R. (2005). Drosophila Nek2 protein kinase knockdown leads to centrosome maturation defects while overexpression causes centrosome fragmentation and cytokinesis failure. Exp Cell Res 303, 1-13.

Prigent, Y., Kann, M.L., Lach-Gar, H., Pechart, I., and Fouquet, J.P. (1996). Glutamylated tubulin as a marker of microtubule heterogeneity in the human sperm flagellum. Mol Hum Reprod 2, 573-581.

Prinz, S., Hwang, E.S., Visintin, R., and Amon, A. (1998). The regulation of Cdc20 proteolysis reveals a role for APC components Cdc23 and Cdc27 during S phase and early mitosis. Curr Biol. 8, 750-760.

Prosser, S.L., Straatman, K.R., and Fry, A.M. (2009). Molecular dissection of the centrosome overduplication pathway in S-phase-arrested cells. Mol Cell Biol 29, 1760-1773.

Pugacheva, E.N., and Golemis, E.A. (2005). The focal adhesion scaffolding protein HEF1 regulates activation of the Aurora-A and Nek2 kinases at the centrosome. Nat Cell Biol 7, 937-946.

Quintyne, N.J., Gill, S.R., Eckley, D.M., Crego, C.L., Compton, D.A., and Schroer, T.A. (1999). Dynactin is required for microtubule anchoring at centrosomes. J Cell Biol 147, 321-334.

Rajagopalan, H., and Lengauer, C. (2004). Aneuploidy and cancer. Nature 432, 338-341.

Raleigh, J.M., and O'Connell, M.J. (2000). The G(2) DNA damage checkpoint targets both Wee1 and Cdc25. J Cell Sci 113 (Pt 10), 1727-1736.

Raynaud-Messina, B., and Merdes, A. (2007). Gamma-tubulin complexes and microtubule organization. Curr Opin Cell Biol. 19, 324-330.

Redon, C., Pilch, D., Rogakou, E., Sedelnikova, O., Newrock, K., and Bonner, W. (2002). Histone H2A variants H2AX and H2AZ. Curr Opin Genet Dev 12, 162-169.

Riballo, E., Kuhne, M., Rief, N., Doherty, A., Smith, G.C., Recio, M.J., Reis, C., Dahm, K., Fricke, A., Krempler, A., et al. (2004). A pathway of double-strand break rejoining dependent upon ATM, Artemis, and proteins locating to gamma-H2AX foci. Mol Cell 16, 715-724.

Rodrigues-Martins, A., Bettencourt-Dias, M., Riparbelli, M., Ferreira, C., Ferreira, I., Callaini, G., and Glover, D.M. (2007). DSAS-6 organizes a tube-like centriole precursor, and its absence suggests modularity in centriole assembly. Curr Biol 17, 1465-1472.

Rogers, G.C., Rusan, N.M., Roberts, D.M., Peifer, M., and Rogers, S.L. (2009). The SCF Slimb ubiquitin ligase regulates Plk4/Sak levels to block centriole reduplication. J Cell Biol 184, 225-239.

Rohlmann, A., Gotthardt, M., Willnow, T.E., Hammer, R.E., and Herz, J. (1996). Sustained somatic gene inactivation by viral transfer of Cre recombinase. Nat Biotechnol 14, 1562-1565.

Rose, A., Schraegle, S.J., Stahlberg, E.A., and Meier, I. (2005). Coiled-coil protein composition of 22 proteomes--differences and common themes in subcellular infrastructure and traffic control. BMC Evol Biol 5, 66.

Rothkamm, K., Kruger, I., Thompson, L.H., and Lobrich, M. (2003). Pathways of DNA double-strand break repair during the mammalian cell cycle. Mol Cell Biol 23, 5706-5715.

Ryu, J.H., Essner, R., Ohta, T., and Kuriyama, R. (2000). Filamentous polymers induced by overexpression of a novel centrosomal protein, Cep135. Microsc Res Tech 49, 478-486.

Sak, A., Fegers, I., Groneberg, M., and Stuschke, M. (2008). Effect of separase depletion on ionizing radiation-induced cell cycle checkpoints and survival in human lung cancer cell lines. Cell Prolif 41, 660-670.

Saladino, C., Bourke, E., Conroy, P.C., and Morrison, C.G. (2009). Centriole separation in DNA damage-induced centrosome amplification. Environ Mol Mutagen 50, 725-732.

Salisbury, J.L. (1995). Centrin, centrosomes, and mitotic spindle poles. Curr Opin Cell Biol 7, 39-45.

Salisbury, J.L. (2007). A mechanistic view on the evolutionary origin for centrin-based control of centriole duplication. J Cell Physiol 213, 420-428.

Salisbury, J.L., Baron, A.T., and Sanders, M.A. (1988). The centrin-based cytoskeleton of Chlamydomonas reinhardtii: distribution in interphase and mitotic cells. J Cell Biol 107, 635-641.

Salisbury, J.L., Suino, K.M., Busby, R., and Springett, M. (2002). Centrin-2 is required for centriole duplication in mammalian cells. Curr Biol 12, 1287-1292.

Sambrook, J., and Russell, D.W. (2001). Molecular Cloning. A Laboratory Manual. Cold Spring Harbour Laboratory Press.

Sancar, A., Lindsey-Boltz, L.A., Unsal-Kacmaz, K., and Linn, S. (2004). Molecular mechanisms of mammalian DNA repair and the DNA damage checkpoints. Annual review of biochemistry 73, 39-85.

Sankaran, S., Crone, D.E., Palazzo, R.E., and Parvin, J.D. (2007). Aurora-A kinase regulates breast cancer associated gene 1 inhibition of centrosome-dependent microtubule nucleation. Cancer Res 67, 11186-11194.

Santamaria, A., Neef, R., Eberspacher, U., Eis, K., Husemann, M., Mumberg, D., Prechtl, S., Schulze, V., Siemeister, G., Wortmann, L., et al. (2007). Use of the novel Plk1 inhibitor ZK-thiazolidinone to elucidate functions of Plk1 in early and late stages of mitosis. Mol Biol Cell 18, 4024-4036.

Sarkar, S., Chaudhuri, S., and Basu, T. (2002). Mechanism of artificial transformation of E. coli with plasmid DNA – Clues. Current Science 83, 1376-1380.

Satir, P., and Christensen, S.T. (2008). Structure and function of mammalian cilia. Histochem Cell Biol 129, 687-693.

Sato, N., Mizumoto, K., Nakamura, M., and Tanaka, M. (2000). Radiation-induced centrosome overduplication and multiple mitotic spindles in human tumor cells. Exp Cell Res 255, 321-326.

Saunders, W. (2005). Centrosomal amplification and spindle multipolarity in cancer cells. Semin Cancer Biol 15, 25-32.

Schatten, H. (2008). The mammalian centrosome and its functional significance. Histochem Cell Biol 129, 667-686.

Schmidt, T.I., Kleylein-Sohn, J., Westendorf, J., Le Clech, M., Lavoie, S.B., Stierhof, Y.D., and Nigg, E.A. (2009). Control of centriole length by CPAP and CP110. Curr Biol 19, 1005-1011.

Schnackenberg, B.J., and Palazzo, R.E. (1999). Identification and function of the centrosome centromatrix. Biol Cell 91, 429-438.

Schockel, L., Mockel, M., Mayer, B., Boos, D., and Stemmann, O. (2011). Cleavage of cohesin rings coordinates the separation of centrioles and chromatids. Nat Cell Biol 13, 966-972.

Sedelnikova, O.A., Pilch, D.R., Redon, C., and Bonner, W.M. (2003). Histone H2AX in DNA damage and repair. Cancer Biol Ther 2, 233-235.

Shan, G. (2010). RNA interference as a gene knockdown technique. Int J Biochem Cell Biol 42, 1243-1251.

Shekhar, M.P., Lyakhovich, A., Visscher, D.W., Heng, H., and Kondrat, N. (2002). Rad6 overexpression induces multinucleation, centrosome amplification, abnormal mitosis, aneuploidy, and transformation. Cancer Res 62, 2115-2124.

Sherr, C.J., Kato, J., Quelle, D.E., Matsuoka, M., and Roussel, M.F. (1994). D-type cyclins and their cyclin-dependent kinases: G1 phase integrators of the mitogenic response. Cold Spring Harb Symp Quant Biol 59, 11-19.

Shiloh, Y. (2006). The ATM-mediated DNA-damage response: taking shape. Trends Biochem Sci 31, 402-410.

Shiloh, Y., and Kastan, M.B. (2001). ATM: genome stability, neuronal development, and cancer cross paths. Adv Cancer Res 83, 209-254.

Shimada, M., and Komatsu, K. (2009). Emerging connection between centrosome and DNA repair machinery. J Radiat Res (Tokyo) 50, 295-301.

Shimura, T., Toyoshima, M., Adiga, S.K., Kunoh, T., Nagai, H., Shimizu, N., Inoue, M., and Niwa, O. (2006). Suppression of replication fork progression in low-dose-specific p53-dependent S-phase DNA damage checkpoint. Oncogene 25, 5921-5932.

Shrivastav, M., De Haro, L.P., and Nickoloff, J.A. (2008). Regulation of DNA double-strand break repair pathway choice. Cell Res 18, 134-147.

Silkworth, W.T., Nardi, I.K., Scholl, L.M., and Cimini, D. (2009). Multipolar spindle pole coalescence is a major source of kinetochore mis-attachment and chromosome mis-segregation in cancer cells. PLoS One 4, e6564.

Singla, V., Romaguera-Ros, M., Garcia-Verdugo, J.M., and Reiter, J.F. (2010). Ofd1, a human disease gene, regulates the length and distal structure of centrioles. Dev Cell 18, 410-424.

Smits, V.A., Klompmaker, R., Arnaud, L., Rijksen, G., Nigg, E.A., and Medema, R.H. (2000). Polo-like kinase-1 is a target of the DNA damage checkpoint. Nat Cell Biol 2, 672-676.

Sonoda, E., Sasaki, M.S., Buerstedde, J.M., Bezzubova, O., Shinohara, A., Ogawa, H., Takata, M., Yamaguchi-Iwai, Y., and Takeda, S. (1998). Rad51-deficient vertebrate cells accumulate chromosomal breaks prior to cell death. EMBO J 17, 598-608.

Soung, N.K., Park, J.E., Yu, L.R., Lee, K.H., Lee, J.M., Bang, J.K., Veenstra, T.D., Rhee, K., and Lee, K.S. (2009). Plk1-dependent and -independent roles of an ODF2 splice variant, hCenexin1, at the centrosome of somatic cells. Dev Cell 16, 539-550.

Spector, D. L., Goldman, R. D., Leinwand, L. A. (1997). Cell synchronization. Cells: A Laboratory Manual Vol. 1, Chap. 14**,**14.1-14.13. Cold Spring Harbor Laboratory Press, New York.

Spektor, A., Tsang, W.Y., Khoo, D., and Dynlacht, B.D. (2007). Cep97 and CP110 suppress a cilia assembly program. Cell 130, 678-690.

Starita, L.M., Machida, Y., Sankaran, S., Elias, J.E., Griffin, K., Schlegel, B.P., Gygi, S.P., and Parvin, J.D. (2004). BRCA1-dependent ubiquitination of gamma-tubulin regulates centrosome number. Mol Cell Biol 24, 8457-8466.

Stearns, T., and Winey, M. (1997). The cell center at 100. Cell 91, 303-309.

Steegmaier, M., Hoffmann, M., Baum, A., Lenart, P., Petronczki, M., Krssak, M., Gurtler, U., Garin-Chesa, P., Lieb, S., Quant, J., et al. (2007). BI 2536, a potent and selective inhibitor of polo-like kinase 1, inhibits tumor growth in vivo. Curr Biol 17, 316-322.

Steere, N., Wagner, M., Beishir, S., Smith, E., Breslin, L., Morrison, C.G., Hochegger, H., and Kuriyama, R. (2011). Centrosome amplification in CHO and DT40 cells by inactivation of cyclin-dependent kinases. Cytoskeleton (Hoboken).

Stiff, T., Walker, S.A., Cerosaletti, K., Goodarzi, A.A., Petermann, E., Concannon, P., O'Driscoll, M., and Jeggo, P.A. (2006). ATR-dependent phosphorylation and activation of ATM in response to UV treatment or replication fork stalling. EMBO J 25, 5775-5782.

Strnad, P., and Gonczy, P. (2008). Mechanisms of procentriole formation. Trends Cell Biol 18, 389-396.

Strnad, P., Leidel, S., Vinogradova, T., Euteneuer, U., Khodjakov, A., and Gonczy, P. (2007). Regulated HsSAS-6 levels ensure formation of a single procentriole per centriole during the centrosome duplication cycle. Dev Cell 13, 203-213.

Stucke, V.M., Sillje, H.H., Arnaud, L., and Nigg, E.A. (2002). Human Mps1 kinase is required for the spindle assembly checkpoint but not for centrosome duplication. EMBO J 21, 1723-1732.

Svendsen, J.M., Smogorzewska, A., Sowa, M.E., O'Connell, B.C., Gygi, S.P., Elledge, S.J., and Harper, J.W. (2009). Mammalian BTBD12/SLX4 Assembles A Holliday Junction Resolvase and Is Required for DNA Repair. Cell 138, 63-77.

Takada, S., Kelkar, A., and Theurkauf, W.E. (2003). Drosophila checkpoint kinase 2 couples centrosome function and spindle assembly to genomic integrity. Cell 113, 87-99.

Takao, N., Kato, H., Mori, R., Morrison, C., Sonada, E., Sun, X., Shimizu, H., Yoshioka, K., Takeda, S., and Yamamoto, K. (1999). Disruption of ATM in p53-null cells causes multiple functional abnormalities in cellular response to ionizing radiation. Oncogene 18, 7002-7009.

Takata, M., Sasaki, M.S., Sonoda, E., Morrison, C., Hashimoto, M., Utsumi, H., Yamaguchi-Iwai, Y., Shinohara, A., and Takeda, S. (1998). Homologous recombination and non-homologous end-joining pathways of DNA double-strand break repair have overlapping roles in the maintenance of chromosomal integrity in vertebrate cells. EMBO J 17, 5497-5508.

Takizawa, C.G., and Morgan, D.O. (2000). Control of mitosis by changes in the subcellular location of cyclin-B1-Cdk1 and Cdc25C. Curr Opin Cell Biol 12, 658-665.

Tanaka, K., and Hirota, T. (2009). Chromosome segregation machinery and cancer. Cancer Sci 100, 1158-1165.

Tang, C.J., Fu, R.H., Wu, K.S., Hsu, W.B., and Tang, T.K. (2009). CPAP is a cell-cycle regulated protein that controls centriole length. Nat Cell Biol 11, 825-831.

Terada, Y., Uetake, Y., and Kuriyama, R. (2003). Interaction of Aurora-A and centrosomin at the microtubule-nucleating site in Drosophila and mammalian cells. J Cell Biol 162, 757-763.

Thacker, J. (2005). The RAD51 gene family, genetic instability and cancer. Cancer Lett 219, 125-135.

Theinert, S.M., Pronest, M.M., Peris, K., Sterry, W., and Walden, P. (2005). Identification of the testis-specific protein 10 (TSGA10) as serologically defined tumour-associated antigen in primary cutaneous T-cell lymphoma. Br J Dermatol 153, 639-641.

Thomas, K.R., and Capecchi, M.R. (1987). Site-directed mutagenesis by gene targeting in mouse embryo-derived stem cells. Cell 51, 503-512.

Toji, S., Yabuta, N., Hosomi, T., Nishihara, S., Kobayashi, T., Suzuki, S., Tamai, K., and Nojima, H. (2004). The centrosomal protein Lats2 is a phosphorylation target of Aurora-A kinase. Genes Cells 9, 383-397.

Tokuyama, Y., Horn, H.F., Kawamura, K., Tarapore, P., and Fukasawa, K. (2001). Specific phosphorylation of nucleophosmin on Thr(199) by cyclin-dependent kinase 2-cyclin E and its role in centrosome duplication. J Biol Chem 276, 21529-21537.

Tournebize, R., Andersen, S.S., Verde, F., Doree, M., Karsenti, E., and Hyman, A.A. (1997). Distinct roles of PP1 and PP2A-like phosphatases in control of microtubule dynamics during mitosis. EMBO J 16, 5537-5549.

Toyoshima-Morimoto, F., Taniguchi, E., Shinya, N., Iwamatsu, A., and Nishida, E. (2001). Polo-like kinase 1 phosphorylates cyclin B1 and targets it to the nucleus during prophase. Nature 410, 215-220.

Tsang, W.Y., Spektor, A., Luciano, D.J., Indjeian, V.B., Chen, Z., Salisbury, J.L., Sanchez, I., and Dynlacht, B.D. (2006). CP110 cooperates with two calcium-binding proteins to regulate cytokinesis and genome stability. Mol Biol Cell 17, 3423-3434.

Tsang, W.Y., Spektor, A., Vijayakumar, S., Bista, B.R., Li, J., Sanchez, I., Duensing, S., and Dynlacht, B.D. (2009). Cep76, a centrosomal protein that specifically restrains centriole reduplication. Dev Cell 16, 649-660.

Tsou, M.F., and Stearns, T. (2006a). Controlling centrosome number: licenses and blocks. Curr Opin Cell Biol 18, 74-78.

Tsou, M.F., and Stearns, T. (2006b). Mechanism limiting centrosome duplication to once per cell cycle. Nature 442, 947-951.

Tsou, M.F., Wang, W.J., George, K.A., Uryu, K., Stearns, T., and Jallepalli, P.V. (2009). Polo kinase and separase regulate the mitotic licensing of centriole duplication in human cells. Dev Cell 17, 344-354.

Tsvetkov, L., and Stern, D.F. (2005). Phosphorylation of Plk1 at S137 and T210 is inhibited in response to DNA damage. Cell Cycle 4, 166-171.

Tsvetkov, L., Xu, X., Li, J., and Stern, D.F. (2003). Polo-like kinase 1 and Chk2 interact and co-localize to centrosomes and the midbody. J Biol Chem 278, 8468-8475.

Tutt, A., Gabriel, A., Bertwistle, D., Connor, F., Paterson, H., Peacock, J., Ross, G., and Ashworth, A. (1999). Absence of Brca2 causes genome instability by chromosome breakage and loss associated with centrosome amplification. Curr Biol 9, 1107-1110.

Uetake, Y., Loncarek, J., Nordberg, J.J., English, C.N., La Terra, S., Khodjakov, A., and Sluder, G. (2007). Cell cycle progression and de novo centriole assembly after centrosomal removal in untransformed human cells. J Cell Biol 176, 173-182.

Uetake, Y., Terada, Y., Matuliene, J., and Kuriyama, R. (2004). Interaction of Cep135 with a p50 dynactin subunit in mammalian centrosomes. Cell Motil Cytoskeleton 58, 53-66.

Utomo, A.R., Nikitin, A.Y., and Lee, W.H. (1999). Temporal, spatial, and cell type-specific control of Cre-mediated DNA recombination in transgenic mice. Nat Biotechnol 17, 1091-1096.

van Vugt, M.A., Smits, V.A., Klompmaker, R., and Medema, R.H. (2001). Inhibition of Polo-like kinase-1 by DNA damage occurs in an ATM- or ATR-dependent fashion. J Biol Chem 276, 41656-41660.

Vasquez, K.M., Marburger, K., Intody, Z., and Wilson, J.H. (2001). Manipulating the mammalian genome by homologous recombination. Proc Natl Acad Sci U S A 98, 8403-8410.

Volarevic, S., Pende, M., and Pullen, N. (1999). Manipulating mammalian genome by gene targeting. Croat Med J 40, 368-374.

Waizenegger, I.C., Hauf, S., Meinke, A., and Peters, J.M. (2000). Two distinct pathways remove mammalian cohesin from chromosome arms in prophase and from centromeres in anaphase. Cell 103, 399-410.

Wang, W.J., Soni, R.K., Uryu, K., and Tsou, M.F. (2011). The conversion of centrioles to centrosomes: essential coupling of duplication with segregation. J Cell Biol 193, 727-739.

Wang, X., Yang, Y., Duan, Q., Jiang, N., Huang, Y., Darzynkiewicz, Z., and Dai, W. (2008). sSgo1, a major splice variant of Sgo1, functions in centriole cohesion where it is regulated by Plk1. Dev Cell 14, 331-341.

Ward, I.M., and Chen, J. (2001). Histone H2AX is phosphorylated in an ATR-dependent manner in response to replicational stress. J Biol Chem 276, 47759-47762.

Warmerdam, D.O., and Kanaar, R. (2010). Dealing with DNA damage: relationships between checkpoint and repair pathways. Mutat Res 704, 2-11.

White, R.A., Pan, Z., and Salisbury, J.L. (2000). GFP-centrin as a marker for centriole dynamics in living cells. Microsc Res Tech 49, 451-457.

Wiese, C., and Zheng, Y. (2006). Microtubule nucleation: gamma-tubulin and beyond. J Cell Sci 119, 4143-4153.

Winding, P., and Berchtold, M.W. (2001). The chicken B cell line DT40: a novel tool for gene disruption experiments. J Immunol Methods 249, 1-16.

Wolff, A., de Nechaud, B., Chillet, D., Mazarguil, H., Desbruyeres, E., Audebert, S., Edde, B., Gros, F., and Denoulet, P. (1992). Distribution of glutamylated alpha and beta-tubulin in mouse tissues using a specific monoclonal antibody, GT335. Eur J Cell Biol 59, 425-432.

Wong, C., and Stearns, T. (2003). Centrosome number is controlled by a centrosome-intrinsic block to reduplication. Nat Cell Biol 5, 539-544.

Xiong, W., and Ferrell, J.E., Jr. (2003). A positive-feedback-based bistable 'memory module' that governs a cell fate decision. Nature 426, 460-465.

Yazdi, P.T., Wang, Y., Zhao, S., Patel, N., Lee, E.Y., and Qin, J. (2002). SMC1 is a downstream effector in the ATM/NBS1 branch of the human S-phase checkpoint. Genes Dev 16, 571-582.

Yuan, S.S., Chang, H.L., and Lee, E.Y. (2003). Ionizing radiation-induced Rad51 nuclear focus formation is cell cycle-regulated and defective in both ATM(-/-) and c-Abl(-/-) cells. Mutat Res 525, 85-92.

Zachariae, W., Schwab, M., Nasmyth, K., and Seufert, W. (1998). Control of cyclin ubiquitination by CDK-regulated binding of Hct1 to the anaphase promoting complex. Science 282, 1721-1724.

Zachos, G., Rainey, M.D., and Gillespie, D.A. (2003). Chk1-deficient tumour cells are viable but exhibit multiple checkpoint and survival defects. EMBO J 22, 713-723.

Zeitlin, S.G., Barber, C.M., Allis, C.D., and Sullivan, K.F. (2001). Differential regulation of CENP-A and histone H3 phosphorylation in G2/M. J Cell Sci 114, 653-661.

Zhang, J., Ahmad, S., and Mao, Y. (2007). BubR1 and APC/EB1 cooperate to maintain metaphase chromosome alignment. J Cell Biol 178, 773-784.

Zhang, J., Ma, Z., Treszezamsky, A., and Powell, S.N. (2005). MDC1 interacts with Rad51 and facilitates homologous recombination. Nat Struct Mol Biol 12, 902-909.

Zhang, J., and Powell, S.N. (2005). The role of the BRCA1 tumor suppressor in DNA double-strand break repair. Mol Cancer Res 3, 531-539.

Zheng, Y., Wong, M.L., Alberts, B., and Mitchison, T. (1995). Nucleation of microtubule assembly by a gamma-tubulin-containing ring complex. Nature 378, 578-583.

Zhou, B.B., and Elledge, S.J. (2000). The DNA damage response: putting checkpoints in perspective. Nature 408, 433-439.

Zou, C., Li, J., Bai, Y., Gunning, W.T., Wazer, D.E., Band, V., and Gao, Q. (2005). Centrobin: a novel daughter centriole-associated protein that is required for centriole duplication. J Cell Biol 171, 437-445.

Zou, H., McGarry, T.J., Bernal, T., and Kirschner, M.W. (1999). Identification of a vertebrate sister-chromatid separation inhibitor involved in transformation and tumorigenesis. Science 285, 418-422.

Zur, A., and Brandeis, M. (2001). Securin degradation is mediated by fzy and fzr, and is required for complete chromatid separation but not for cytokinesis. EMBO J 20, 792-801.

Zyss, D., and Gergely, F. (2009). Centrosome function in cancer: guilty or innocent? Trends Cell Biol. 19, 334-346.

Appendix 1

Full length chicken Cep135 cDNA sequence with ATG and STOP codon underlined indicated in red and 5` UTR in blue**.**

```
   1 CACGTCCGGC GTCTCCTCAG TGGTTTGCTC TGGAAGAATT TACCTTCAGC
  51 AGCGTGTCGG TGTCCTTTTT TTCCTGAATT TTACAAAAGC CACTTTGGAT
 101 CTGTGTTTAC AATGACGACA ACAGCGGAGC GGAAGTTTGT TAACCTCAGG
 151 AAACGTCTGG ATCAGCTGGG CTATCGGCAG CCCTTGGGAG TGGAGAGTTT
 201 ACCTTTGGTG GAAAAGCTTT TCAGTGACCT TGTTCATACA ACAGAGAGCC
 251 TGCGCAGTGC AAAGTTATCT GCTGGAAAAA TTGAAAAAGA GTGCAGCAAT
 301 TACGATGCTA TCATAGAGCC ATATAAAACT GAGACTGCAA AACTTACCAG
 351 GGAAAATAAT GAGCTGCATT TGGAAGTATT AAAACTGAAA GAGCAATCTG
 401 ATCATCATAT TAAAGATTTG AAAGCCAGCT TAAGGAGAGC TGAAAATGAA
 451 GCAGCTGACT TGAGATTCCT GAATAACCAG TATGTGCATA AAATCAAACT
 501 GCTGGAAAAA GAGAGCAAAG CCAAGACTGA AAAAATTCAG CAGCTTCAGG
 551 AGAAGAATCT GCAAGCAGTG GTGCAAACTC CTGGTGGCAG AAAAAGAAAC
 601 ATCCCATTCA GGCGTCAACG CATGCAGATA GACCAGCCTG TTCCTCCATC
 651 AGCTGTTAGT GCTTATCCAG TGCCTCAGCC AGAGGACCCG TACATTGCAG
 701 ACCTTCTTCA GGTGGCTGAT AATCGAATAC AAGAACTTCA GTCAGAAGTA
 751 ACACAGTTAC AAGAAAAGCT AGAGATATCA GAAAATGGAA AGAAGAATTA
 801 CAGCAAGCAG GTTGAGCTTA GAGACAAAGA AATAGAACGC CTCATGCTAG
 851 CATTGGATGG TGGTCGTTCT CATGAAGTTA TATCTCTGGA ATCAAGAAGT
 901 AAAAGCAATG AGAAACTTAT TGCCCAATTA AATTTGCAGG TTGAATATCT
 951 TCAGCAGTCA AACAAAGAAC TTGAAAATCG CATTCAAGAC CTCTTGGACA
1001 CAAAAAAAAA TGTGACTAGT GAGGTAGTGC ACTTAAGCAA TAAAAATGAA
1051 GAACTCTGTC AAGAACTGAA TGAAATAGAC CATTTGGCAC AGCAGTTGGA
1101 AAGACATAAG GAAATTGTGC TTGAAACTGC AGATAAAGAA ATAGGAGAAG
1151 CAAAGAAGGA AATTGAGAGA AAGGACAGTG AAATACAGGA TCTTGAAGAA
1201 ACAATAACGA GGCTTAAATC AGAGTTGAGC TCGTGTCGTC GACAGAACGA
1251 GAGATTGAGT GAAGAACTAT TTGGAAAAGC AGATGATAAA GAGAATCTTG
1301 AACTACTGCT GAACCAGCTT GAACAAGAAA AACAGAGGCT GACAGAAAAA
1351 ACAGAGAACT TTGAAATAAA AGAACGAGAA CTTGTCCTAG AAATAGAAAG
1401 AATGAGATTA GAATACGGTA TAGCTCTAGG AGACAAATCT CCATCTCGTC
1451 TAGATGCATT TGTCAAAACT TTAGAAGATG ACAGAGATTA TTATAAAAGA
1501 GAATTAGAGT ATCTTCAGAA AATGATAAAA CGAAGACCTA GCCCAAGTCG
1551 TAGGAGTCCA GAGAAGAGTG AAGATCTGAG ATTGATCACT AGAGAAAGAG
1601 ATGAGCTACA GTCCATGTTA GACAGATTTG AAAAGCATAT GATAGAAATT
1651 CAATCCAATG TCAAGCTACT GACTGCAGAA AGAGACAGAT TAAATATTCT
1701 TTATGAGCAA TCTCAGAGTG AATTAAACAG ACTGAGAAGA GAAGCAAAAC
1751 ATAATTTAGT TTCTCAAAGT CATGTGGGAG AAGATGGAGA TGCTTCACTG
1801 GCAGACTTTA GAAGACTGAT GGCAGAAAAG GAAAGTCTAA GAGAAAAGTT
1851 AAAGATTCAG CAAGAAGCGG CTAACCTTGA AAAATCAAAG ATGCAGCATG
1901 ATATTTCAGT ACTGGAAAAT AATATCCAAC AATTTGAGTT GGAAAGGTGT
1951 GAACTAAAGA GTACAATCTC TATCCTGAAA GAAAGAATAA AGTCTTTGGA
2001 AAATGAATTA AAATTGAAGT CCAGTAAACT TATCCAAACA TCTGATGATT
2051 CTTCACAACT TAAAGCTGAA CTTTGCTCAC TTCACCTCTT AAATGAACAA
2101 CTTCAGAGGA CTGTGGAAGA CTTACAGCAC CGATTGTCTC TCAAAAAGGA
2151 TGAACTTCAG TCAGCTCAAG AAGAAATTGT AAAGCTAGAG GAGAAAATAG
2201 ATAGGTTAAA CCAGAAGAGC ACTTCACAGG ATGAGGCAGT CAATGTGCTT
2251 AGAAGTACTA TAACTGTTTT GGACAAAGAA AAGGATAATC TTCAAGAAAC
2301 TGTAGATGAA AAAACAGAAA AAATTGCGTG CTTAGATGAC AACTTAGCTA
2351 ACAAGGAAAA GACAATTACT CACTTACGGC TAACGCTCTC TGAGCTGGAG
2401 TCATCCACAG ACCAGCTAAA GGACCTCCTG AGCAGCAGAG ACCGTGAAAT
2451 ATCTAGCTTA CGTCGCCAGC TTGATGCATC CCACACAGAG ATTGCAGAAA
2501 CAGGAAGAGT AAAGGAAATA GCTCTGAAAG AAAATAGGCG ACTACAGGAT
2551 GACCTAGCTA CAATGACCAG AGAAAACCAG GCTGTCAGTT CTGAGCTCGA
2601 AGATGCAATA CGTGAGAAGG AAGAAATGAA AACTAGAGTT CATAATTATA
2651 TAACTGAAGT TTCCAGATTT GAGAGTCTGA TAGCTTCAAA GGAAAAAGAA
2701 AACCAAGAAT TATTAGAGAA GTTCCGAATG CTCCATACAC AAGCTGAGGA
2751 CTGGGAAATC AAGGCTCATC AAGCTGAAGG GGAAAGCAGC TCAATACGAC
2801 TTGAACTCCT TTCTGTAGAT ACGGATCGGA GACATCTTCG AGAGAGAGTA
2851 GAACTTCTGG AGAAAGAGAT TCAAGAGCAT ATGATTGCAC ATCAAGCTTA
2901 TGAATCTCAG ATCTCCTCCA TTACAAAAAA TATGTCTAAA TTGGAAGAGG
2951 ACATTAAACG TGAACATCAG GATAAGTCCT CCGTGCTGGC TGACCTGACT
3001 TCTGTGAGAG AACTTTGTGT TAAGCTTGAA GCTAGCAAAG ACCTTTTATC
3051 TCGACAGCTT GCATCTAAAA GCATGGATTA TGAAAAGGTT CTAGGTGAAT
3101 TAGAAGATGT TAAATCAGAA GCAGAGTTGC TGAAAAAGCA GTTATCCAGT
3151 GAGAGACTTA CAATTCAGAA TCTTGAAACA TTGCTGGCTA CCAGTAGAGA
3201 TAAAGAATTT CAGAACCATT TAACGTCTCA CGAAAAAGAT TCAGAAATCC
3251 AGTTACTGAA AGACAAGTTA ACACTTGCCG AGGGGAAACT AAGCAGTCAT
3301 AATAGAGAGG TTTCCATGCT TCGAAGTAAA GTTGCACAGC TGCAGACTGA
3351 CTATGATGTT TTAAAAAGAC AGCTGACGAC TGAAAGATTT GAACGAGAGC
3401 GTGCAATTCA GGAGATGCGT CGACACGGTC TCTCTACGTC GTCATTACGT
3451 GCTTCACCTC CTCTCAGTTC TACATTAAGG TCTCCCTCAC ATTCTCCGGA
```

```
3501 TCGTGCAGTT GCAAGGACAG CTGATCAAGC AGCTGCTGAA AAAAACGTGAGCTTCAAGGA GTAA
```

Appendix 2

A list of the primers used for PCR-based cloning and DNA sequencing is given in Table A1. Primers were obtained from Sigma-Aldrich Ireland.

Table A1 Primers used for PCR and DNA sequencing

Primer name	Sequence 5`-3`	Use
Cep135-5`Pro-F1	ATGCAGAACGACGAGGAGAT	For cloning 5` external probe
Cep135-5`Pro-R1	GAACTCCCAAAGGACAACCA	
Cep135-3`Pro-F1	AAAAACAACCCACAAACAACTTT	For cloning 3` external probe
Cep135-3`Pro-R1	TCTGATGAGATTACATGCAGAGC	
Cep135-5`Pro-F2	GGCAGAACTTAAAAATACTGAGC	For cloning new 5` external probe
Cep135-5`Pro-R2	TTCACACGTAGGCTTAGAAAAG	
Cep135-3`Pro-F2	GGTCCTCACCTTTGCAAGAA	For cloning new 3` external probe
Cep135-3`Pro-R2	ATCTCAACCTAACAGAGGTGCTG	
Cep135-5`Arm-F	GCGGCCGCTGTGGGTTGACCTGTCTCT	For cloning 5` arm
Cep135-5`Arm-R	GGATCCTAAAATATCGTTTGTTACAGC	
Cep135-3`Arm-F	GGATCCCTATACAGGATTTACTCTTG	For cloning 3` arm
Cep135-3`Arm-R	GGTACCTTGTTTTGACTAATCAACAGC	
Cep135-GSP1	GTACGGGTCCTCTGGCTG	For 5` RACE PCR of *cCep135*
Cep135-GSP2x	TGCATGCGTTGACGCCTGAA	
Cep135-GSP3x	TTCTGCCACCAGGAGTTTGC	
Cep135-F	CCGCGGATGACGACAACAGCGGAGC	For cloning of *cCep135* cDNA
Cep135-R	GGATCCTTACTCCTTGAAGCTCACGTTT	
CP110-F	AACCTCGAGATGGAGGACTACGAAACGT	For cloning of *cCp110* cDNA
CP110-R	GGATCCTCATCCAAGTGAGTGCTGTC	
5`armExoc1	TGACTGCTTCTATGGATGATT	For sequencing exons of *cExoc1* gene in the 5` arm
5`armExoc2	ATGATGAGTTAAGTGTGCCTT	
Cep135seq	GTGGTCGTTCTCATGAAGTTATATC	For sequencing middle of *cCep135* cDNA
Cp110seq1	GGGAGTACATAGAGAAAGAG	For sequencing middle of *cCp110* cDNA
Cp110seq2	GTAGAGACTGGTACTGTAGGTT	
Primer C1	TACGAGGAGCGCTTTTGTTTTGTATTG	Primers used for screening targeted integration of the *cCep135* knockout construct
Primer C2	AGCCAAGCTGGGCGTAATCAT	
Primer G	GACCCGTACATTGCAGACCT	
Primer R	ACAAGAAACTACCACCTAAAAAGCA	

Appendix 3

Full length chicken CP110 cDNA sequence with ATG and STOP codon underlined and indicated in red.

```
   1 ATGGAGGACT ACGAAACGTT CTGTAAGAAG CATCTGTCCA GAATCCAAGA
  51 AGAGGCAACA AAAGGGGAAA ACTCATCCAC CTCGTTGGAC AGAAATGTCT
 101 CCCTCATTCA ATTCCATGGA GTTCCAGTGC TCTCCCCTCT GCTGAGCTTT
 151 GAAAAGAGAA AGGAAATACA GCAGTATCGA CAGAAAGCAC TGGATCTAGA
 201 GACTTGGAGA CAGAACTCCC ACAAAAGAGC CTTACTGAAT CGTGTTCAGG
 251 AGATTCTAGA AAACATTCAG AACAGGAAAG TATCTGGTAA GAGTGATGTG
 301 AACACGTGGG ATGCTGAGAA CACCTGCCCC GATTCAGACT CAAAAGCTTT
 351 AACTGATCTC GCAGCTGTGT CAGATGCCAA CTTGCCATGT TCTCCCGAAA
 401 GGCATTGTTC TGTGCAGCTT GAAAAAAGCC AAGAGCTTTT GCCACCAGAC
 451 TCTATGCAAC AAGTGACATC AAATGCAACA GAAGTAGGTA AACCAGCAGA
 501 AGAAAATGTT CCTTCAAAGG AAAGTGGGAG TCACTTCTCA AGAGATGTAC
 551 CTTGTCCGAG GGCTGCATCT CCTGACAGTG TACAGAGTAA ACTTGTGTCC
 601 CCTGCTTTGC AAAAGCAAGA GGGACAAGGA GTGCCATCAT CTGACAAGGA
 651 AGTCCAAGAT CCATATGCAG TGAGTCTTCA GAACCTGATG AAAAAGTCTA
 701 GGGAGTACAT AGAGAAAGAG CAAAGCAGGC GTAGCTCAAA AAGCAGTTCA
 751 AAGAAGAGTA TGAATGAAAG CCATTCAGAT AAAGAAAATG ATGCAGTTAA
 801 AACATCGGAC CCTGTGAAAG AGAGGGTAAA GCTTACAGGC AGAAGTTCCA
 851 CTGCTCTGCC ACTTGATAAA CCCTGTCTTA ATAAATCAAA TGCTCATATT
 901 CAAGGTGCCT CTACTCATAC AAGTAACACA AGTATGTCAA CTTTATCCAG
 951 TTTTTCTAAA GTGGATATAC CTATGAGAGT TGGAACACCC CCGTTGGTGG
1001 ATTCGGATTC AGATGAAGAA TTTAAAAATA CTTCCACCAT TGATCGTGAC
1051 AGTAGCATTG TCAGGAGCCT CACAGGGTCG TATACCAAAC TGCCAAGCCC
1101 AGAGCCAAGC ATGAGTCCAA AAATGCACCG GAGGCGCCCA AGGCCTCTAT
1151 CAATGGGGCA CATAGTTATA AATAACCCTG TGAATGCTTA TGAATTAAGT
1201 CCCAAAGGCA AGGGTAGAGC AATGGATTTA ATTATGCAAG ATATTGCAGA
1251 TAAAAATAAT GTGTCTGAGT CAGTGCCAAA GTTCATGATG GACTTCAGTA
1301 TGCTTTGCCC TAGCAGAGTT CCTGGTGTCC TGAGGAGTTC TTCAGGCCCT
1351 TCTGACGGGT TGCTGGTTGG CAAACCAAAT AGACATTCCT TTGGGCACTC
1401 AGAAGGCAAA GGGACGTTGT CTGCTGCAAT GGAAGGACAG ATAGTGATGG
1451 ACAACAGGGG ACCGTATAAA GTAGAGACTG GTACTGTAGG TTCAAAACTG
1501 AATGAGCCAT TTTCCATTAA TCAGTCTACA GTAACACAGA AGCTCCTAGC
1551 TGTGAACGAA ACCAAGGCAT CCAGTTTGCA AGAAAATACT AAATCTCCAG
1601 TAGAACTCAA TAAATCTTAC GATGTAGAAA GCCCATCCCC ACTACTAATG
1651 CAGAGCAAGA GTATGCACCA GCAGATGGAT ACTCCAAGTG TTCCCCCAGC
1701 AAATGAACAG TTTCTAGAAA ACAGTTTTGA AAAGGTAAAA CGTAGACTTG
1751 ATTTGGACAC TGACGACTGC CAGAAAGATA ACAACCCCTG TGTTGTAACA
1801 GTTGGAATGG AGGAACAAGA GAGGCAATGG TTGCAAGAGC AGAAATATCC
1851 CGTGACGTCA GTTTACATTA CCAAGAATGC AGCCTCTGAT TCAAGTATGG
1901 CAAAAGAAGA GATTTTAAAG ACTAAAATGT TGGCCTTTGA AGAAATGAGG
1951 AAGAGACTCG AAGAGCAGCA TGCACAACAG CTGTCAATTC TGATAGCAGA
2001 ACAAGAGCGA GAGCAGGAGA AATTGCAGAA GGAACTGGAG GAACAGGAGA
2051 GAAAGGGAAA GAAGATCGCT ACGACAGAAA TAGAGATTTC CAAAGTGAAT
2101 ATTAACAGTA GGATGGAGTT GGAGTGGAGA AAAAGTGAAA GCGGTTTAGT
2151 GGAAAGTGTG CAGTCTCAGC TGGAGACGAT CCATAATGCC AACTCCACAA
2201 GCATTGGTTT TGCTCATACT ACATCACCTA ACACCTTCAC TTCAACAAGT
2251 GAAACTTCCT TCTTTCTCTG GGGACCATCA GGCAGCGGAG TTATAAAAAC
2301 CTCAGTATCT AGGCCAAGTA ACAGGATCAA AACTAGGTGG ACCCAGATTT
2351 TCACTCCGGA GATACAAATG AAGTTTGATA AGATAACTGC TGTGGCAAAG
2401 GGGTTTCTTA CGCGTCGGCT CCTACAGACA GAGAAACTGA AACATCTCAA
2451 GCAGACTGTA AAAGATACCA TGGAGTTCAT AAGAAATTTT CAGTCTGAAG
2501 CTCCATTAAA AAGAGGAAGT GTTTCAGCAC AAGATGCATC CCTTCATGAG
2551 AGAGTAATGG CTCAGCTTCG AGCTGCTCTG TATGATATCC ATGACATATT
2601 TTTCACGATG GAGGCATCAG AAAGAATGAA CATTCTGCGT CACGATCGTG
2651 AAGTTCGTAA AGAGAAGATG CTCAGGCAAA TGGATAAAGT AAAGAGTCCA
2701 AGAGAGAGAG CAACGCTTTC AACAGCTACG CAGAAATCTC TGGATAGGAA
2751 AAAGTACATG AAGGCTTCAG AAATGGGAAT GCCTAGTAAA AAAATAGTCA
2801 TAAAACAAAG AAGTCCTGAG AGCCGAGTGC TTCAACCAAA TCAAGGACAG
2851 AATGCCCCAG TTCATAGATT ACTTTGCAGA CAAGGAACCC CTAAGACCTC
2901 AATGAAGGGG GTTGAGCAAA ATAGAAAGAA GGCCTCAGAG AGCAGAGTGT
2951 CTAACAAGGC GGTTTCAGGA GCATATGCAG GAAGAACCCA AAGAAAGAAG
3001 CCAAATGTTG TGACAATTTA A
```

Appendix 4

Poster presentations and Publications

Publications

- **Inanç, B.,** Dodson, H. and Morrison, C.G. (2010). A centrosome-autonomous signal that involves centriole disengagement permits centrosome duplication in G2 phase after DNA damage. Mol. Biol. Cell, 21: 3866-3877.
- **Inanç, B.** and Morrison, C.G. (2011). Getting permission: How DNA damage causes centrosome amplification. Cell Cycle, 10: 1890-1891.

In preparation

- **Inanç, B.**, Puetz, M., Dantas, T. J., Lalor, P., Dockery, P., Gergely, F. and Morrison, C.G. Abnormal centrosomal structure and duplication in Cep135-deficient vertebrate cells.

Poster Presentations

- **Inanç, B.,** Dodson, H. and Morrison, C.G. Testing a Licencing Model for DNA-Damage Induced Centrosome Amplification. Poster presented to the American Society for Cell Biology at the Annual ASCB meeting, December 5-8 2009, San Diego, CA, USA.
- **Inanç, B.,** Dodson, H. and Morrison, C.G. Mechanisms of DNA-damage Induced Centrosome Amplification. Poster presented to the Irish Association for Cancer Research for the Annual meeting, March 3-5 2010, Galway, Ireland.